Novel Molecular Targets in Advanced Prostate Cancer

Trinity College Dublin

The University of Dublin

A thesis submitted to the University of Dublin, Trinity College for the degree of

Doctor of Philosophy (Ph.D.)

by

Dr. John Patrick Greene

Supervisors:

Prof Stephen Finn, Trinity College Dublin

Prof Raymond McDermott, Tallaght University Hospital

April 2019

Declaration

I declare that this thesis has not been submitted as an exercise for a degree at this or any other university and it is entirely my own work.

I agree to deposit this thesis in the University's open access institutional repository or allow the Library to do so on my behalf, subject to Irish Copyright Legislation and Trinity College Library conditions of use and acknowledgement.

_____

John Patrick Greene

Summary

Prostate Cancer (PCa) is the most commonly diagnosed cancer in men and a leading cause of morbidity and mortality among men in the United States and Western Europe. The aim of initial treatment in advanced PCa is to reduce circulating levels of androgens in the body by blocking their effect through inhibiting the androgen receptor (AR) through androgen deprivation therapy (ADT). Additional agents that target the AR can be used when disease progresses on ADT. A number of patients will not respond to these agents, while others will eventually develop secondary resistance. Identifying those patients who will not respond to these agents is a key focus of ongoing research.

In the study, the safety and tolerability of radium-223 combined with enzalutamide was assessed in patients with castration-resistant PCa (CRPC). Both these drugs are approved for use as single agents, however the safety of combining the drugs is unknown. In this study, it was found that the combination was safe and tolerable. The effect of the combination therapy on circulating tumour cells (CTCs) was also assessed, however it did not serve as a potential surrogate marker of response.

PCa tends to have a long natural history and may require treatment with multiple modalities over many years, however repeat biopsies are not routine in the clinical setting. To address this, patients with metastatic PCa were enrolled in a translational study named iPROSPECT. All patients were offered an optional biopsy which could be either a bone marrow biopsy or a CT guided biopsy. It was observed that image guided biopsies provided more information than bone marrow biopsies and were more accurate at obtaining tissue. These

tissue biopsies were further analysed using next generation sequencing (NGS) and compared to their primary biopsies. A number of gene targets were identified, with a higher incidence of mutations detected in patients with more advanced disease. Furthermore, gene expression differed between primary and metastatic biopsies indicating the significance of performing repeat biopsies in patients with advanced PCa.

Similarly, having access to repeat biopsy material in advanced PCa allows for further testing using immunohistochemistry (IHC) which can identify alterations in the AR such as AR-V7 or neuroendocrine differentiation. In this study, both AR-V7 and neuroendocrine differentiation were noted in patients who had undergone a biopsy of a metastatic deposit. This underscores the importance of repeat biopsy, given that it could guide clinical decision making.

To further identify biomarkers in advanced PCa, circular RNAs (circRNAs) were profiled in a cell line model of the disease. circRNAs are a novel type of non-coding RNA which appear to have a role in regulating microRNAs (miRNAs) and may have a role in cancer initiation and resistance to treatment. This study profiled PCa and benign cell lines and found circRNAs to be differentially expressed between malignant and benign cell lines and between androgen dependent and independent cell lines. Furthermore, hsa_circ_0004870 appears to be associated with AR-V7 and may play a role in the development of resistance to enzalutamide.

The data generated in this project determined the combination of radium-233 and enzalutamide is safe and well tolerated and has identified new

therapeutic targets in advanced PCa. Therefore, this could lead to real world clinical benefits for patients living with this disease.

Acknowledgements

I would like to gratefully acknowledge the support and guidance of my supervisors, Professor Ray McDermott and Professor Stephen Finn, during the course of this project. Their constant enthusiasm and belief in me over the last few years has been invaluable. I would also like to thank Dr. Steven Gray for his advice during all stages of the research.

My grateful thanks also to the following people for assistance at various stages of the project; Dr. Orla Casey, Dr. Lauren Brady, Dr. Gordon Blackshields, Dr. Odharnaith O'Brien, Dr. Tatjana Vlajnic, Dr. Paul Smith, Dr. Brian Hayes, Dr. Cathal O'Brien, Dr. Martin Barr, the staff at Cancer Trials Ireland, the iPROSPECT investigators, the staff in the histopathology laboratory in St. James's Hospital and the staff in the clinical trials unit at Tallaght University Hospital. A special thank you to Dr. Anne-Marie Baird, without her help this project would never have been possible.

I would like to especially acknowledge the patients who participated in the clinical trials in this study.

Finally, I would particularly like to acknowledge the encouragement and support of my wife, my parents and my family over the last few years, without whom this thesis could not have been completed.

This work was supported by the Irish Cancer Society and the Prostate Cancer Foundation

List of Tables

Table 1.1. Cancer associated circRNAs. 22

Table 2.1. Cell lines categorised according to AR status. 28

Table 2.2. PCR conditions for mycoplasma testing. 33

Table 3.1. ECOG Performance Status Grading System. 62

Table 3.2. ECOG Performance Status for patients recruited to ICORG 13-21. 63

Table 3.3. Baseline Characteristics of Patients recruited to ICORG 13-21. 63

Table 3.4. The most frequent AEs. 65

Table 3.5. Combination therapy AEs leading to discontinuation or delay of radium-223 and enzalutamide. 66

Table 4.1. Baseline characteristics of patients recruited to cohort 1 and cohort 2 86

Table 4.2. NGS Biopsy Results. 103

Table 5.1. Custom designed BaseScope™ probes for AR-FL and AR-V7. ..138

Table 6.1. Human Prostate Cancer Cell Lines. 167

Table 6.2. Different methods attempted to optimise RNase R. 174

Table 6.3. List of miRNAs and their predicted circRNAs. 176

Table 6.4. List of circRNAs selected for validation. 177

Table 6.5. List of circRNAs qPCR values beyond 30 cycles that were not further tested. 178

Table 6.6. Top ten upregulated circRNAs in PCa (malignant *vs.* benign cell lines)..... 181

Table 6.7. Top ten downregulated circRNA in PCa (malignant *vs.* benign cell lines)..... 182

Table 6.8. Top ten upregulated circRNAs in androgen independent cell lines. 188

Table 7.1 The top 5 up-regulated and down-regulated circRNAs in control *vs.* clone 1 based on FC. 210

Table 7.2 The top five up-regulated and down-regulated circRNAs in clone 9 *vs.* control based on FC. 213

List of Figures

Figure 1.1. Androgen production in the male. 4

Figure 1.2. Schematic image of the AR and potential drug targets 5

Figure 1.3. The molecular structure of the AR gene and protein, showing the domain regions. 9

Figure 1.4. AR-FL and AR splice variants. 11

Figure 1.5. Image of CTC. 13

Figure 1.6. circRNA splicing. 16

Figure 1.7. circRNA validation. 18

Figure 1.8. circRNA sponges. 20

Figure 2.1. CircRNA microarray. 42

Figure 2.2. The ScreenCell® Device. 45

Figure 2.3. The Oncomine™ Focus Assay gene list and workflow. 49

Figure 2.4. RNAscope® 2.5 Assay. 51

Figure 2.5. RISH semi-Quantitative Analysis. 53

Figure 3.1. Study schema for CTRIAL (ICORG) 13-21 trial. 59

Figure 3.2. Representative images of CTCs on ScreenCell® filters stained with MGG. 68

Figure 3.3. CTC counts throughout treatment with the combination of radium-223 and enzalutamide. 69

Figure 3.4. CTC counts in patients who progressed rapidly on ADT (within 18 months). 71

Figure 3.5. CTC counts in patients who progressed on ADT after 18 months 72

Figure 4.1. Schema of iPROSPECT study. 82

Figure 4.2. Site of metastases for cohort 1. 84

Figure 4.3. Sites of metastatic disease for cohort 2. 87

Figure 4.4. CTC counts in patients recruited to iPROSPECT cohort 1 and cohort 2. 89

Figure 4.5. Total number of biopsies performed in iPROSPECT sub-studies. 90

Figure 4.6. Sensitivity of bone marrow biopsies *vs.* CT guided biopsies. 92

Figure 4.7. Bone marrow sampling in a patient recruited to iPROSPECT with metastatic PCa. 93

Figure 4.8. Alkaline phosphatase value comparisons of positive and negative bone marrow biopsies. 95

Figure 4.9. PSA value comparisons of positive and negative bone marrow biopsies. 96

Figure 4.10. Lymph node biopsy showing metastatic adenocarcinoma. 97

Figure 4.11. Liver biopsy showing metastatic adenocarcinoma. 98

Figure 4.12. H&E of liver biopsy from iPROSPECT sample. 100

Figure 4.13. Heatmap showing alterations in metastatic biopsy samples using the Oncomine™ panel. Darker blue reflects higher copy number gain. Red boxes indicate alterations identified in genes. 104

Figure 4.14. CTC counts measured at time of biopsy according to the presence or absence of carcinoma. 106

Figure 5.1. Standard curve method for AR-FL. 119

Figure 5.2. AR-FL copy number expression. 120

Figure 5.3. AR-V7 standard curve. 121

Figure 5.4. RNA copy number expression of AR-V7.....122

Figure 5.5. AR-FL expression in a cell line model of enzalutamide resistance. 124

Figure 5.6. AR-V7 expression in a cell line model of enzalutamide resistance. 125

Figure 5.7. IHC for AR-V7. 127

Figure 5.8. RNAscope® and BaseScope™ positive and negative controls using HeLa cells. 130

Figure 5.9. AR-FL and AR-V7 expression in 22Rv1 cell lines using RNAscope®. 133

Figure 5.10. AR-FL and AR-V7 expression in VCaP cell lines using RNAscope®. 135

Figure 5.11. AR-FL and AR-V7 expression in PC3 cell lines using RNAscope®. 137

Figure 5.12. Custom designed BaseScope™ probes for AR-FL and AR-V7. 138

Figure 5.13. AR-FL and AR-V7 expression in VCaP using BaseScope™. ..141

Figure 5.14. LNCaP Control cell line stained using BaseScope™. 143

Figure 5.15. LNCaP clone 1 cell line stained using BaseScope™. 145

Figure 5.16. LNCaP clone 9 stained using BaseScope™. 147

Figure 5.17. Androgen independent PC-3 using BaseScope™ showing no expression of AR expression. 149

Figure 5.18. Images obtained from RNAscope® staining on radical prostatectomy sample specimen. 152

Figure 5.19. AR-FL and AR-V7 expression in a patient sample using BaseScope™. 155

Figure 5.20. Compatibility of RNAscope® with ScreenCell® filters. 157

Figure 6.1. Boxplot distributions of circRNA expression 168

Figure 6.2. Principle Component Analysis plot. 170

Figure 6.3. circBICC1 expression in HeLa Cells..... 172

Figure 6.4. Expression of hsa_circ_0090923 and AR-FL with and without RNase R 173

Figure 6.5. Clustering heat map of microarray data showing differential expression of circRNAs between malignant and benign cell lines..... 180

Figure 6.6. hsa_circ_0004870 expression according to malignancy status. .. 184

Figure 6.7. hsa_circ_0083092 expression in PCa. 185

Figure 6.8. Clustering heat map of microarray data. 187

Figure 6.9. hsa_circ_0004870 expression according to androgen dependency. 191

Figure 6.10. hsa_circ_0083092 expression according to androgen dependency. 192

Figure 6.11. circRNAs identified from circBase using the AR and AR-V7 sequences. 193

Figure 6.12. Alignment of the four identified circRNAs from circBase to the AR transcript (NM00044.3) and AR-V7. 195

Figure 6.13. hsa_circ_0090923 sequence and alignment to the AR from circBase. 196

Figure 6.14. Relative expression of hsa_circ_0090923 in known AR dependent cell lines 197

Figure 6.15. circRNA products post qPCR. 197

Figure 7.1. circRNAs and cancer development. 204

Figure 7.2. Clustered heatmap of enzalutamide resistant clones 1 and 9 vs. less resistant control 207

Figure 7.3. Heatmap and corresponding scatterplot showing expression levels for control *vs.* clone 1 cells. 209

Figure 7.4. Heatmap and corresponding scatterplot showing expression levels for control vs. clone 9 cells 212

Figure 7.5. Detailed annotation for predicting circRNA/miRNA interaction for miR-145 and hsa_circ_000487. 214

Figure 7.6. Validation of circRNAs. 217

Figure 7.7. hsa_circ_0004870. 220

Figure 7.8. RBM39 expression. 222

Figure 7.9. U2AF65 expression. 223

Figure 7.10. miR-125b expression. 225

Figure 7.11. Relative expression of hsa_circ_0083092 in cell culture media. 226

Figure 7.12. Using BaseScope® technology to design circRNAs probes. 227

Figure 7.13. RISH in cell lines for hsa_circ_0083092 using BaseScope®. .. 228

Figure 7.14. RISH in metastatic lymph node biopsy sample for hsa_circ_0083092 using BaseScope®. 229

Abbreviations

ADT	androgen deprivation therapy
AE	adverse event
AGO	Argonaute Protein
ALL	acute lymphoblastic leukaemia
AMNCH	Adelaide and Meath National Children's Hospital
ANOVA	analysis of variance
AR	androgen receptor
AR-FL	androgen receptor full length
ARV7	androgen receptor variant 7
ASI	androgen signalling inhibitors
ATCC	American Type Culture Collection
BCL-2	B-cell lymphoma 2
BCR	biochemical recurrence
BPH	benign prostatic hyperplasia
ceRNA	competitive endogenous RNA
CircRNA	circular RNA
CRP	C – reactive protein
CRPC	castrate resistant prostate cancer
Ct	cycle threshold
CT	computerized tomography
CTC	circulating tumour cell
CTCAE	Common Terminology Criteria for Adverse Events
CTRIAL	Cancer Trials Ireland
CYP-17	Cytochrome P450 17
DHT	dihydrotestosterone

DMEM	Dulbecco’s modified eagle’s medium
DNA	Deoxyribonucleic acid
ECOG	Eastern Cooperative Oncology Group
EDTA	Ethylenediaminetetraacetic acid
EGF	epidermal growth factor
EMT	epithelial mesenchymal transition
EORTC	European Organisation for Research and Treatment of Cancer
EpCAM	epithelial cell adhesion molecule
ERG	ETS-related gene
ERK	extracellular receptor kinase
ETS	E26 transformation specific
ETV1	ETS variant 1
FBS	foetal bovine serum
FC	fold change
FDR	false discovery rate
FFPE	formalin fixed paraffin embedded
FGF	fibroblast growth factor
H&E	Haematoxylin and Eosin
Hb	haemoglobin
HIPK2	Homeodomain-interacting protein kinase 2
ICORG	All Ireland Co-Operative Oncology Research Group
IGF-1	insulin growth factor
IHC	immunohistochemistry/Immunohistochemical
IMS	industrial methylated spirits
iPROSPECT	Irish Programme for Stratified Prostate Cancer Therapy
LBD	ligand binding domain

LDH	lactate dehydrogenase
LHRH	Luteinizing hormone-releasing hormone
LncRNAs	long non-coding RNAs
LRTI	lower respiratory tract infection
MEM	minimum essential medium eagle
MetS	metabolic syndrome
MGG	May Grunwald Giemsa
miRNA	microRNA
mTOR	mammalian target of rapamycin
MYC	myeloctomatosis oncogene cellular homolog
MRE	miRNA response elements
mRNA	Messenger RNA
MRI	Magnetic resonance imaging
NCBI	National Centre for Biotechnology
ncRNA	noncoding RNAs
NGS	next-generation sequencing
PMBC	peripheral blood mononuclear layer
PBS	phosphate buffered saline
PBST	PBS tween
PCa	Prostate cancer
PCR	polymerase chain reaction
PCRC	Prostate Cancer Research Consortium
PCWG2	Prostate Cancer Working Group 2
PPIB	peptidyl-prolyl cis-trans isomerase B
PPSA	proPSA
PSA	prostate specific antigen

PSAP	prostatic specific acid phosphatase
PTEN	phosphatase and tensin homologue
QoL	quality of life
OS	overall survival
RBP	RNA-binding proteins
RISH	RNA in situ hybridisation
RNA	Ribonucleic acid
RNase R	Ribonuclease R
RT	room temperature
SEM	standard error of the mean
SFM	serum free media
TBS	tris-buffered saline
TE	Tris-EDTA
TMPRSS2-ERG	transmembrane protease serine ETS-related gene fusion
TMA	tissue microarray
TNF	tissue necrosis factor
TTF-1	thyroid transcription factor 1
VEGF	vascular endothelial growth factor
WCC	white cell count
WHO	World Health Organisation
WT	wildtype

Units

bp	base pairs
°C	degrees Celsius
g	grams
h	hour(s)
IU	International Units
µg	microgram
µL	microlitre
µM	micrometre
µM	micromolar
kB	kilobases
kDa	kilodaltons
kg	kilograms
hz	hertz
L	litre(s)
M	molar
mA	miliamp
mg	milligram
min	minutes
mL	millilitre
mM	millimolar
mm	millimetre
n	number (sample size)
nM	nanometres
ng	nanogram
pg	pictogram

rpm	revolutions per minute
s	second(s)
U	unit(s)
V	Volt
w/v	weight per volume
v/v	volume per volume

Publications and presentations

Oral presentations

Circular RNAs as a potential novel biomarker in prostate cancer. 8th Annual ToPCaP Retreat 2015.

Publications

Lim MCJ, Baird AM, Aird J, **Greene J,** Kapoor D, Gray SG, McDermott R, Finn SP. RNAs as Candidate Diagnostic and Prognostic Markers of Prostate Cancer-From Cell Line Models to Liquid Biopsies. Diagnostics (Basel). 2018 Aug 30;8(3). PMID: 30200254

Greene J, Baird AM, Brady L, Lim M, Gray SG, McDermott R, Finn SP. Circular RNAs: Biogenesis, Function and Role in Human Diseases. Front Mol Biosci. 2017 Jun 6;4:38. PMID: 28634583

Ridge SM, Bhattacharyya D, Dervan E, Naicker SD, Burke AJ, Murphy JM, O'Leary K, **Greene J**, Ryan AE, Sullivan FJ, Glynn SA. Secreted factors from metastatic prostate cancer cells stimulate mesenchymal stem cell transition to a pro-tumourigenic 'activated' state that enhances prostate cancer cell migration. Int J Cancer. 2018 May 15;142(10):2056-2067. PMID: 29266277

Poster presentations

McDermott R, **Greene J**, Deignan O, McCaffrey J, Parker I, Bowes I, Teiserskiene T, Feeney J, Thirion P, Finn S, Kelly P; Phase II safety and tolerability study of Radium-223 (R223) in combination with enzalutamide (ENZA) in patients (pts) with metastatic castration-resistant prostate cancer

(mCRPC): CTRIAL-IE (ICORG) 13-21. J Clin Oncol 36, 2018 (suppl; abstr 5050) **Greene J**, Baird AM, Brady L, Gray S, Finn S, McDermott R. hsa_circ_0004870 is related to AR-V7 expression and may confer resistance to enzalutamide in castration-resistant prostate cancer. Annals of Oncology (2017) 28 (suppl_5): v573-v594. 10.1093/annonc/mdx390

Greene J, Blackshields G, Casey O, Brady L, Baird A.M., Gray S, Finn S, McDermott R. circular RNA: A novel regulatory non-coding RNA expressed in prostate cancer. Annals of Oncology (2016) 27 (6): 526-544. 10.1093/annonc/mdw392

Glynn S, **Greene J** et al. The Prostate Cancer – Bone Marrow Mesenchymal Stem Cell Para-endocrine Axis in the Metastatic Tumour Microenvironment. Keystone Symposia on Molecular and Cellular Biology 2016

Greene J, Casey O, O'Leary K, Fahey C, Bracken S, Glynn S, Perry A, Watson W, Finn S McDermott R. The Irish Programme for Stratified Prostate Cancer Therapy (iPROSPECT)) J Clin Oncol 34, 2016 suppl 2S; abstr 335

Book chapters

Greene J.P., Finn S.P. (2018) Genetic Susceptibility. In: Robinson B., Mosquera J., Ro J., Divatia M. (eds) Precision Molecular Pathology of Prostate Cancer. Molecular Pathology Library. Springer.

Awards

Health Research Board Travel Grant to attend the Summer Curriculum in Cancer Prevention Course, National Cancer Institute, Bethesda, MD, USA, 2015

ESMO Travel Grant to attend the Prostate Cancer Preceptorship in Barcelona, Spain, 2015

Postgraduate Certificate in Statistics awarded by Trinity College Dublin, 2016

Table of Contents

Declaration i

Summary iv

Acknowledgements vii

List of Tables viii

List of Figures ix

Abbreviations xvi

Units xx

Publications and presentations xxii

Table of Contents xxv

Chapter 1: Introduction 1

1.0 Introduction 2

6.0 Prostate cancer 2

6.1 Management of advanced disease 6

6.2 Androgen receptor 8

6.3 AR-V7 9

6.4 Circulating Tumour Cells 12

6.5 circular RNAs 14

6.6 Irish clinical trials in advanced prostate cancer 23

1.1.1 C-TRIAL 13-21 (radium-223 and enzalutamide) 23

1.1.2 iPROSPECT 23

6.7 Aims and objectives 24

Chapter 2: Materials and Methods 26

2.0 Materials and methods 27

6.8 Preparation and handling of materials 27

6.9 Cell culture 27

2.1.1 Cell culture conditions 27
2.1.2 Prostate cell lines 27
2.1.3 Cryopreservation 31
2.1.4 Propagation of cells from storage 31
2.1.5 Cell sub-culture 31
2.1.6 Cell counting 32
2.1.7 Mycoplasma testing 32

6.10 RNA isolation and quantification 33

2.1.8 Trizol® RNA isolation protocol 34
2.1.9 RNeasy Mini Kit 35
2.1.10 RNA quantification 36

6.11 Gene expression analysis 38

2.1.11 cDNA Synthesis for gene expression analysis 38
2.1.12 cDNA Synthesis for miRNA expression analysis 38
2.1.13 TaqMan® Probe-based gene/miRNA expression 38
2.1.14 SYBR Green-based gene expression analysis 39
2.1.15 qRT-PCR data analysis 39
2.1.16 Standard curve method 40
2.1.17 Agarose gel electrophoresis 40

6.12 circRNA microarray 41

2.1.18 Microarray 41
2.1.19 Microarray data analysis 43
2.1.20 Delineation of circRNA/miRNA interactions 43

6.13 Circulating Tumour Cells (CTCs) 43

2.1.21 Blood collection for CTC isolation 43
2.1.22 CTC isolation 44
2.1.23 Staining 44

6.14 Archival tissue 46

2.1.24 Ethical approval 46
2.1.25 FFPE sample preparation 46
2.1.26 FFPE sections 46

6.15 Metastatic biopsies 47

2.1.27 Bone marrow biopsy 47
2.1.28 CT guided biopsy 47

6.16 Next generation sequencing (NGS) 48

6.17 RNA *in situ* hybridisation 50

2.1.29 Culture adherent cells 50
2.1.30 RNAscope® 50
2.1.31 BaseScope™ 52
2.1.32 Interpretation of RISH Results 52

6.18 Statistical Analysis 54

Chapter 3: Analysis of Safety Data and Circulating Tumour Cells in patients treated with Radium-223 in combination with Enzalutamide 55

6.19 Introduction 56

6.20 Results 59

3.1.1 ICORG 13-21 59
3.1.2 Criteria for Definition of Progression of Disease 60
3.1.3 Patient characteristics 60
3.1.4 Safety data 64
3.1.5 CTC collection 67
3.1.6 Effect of Radium-223 and enzalutamide on CTC numbers 67
3.1.7 CTC counts according to prior response to ADT 70

6.21 Discussion 73

Chapter 4: Tumour heterogeneity in Metastatic Prostate Cancer 77

6.22 Introduction 78

6.23 Results 81

4.1.1 iPROSPECT Study 81
4.1.2 Patient characteristics 83
4.1.3 CTCs 88
4.1.4 Metastatic biopsies in prostate cancer 88
4.1.5 Sensitivity of bone marrow *vs*. CT guided metastatic biopsies 91
4.1.6 Bone marrow biopsies 91
4.1.7 Biochemical data 94
4.1.8 Lymph node, liver and bone biopsies 94
4.1.9 Neuroendocrine differentiation in PCa 99
4.1.10 Next Generation Sequencing of matched primary and metastatic samples 101
4.1.11 CTCs and metastatic biopsies 105

6.24 Discussion 107

Chapter 5: Assessment of Methods and Sample types for identifying AR-FL & AR-V7 in Prostate Cancer 115

6.25 Introduction 116

6.26 Results 118

5.1.1 AR-FL expression in a panel of PCa cell lines 118

5.1.2 AR-V7 expression in a panel of PCa cell lines....118
5.1.3 AR-FL and AR-V7 expression in an isogenic model of enzalutamide resistance....123
5.1.4 AR-V7 expression using IHC....126
5.1.5 Comparison of RISH methods to detect AR-FL and AR-V7....126
5.1.6 Assessment of RISH techniques....128
5.1.7 AR-FL and AR-V7 expression using RISH....131
5.1.8 RISH using BaseScope™....138
5.1.9 Assessment of RISH on patient tissue samples....150
5.1.10 AR-FL and AR-V7 using BaseScope™ RISH....153
5.1.11 Assessing the sensitivity of BaseScope™ in other PCa subtypes 153
5.1.12 CTC filters and RISH....156

6.27 Discussion....158

Chapter 6: Circular RNA expression in Prostate Cancer....163

6.28 Introduction....164

6.29 Results....166

6.29.1 circRNA profiling of Prostate Cancer cell lines....166
6.29.2 Differentially expressed circRNAs....169
6.29.3 Proof of concept to determine the utility of qPCR to detect circRNAs....171
6.29.4 RNAse R....171
6.29.5 circRNAs and their miRNA binding sites....175
6.29.6 circRNAs and their associated miRNAs identified from microarray....175
6.29.7 circRNAs are differentially expressed in Prostate Cancer....179
6.29.8 circRNAs are differentially expressed according to AR status. 183

6.30 Discussion....198

Chapter 7: Circular RNAs and their association with resistance to enzalutamide 202

6.31 Introduction....203

6.32 Results....206

7.1.1 circRNA screening identified differentially expressed profiles within an isogenic enzalutamide resistant cell line model....206
7.1.2 Associated circRNA parental genes are involved in pro-oncogenic activities and is further altered depending on the extent of enzalutamide resistance....208
7.1.3 miRNAs associated with circRNAs....211
7.1.4 Validation of circRNAs....215
7.1.5 hsa_circ_0004870 is downregulated in cancer cells and androgen dependent PCa....218

7.1.6 RBM39 and U2AF65 are down-regulated in enzalutamide resistant PCa 221
7.1.7 miRNAs 223
7.1.8 circRNA expression in media 224
7.1.9 RISH for circRNA detection 227

6.33 Discussion 230

Chapter 8: Discussion and future directions 233

6.34 Overall discussion 234

6.35 Future work 240

6.36 Overall conclusions 242

References 244

Chapter 1: Introduction

1.0 Introduction

6.0 Prostate cancer

Prostate cancer (PCa) is the most commonly diagnosed cancer in men in Ireland (excluding non-melanoma skin cancers) and a leading cause of morbidity and mortality among men in the United States and Western Europe (1). In Ireland, the rate of PCa has increased from 1,162 in 1995 to 3,122 in 2010 (2). One in 5 men will develop metastases (stage IV disease) and die of their cancer within 10 years. In addition, approximately 200 men per year have metastatic disease at the time of diagnosis, from whom only 19% are alive after five years (3). Treating metastatic disease effectively in these individuals presents significant clinical challenges. The clinical behaviour of PCa ranges from a microscopic, well-differentiated localised cancer, that may never be clinically significant, to an aggressive cancer that may metastasize to other parts of the body (4). PCa tends to have a long natural history and may require treatment with multiple modalities over many years. For PCa, the median age at diagnosis is 68 years, and it is generally considered a disease of men aged >70 years. The incidence of PCa is higher in patients aged between 70-79 years as compared to those aged between 50-69 (5). Men diagnosed with advanced PCa usually have a long median survival and it may be sometimes described as a chronic disease. In fact, it has been estimated that the median survival of patients with newly diagnosed metastatic PCa is over 42 months (6).

PCa is usually diagnosed through either prostate specific antigen (PSA) testing, performed as part of routine screening, or due to symptom presentation such as urinary frequency, urgency, and nocturia. Once a diagnosis of PCa is established, further evaluation that incorporates known risk factors is required

to determine the next appropriate treatment step. Localised disease is managed through a combination of surgery and radiotherapy depending on the extent of the disease (Gleason Score, PSA and T stage) and the performance status of the patient. Metastatic disease may present many years after a patient's previous treatment for localised disease, however some men will present acutely with *de novo* metastatic PCa.

PCa growth, at least initially, is dependent upon androgens and the androgen receptor (AR) (7). Androgen production occurs primarily in the testes (Fig 1.1), which accounts for more than 90% of total circulating testosterone (8). Testicular production of androgens is regulated through hypothalamic pituitary feedback and the adrenal glands produce the remainder of the circulating androgens. The mainstay of initial treatment in advanced PCa is to block the effect of these androgens by reducing circulating levels of androgens in the body or by blocking their effect through inhibiting the AR (Fig 1.2) (9). This is achieved through the use of androgen deprivation therapy (ADT), and is the standard initial approach for patients when systemic therapy is indicated for metastatic PCa (10). LHRH agonists (e.g. leuprolide) and antagonists (e.g. degarelix) suppress LH production through different feedback mechanisms and lower the level of circulating androgens. This results in a rapid reduction in the level of PSA and leads to an improvement in symptoms if present (less pain and improved urinary symptoms) (11). Appropriate men who start ADT may also be offered docetaxel chemotherapy (75 mg/m^2 every 3 weeks without prednisolone) as part of their initial treatment based on recent data from the CHAARTED and

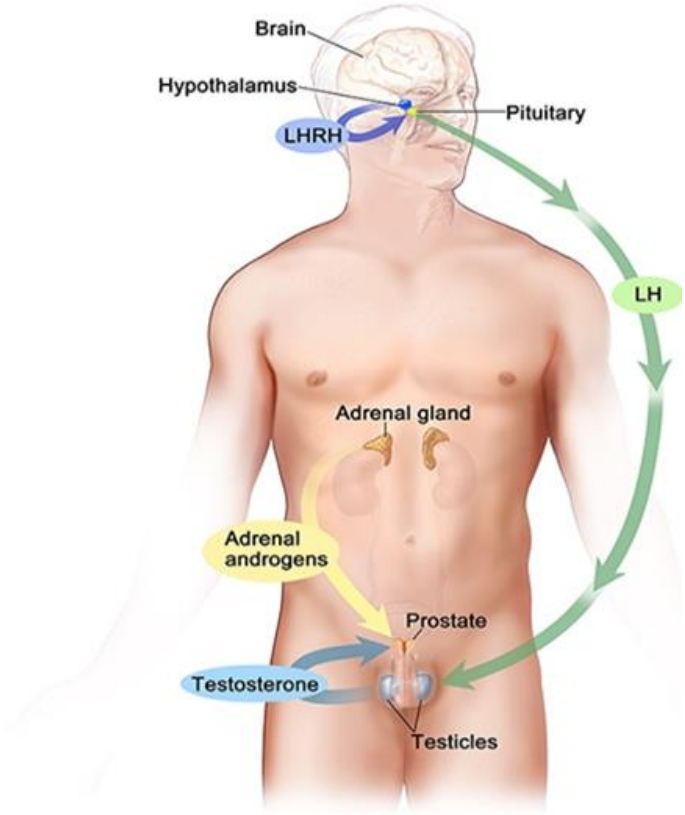

Figure 1.1. Androgen production in the male.

Androgen production in the male is regulated through hypothalamic pituitary feedback system. Image shows that testosterone production is regulated by luteinizing hormone (LH) and luteinizing hormone-releasing hormone (LHRH). The hypothalamus releases LHRH, which stimulates the release of LH from the pituitary gland. LH acts on specific cells in the testes to produce the majority of testosterone in the body. Most of the remaining androgens are produced by the adrenal glands. Androgens are taken up by prostate cells, where they either bind to the AR directly or are converted to dihydrotestosterone (DHT), which has a greater binding affinity for the AR than testosterone.

Image taken from Heidenreich *et al.* (9).

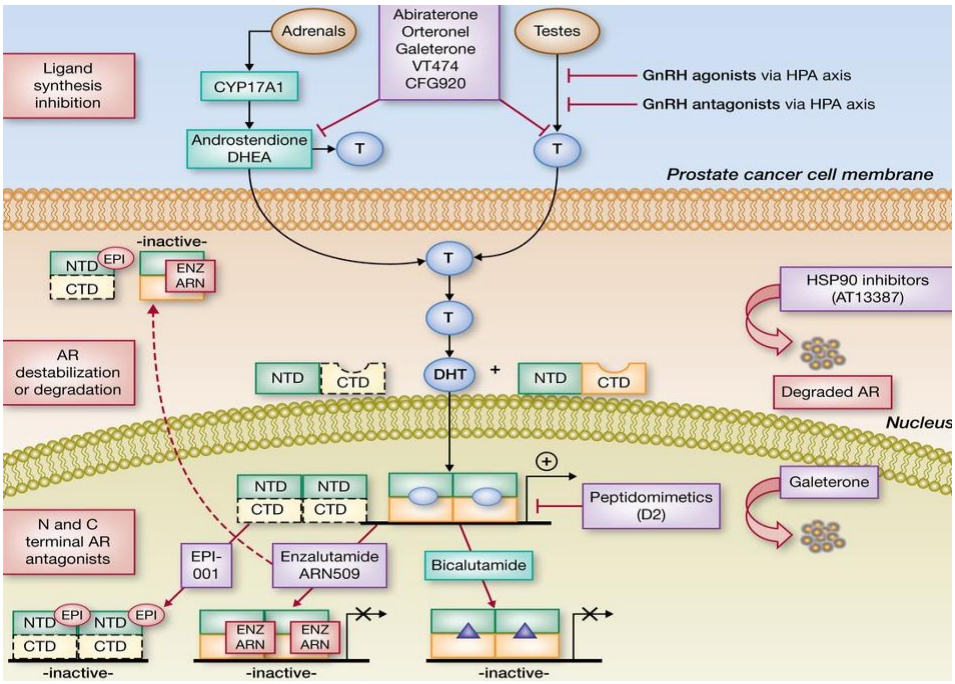

Figure 1.2. Schematic image of the AR and potential drug targets.

Inhibition of AR ligand production: Inhibition of CYP17A by Abiraterone, Orteronel, Galeterone, VT474, or CFG920 suppresses testicular, adrenal and tumour androgen synthesis. Galeterone can suppress CYP17A, antagonize androgens and reduce AR levels. Abiraterone at high doses can inhibit AR and HSD3B.

AR degradation: AR can be destabilized through inhibition of HSP90 binding. *AR-cofactor association:* Peptidomimetics (e.g. D2) can disrupt AR interaction with cofactors, decreasing AR driven gene transcription.

AR antagonism: Enzalutamide and ARN509 block ligand/receptor interactions at the LBD, reduce AR-DNA association and AR nuclear accumulation. EPI-001 blocks AR NTD-coactivator association and nuclear accumulation and is

active against truncated AR variants lacking the C terminal domain (CTD). Image modified from Mostaghel *et al.* (12).

STAMPEDE trials, which have shown a significant survival benefit (9% absolute survival benefit) if given jointly with ADT (13, 14). Further to this, abiraterone may be added to ADT based on data from STAMPEDE and LATITUDE clinical trials (15, 16).

6.1 Management of advanced disease

Multiple therapies are now available, which prolong survival and improve symptoms in men with advanced PCa (14, 17-19). However, resistance to these treatments develops eventually in all men (20). The goal of ongoing current research is to discover biomarkers that may identify patients who will not respond to certain treatments and therefore tailor treatments that may work better for them. Most men will initially respond to ADT for a period of around 18 months on average, but eventually they will progress and become resistant to their LHRH therapy (7). This manifests itself with rising PSA, altered clinical symptoms or radiological progression. Patients who have evidence of disease progression while being managed with ADT have now what is termed castration resistant PCa (CRPC) (9). The presence of castration resistant disease does not imply that disease is totally independent of androgens, therefore ADT should be continued with the addition of antiandrogens. Older antiandrogens such as bicalutamide, primarily act by blocking the binding of DHT to the AR (11). Newer second-generation agents abiraterone and enzalutamide have largely replaced bicalutamide as first line antiandrogen treatment for CRPC (17, 18).

Abiraterone is an orally administered small molecule that irreversibly inhibits the *CYP17* gene and, in doing so, it blocks the synthesis of androgens in the tumour as well as in the testis and adrenal glands (18). In clinical trials, abiraterone plus prednisone prolonged overall survival (OS) compared with prednisone alone in men who had previously been treated with docetaxel (18) and in those who were chemotherapy naïve (21). Enzalutamide is another second-generation antiandrogen agent, which is orally administered and affects a multitude of mediators in the AR signalling pathway, including blocking the binding of androgens to the AR (22). Enzalutamide has improved OS in men who have previously been treated with docetaxel (23) and in those who are chemotherapy naïve (24). Both abiraterone and enzalutamide have significantly improved OS compared with placebo in trials with CRPC patients, however, there appears to be limited activity for these agents in men who have progressed on either agent previously (25, 26). For men who have progressed on either drug, consideration should be given towards cytotoxic chemotherapy (e.g. taxanes) in selected suitable candidates (27).

The majority of men who develop metastatic PCa disease will develop bone metastases only (28). Skeletal related events are a significant cause of morbidity including pain. Treatments that aid bone protection and help reduce skeletal related events include bisphosphonates and receptor activator of nuclear factor κ B (RANK-L) inhibitors (29). A novel type of bone-targeted therapy in PCa is radium-223, an alpha particle emitting radiopharmaceutical that is given intravenously on a monthly basis for a maximum of 6 treatments (30). Radium-223 has a bone-seeking element, which emits high-energy short wave radiation to the tumour with minimal toxicity to normal bone marrow and

other organs. Treatment with radium-223 is well tolerated and has been shown to increase both OS and time to first symptomatic skeletal-related event. It should be considered in patients with symptomatic bone metastases and no known visceral metastases (30).

6.2 Androgen receptor

The AR plays essential roles in the initiation and progression of PCa (31). Structurally, the human AR gene (Fig 1.3) is composed of eight exons and encodes a multi-domain protein consisting of an N-terminal transactivation domain (NTD), a central DNA-binding domain (DBD), a hinge region, and a C-terminal ligand-binding domain (LBD).

The mainstay of initial treatment is to directly block production of these androgens by using anti-androgens (e.g. abiraterone) or AR inhibitors (e.g. enzalutamide) (32). A number of patients will not respond at all to these agents at the beginning of treatment, while others will eventually develop secondary resistance (33). Several hypotheses for treatment failure have been suggested such as hypersensitivity to non-testicular anti-androgens, increased androgen biosynthesis from adrenal precursor steroids or mutations in the AR gene (31). AR aberrations have been identified in approximately 10–40% of patients with CRPC treated with anti-androgens (34). Recently, aberrations in the LBD of the AR including AR-V7, and the F876L missense mutation have been shown to be associated with resistance to therapy (35).

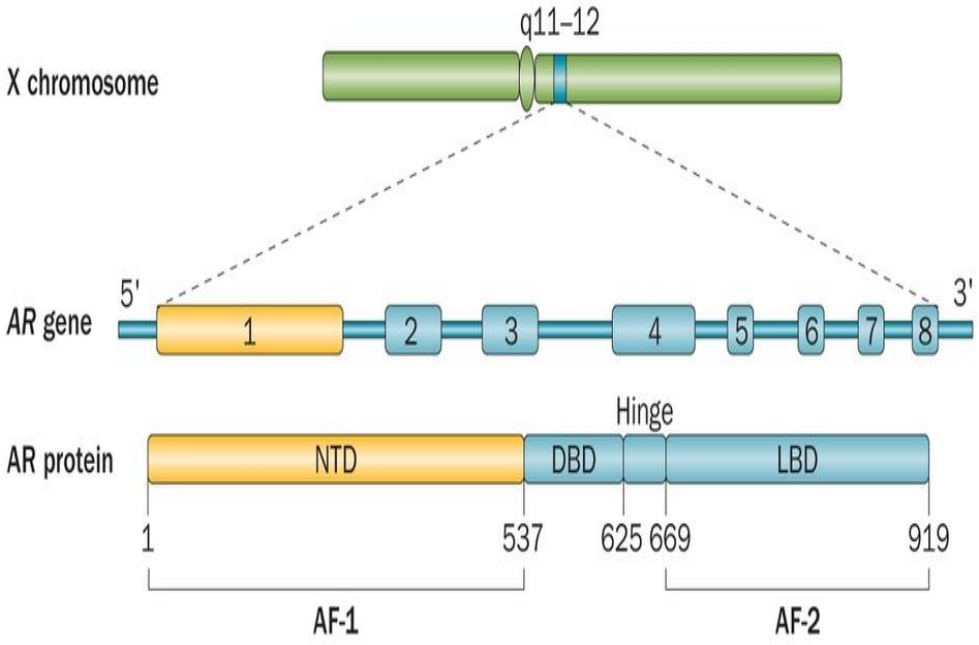

Figure 1.3. The molecular structure of the AR gene and protein, showing the domain regions.

The AR is 920 amino acids long and consists of 4 functional domains encoded by 8 exons. The AR is composed of the ligand-independent amino-terminal transactivation domain (NTD; exon 1), DNA-binding domain (DBD; exons 2–3), the hinge region (exon 4) and the ligand-binding domain (LBD; exons 4–8) Image taken from Lorente *et al*. (32).

6.3 AR-V7

AR splice variant-7 (AR-V7) is a truncated form of the AR that lacks the LBD, which is the target of enzalutamide and abiraterone (Fig 1.4). This alternatively spliced variant encodes a truncated AR protein that lacks the C-terminal binding domain but retains the transactivating N-terminal domain (36-38). It is also unique in containing a cryptic exon (33, 39-41). The AR remains constitutively active as a transcription factor in PCa, but it has been shown that

the presence of AR-V7, detected with qPCR on RNA extracted from circulating tumour cells (CTCs), may be associated with resistance to drugs that normally exert their function at the ligand-binding domain of the AR (125-128). Qu *et al.* have shown that AR-V7 was detectable in 58.7% of patients with CRPC using immunohistochemistry (IHC) (42).

Patients with AR-V7 appear less likely to respond to therapies such as abiraterone and enzalutamide (33, 40, 43). Interestingly, Antonarakis *et al.* have also shown that treatment with taxanes appeared superior to AR-directed therapy in AR-V7 positive men (40). Within this population, the PSA responses were 41% (7 of 17) in taxane-treated patients and 0% (0 of 18) in enzalutamide or abiraterone treated patients ($p < 0.001$). Median PSA progression free survival (PFS) was longer in taxane treated men compared with enzalutamide or abiraterone treated men (HR, 0.22 [95% CI, 0.09-0.53]; $p < 0.001$). In addition, among men with detectable AR-V7 at baseline (n=12), 7 patients (58%) became AR-V7 negative during taxane therapy. This indicates that AR-V7 status could be used to determine the administration of sequential treatment in CRPC. The majority of previous studies have detected the presence of AR-V7 using mRNA isolated from CTCs, which is not yet feasible in the clinical setting (33, 40).

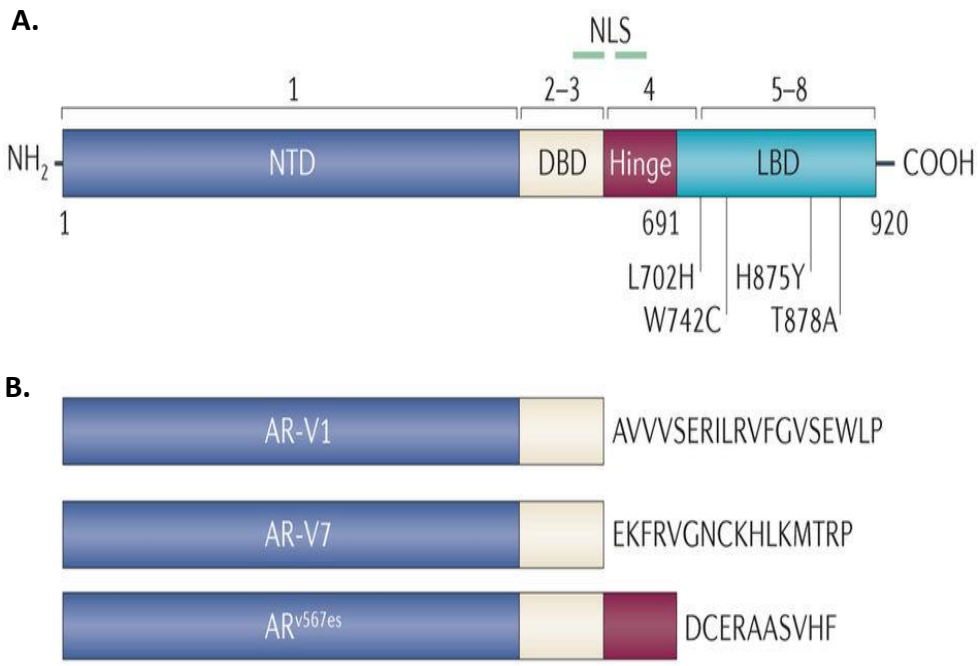

Figure 1.4. AR-FL and AR splice variants.

(A) The AR with recurring missense mutations noted (L701H, W741C, H874Y and T877A).

(B) The protein structures of representative AR splice variants, including AR-V7, are shown with the in-frame variant specific amino acids derived from the alternative splicing events.

Image taken from Watson *et al*. (43).

Other methods of detection include immunohistochemistry (IHC) and RNA *in situ* hybridisation (RISH) (44).

6.4 Circulating Tumour Cells

Recently, the investigation of CTCs and circulating nucleic acids (cNAs) as a form of "liquid biopsy" may allow for the possibility of avoiding repeated tissue biopsies but still provide the histopathological information at any stage of the disease process (45). CTCs are rare malignant cells that originate from the primary tumour or from other metastatic sites and can be detected in peripheral blood (46). CTCs and cNAs can be optimally exploited by high value analysis with technologies such as next generation sequencing (NGS), high throughput proteomic and epigenetic profiling. There is increasing evidence that numbers of CTCs may have a prognostic role in advanced PCa (47-49). Unfavourable CTC counts (≥5 cells/7.5 mL) before therapy are associated with shorter OS than a favourable CTC count (<5 cells/7.5 mL) in metastatic CRPC (mCRPC) patients (50). CellSearch® is the only US Food and Drug Administration (FDA) approved device for CTC detection and enumeration, however, it still has limitations, including a comparatively low detection rate and reduced sensitivity in patients with low CTC counts (51). These limitations may be due to the inability of the CellSearch® system to detect CTCs that have undergone epithelial-mesenchymal transition (EMT), which results in lost expression of epithelial cell markers and re-expression of stem cell markers (52). A size-based filtration technique can also be used owing to its ability to isolate CTCs without the need for antibody detection

(53). The filtration technique preserves the CTC morphology and maintains the presence of CTC clusters (Fig 1.5).

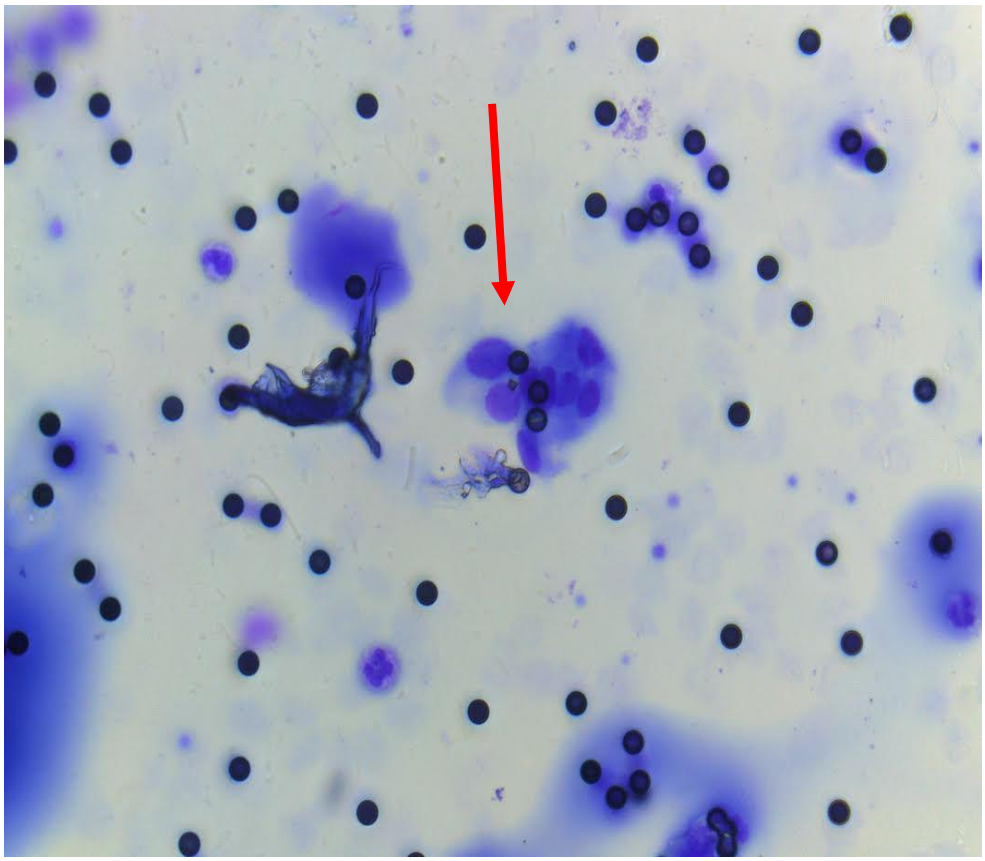

Figure 1.5. Image of CTC.

Representative image of CTC cluster (as indicated by red arrow) in a patient with metastatic PCa using a size-based filtration device (ScreenCell®). CTCs were stained using a modified May-Grünwald Giemsa (MGG) stain (Magnification 40X).

Image taken from Greene *et al. (Manuscript in preparation).*

These types of filters can also be used for ancillary studies such as Fluorescent *in situ* hybridization (FISH), IHC, cell culture, and Polymerase Chain Reaction (PCR) (54). Higher CTC counts have also been observed in patients with bone predominant metastases as compared with patients with visceral spread, which suggests a prognostic potential for CTC testing in monitoring patients with bone metastases in PCa (50). Radium-223 is a bone targeting agent with no known effect on CTC numbers. Enzalutamide has proven efficacy in converting unfavourable CTC counts (≥5 cells/7.5 mL) to favourable (<5 cells/7.5 mL) (55). Currently, there is no data available on the effect of radium-233 alone or in combination with enzalutamide, and CTC counts.

6.5 circular RNAs

Mechanisms of resistance to antiandrogens are poorly understood, however one such mechanism that may contribute to resistance are noncoding RNAs (ncRNAs), which include short microRNAs (miRNAs) and long non-coding RNAs (lncRNAs) (56-58). ncRNAs account for 95% of total RNA in eukaryotic transcription, and are being increasingly appreciated to have an important function in gene regulation (59-61). circRNAs, a recently discovered ncRNA, are generated from the backsplicing of exons, introns, or both to form exonic or intronic circRNAs (60). The first examples of circRNA transcripts were identified in the early 1990's, however at that time they were thought to represent errors in RNA splicing (60, 62-64). It wasn't until recently that interest in circRNA research was re-established by Salzman *et al*., who identified circRNAs in RNA sequencing (RNA-seq) samples of cancer and non-cancer cell lines (65). This development has led to the identification of

thousands of individual circRNAs that are endogenous to mammalian cells and are both highly stable and abundant *in vivo* compared to their linear counterparts (66). More recently, advances in high-throughput sequencing, novel bioinformatics approaches and corresponding experimental validation, have proven that circRNAs represent a distinct class of ncRNAs (66). Unlike linear RNA, the 3′ and 5′ ends in circRNA, normally present in an RNA molecule, are joined together, forming a covalently closed continuous loop, which prevents degradation by RNA exonucleases. This confers stability on circRNAs, resulting in their abundance in the cytoplasm (60). circRNAs may arise from exons or introns leading to the formation of three different types of circRNAs; exonic, intronic and exon-intron circRNAs (Fig 1.6) (60).

The formation of exonic circRNAs are a result of pre-mRNA splicing when the 3′ splice donor attaches to the 5′ splice acceptor forming an exonic circRNA (60, 66). In some cases, this happens with a single exon, whereas in others the start of an upstream exon splices to the end of a downstream exon, with the intervening RNA circularised, producing circRNAs from multiple exons. Alternatively, if the intron between the exons is retained, the resulting circular transcript is referred to as exon–intron circRNA (67). Finally, intronic circRNAs can be produced from intron lariats that are resistant to degradation by de-branching enzymes (60, 67). Intronic circRNAs contain a single unique 2′ to 5′ linkage that distinguishes them from exonic circRNAs (66). The formation of intronic circRNAs relies on GU-rich sequences near the 5′ splice site and C-rich sequences near the branch point (68). During the backsplicing

process, the two segments bind into a circle first, the exonic and intronic sequences in the

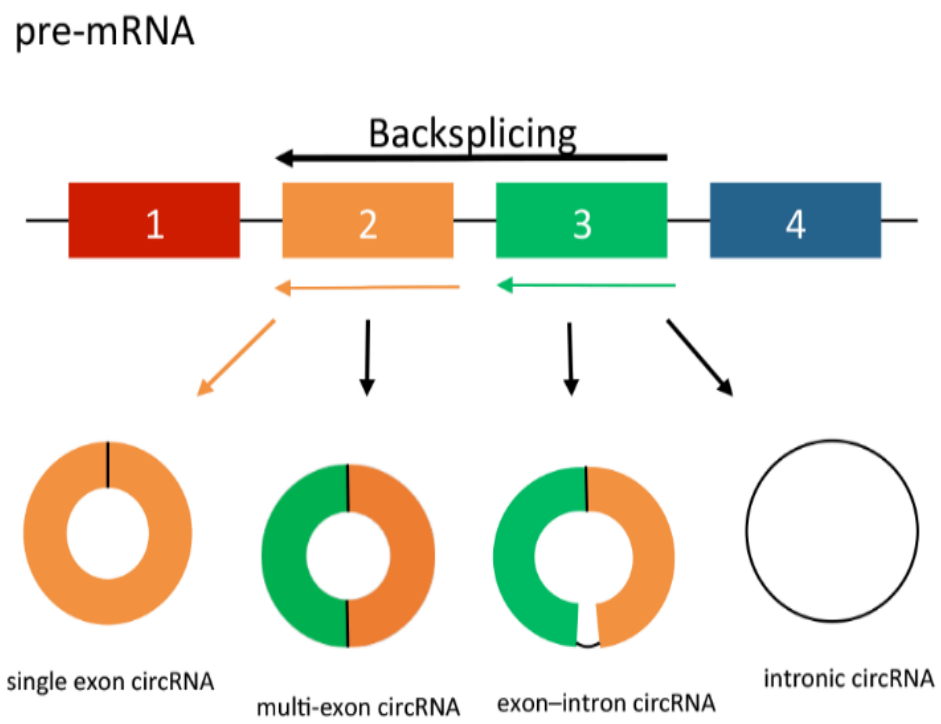

Figure 1.6. circRNA splicing.

circRNAs are created by non-canonical splicing process known as 'backsplicing'. A downstream splice donor is joined to an upstream splice acceptor. circRNAs can be exonic, intronic or a combination of both.

Coloured bars - exons; Black lines - introns.

Image taken from Greene *et al*. (69).

binding part are cut out by the spliceosome with the remaining introns brought together to form an intronic circRNA.

Advances in sequencing technology have enhanced the methods of detection of cirRNAs including deeper sequencing with longer read lengths, the development of better algorithms for mapping RNA and the use of enriched RNA libraries. Salzman *et al.*, originally looking for genomic rearrangements in RNA-seq samples from patients with acute lymphoblastic leukaemia (ALL), found there was an unexpected abundance of fragments in which two read pairs mapped to the same gene but were in the opposite order (65). This method was further developed by scanning for out-of-order paired end reads for specific genes which then allowed for quantitative PCR (qPCR) validation in cancer and non-cancer cell lines (65). The detection of circRNAs was further developed by Jeck *et al.* and Memczak *et al.* using bioinformatic analyses on RNA-seq libraries to identify specific back-splice junctions *de novo* (60, 70). One way to differentiate circRNAs from linear RNAs is by using an RNA exonuclease enrichment strategy. Ribonuclease R (RNase R) is a magnesium-dependent 3′→5′ exoribonuclease that digests essentially all linear RNAs but does not digest circRNA structures due to lack of free ends (71). Using this strategy, thousands of circRNAs have been identified that can contain one or more coding exons from linear messenger RNAs and can be hundreds to thousands of nucleotides in length (72). qPCR can then be used to assess the relative abundance of circRNA across samples using divergent primers (Fig. 1.7) that are designed to specifically amplify and detect the backsplice junction (60). Other

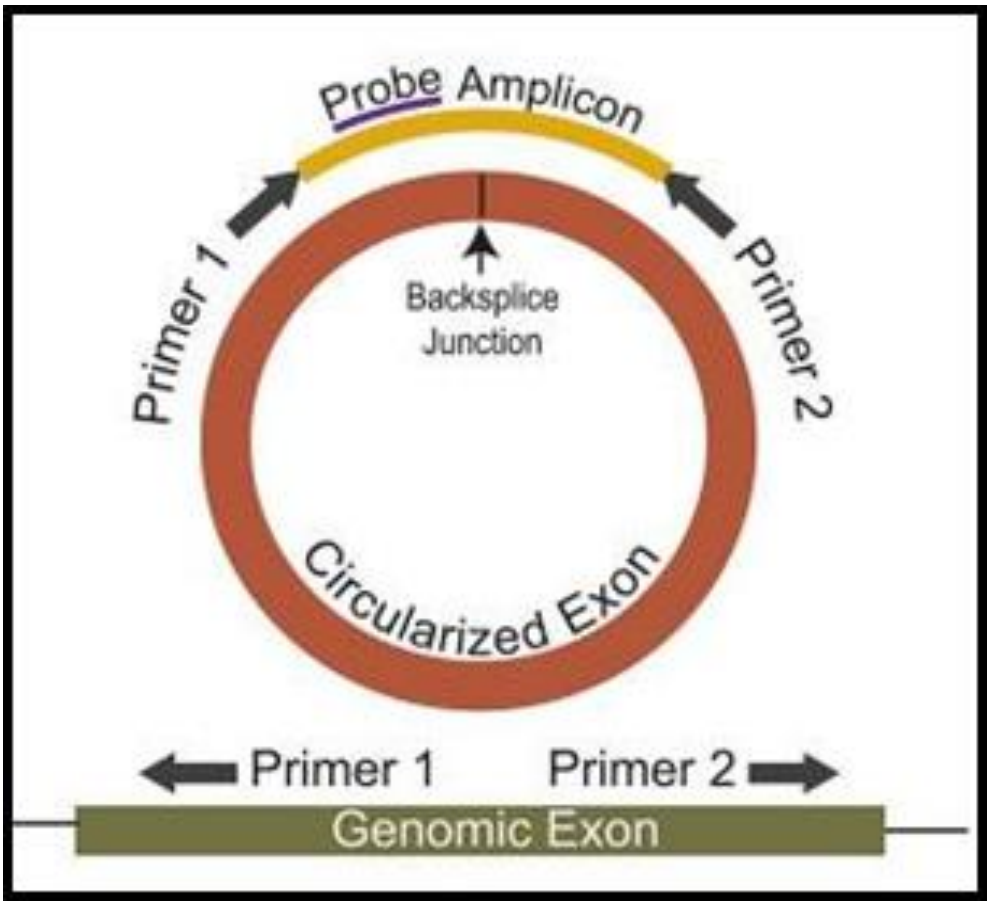

Figure 1.7. circRNA validation.

Validation of circRNAs can be achieved using qPCR-based assays designed using outward facing primers as illustrated.
Image taken from Jeck *et al*. (66).

methods which enrich for circRNAs in sequencing libraries, include the use of ribosomal RNA (rRNA) and polyA depletion techniques (73).

However there remains non-uniformity in RNA-Seq data sets, in part due to circRNAs having relatively low abundance compared with their linear counterparts and also due to the fact that some data sets were generated in the absence of RNase R enrichment (73). Other methods of detection include the use of high throughput microarrays using RNA samples enriched with RNase R (74). Zhong *el al.* used this method to identify circRNAs expressed in bladder cancer (75). A number of bioinformatic algorithms and online resources have been developed for identifying circRNAs (76). CircBase provides online merged and unified data sets of circRNAs and the evidence supporting their expression can be accessed and scripts are available to identify known and novel circRNAs in sequencing data (77).

Ongoing research into the role and function of circRNA has initially focused on their potential regulatory role. The competitive endogenous RNA (ceRNA) network hypothesis proposes that specific RNAs can impair miRNA activity through sequestration (Fig. 1.8), thereby upregulating or downregulating miRNA target gene expression (78).

To date, a small number of circRNAs have been identified as miRNA sponges (79). An important function of miRNAs is the ability to regulate hundreds of targets, as well as to collectively function in networks in which a single target may have multiple MREs (80). Pipelines have been created using algorithms for miRNA target prediction, which allows for the identification of

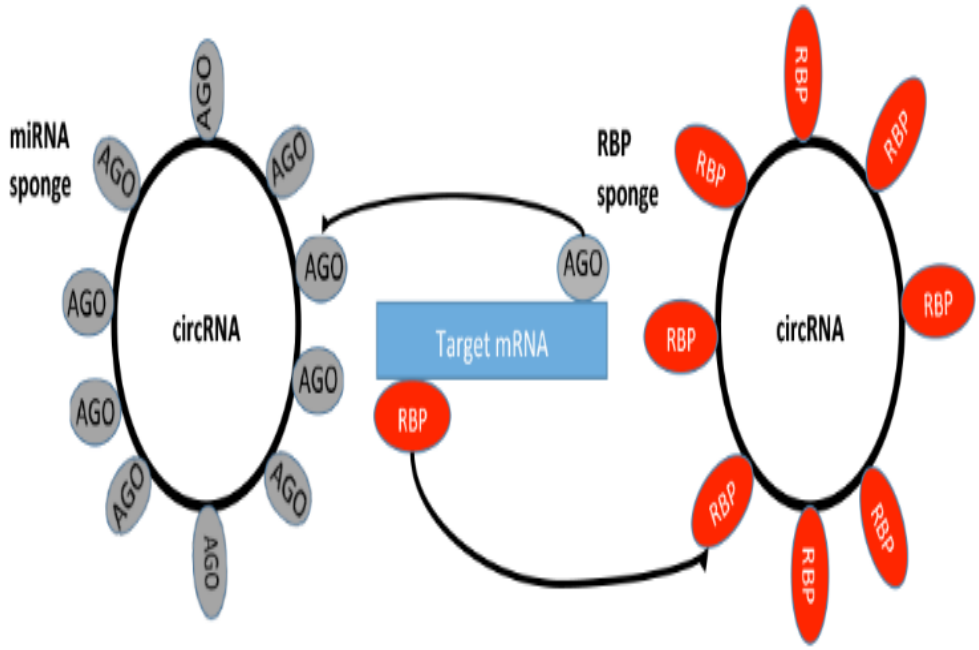

Figure 1.8. circRNA sponges.

circRNAs can bind miRNA from its mRNA targets via RBPs and AGO proteins.

RBP = RNA Binding Protein; AGO = Argonaute Protein

Image taken from Greene *et al*. (69).

candidates for experimental validation (77). Recent evidence suggests circRNAs may have a role in the development and progression of cancer (81-83). The fact that circRNAs appear to behave as miRNA sponges, has only increased this interest (84). The expression of miRNA is dysregulated in human cancer through various mechanisms, including amplification or deletion of miRNA genes, abnormal transcriptional control of miRNAs, dysregulated epigenetic changes and defects in the miRNA biogenesis machinery (85). It has been proposed that circRNAs regulate gene expression at the transcriptional or post-transcriptional level by interacting with miRNAs and that circRNAs may have a role in regulating miRNA function in cancer initiation and progression (86, 87). Zheng *et al.* have identified over 27,000 circRNA candidates from the sequencing data of six human normal tissues (brain, lung, heart, stomach, colon and liver) and seven human cancers (bladder, breast, colorectal, gastric, hepatocellular carcinoma, kidney clear cell carcinoma and prostate adenocarcinoma) (88). circRNAs appear to be more often downregulated in tumour tissue compared to normal tissue and this may be due to (i) errors in the back-splice machinery in malignant tissues, (ii) degradation of circRNAs by deregulated miRNAs in tumour tissue or (iii) increasing cell proliferation leading to a reduction by thinning out circRNAs (89). Upregulation of circHIPK3, a proposed miRNA sponge, has been identified in cancerous tissues including prostate and renal cell carcinoma (88). More recently, an androgen-responsive circRNA called circSMARCA5, which promotes cell proliferation, has been found to be up-regulated in PCa (90). Numerous other studies have identified circRNAs to be up or downregulated in different cancer subtypes (Table 1.1).

Table 1.1. Cancer associated circRNAs.

Cancer type (ref)	circRNA	Expression
Gastric* (91)	hsa_circ_002059	down
Colon (92-94)	circ6229	down
	cirITCH	down
Bladder (75)	circFAM169A	down
	circTRIM24	down
	circTCF25	up
	circZFR	up
	circPTK2	up
	circBC048201	up
Hepatocellular (95-97)	hsa_circ_0001649	down
	ciRS-7	up
	hsa_circ_0005075	up
Oesphageal (98)	cirITCH	down
Lung (99)	cirITCH	down

*Tumour tissue and plasma

6.6 Irish clinical trials in advanced prostate cancer

Two clinical trials enrolled patients with metastatic PCa; a phase II trial examining the combination of radium-223 and enzalutamide; and a translational longitudinal study prospectively collecting biospecimens.

1.1.1 C-TRIAL 13-21 (radium-223 and enzalutamide)

Both radium-223 and enzalutamide have proven efficacy in mCRPC as single agents and given their differing modes of action and non-overlapping toxicity profiles, there is considerable interest in defining the correct combination or sequencing of these novel approaches. A phase II study (C-TRIAL 13-21) of radium-223 in combination with enzalutamide in progressive mCRPC was developed (clinicalTrials.gov Identifier: NCT02225704). The primary objective was to determine the safety and tolerability of the combination treatment. Radium-223 was administered as a slow bolus intravenous (IV) injection of 50 kBq/kg on day 1 of every four-week cycle, for 6 doses maximum with enzalutamide 160 mg orally (PO) daily until disease progression. This study also examined CTC enumeration at baseline and throughout the study (Protocol provided in Appendix I).

1.1.2 iPROSPECT

There has been an absence of predictive biomarkers in metastatic PCa and there has been no incentive and few opportunities to systematically collect biospecimens longitudinally during the course of this disease. An example of how systematic longitudinal collection of biospecimens in the current population can inform stratification of patients for treatment is supported by the knowledge of neuroendocrine differentiation in PCa (49, 100-102). In a

subset of patients, therapeutic resistance to AR-targeting therapy is accompanied by the emergence of a histologic subtype that morphologically resembles de novo small-cell PCa (103). Such tumours can be identified histologically if a repeat biopsy is performed and have been shown to be more clinically aggressive (radiologically and symptomatically) and respond briefly to chemotherapy but not to hormonal therapies. It is, therefore, potentially justifiable to perform repeated biopsies to identify and stratify patients whose tumours have histologically altered by developing neuroendocrine features at a given sampling point.

The Irish Programme for Stratified Prostate Cancer Therapy (iPROSPECT) was a national prospective translational study (clinicalTrials.gov Identifier: NCT03162003) that investigated how clinical and biological patterns change over time and relate to each individual's treatment response and progression of disease. The aim of iPROSPECT was to deliver a programme of stratified therapies for patients with PCa, based on a greater understanding of the intra- and inter-cellular signalling pathways driving disease progression (Protocol provided in Appendix II).

6.7 Aims and objectives

The aim of this study was to assess novel treatments for advanced PCa and to detect markers that may be associated with resistance.

The objectives of this project were:

- To assess the baseline characteristics of patients recruited to a phase II clinical trial examining the combination of radium-223 and enzalutamide and to assess the safety of this combination

- To assess the baseline characteristics of patients with advanced PCa recruited to a translational study, iPROSPECT
- To collect primary biopsy tissue, metastatic biopsy tissue and longitudinal blood samples, including CTCs, from patients enrolled in the radium-223 and enzalutamide clinical trial, and the iPROSPECT translational study
- To determine the use of CTC numbers as a surrogate response read out to the combination treatment of radium-223 and enzalutamide
- To compare bone marrow biopsies to CT guided biopsies for obtaining biopsy material from metastatic sites in patients recruited to iPROSPECT
- To molecularly profile matched primary biopsy tissue and metastatic tissue samples
- To assess different molecular methods for detecting AR-V7 in PCa
- To profile PCa for circRNA expression and to identify novel circRNA mediated mechanisms of resistance to enzalutamide

Chapter 2: Materials and Methods

2.0 Materials and methods

6.8 Preparation and handling of materials

Reagents and chemicals used in the laboratory were of analytical grade and stored in accordance with manufacturers' instructions. All chemicals and waste resulting from any experiments was disposed of according to local guidelines. Chemicals were purchased from Merck KGaA (Darmstadt, Germany), Sigma Aldrich (St. Louis, MO, USA) unless stated otherwise. Cell culture reagents were purchased from Sigma Aldrich, with exceptions noted.

6.9 Cell culture

2.1.1 Cell culture conditions

Cell culture work was performed aseptically in accordance with good laboratory practice in an ABS optimale 18 laminar air flow unit (LAF) (Aulnay Sous Bois, France). The LAF was allowed to run for at least 20 min prior to use and sanitised using 70% industrial methylated spirits (IMS) in dH_2O. Cell culture reagents were warmed in a 37°C incubator for approximately 30 min prior to use, unless stated otherwise. All cells were cultured in a 5% CO_2 humidified atmosphere.

2.1.2 Prostate cell lines

Eleven PCa cell lines were used in this project; PC-3, 22Rv1, DU145, LNCaP, VCaP, BPH-1, PWR-1E, RWPE-1 (Table 2.1), and three LNCaP clones. All cell lines were obtained from American Tissue Culture Collection (ATCC-LGC Standards, Middlesex, UK) except the three LNCaP clones, which were gifted from Novartis (Dublin, Ireland). Cell lines were cultured in complete media containing 10% foetal bovine serum (FBS) and 1% penicillin

streptomycin (P/S) (5000 U/mL penicillin, 5000 U/mL streptomycin), unless stated otherwise.

Table 2.1. Cell lines categorised according to AR status.

AR positive	22Rv1	androgen-dependent CWR22 xenograft
	VCaP	vertebral bone metastasis
	LNCaP	lymph node metastasis
AR negative	PC-3	bone metastasis
	DU 145	brain metastasis
Benign	BPH-1	human prostate tissue
	PWR-1E	prostatic epithelial cells
	RWPE-1	normal adult human prostate

2.1.2.1 22Rv1 (ATCC® CRL-2505™)

22Rv1 is a human prostate carcinoma epithelial cell line derived from a xenograft that was serially propagated in mice after castration-induced regression and relapse of the parental, androgen-dependent CWR22 xenograft. Cells were cultured in complete RPMI-1640 Medium.

2.1.2.2 LNCaP clone FGC (ATCC® CRL-1740™)

LNCaP clone FGC was isolated in 1977 by J.S. Horoszewicz, *et al*. (104), from a needle aspiration biopsy of the left supraclavicular lymph node of a 50-year-old Caucasian male (blood type B+) with a confirmed diagnosis of metastatic PCa. Cells were cultured in complete RPMI-1640 Medium.

2.1.2.3 VCaP (ATCC® CRL-2876™)

This line was established in 1997 from a vertebral bone metastasis from a patient with hormone refractory PCa. It was passaged as xenografts in mice then cultured *in vitro*. It is androgen sensitive *in vitro* and *in vivo*. Cells were cultured in complete Dulbecco's Modified Eagle's Medium.

2.1.2.4 DU 145 (ATCC® HTB-81™)

DU 145 is not detectably hormone sensitive and is only weakly positive for acid phosphatase and isolated cells form colonies in soft agar. The cells do not express prostate antigen. Cells were cultured in complete Eagle's Minimum Essential Medium.

2.1.2.5 PC-3 (ATCC® CRL-1435™)

The PC-3 cell line was initiated from a bone metastasis of a grade IV prostatic adenocarcinoma from a 62-year-old male Caucasian. It does not express androgens. Cells were cultured in complete F-12K Medium.

2.1.2.6 BPH-1 (DSMZ no.: ACC 143)

An epithelial cell line developed from human prostate tissue obtained by transurethral resection. The base medium was RPMI 1640. Complete growth medium contained the following supplements: 10% FBS, 1% P/S, 20 ng/mL testosterone (SERVA Electrophoresis GmbH, Heidelberg, Germany), 5 µg/mL transferrin, 5 ng/mL sodium selenite and 5 µg/mL insµLin (Thermo Fisher Scientific).

2.1.2.7 PWR-1E (ATCC® CRL-11611™)

Human prostatic epithelial cells, derived from a normal prostate with mild hyperplasia, were immortalized with an adenovirus 12-SV40 hybrid virus (Ad12-SV40) (105). This cell line was cultured in Keratinocyte Serum Free Media (Thermo Fisher Scientific), containing 0.05 mg/mL bovine pituitary extract (BPE) and 5 ng/mL Epidermal growth factor (EGF) (Thermo Fisher Scientific) and 1% P/S.

2.1.2.8 RWPE-1 (ATCC® CRL-11609™)

Epithelial cells derived from the peripheral zone of a histologically normal adult human prostate were transfected with a single copy of the human papilloma virus 18 (HPV-18) to establish the RWPE-1 cell line (106). These cells were cultured in the same media as PWR-1E.

2.1.2.9 Isogenic model of Enzalutamide resistance

This isogenic model was gifted from Novartis and generated from single clones as described by Korpal *et al.* (35). Cell lines were cultured in complete RMPI-1640 Medium. The model consisted of three aged-matched cell lines; the control (drug sensitive), Clone 1 (highly drug resistant) and Clone 9 (moderately drug resistant).

2.1.3 Cryopreservation

Cells were trypsinised and counted as described previously, and re-suspended in Cellbanker® cryopreservation media (AMS Biotechnology, Abingdon, UK) at a concentration of 1-1.5 x 106 cells/mL. Aliquots were stored at -80°C.

2.1.4 Propagation of cells from storage

Complete media was warmed to 37°C. Cells were removed from storage and thawed rapidly in a 37°C water bath for 2 min. Once thawed, the cells were added to 9 mL complete media in a 15 mL tube. The cells were then centrifuged at 300 χ g for 5 min. The supernatant was decanted and the cell pellet was re-suspended in 1 mL warmed complete media. The cells were added to a tissue culture flask with the required volume of media. The cells were then incubated in a humidified atmosphere at 37°C with 5% CO_2.

2.1.5 Cell sub-culture

Cells were visualised daily using an inverted phase-contrasted microscope (Nikon Corp., Tokyo, Japan). Sub-culturing was performed when cell cultures reached 80-90% confluency. Cell culture medium was decanted and the cells were washed with 5 mL 1X PBS (Thermo Fisher Scientific) to remove residual FBS. One mL trypsin ethylene-diamine tetra-acetic acid (EDTA) (Thermo Fisher Scientific) was added to the flasks. Flasks were incubated at 37°C for approximately 5 min to remove adherent cells from the surface. Nine mL complete medium was then added to the flasks to inactivate the trypsin. Cells were transferred to a sterile 15 mL tube and pelleted by centrifugation at 1300 χ g for 3 min in an Eppendorf™ 5804 centrifuge (Thermo Fisher Scientific). The supernatant was discarded and the cell pellet re-suspended in 10 mL

complete medium. This suspension was used to seed fresh flasks at a number of different densities.

2.1.6 Cell counting

Cells were seeded at specific densities depending on experimental set up. A bright line haemocytometer (Hausser Scientific, Horsham, PA, USA) was used in conjunction with Trypan Blue (0.4% v/v) for cell counting and viability. Cells were pelleted as above and re-suspended in a specific volume of media until a single cell suspension was obtained. A 20 µL aliquot of this suspension was added to 180 µL Trypan Blue and mixed. A coverslip was placed on the haemocytometer. The edge of the cover slip was touched gently by a pipette tip and the chamber filled by capillary action. The number of cells/mL was calculated using the following equation:

Average no. of cells counted x 10,000 x 10 = no. of cells/mL

Where, 10,000 equals the µL volume under the cover slip and 10 equals the dilution factor.

2.1.7 Mycoplasma testing

At 70-80% cell confluence, media was removed from T75 cm^3 flasks for mycoplasma testing. Prior to use, the cell supernatant was centrifuged at 300 χ g to remove cellular debris. A PCR based reaction, adapted from Young *et al.* (107), was used to determine the presence/absence of mycoplasma. The primers were designed to encompass common mycoplasma species:

FWD 5´ - GGGAGCAAACAGGATTAGATACCCT-3´;

REV 5´ - TGCACCATCTGTCACTCTGT TAACCTC-3´

The PCR reaction consisted of the following: 12.5 µL Green 2X GoTaq (Promega, WI, USA), 0.5 µL FWD primer (10 µM) (Merck KGaA), 0.5 µL REV primer (10 µM) (Merck KGaA) and 10.5 µL DNase free water (Thermo Fisher Scientific). The total reaction volume was 25 µL, which included 1 µL cell supernatant. The PCR reaction was run under the conditions laid out in Table 2.2. The resulting PCR products were electrophoresed on a 2.5% agarose gel. A PCR negative control and a known mycoplasma positive control were included. A band at 270 bp was indicative of a positive result. All cell lines were examined for mycoplasma infection every 3 months.

Table 2.2. PCR conditions for mycoplasma testing.

Temperature	Time	
95°C	5 min	
94°C	30 sec	40 Cycles
55°C	30 sec	
72°C	1 min	
72°C	10 min	

6.10 RNA isolation and quantification

Two different methods were used to isolate RNA from cells. The first method used TRIzol® Reagent (Thermo Fisher Scientific) and was utilised as a standard protocol to isolate RNA. The second method used the RNeasy Mini Kit (Qiagen, Sussex, UK) for circRNA experiments.

2.1.8 Trizol® RNA isolation protocol

The cell culture supernatant was decanted and adhered cells were directly lysed by adding 2 mL TRIzol® Reagent (Thermo Fisher Scientific) to the flask surface and cells were dislodged with a cell scraper. The cell lysate was mixed several times using a pipette. For phase separation, 200 µL chloroform (Merck KGaA) was added to the cell lysate, vortexed vigorously for 15 sec and then incubated at RT for 5 min. The samples were centrifuged at 12,000 χ g for 15 min at 4°C. The upper aqueous phase was transferred into a fresh tube without disturbing the interphase. To precipitate the RNA from the aqueous phase, 400 µL isopropyl alcohol (Merck KGaA) was added to the sample. The sample was mixed and incubated for 5 min at RT. The sample was centrifuged at 12,000 χ g for 15 min at 4°C. The precipitate was removed and the RNA pellet was washed with 1 mL 75% EtOH (Merck KGaA). The sample was then centrifuged at 12,000 χ g for 10 min at 4°C. The EtOH was removed and a repeat pulse centrifuge step was performed. Surplus EtOH was removed and the pellet was allowed to air dry for 20 min. The sample was re-suspended in RNase-Free H_2O and stored at –80°C.

2.1.8.1 DNase Treatment

Ambion® TURBO DNA-free™ DNase Treatment (Thermo Fisher Scientific) and Removal Reagents are designed to remove contaminating DNA from RNA preparations, and to subsequently remove the DNase and divalent cations from the sample. A 0.1 volume of 10X DNase I Buffer and 1 µL DNase I was added to RNA samples, and mixed gently. Samples were incubated at 37°C for 30 min. DNase Inactivation Reagent (0.1 volume) was added and mixed well.

Samples were incubated for 2 min at RT, with occasional mixing. Samples were centrifuged at 10,000 χ g for 1.5 min and the RNA was transferred to a fresh tube.

2.1.8.2 RNA Clean Up

In order to remove any contaminating residual products after DNase treatment, an RNA clean-up step was performed. One hundred % EtOH was added to the sample followed by 3 M Sodium Acetate (Thermo Fisher Scientific). The sample was mixed well by inversion and incubated at RT for 20 min. The sample was centrifuged for 10 min at 12000 χ g at 4°C and the supernatant was removed. The sample was washed with 1 mL 75% EtOH and centrifuged again at 12000 χ g at 4°C for 10 min. The supernatant was removed and re-suspended in RNase-Free H_2O.

2.1.9 RNeasy Mini Kit

A second method was also used to isolate RNA. This was done in order to reduce potential 'nicking' of circRNAs that would prevent their detection by qPCR. This was performed using the RNeasy Mini Kit (Qiagen). Cells were disrupted by the addition of 350 µL Buffer RLT and vortexed. One volume of 70% EtOH was added to the homogenized lysate and mixed well by pipetting. Up to 700 µL of the sample was added to a RNeasy spin column and centrifuged for 15 sec at 8000 χ g. The flow-through was discarded. Genomic DNA contamination was eliminated as follows; 350 µL Buffer RW1 was added to the RNeasy spin column and centrifuged for 15 sec at 8000 χ g, with the flow-through discarded. Next, 10 µL DNase I solution was added to 70 µL

Buffer RDD and mixed by gently inverting the tube. The DNase I mix was added directly to the RNeasy spin column membrane and incubated at RT for 15 min. Following the incubation, 350 µL Buffer RW1 was added to the spin column and centrifuged for 15 sec at 8000 χ g. Next, 500 µL Buffer RPE was added to the RNeasy spin column and centrifuged for 15 sec at 8000 χ g and the flow-through discarded. An additional 500 µL Buffer RPE was added to the RNeasy column and centrifuged for 2 min at 8000 χ g to dry the membrane. The RNeasy column was then placed into a fresh 2 mL collection tube and the assembly centrifuged for 1 min to avoid any carry-over of Buffer RPE. The RNeasy spin column was placed in a new 1.5 mL collection tube and 30-50 µL RNase-free H_2O was added directly to the spin column membrane. The assembly was centrifuged for 1 min at 8000 χ g to elute the RNA. The eluate containing RNA was stored at -80°.

2.1.10 RNA quantification

2.1.10.1 RNA quantification using the Nanodrop

RNA was quantified using a NanoDrop 1000 spectrophotometer (Thermo Fisher Scientific). The instrument was first initialised and blanked with 1 µL RNase/DNase-free H_2O. One µL of each sample was loaded individually onto the NanoDrop. The instrument was cleaned between each sample. The NanoDrop returned the nucleic acid concentration in ng/µL and also the 260:280 and 260:230 purity ratios. A 260/280 ratio of ~1.8 is generally accepted as “pure” for DNA; a ratio of ~2.0 is generally accepted as “pure” for RNA.

2.1.10.2 RNA quantification using the Agilent RNA 6000 Nano Kit

RNA for microarray studies underwent a quality assessment using the Agilent 2100 Bioanalyzer (Agilent, CA, US). The samples were loaded at 100 ng per well based on the original concentration values obtained by the spectrophotometer. The Agilent 2100 Bioanalyzer uses a 635 nm diode laser with an emission filter of 670–700 nm to detect fluorescence after dye intercalation into nucleic acids. To estimate nucleic acid purity, the ratio of the absorbance contributed by the nucleic acid to the absorbance of the contaminants is calculated. Requirements for A260/A280 ratios are 1.8–2.2, while requirements for A260/A230 ratios are generally >1.7.

2.1.10.3 RNA Quantification using the Qubit® Fluorometer

In order to perform RNA Quantification using the Qubit® Fluorometer (Thermo Fisher Scientific), two assay tubes for the standards were set up and one assay tube for each sample to be tested. The Qubit® Working Solution was prepared by diluting the Qubit® reagent 1:200 in Qubit® buffer. Two hundred µL Working Solution was prepared for each standard and sample. Standard 1 was prepared by adding 190 µL of the working solution to 10 µL of kit standard 1. Standard 2 was prepared by adding 190 µL of the working solution to 10 µL of kit standard 2. Samples were prepared for quantification by adding 198 µL working solution to 2 µL RNA sample to be quantified. All assay tubes were vortexed for 2-3 sec and incubated at RT for 2 min. The samples were read in the Qubit® Fluorometer and the resultant reading multiplied by the dilution factor to determine concentration of original RNA sample.

6.11 Gene expression analysis

2.1.11 cDNA Synthesis for gene expression analysis

cDNA was synthesised using the High Capacity cDNA Reverse Transcription Kit (Thermo Fisher Scientific) by the addition of the following components into a sterile, nuclease-free tube on ice; 1 µg total RNA, 2 µL 10X RT Buffer, 0.8 µL 25X dNTP Mix, 2.0 µL RT Random Primers, 1.0 µL Multiscribe Reverse Transcriptase, 1.0 µL RNase inhibitor and 3.2 µL Nuclease-free H_2O to a final volume of 20 µL. The thermal cycling conditions were as follows; 10 min at 25°C, 120 min at 37°C, 5 min at 85°C. cDNA was stored at -20°C until use.

2.1.12 cDNA Synthesis for miRNA expression analysis

cDNA for use in miRNA expression analysis was synthesised using the TaqMan© miRNA Reverse Transcription Kit (Thermo Fisher Scientific) by the addition of the following components into a sterile, nuclease-free tube on ice; 1 µg total RNA, 0.15 µL 100 mM dNTPs, 3 µL 5X RT Primer, 1 µL Multiscribe Reverse Transcriptase, 1.5 µL 10X RT Buffer, 0.19 µL RNase Inhibitor, 4.16 µL Nuclease-free H_2O to a final volume of 15 µL. The thermal cycling conditions were as follows; 30 min at 16°C, 30 min at 42°C, 5 min at 85°C. cDNA was stored at -20°C until use.

2.1.13 TaqMan® Probe-based gene/miRNA expression

cDNA generated using the protocols described above were used for gene expression analysis using TaqMan® probes (Thermo Fisher Scientific). Each PCR reaction was prepared in a 96-well plate as follows; 1.0 µL 20X TaqMan® gene expression assay (in the case of miRNA expression analysis

1.0 µL 20X TaqMan® small RNA assay), 10 µL TaqMan® Universal Master Mix, 4 µL cDNA template, 5.0 µL RNase-free H_2O to a final volume of 20 µL. The negative control for each reaction consisted of 1 µL RNase-free H_2O substituted for template cDNA. The plates were loaded onto the 7500 Fast Real-Time PCR Machine (Thermo Fisher Scientific). The thermal cycling conditions were as follows: 2 min at 50°C, 10 min at 95°C, and 40 cycles of 15 sec at 95°C and 1 min at 60°C. Data were normalized using the ΔΔCt method based on *GAPDH* expression as a housekeeping gene.

2.1.14 SYBR Green-based gene expression analysis

cDNA was generated using the protocol previously described. Each PCR reaction was prepared in a 96-well plate. The expression of target gene transcripts was determined with real-time qPCR using SYBR Green PCR Master Mix (Thermo Fisher Scientific). Each PCR reaction was carried out in a final volume of 20 µL containing 10 µL 2X SYBR Green Master Mix, 0.5 µL each 10 pmol/µL FWD and REV primers (Eurofins Genomics, Ebersberg, Germany) (Appendix IV) and 9 µL RNase-Free H_2O. PCR amplification was performed over 40 cycles using the following conditions: 95ºC for 10 min, 95ºC for 15 sec, 55ºC for 30 sec and 60ºC for 60 sec. Data were normalized using the ΔΔCt method based on *GAPDH* expression as a housekeeping gene.

2.1.15 qRT-PCR data analysis

The ΔΔCt method was used to calculate the relative expression of gene/miRNA targets. The delta-delta Ct method, also known as the 2–ΔΔCt method, was used to calculate the relative fold change in gene expression.

2.1.16 Standard curve method

Standard dilution curves for known gene copy numbers using gBlocks® gene fragments (Integrated DNA Technologies, CA, US) were designed for AR-FL and AR-V7. A standard curve was prepared using AR-FL and AR-V7 present at 300,000 copies, 30,000 copies, 3,000 copies, 300 copies and 30 copies. The mass of gDNA was calculated using the copy numbers of interest. A serial dilution was then performed. Threshold cycle numbers in quantitative PCR reactions were determined for cDNA specific to gene copy number at 6 dilutions containing the indicated number of copies of each transcript. Formulas were derived to quantify the absolute copy numbers on the basis of Ct values.

2.1.17 Agarose gel electrophoresis

PCR products were visualised on 1% agarose gels. The agarose was dissolved in Tris-Acetate-EDTA (TAE) buffer (40 mM Trizma base, 20 mM acetic acid, 1 mM EDTA) by boiling in a microwave for 2- 3 min. Ten µL DNA SYBR Safe gel (Thermo Fisher Scientific) was added to the solution. The solution was poured into a gel tray with well forming combs and allowed to set. A 1/6 volume of 6X DNA Loading Dye (Thermo Fisher Scientific) was added to the PCR sample and loaded on to the gel. A DNA ladder (Thermo Fisher Scientific) was also added to the gel. Electrophoresis of the samples was carried out using 1X TAE as running buffer. The voltage was kept constant at 100 V and gels electrophoresed for approximately 60 min. The bands were

visualised and photographed under UV light using a Biospectrum Imaging System (Ultra Violet Products, Cambridge, UK).

6.12 circRNA microarray

2.1.18 Microarray

Profiling of cell lines was performed using the human circRNA Array version 2 (Arraystar, MD, US). Total RNA was isolated from each sample and was quantified using the NanoDrop ND-1000. RNA integrity was assessed by Arraystar using electrophoresis on a denaturing agarose gel. The sample preparation and microarray hybridization were performed according to Arraystar's instructions (Fig. 2.1). Briefly, total RNA was digested with RNAse R (Epicentre, WI, US) to remove linear RNAs and enrich for circRNAs. The enriched circRNAs were amplified and transcribed into fluorescent cRNA utilizing a random priming method (Arraystar Super RNA Labeling Kit). The labelled cRNAs were hybridized onto the Arraystar Human circRNA Array V2 (8x15K). The array slides were washed and scanned on the Agilent Scanner G2505C (Agilent). Agilent Feature Extraction software (version 11.0.1.1) was used to analyse acquired array images.

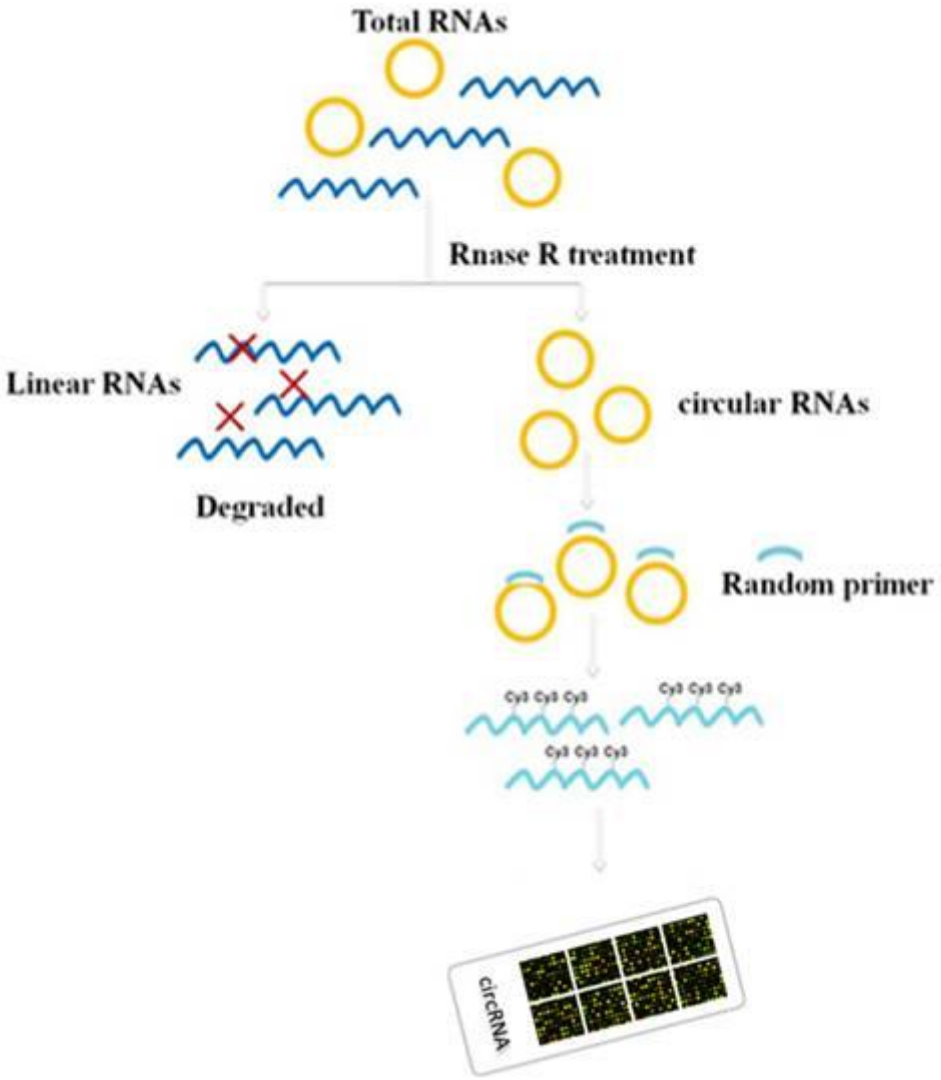

Figure 2.1. CircRNA microarray.

A random primer-based labelling system was coupled with RNase R-based sample pre-treatment to efficiently remove linear RNAs, and specifically label circular RNAs (Image taken from the Arraystar product information leaflet).

2.1.19 Microarray data analysis

Quantile normalization and subsequent data processing were executed using R (http://www.R-project.org) (108). circRNAs with at least 4 out of 8 samples that were flagged (an attribute that denotes the quality of the entities) as Present or Marginal were considered to be target circRNAs according to GeneSpring software's (Agilent Technologies) definitions and instructions. These target circRNAs were retained for further differential analysis. Comparing two groups, the fold change (i.e. the ratio of the group averages) for each circRNA was computed. A student's paired *t* test was used to identify significantly altered circRNAs. The false discovery rate (FDR) was applied to determine the threshold of P-value. An FDR of < 0.05 was recommended.

2.1.20 Delineation of circRNA/miRNA interactions

The circRNA/miRNA interaction was predicted using Arraystar's miRNA target prediction software based on miRanda (109) and TargetScan (110). To establish a circRNA-miRNA network, the top five predicted miRNA Response Elements (MREs) for each circRNA were identified.

6.13 Circulating Tumour Cells (CTCs)

2.1.21 Blood collection for CTC isolation

Patients with metastatic CRPC recruited to the clinical trial ICORG 13-21 and iPROSPECT had blood collected for CTC analysis. Three mL whole blood was drawn into EDTA tubes (BD Biosciences, CA, US). Blood samples were refrigerated at 4ºC until filtration. To ensure optimal CTC isolation, filtration occurred within 4 h of blood sampling.

2.1.22 CTC isolation

This study used a filtration device (ScreenCell®, Sarcelles, France) which can isolate CTCs from a blood sample. In the ScreenCell® device, blood flow passes through a microporous membrane filter allowing size-selective isolation of CTCs under fully reproducible and standardised conditions. Three mL whole blood was diluted with 4 mL filtration buffer (ScreenCell®), incubated at RT for 8 min and passed through a Cyto microporous filter (ScreenCell®), using vacuum-assisted filtration to separate CTCs from other blood cells (Fig 2.2). Following filtration, 1.6 mL 1X PBS was passed through the filter to wash away debris. Filters were allowed to dry overnight on filter paper. Two filters were generated at each time point for each participant.

2.1.23 Staining

Filters were stained with MGG stain. Briefly, filters were placed in the following baths of stain: 100% MG for 2.5 min; 50% MG for 2.5 min; 10% Giemsa for 10 min. The filters were then washed in a bath of H2O. Filters were reviewed and enumerated by a trained histopathologist.

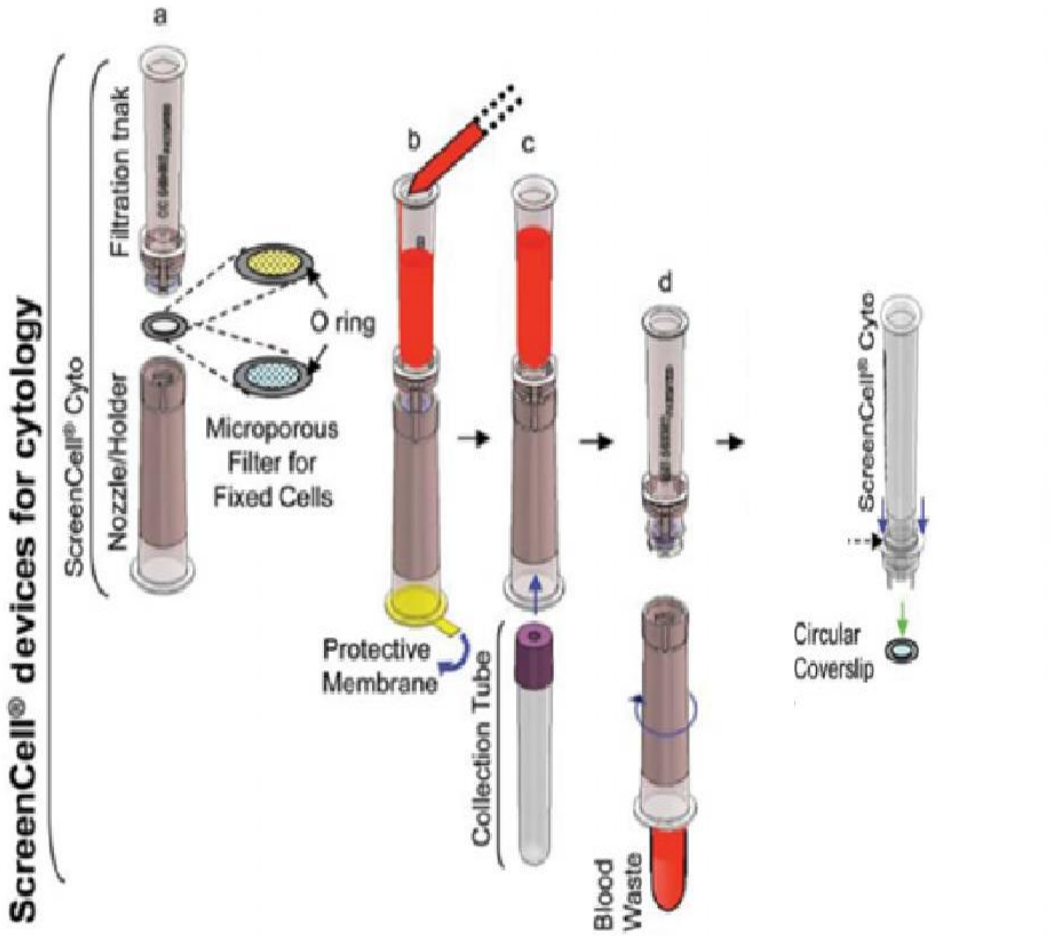

Figure 2.2. The ScreenCell® Device.

Filtration devices comprised of a filtration tank, a filter capped by a removable nozzle/holder (a) which, after removal of a protective membrane (b), allows insertion and guidance of a collection tube (c). At the end of filtration, the filter was released by pushing down a rod located at the bottom part of the filtration device (Image adapted from ScreenCell® Device protocol insert).

6.14 Archival tissue

2.1.24 Ethical approval

Ethical approval was obtained for iPROSPECT and ICORG 13-21 translational studies from the relevant hospital bodies. Both studies were co-ordinated by Cancer Trials Ireland. Archival radical prostatectomy or metastatic biopsy formalin-fixed paraffin-embedded (FFPE) samples from enrolled patients were collected if available. Slides had previously been reviewed by a pathologist and the diagnosis confirmed according to the World Health Organisation (WHO) classification guidelines.

2.1.25 FFPE sample preparation

2.1.25.1 Cell lines

Cells were recovered from the culture flasks as previously described. The cell suspension was diluted with 50 mL complete media and centrifuged at 200 χ g for 5 min. Bovine thrombin (Instrumentation Laboratory, Munich, Germany) and human plasma (Instrumentation Laboratory) reagents were reconstituted with dH_2O. One drop of reconstituted plasma reagent was added to the pellet, followed by 3 drops of reconstituted thrombin. The sample was incubated for 3 min undisturbed allowing a clot to form. It was placed into a white cell safe biopsy capsule, and then placed into an appropriately labelled cassette. The cassette was closed with a metal clip and placed in a specimen pot containing 10% buffered formalin (Thermo Fisher Scientific). The sample was then processed and embedded using standard laboratory protocols.

2.1.26 FFPE sections

FFPE samples were sectioned at 4 μm using a HM325 rotary microtome (Thermo Fisher Scientific). The sections were floated in a 56°C waterbath and

mounted onto TOMO® adhesion slides (Matsunami Glass, Osaka, Japan). The sections were dried overnight by placing the slides on a heating block heated at 40°C. Slides were used immediately or stored in the laboratory at RT.

6.15 Metastatic biopsies

2.1.27 Bone marrow biopsy

Informed consent was obtained from all patients before any procedure was performed. With the patient positioned, the iliac crest was palpated and the preferred sampling site marked with a pen. The skin and the underlying tissue to the periosteum was infiltrated with a local anaesthetic. A skin incision was made with a small surgical blade, through which the bone marrow needle, with a stylet locked in place, was inserted. Once the needle touched the bone surface, the stylet was removed. With firm pressure applied, the needle was slowly rotated in an alternating clockwise-counter clockwise motion and advanced into the bone marrow cavity to obtain an adequate bone marrow specimen measuring approximately 1.6-3 cm in length. After this procedure, the needle was slowly pulled out while being rotated in an alternating clockwise and counter clockwise motion. The specimen was removed and placed in formalin solution for histologic processing.

2.1.28 CT guided biopsy

Informed consent was obtained from all patients before biopsy procedures. In all patients, the biopsy was performed using non-coaxial technique using an automated biopsy gun with an 18-gauge cutting needle. After puncturing the skin, the position of the needle tip was confirmed by obtaining limited CT images around the lesion at 5-mm thickness. If clinically feasible, 3 core

biopsies were taken and placed in formalin solution and then processed to FFPE blocks using standard laboratory procedures.

6.16 Next generation sequencing (NGS)

NGS was performed using 2- 4 sections measuring 10 µM from FFPE blocks. Total nucleic acids were extracted using the Agencourt FormaPure system (Beckman Coulter, CA, US) according to manufacturer's instruction. DNA and RNA were quantified using Qubit™ fluorometric quantitation. DNA and RNA library preparation was performed using the Oncomine™ Focus Assay (Thermo Fisher Scientific). Sequencing for mutations and copy number was performed on the DNA library and fusions were performed on the RNA library (Fig 2.3). Bioinformatics was performed using Ion Reporter™ Software (Thermo Fisher Scientific).

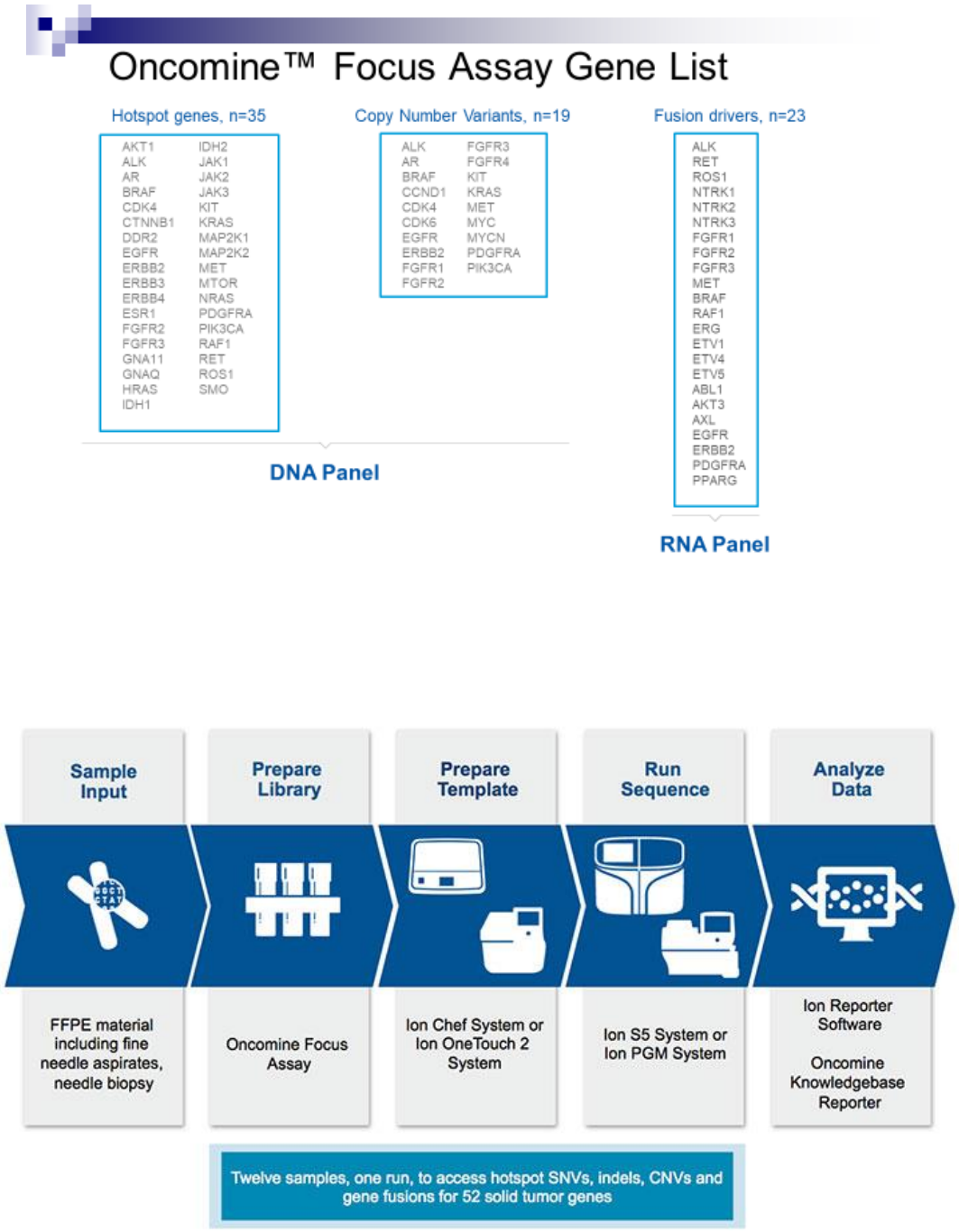

Figure 2.3. The Oncomine™ Focus Assay gene list and workflow.

(Image taken from Thermo Fisher Scientific protocol insert).

6.17 RNA *in situ* hybridisation

2.1.29 Culture adherent cells

In order to perform RISH directly on cell lines, a number of cell lines were cultured on Nunc™ Lab-Tek™ II Chamber Slides™ (Thermo Fisher Scientific). Cells were fixed in 10% buffered formalin for 60 min.

2.1.30 RNAscope®

RISH was performed using the RNAscope® (Advanced Cell Diagnostics, CA, US) assay. This was performed manually according to the manufacturer's instructions (Fig 2.4). Briefly, the RNAscope® assay procedure included the following steps: FFPE tissue sections were deparaffinized and treated sequentially with pre-treatment 1 (10 min at RT), pre-treatment 2 (boiling for 20 min), and pre-treatment 3 (30 min at 40°C) to allow for target probe access. Target probes were added onto the slides and incubated in the HybEZ oven (Advanced Cell Diagnostics) for 2 h at 40°C to allow probe hybridization to RNA targets. The slides were washed and incubated with a series of signal amplification solutions: amplification 1 (30 min at 40°C), amplification 2 (15 min at 40°C), amplification 3 (30 min at 40°C), amplification 4 (15 min at 40°C), amplification 5 (30 min at RT), and amplification 6 (15 min at RT). The slides were then dehydrated. Signals were generated by chromogenic reaction using horseradish peroxidase with 3,3-diaminobenzidine (10 min at RT). The slides were counterstained with haematoxylin solution, Gill No. 3 (Merck KGaA) and mounted with Cytoseal mounting medium (Thermo Fisher Scientific). Assays using archival FFPE specimens were performed in parallel with positive and negative controls, to ensure interpretable results. The endogenous housekeeping gene, PPIB, was used as a positive control to assess

both tissue RNA integrity and assay workflow. Positive staining with signals easily visible under a 10X objective lens was considered to be adequate. The bacterial gene, dapB, was used as negative control to assess background signals.

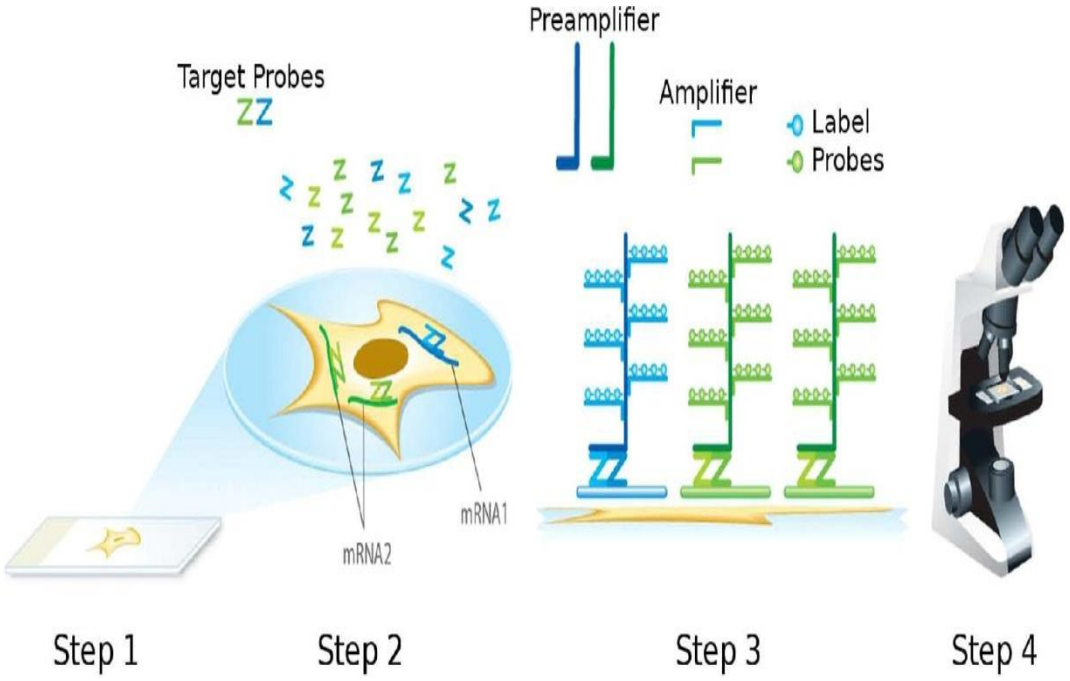

Figure 2.4. RNAscope® 2.5 Assay.

Workflow for FFPE sample preparation, pre-treatment and detection for the RNAscope® 2.5 Assay (Image taken from the RNAscope® 2.5 Assay protocol insert).

2.1.31 BaseScope™

The BaseScope™ (Advanced Cell Diagnostics) assays were performed manually according to the manufacturer's instructions. Briefly, the BaseScope™ assay procedure included the following steps: The FFPE tissue sections were deparaffinized and treated sequentially with pre-treatment 1 (10 min at RT), pre-treatment 2 (boiling for 20 min), and pre-treatment 3 (30 min at 40°C) to allow for target probe access. Target probes were added onto the slides and incubated in the HybEZ oven (Advanced Cell Diagnostics) for 2 h at 40°C to allow probe hybridization to RNA targets. The slides were washed and incubated with a series of signal amplification solutions: amplification 1 (30 min at 40°C), amplification 2 (15 min at 40°C), amplification 3 (30 min at 40°C), amplification 4 (15 min at 40°C), amplification 5 (30 min at RT), and amplification 6 (15 min at RT). Signals were generated by chromogenic reaction using horseradish peroxidase with 3,3-diaminobenzidine (10 min at RT). The slides were counterstained with haematoxylin and mounted with Cytoseal mounting medium.

2.1.32 Interpretation of RISH Results

Stained tissues were examined by a pathologist using brightfield microscopy. RNAscope® positive staining appeared as brown, whereas BaseScope™ positive staining appeared as red (Fig 2.5). The number of dots correlated to the number of RNA copy numbers, whereas dot intensity reflected the number of probe pairs bound to each molecule. Semi-quantitative scoring was used e.g., 1+ to 4+ based on number of dots per cell to interpret staining patterns.

Score	Criteria
0	No staining or <1 dot/10 cells
1	1-3 dots/cell
2	4-9 dots/cell. None or very few dot clusters
3	10-15 dots/cell and <10% dots are in clusters
4	>15 dots/cell and >10% dots are in clusters

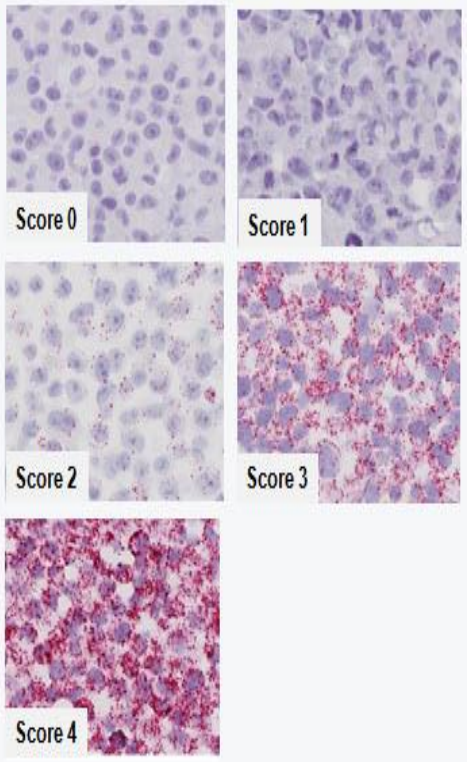

Figure 2.5. RISH semi-Quantitative Analysis.

Samples were visually scored based on the average number of dots per cell using the following criteria: 0 (negative, 0–1 dot/tumour cell or 2–3 dots/tumour cell in <50% of tumour cells), 1+ (2–3 dots/tumour cell in >50% of tumour cells), 2+ (4–10 dots/tumour cell), 3+ (>10 dots/tumour cell in >50% of tumour cells), and 4+ (>10 dots/tumour cell in >50% of tumour cells with clusters of the signal) (Image taken from ACD protocol insert).

6.18 Statistical Analysis

Statistical packages IBM SPSS Statistics 24 (IBM, Ireland) and Graphpad PRISM 7 (Graphpad, CA, USA) were used for the majority of statistical analysis in this thesis. Data is graphed as mean ± SEM. Significance was determined via one way analysis of variance (ANOVA), where the number of groups in the experiment was three or more, or a paired student *t* test where the number of groups did not exceed two. A probability of $p<0.05$ was considered to represent a significant difference between the groups. A *post hoc* test was necessary after ANOVA to determine which groups were significantly different to each other. For ICORG 13-21 patient data, statistical analysis was completed in conjunction with Dr. Imelda Parker, Cancer Trials Ireland. The specifics of each statistical test utilised, are outlined in each results section.

Chapter 3: Analysis of Safety Data and Circulating Tumour Cells in patients treated with Radium-223 in combination with Enzalutamide

6.19 Introduction

Evaluating drugs to treat metastatic PCa has previously posed unique challenges due to the biology and natural history of the disease. In recent years, several new agents have been developed, which have demonstrated significant survival benefits in patients with advanced CRPC when administered prior to and/or post chemotherapy. These include the anti-androgen - enzalutamide (22), the CYP-17 inhibitor - abiraterone (21), the radioisotope - radium-223 (30) and the novel taxane - cabazitaxel (19). Given their differing modes of action and non-overlapping toxicity profiles, there is considerable interest in defining the correct combination or sequencing of these novel therapies. Radium-223 and enzalutamide are both well-tolerated agents, and the combination of both with their differing modes of action, could lead to potential synergy and increased treatment efficacy. However, data is lacking for a combination regimen consisting of radium-233 and enzalutamide.

Radium-223 is indicated for the treatment of adults with CRPC, who have symptomatic bone metastases and no known visceral metastases (30). Radium-223 is a therapeutic alpha particle-emitting pharmaceutical. It is administered as 6 intravenous injections (50 kBq/kg), given every 4 weeks. Radium-223, through its active moiety, mimics calcium and selectively targets bone, specifically areas of bone metastases, by forming complexes with the bone mineral, hydroxyapatite. The high linear energy transfer of alpha emitters (80 keV/μM) leads to a high frequency of double strand DNA breaks in adjacent tumour cells, resulting in a potent cytotoxic effect. Additional effects on the tumour microenvironment including osteoblasts and osteoclasts also contribute to the *in vivo* efficacy. The alpha particle range from radium-223 is

less than 100 μM (less than 10 cell diameters), which minimises damage to the surrounding normal tissue.

Enzalutamide (MDV3100) is a novel anti-androgen, which binds the AR LBD and inhibits growth of castration-resistant xenografts (22). Enzalutamide is administered orally as a once daily dose of 160 mg. Unlike older antiandrogens such as bicalutamide, enzalutamide impairs AR nuclear translocation and blocks DNA binding (20). Data from early phase trials have shown that enzalutamide was active in both pre- and post-chemotherapy-treated patients showing a decrease of PSA and CTCs, while prolonging OS in phase III clinical trials (22, 24). However, intrinsic and acquired resistance to the drug have been observed. Mechanisms of resistance are not fully understood, but may include splice variants of the AR such as AR-V7 (33), copy number gain of the AR (111), and AR mutations including F876L (35).

CTCs are rare malignant cells that originate from the primary tumour or from other metastatic sites and can be detected in the peripheral blood (45). CTCs may act as a 'liquid biopsy' to monitor changes in response to treatment including the development of resistance (41). Higher CTC counts have been observed in patients with bone predominant metastases as compared with patients with visceral spread, which suggests a potential prognostic use for CTC testing in monitoring patients with bone disease in PCa (50). Enumeration of CTCs also represents a potential method for monitoring response to treatment over time. In addition, CTCs and circulating nucleic acids provide a substrate for serial biomarker assessment and investigation of the mechanisms of castration resistance. Prospective information on the effect of radium-223

combined with enzalutamide on CTCs is lacking, as are potential mechanisms of resistance.

The aims of this chapter were to (i) determine the safety and tolerability of the combination of radium-223 and enzalutamide in progressive mCRPC, (ii) examine if a combination of enzalutamide and radium-223 results in decreased CTC numbers throughout the study and (iii) determine if CTCs can be used as a potential surrogate response read out.

6.20 Results

3.1.1 ICORG 13-21

A phase II clinical trial (CTRIAL (ICORG) 13-21) of radium-223 in combination with enzalutamide in progressive mCRPC was initiated, with accrual in 4 cancer centres throughout Ireland. Each enrolled patient received the combination of radium-223 and enzalutamide for 6 cycles (Fig 3.1) until the patient discontinued the trial due to progressive disease as defined by the Prostate Cancer Working Group Criteria (PCWG2) criteria or due to unacceptable toxicity (Protocol is provided in Appendix I).

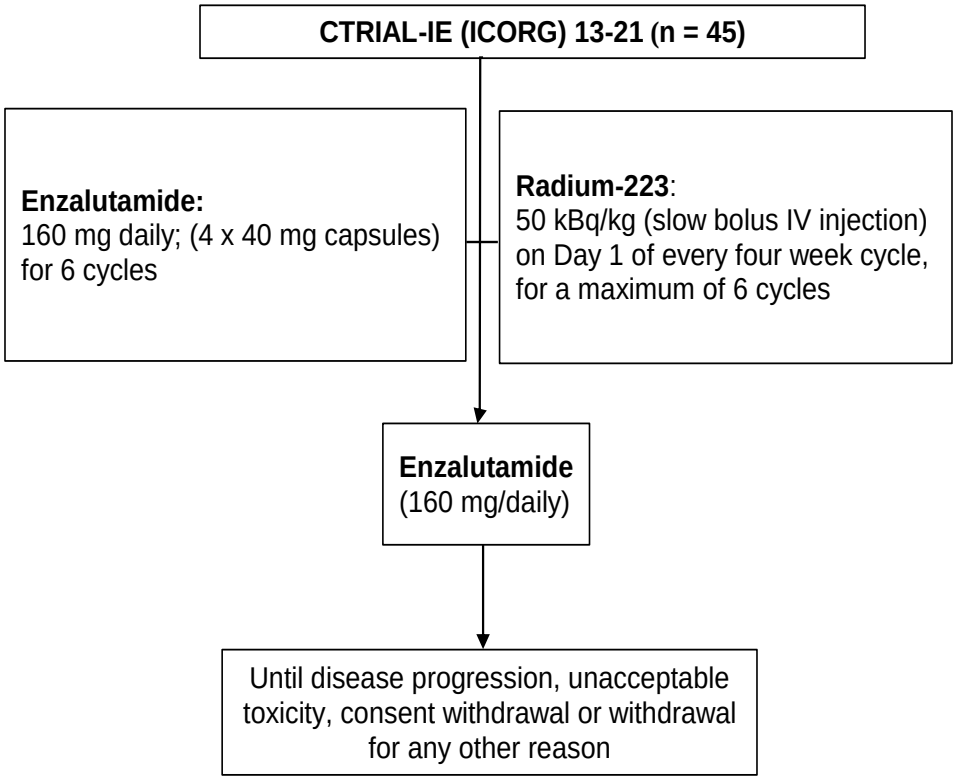

Figure 3.1. Study schema for CTRIAL (ICORG) 13-21 trial. All enrolled patients received six cycles of radium-223 and continuous daily enzalutamide until study discontinuation.

The trial was registered with Cancer Trials Ireland (formerly the All-Ireland Cooperative Oncology Research Group (ICORG)) as CTRIAL-IE (ICORG) 13-21 and with clinicalTrials.gov as NCT02225704. An enrolment period of 12 months from initiation was expected, however, an extension was granted to meet the defined target accrual.

3.1.2 Criteria for Definition of Progression of Disease

The Prostate Cancer Working Group (PCWG2) criteria (see Appendix 3) emphasises the importance of keeping patients on trial until radiographic or symptomatic progression and that an effort is made not to discontinue therapy solely on the basis of a rise in PSA in the absence of other indicators of disease progression (112).For the purpose of this study, clinical disease progression was defined using the radiologic criteria from PCWG2 and/or on the basis of symptoms attributable to the cancer. PSA progression alone was not used as a rationale for patient withdrawal from study.

3.1.3 Patient characteristics

Eligible patients for the study required histologically or cytologically confirmed adenocarcinoma of the prostate, and without neuroendocrine differentiation or small cell histology. Metastatic disease was confirmed by CT, MRI or bone scan. Patients were required to have documented progressive disease either by radiographic or PSA criteria. Prior docetaxel chemotherapy for metastatic hormone sensitive PCa was allowed. The Eastern Cooperative Oncology Group (ECOG) performance status was used at screening to assess all patients (Table 3.1). Patients must have had an ECOG performance status ≤ 2 to be eligible for the study. From July 2015 to July 2017, 45 patients were

enrolled in Ireland. The majority of patients had a ECOG performance status of 0-1 (n=44, 97.7%) (Table 3.2).

The median age of patients recruited was 67.6 years (range 51 – 79 years) (Table 3.3). Forty-two patients (93.3%) received all 6 cycles of combination therapy. The median baseline PSA for patients was 73.2 ng/mL (range 2.1 – 907.3 ng/mL). The median haemoglobin at baseline was 13.1 g/dL (range 9.7 - 15.9) and the median alkaline phosphatase was 158.2 IU/L (range 30 – 964) (Table 3.3).

Table 3.1. ECOG Performance Status Grading System.

ECOG Performance Status	
Grade	**ECOG**
0	Fully active, able to carry on all pre-disease performance without restriction
1	Restricted in physically strenuous activity but ambulatory and able to carry out work of a light or sedentary nature, e.g., light house work, office work
2	Ambulatory and capable of all self-care but unable to carry out any work activities. Up and about more than 50% of waking hours
3	Capable of only limited self-care, confined to bed or chair more than 50% of waking hours
4	Completely disabled. Cannot carry on any self-care. Totally confined to bed or chair
5	Dead

Table 3.2. ECOG Performance Status for patients recruited to ICORG 13-21.

ECOG	Frequency (n)	Percent (%)
0	17	37.78
1	27	60.00
2	1	2.22

Based on all enrolled patients (n=45).

Table 3.3. Baseline Characteristics of Patients recruited to ICORG 13-21.

Characteristic	Median (range)
Age	
Years	68 (51 - 79)
Biochemical values	
Total alkaline phosphatase (IU/L)	158.2 (39 – 964)
Haemoglobin (g/dL)	13.1 (9.7 – 15.9)
PSA (ng/mL)	73.2 (2.1 – 907.3)

Based on all enrolled patients (n=45).

3.1.4 Safety data

Adverse events (AEs) were graded 1 to 4 as per the Common Terminology Criteria for Adverse Events (CTCAE) version 4.0. The most common adverse events of all grades are shown (Table 3.4). Fatigue was the most common event occurring in 55.5% of all patients. Nausea was the second most common event, occurring in 46.6% of patients. Back pain was present in 22.2% of patients. Neutropaenia occurred in 20% of patients and hypertension was reported in 11.1% of patients.

A total of 13 patients (28.9%) had grade 3/4 toxicities (CI: 15.6% - 42.1%). Of these, 11 patients (24%) had grade 3/4 toxicities that were considered to be therapy related. The most frequent grade 3/4 AEs were neutropaenia (n=3, 6.6%) and fatigue (n=3, 6.6%) followed by nausea, LRTI, lymphocytopaenia, leukopaenia, hyperkalaemia, hypokalaemia, back pain, headache, urticaria, syncope and hypertension (all n=1, 2.2%). A total of 4 patients (9%) had serious combination therapy related AEs. Events that were considered serious were grade 3/4 neutropaenia, grade 2 fatigue, grade 2 LRTI, grade 1 iron deficiency, grade 1 elevated CRP and grade 2 back pain. Two patients (4.4%) discontinued treatment due to AEs: grade 3 LRTI (n=1), and grade 2 nausea and pain (n=1) (Table 3.5). Only 2 patients had their treatment delayed due to a AEs. There were no therapy-related deaths. Disease progression was confirmed using the PCWG2 criteria from 2007. Only one patient was withdrawn from the study during the combination treatment arm due to progressive disease.

Table 3.4. The most frequent AEs.

AE	Grade 1	Grade 2	Grade 3	Grade 4	Total (n) (%)
Fatigue	14	8	3	0	25 (55.5)
Nausea	14	6	1	0	21 (46.6)
Back pain	6	3	1	0	10 (22.2)
Neutropaenia	1	5	2	1	9 (20)
Headache	4	1	1	0	6 (13.3)
Lymphocytopaenia	1	3	1	0	5 (11.1)
Leukopaenia	2	2	1	0	5 (11.1)
Hypertension	0	4	1	0	5 (11.1)
LRTI	0	3	1	0	4 (8.8)
Urticaria	0	0	1	0	1 (2.2)
Syncope	0	0	1	0	1 (2.2)
Hypokalaemia	0	0	1	0	1 (2.2)
Hyperkalaemia	0	0	1	0	1 (2.2)

AEs based on all enrolled patients (n=45).

Table 3.5. Combination therapy AEs leading to discontinuation or delay of radium-223 and enzalutamide.

AE	Grade 2	Grade 3	Total
Neutropaenia	0	1	1
Nausea	1	0	1
Pain	1	0	1
LRTI	0	1	1
Urticaria	0	1	1

AEs based on all enrolled patients (n=45).

3.1.5 CTC collection

CTCs were collected using a ScreenCell® filtration device (refer to Methods 2.7). CTCs were collected at baseline and every four months (± 1 month) as per trial protocol (Appendix I). CTC filters were stained with a modified MGG, and CTCs were enumerated in conjunction with a consultant histopathologist (Dr Brian Hayes, Cork University Hospital) (Fig 3.2). The change in CTC number over time was assessed.

3.1.6 Effect of Radium-223 and enzalutamide on CTC numbers

CTCs were collected at baseline and throughout treatment with the combination treatment, and after the patient completed the combination and continued enzalutamide alone. CTCs were analysed per 6 mL volumes of blood (Fig 3.3). The average CTC count at baseline (n=44 patients) was 19.6 (SEM ± 3.0). After 3 cycles of radium-223 and enzalutamide, repeat CTC counts were performed (n=44). The average CTC count prior to receiving their fourth cycle (C4D1) of combination treatment was 17.8 (SEM ± 2.7). CTC counts were measured 4 weeks after completion of radium-223 and enzalutamide on cycle 7 day 1 (C7D1) (Fig 3.3). The average count was 22.6 for 45 patients (SEM ± 2.9). Following completion of combination therapy, patients continued on enzalutamide alone and CTC counts continued to be enumerated. CTC counts initially dropped to 17.2 (SEM ± 2.6) 12-20 weeks post radium-223. However, on subsequent analysis (20 weeks post radium-233) there was a steady increase in CTC numbers on enzalutamide alone. At timepoint 5, the CTC count was 19.1 (SEM ± 4.4) and 26.9 (SEM ± 3.9) at timepoint 6. There was no statistical difference in CTC counts over time.

A.

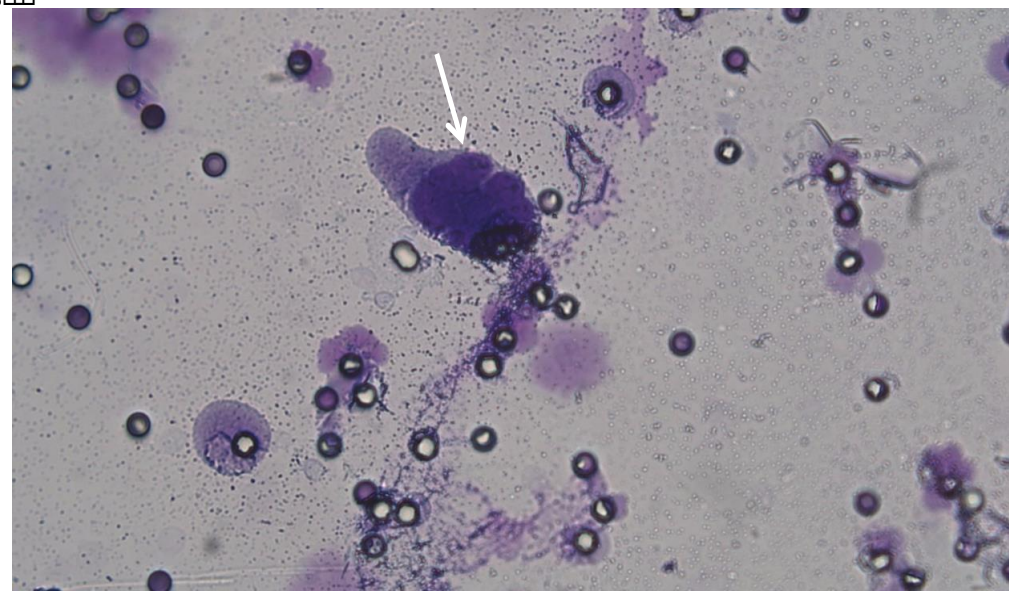

B.

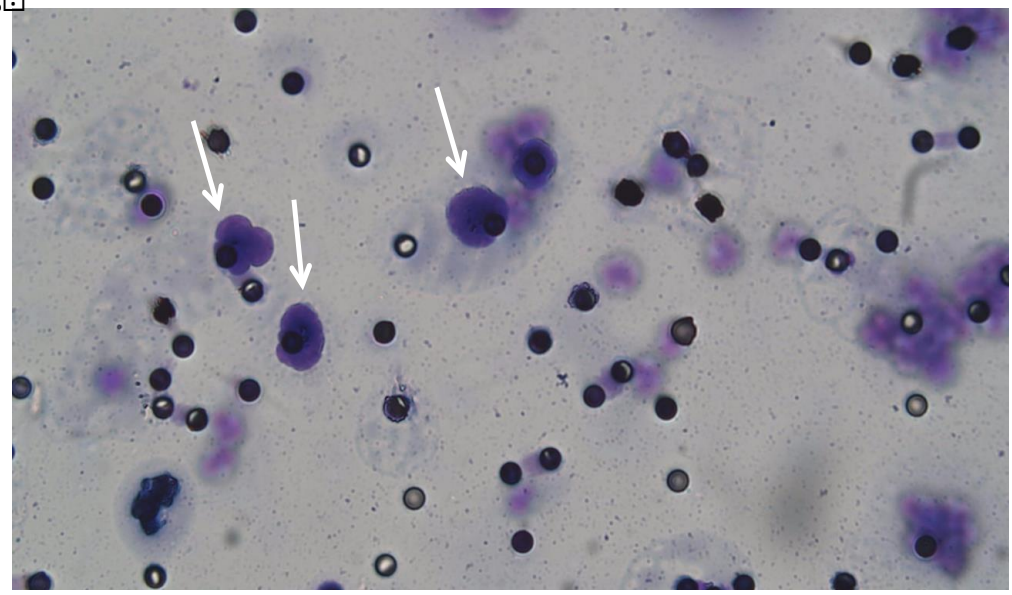

Figure 3.2. Representative images of CTCs on ScreenCell® filters stained with MGG.

White arrows indicate (A) A single visible CTC and (B) A cluster of CTCs.

(Magnification at 40X)

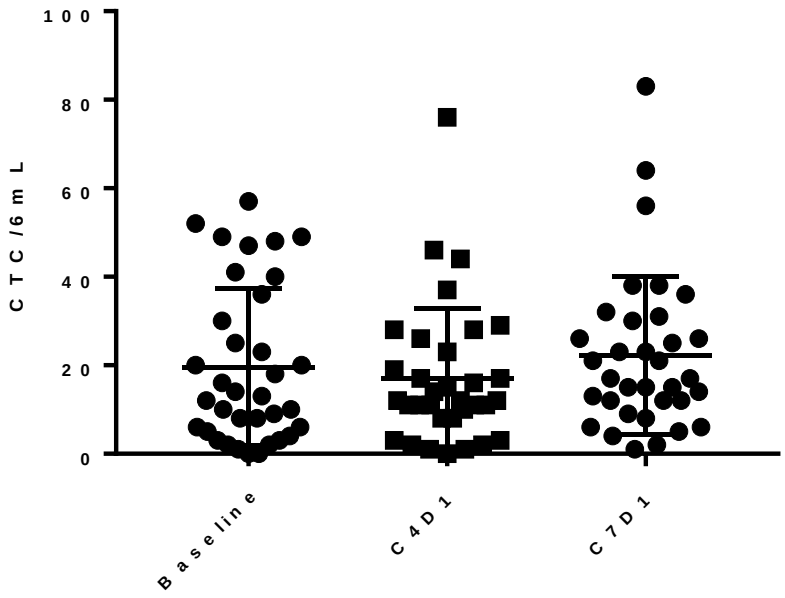

Figure 3.3. CTC counts throughout treatment with the combination of radium-223 and enzalutamide.

(Baseline n=44*, C4D1 n=44*, C7D1 n=45; Data graphed as raw values)

(Note: Enzalutamide only data not shown; post C7D1)

* One patient CTC count excluded due to insufficient volume of sample

3.1.7 CTC counts according to prior response to ADT

CTC counts were analysed in a cohort of 23 patients, who were stratified based on prior ADT response. Those that progressed quickly on ADT (<18 months) to become castration resistant were classed as poor responders (n=11). Those patients who demonstrated longer response rates to ADT (>18 months) and remained hormone sensitive were classed as good responders (n=12). In both groups, radium-223 combined with enzalutamide resulted in a decline in CTC numbers, however this was not significant (Fig 3.4 and Fig 3.5). Poor responders had a baseline average CTC count of 22.5/6 mL (SEM ± 5.9) with an average count of 19.4/6 mL (SEM ± 7.0) by cycle 4, however after completion of radium-223 (C7D1) the average CTC count had risen to 22.9 (SEM ± 4.9) (Fig 3.4).

There was also no significant difference in CTC numbers in those classed as good responders. Average baseline CTCs were 14.4/6 mL (SEM ± 4.9), which dropped to 12.5/6 mL (SEM ± 2.1) by cycle 4. Upon stopping radium-223, the average CTC count at cycle 7 increased to 14.7 (SEM ± 3.5) (Fig 3.5). CTC numbers were lower in good responders *vs.* poor responders from baseline through until C7D1.

Correlation of CTC counts with PSA, alkaline phosphatase and haemoglobin at base line was performed. There was no statistically significant correlation in these laboratory parameters and CTC counts.

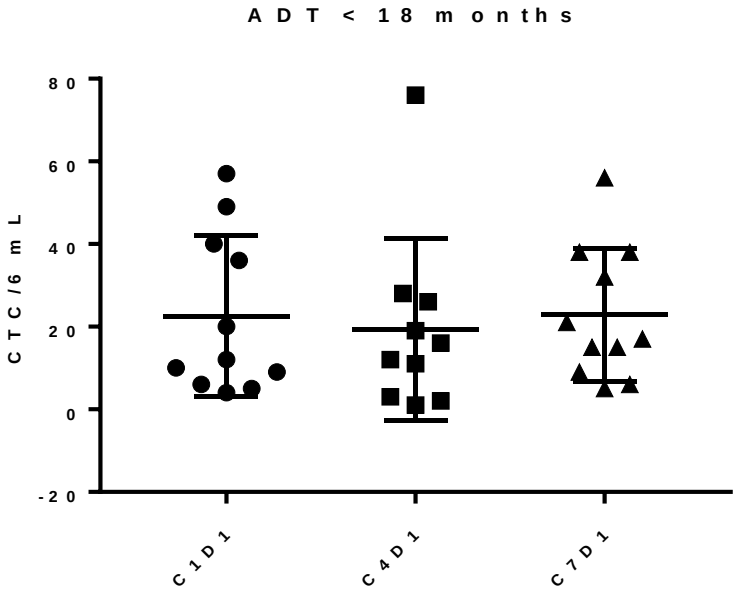

Figure 3.4. CTC counts in patients who progressed rapidly on ADT (within 18 months) treated with radium-223 and enzalutamide combination therapy. (n=11; Data graphed as raw values)

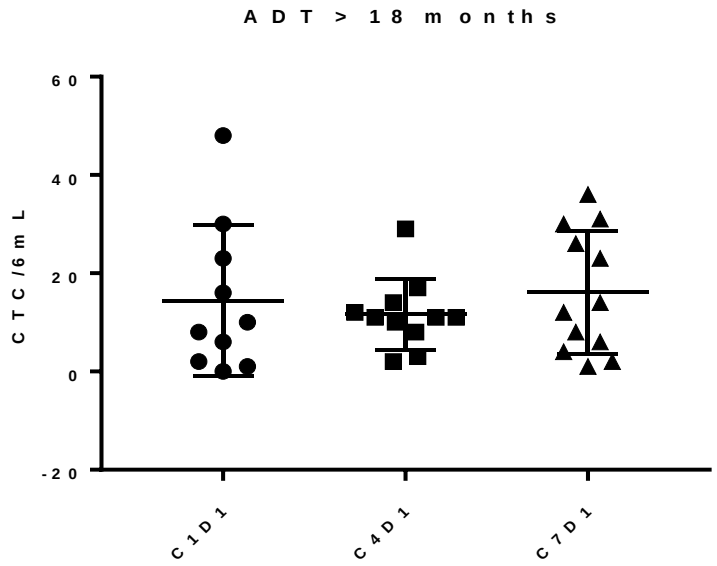

Figure 3.5. CTC counts in patients who progressed on ADT after 18 months treated with radium-223 and enzalutamide combination therapy.

(C1D1 n=10, C4D1 n=11, C7D1 n=12; Data graphed as raw values).

6.21 Discussion

Evaluating drugs to treat PCa has previously posed unique challenges due to its biology and long natural history. The combination of radium-223 and enzalutamide is of interest as they are well-tolerated agents, which have differing modes of action (24, 30). Therefore, a phase II clinical trial of radium-223 in combination with enzalutamide in progressive mCRPC was designed. The primary endpoint was safety analysis for the combination treatment. A translational study was also developed alongside the clinical study in order to collect and analyse CTCs, blood samples and archival tissue from these patients for research purposes (Full protocol provided in Appendix I).

Forty-five patients were enrolled on to the trial by June 2017. All patients had confirmed mCRPC to bone that had progressed on ADT and met all eligibility criteria as per the protocol (Appendix I). The baseline characteristics of patients recruited to this study were similar to other studies in this subgroup of patients (30). The median age was 68 (51 – 79), reflecting the older age population group witnessed in PCa. The median PSA at screening was 73.2 ng/mL with a range of 2.1 ng/mL – 907.3 ng/mL. The majority of patients had an ECOG performance status of 0 to 1, with only 1 patient presenting with an ECOG of 2 at screening. This reflected a subgroup of men with mCRPC with an excellent performance status and few comorbidities. This would be in keeping with prior clinical trials that have recruited patients with a good performance status. Indeed, in the ALSYMPCA study, a phase III study by Parker *et al.* examining radium-223 in patients with mCRPC, 87% of patients had an ECOG performance status of 0-1 (30).

In this study, the majority of patients completed all six cycles of radium-223 and enzalutamide combination therapy, meaning this combination was a well-tolerated and acceptable regimen for patients. A total of 13 patients (28.9 %) had grade 3 or 4 toxicities. Of these, a total of 11 patients (24 %) had grade 3/4 toxicities that were considered to be therapy related. This rate was lower than expected when compared to previous studies examining these agents as single therapies. In the previous phase III ALSYMPCA study, 56% of patients developed grade 3/4 toxicity (30). Similarly, in the PREVAIL study by de Beer *et al.*, 43% of patients treated with enzalutamide for mCRPC developed grade 3/4 toxicities (17). In this study, the most frequent grade 3/4 adverse events were neutropaenia (n=3, 6.6%) and fatigue (n=3, 6.6%). Neutropaenia was most likely related to radium-223. This is consistent with data reported in previous studies looking at this agent (30). Similarly, fatigue was a commonly reported AE in prior enzalutamide studies (17). In this study, only 2 patients (4.4%) discontinued treatment due to AEs. One patient had a grade 3 LRTI (n=1) and the second patient had both grade 2 nausea and pain (n=1). A total of 2 patients had their treatment delayed due to an AE. There were no therapy-related deaths.

As a possible surrogate read out to treatment response, CTCs were enumerated throughout the course of treatment. A previous study has identified a CTC count of <5 CTCs/7.5 mL of blood, prior to treatment, to be associated with a favourable survival compared with patients with ≥5 CTCs/7.5 mL of blood (50). All enrolled patients in ICORG 13-21 had blood drawn at baseline for CTC analysis and at subsequent four-month intervals throughout therapy (±

1 month). A size-based filtration assay, ScreenCell®, was employed in combination with an MGG stain to visualise CTCs under the microscope. A consultant histopathologist assessed CTC numbers. Available CTC results were analysed at baseline, cycle 4 day 1 (C4D1) and after completion of radium-223 at cycle 7 day 1 (C7D1). CTC levels were reported per 6 mL of blood; however, some samples were omitted due to low blood volumes and were excluded from the analysis. There was a decline in CTC counts during treatment identified at C4D1, however this was not sustained at C7D1 after completing radium-223. There was no significant difference in CTC numbers over time with the combination of radium-223 and enzalutamide. Similarly, when clinical data such as PSA, haemoglobin and alkaline phosphatase were assessed, there was no correlation between these clinical parameters and CTC numbers.

A cohort of patients were stratified based on ADT response. Patients who progressed to castration-resistant disease while on ADT for less than 18 months (poor responders) (n=11) were compared to patients who had remained on their ADT for longer than 18 months (good responders) (n=12). Patients who progressed rapidly to CRPC on ADT are known to have an overall worse prognosis (7). CTC counts between the two groups at baseline were measured. CTC counts were higher at baseline in the poor responders group compared to the good responders. After four cycles of treatment with radium-223 and enzalutamide combination therapy, there was a noticeable reduction in CTC numbers in both groups. After withdrawal of radium-223 CTC numbers

increased in poor and good responders. However, this was not statistically significant, perhaps due to small number of patients in both groups.

The combination of radium-223 and enzalutamide is safe and well tolerated, with the majority of patients completing all planned cycles of combination treatment. Furthermore, the combination of radium-223 and enzalutamide appears to be effective in reducing CTC numbers in patients. One proposed hypothesis for radium-223's effect on CTCs is osteomimicry, a form of epithelial plasticity leading to an osteoblastic phenotype of CTCs, which may contribute to the uptake of radium-223 within bone metastases and may thereby enhance the therapeutic benefit of radium-223 (113, 114). This could lead to CTCs being potentially used as a surrogate read out for the effect of radium-223 and could allow for continuous ongoing monitoring of response to treatment. Therefore, CTCs could have the potential to be used as a predictive biomarker for response to treatment. Future studies examining radium-233 as a single agent *vs*. combination treatment may be warranted, however a more detailed analysis of the results of this trial is awaited, including clinical outcomes. These outcomes, including clinical parameters, will be correlated to CTC numbers and may lend further knowledge to the link between osteomimicry and radium-223 treatment. Long-term efficacy data is awaited and will be reported in time; however, this is outside the scope of this thesis.

Chapter 4: Tumour heterogeneity in Metastatic Prostate Cancer

6.22 Introduction

In recent years, several new treatments for metastatic PCa have become available, such as abiraterone and enzalutamide, which has expanded the options for patients (17, 18). Not all patients respond in the same way to these treatments; therefore, it is important to find markers to stratify patients for therapy and to give an indication of an individual patient's response. Although PCa is the most common malignancy to affect men in the Western world, the molecular mechanisms underlying its development and progression remain poorly understood (4). Like other cancers, PCa has a genetic contribution that is characterized by multiple genomic alterations, including point mutations, microsatellite variations, and chromosomal alterations (115). The development and application of novel sequencing technologies has significantly accelerated the detection of genomic alterations, revealing the complex nature and heterogeneity of the disease. However, the assessment of the genomic landscape of advanced PCa has been difficult, primarily because of limited access to tissue and technologies that require large amounts of DNA and RNA, and the fact that most patients with advanced PCa do not undergo repeat biopsies of metastases as part of routine clinical care.

Bone metastases, characteristically osteoblastic, are the most frequent site for the spread of PCa with pelvic bones, vertebrae, and ribs, the most common sites to harbour metastatic deposits (116). The use of a bone marrow biopsy (performed without real time imaging) in metastatic PCa, as a method of tissue acquisition, was previously described in 1952 by Rubinstein *et al.* (117). However, bone marrow biopsies are not standard of care in the management of men with metastatic PCa, due to the lack of sensitivity and

associated morbidity, but may be used for research purposes to acquire metastatic samples from bone lesions. Targeted (performed using real time imaging e.g. CT guided) metastatic biopsy is also an important tool in the evaluation of metastatic lesions. Several factors have been shown to affect biopsy yield in metastatic PCa and should be considered. They include the use of image guidance (real time, non-real time, none), type of biopsy and number of attempts (fine needle aspiration, core biopsy), and eventual processing or analysis (decalcification, IHC, DNA analysis, RNA analysis, etc.) (118). Bone metastases, nodal disease or visceral lesions constitute indications for CT-guided percutaneous biopsy.

Having sufficient tissue samples is important in order to allow for intensive testing including NGS. NGS studies have led to significant advances in the understanding of the cancer genome of several tumour types, and current efforts are aimed toward bringing sequencing discoveries into the clinic in the form of biomarkers (diagnostic, prognostic, and predictive) and biomarker-designed clinical trials. The Irish Programme for Stratified Prostate Cancer Therapy (iPROSPECT) translational study (Full protocol provided in Appendix II) was developed in order to allow researchers to prospectively collect clinically relevant bio-specimens from patients with metastatic PCa with matched clinical data. iPROSPECT consists of several interconnected projects, each of which aims to analyse patients' samples throughout the course of the disease and integrate their results with the clinical information in order to understand and better predict response to treatments.

The aims of this chapter were to (i) enumerate CTCs throughout the course of the study, (ii) collect metastatic biopsy samples from patients recruited to iPROSPECT and determine the optimal biopsy method, and (iii) molecularly characterise metastatic advanced PCa and to identify potential predictive novel targets.

6.23 Results

4.1.1 iPROSPECT Study

To date 56 patients have been enrolled on the iPROSPECT study (accrual target 60), across two cohorts of patients (Fig 4.1). Cohort 1 recruited 15 patients, which included patients with visceral and/or bone lesions (excluding patients who had only nodal metastatic disease), who had commenced or were about to commence ADT and whose disease had not shown any evidence of castration resistance (hormone-sensitive). Cohort 2 recruited 41 patients, which included patients with visceral disease and/or bone lesions, who had developed castration-resistant disease while receiving ADT. Advanced metastatic PCa was confirmed by CT, MRI or by bone scan. Archival FFPE samples from the standard diagnostic biopsy or radical prostatectomy was accessed for all cohorts if available. Clinical data was collected for each patient including PSA, Gleason Score, alkaline phosphatase, lactate dehydrogenase (LDH) and medical history including prior treatments.

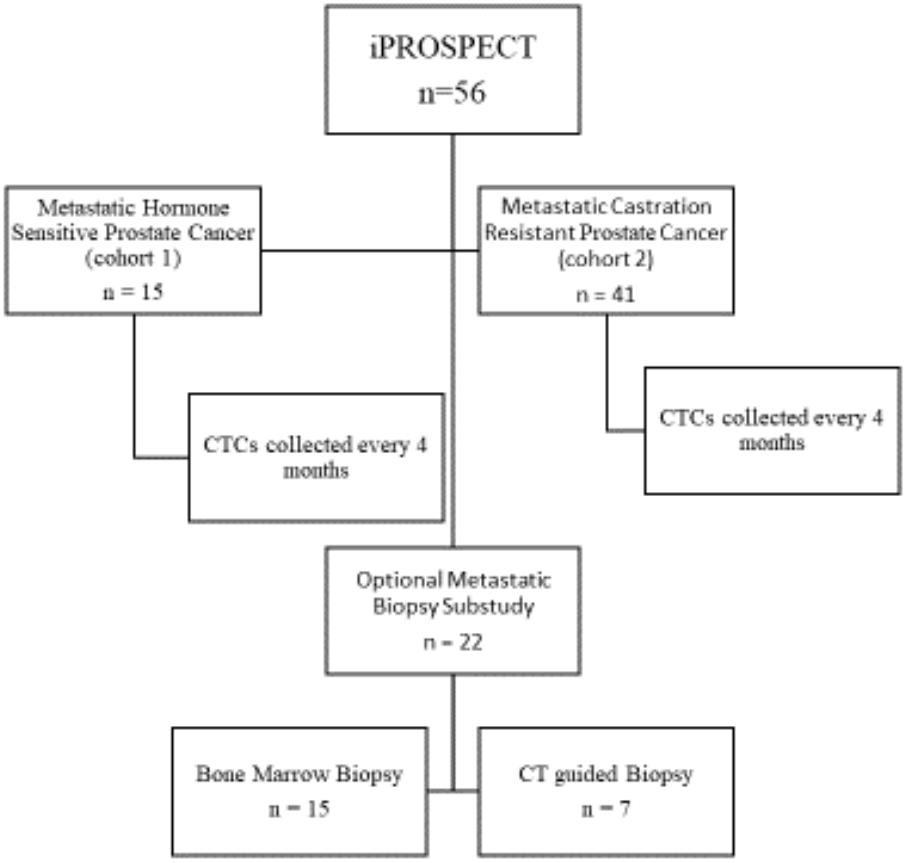

Figure 4.1. Schema of iPROSPECT study. Optional sub-studies included a bone marrow biopsy or a CT guided biopsy of a metastatic deposit.

4.1.2 Patient characteristics

A total of 15 patients with hormone sensitive PCa were recruited to cohort 1. The baseline characteristics for cohort 1 are listed in Table 4.1. The mean age for patients was 67 years (range 51 - 81). The median baseline PSA at recruitment was 31 ng/mL (range 0.3 - 261.2 ng/mL) and the average Gleason Score for this cohort was 8 (range 7- 9). All patients recruited to the study had baseline blood tests performed including alkaline phosphatase and LDH levels. Overall, the median LDH at baseline was 263 IU/L (range 170 – 402 IU/L). Four patients were excluded from this analysis as they had no LDH measurement taken at baseline. The median alkaline phosphatase at baseline was 298 IU/L (range 35 – 2145 IU/L). All patients recruited to cohort 1 had bone metastatic disease (Fig 4.2). Two patients had both bone and lymph node metastases (13%).

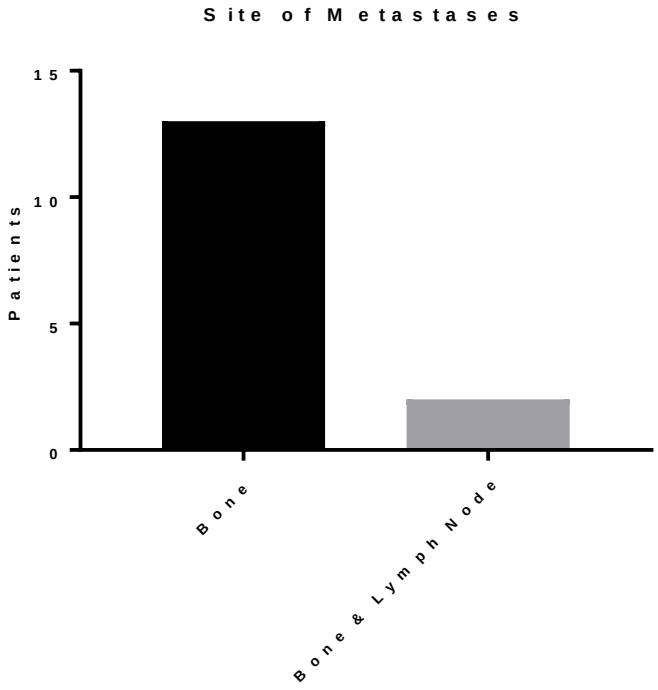

Figure 4.2. Site of metastases for cohort 1. Bone metastases were the most prominent.

(n=11)

A total of 41 patients with CRPC were recruited to cohort 2. Baseline characteristics are listed in Table 4.1. The median age at screening was 69 years of age (range 57 - 85). PSA data was available for 34 patients. The median PSA at screening for these patients was 173 ng/mL (range 2 – 1337 ng/mL). For the available biopsy results (n=27), the average Gleason score was 8 (range 6 - 10).

The median LDH at screening was 378 IU/L (range 167 – 1323 IU/L) and the average alkaline phosphatase was 195 IU/L (range 43 – 1060 IU/L). All patients had bone metastatic disease (Fig 4.3). Of these, 13 patients also had lymph node involvement (42%) and 9 patients (27%) also had visceral involvement (lung n=7, liver n=4, and adrenal metastases n=1).

Table 4.1. Baseline characteristics of patients recruited to cohort 1 and cohort 2.

	Cohort 1 (n=15)	**Cohort 2 (n=34)**	**p value ***
Age (Years)			
Median (range)	67 (51 - 81)	69 (57 - 85)	0.3010
Gleason Score			
Median (range)	8 (7 – 9)	8 (6 – 10)	0.5738
Median biochemical values (range)			
Total alkaline phosphatase (IU/L)	298 (35 – 2145)	195 (43 – 1060)	0.3403
LDH (IU/L)	263 (70 – 402)	378 (167 – 1323)	0.2216
PSA (ng/mL)	31 (0.3 - 261.2)	173 (2 – 1337)	0.0888

* Student t test, unpaired

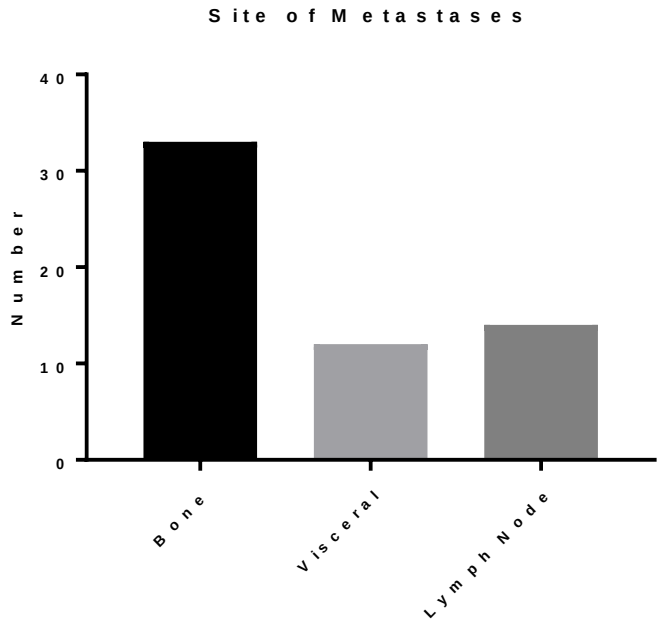

Figure 4.3. Sites of metastatic disease for cohort 2. Bone was the most common site followed by lymph node involvement and visceral involvement

4.1.3 CTCs

Patients recruited to iPROSPECT had CTCs drawn at baseline, when starting a new treatment and at 4-month intervals (± 1 month) throughout their treatment. In cohort 1, the mean baseline CTC count was 20/6 mL of whole blood (SEM ± 5.0) which rose to 29.5/6 mL (SEM ± 5.8) at follow up 1 (FU1) and then reduced to 13.9/6 mL (SEM ± 3.1) at follow up 2 (FU2) (Fig 4.4). In cohort 2, the mean CTC count was 14.4/6 mL (SEM ± 2.6) at baseline then rose to 17.4/6 mL (SEM ± 4.8) at FU1 and reduced to 11.6/6 mL (SEM ± 2.4) at FU2 (Fig. 4.4). There was no statistical difference between the groups.

4.1.4 Metastatic biopsies in prostate cancer

Optional metastatic sub-studies were offered to all eligible patients. All patients undergoing a procedure had informed consent taken for their sub-study. From 56 patients on trial, 22 patients (39.3%) consented to undergo an optional biopsy (CT guided or bone marrow biopsy) of a metastatic lesion (Fig 4.5). Of these, 15 patients with bone metastases (68.2%) underwent a bone marrow biopsy, 3 patients (13.8%) underwent a CT guided liver biopsy due to the presence of liver metastases, 2 patients (9%) had a CT guided biopsy of an enlarged lymph node and 2 patients (9%) had a targeted bone biopsy (one patient underwent a CT guided biopsy of a bone lesion and a second patient had a bone lesion surgically resected).

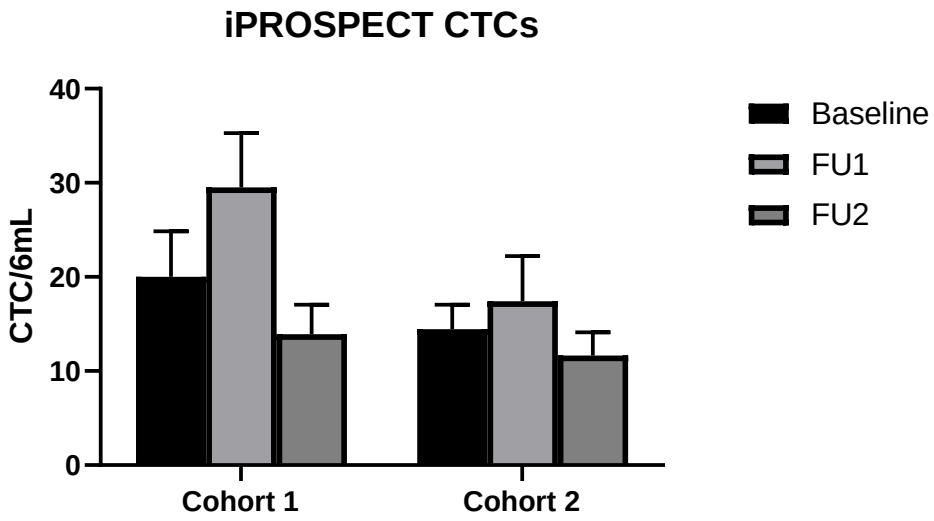

Figure 4.4. CTC counts in patients recruited to iPROSPECT cohort 1 and cohort 2. Using an ANOVA comparing all means (i.e. C1 vs C2, and timepoints vs each other) – no significance. (For cohort 1, baseline n=15, FU1 n=12, FU2 n=10; Data graphed as mean ± SEM. For cohort 2, baseline n=43, FU1 n=36, FU2 n=28; Data graphed as mean ± SEM).

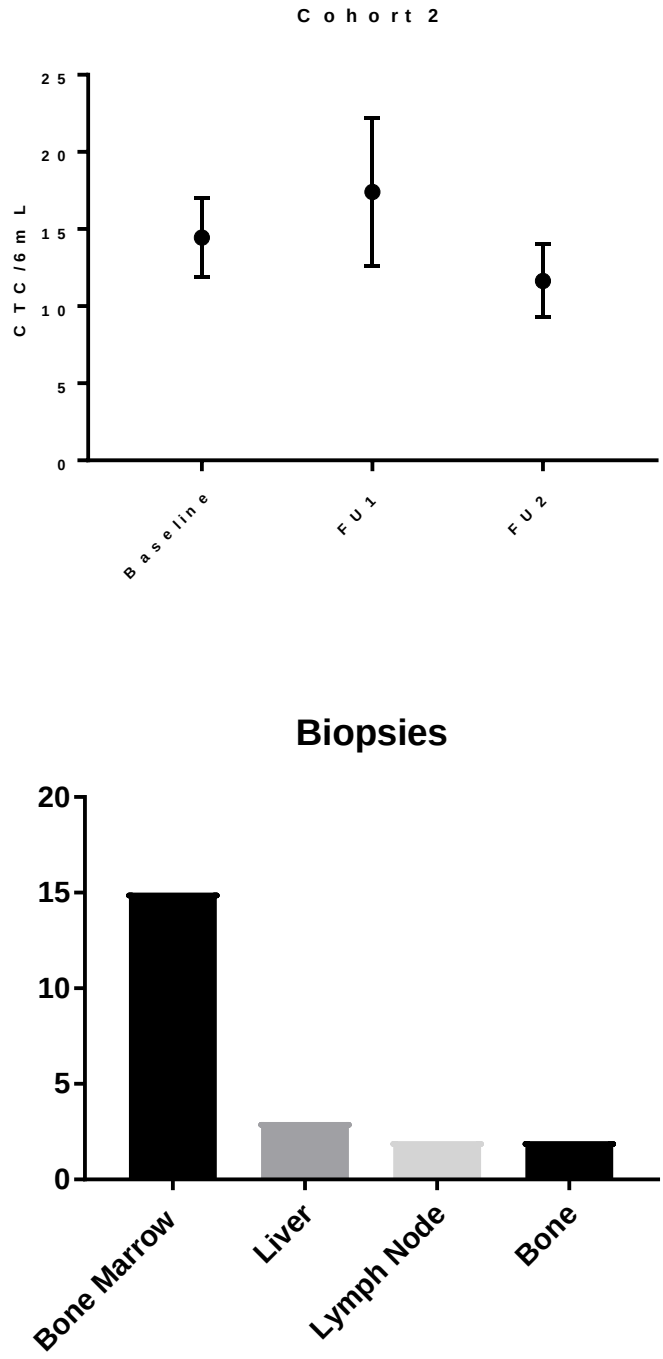

Figure 4.5. Total number of biopsies performed in iPROSPECT sub-studies. The majority of patients had a bone marrow biopsy performed (68.2%). Other patients underwent a CT guided biopsy of a liver lesion (13.8%), lymph node (9%) or bone metastases (9%).

4.1.5 Sensitivity of bone marrow *vs.* CT guided metastatic biopsies

CT guided biopsies were compared to bone marrow biopsies by assessing the pathological reports for each biopsy. The presence or absence of carcinoma was recorded using IHC. For the 15 bone marrow biopsies performed without any real-time imaging guidance, four samples (26.67%) were positive for carcinoma compared to all six samples being positive (100%) for carcinoma performed using real-time imaging guidance by CT guided techniques. Overall, CT guided biopsies were more sensitive ($p \leq 0.01$) at diagnosing carcinoma than bone marrow biopsies in patients with metastatic PCa (Fig 4.6).

4.1.6 Bone marrow biopsies

Patients with bone metastases were offered a bone marrow biopsy to obtain tissue from a metastatic deposit to allow further analysis including IHC and NGS. Bone scans were reviewed prior to the procedure to confirm the presence of bone metastases. Bone marrow biopsies were performed on an oncology dayward. Specimens were processed into FFPE as per local hospital guidelines (Appendix III). All bone samples underwent a decalcification process. Slides were reviewed and reported at the local hospital site. A second review was undertaken at the St. James's Hospital Central Pathology Laboratory. A sample bone marrow infiltrated with adenocarcinoma is shown in Fig 4.7A/B, stained with H&E. Staining with pan cytokeratin AE1/AE3 was used to confirm the presence of malignant cells (Fig 4.7C).

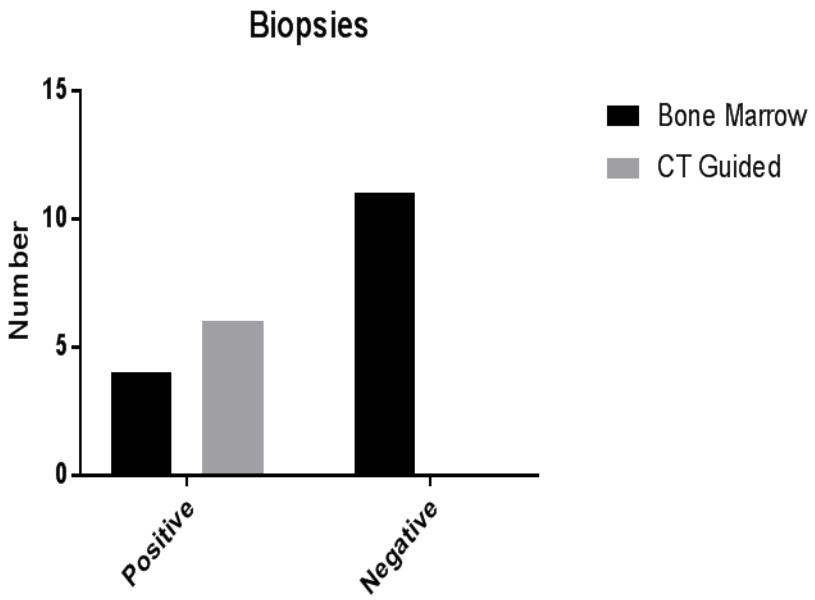

Figure 4.6. Sensitivity of bone marrow biopsies *vs.* CT guided biopsies. CT guided biopsies using real time imaging were more sensitive at collecting metastatic sample compared to using a bone marrow biopsy. Data analysed using a chi-square test. ($p < 0.01$; CT guided positive biopsies *vs.* bone marrow positive biopsies).

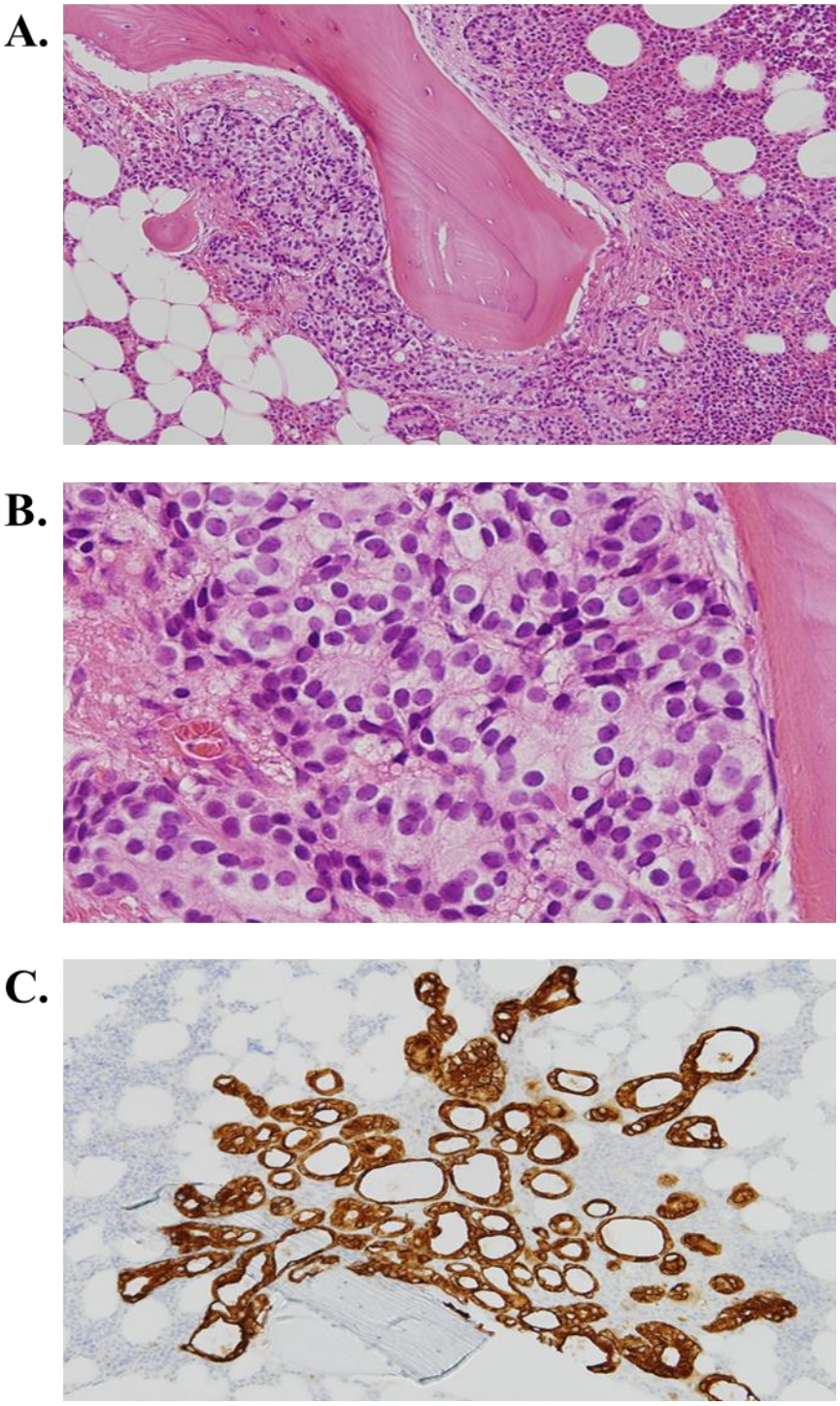

Figure 4.7. Bone marrow sampling in a patient recruited to iPROSPECT with metastatic PCa. (A) H&E showing metastatic adenocarcinoma (10X), (B) H&E showing metastatic adenocarcinoma (40X), (C) Pan Cytokeratin AE1/3 positivity (10X).

4.1.7 Biochemical data

Alkaline phosphatase is a bone marker that is elevated when the bone marrow is infiltrated with carcinoma (116). Alkaline phosphatase levels were reviewed to determine if there was any association with a positive bone marrow result. The mean alkaline phosphatase for patients with positive bone marrow for carcinoma was 296 IU/L (range 104 – 438 IU/L) and for patients with no evidence of carcinoma was 148 IU/L (range 43 – 740 IU/L). There was no significant correlation between alkaline phosphatase levels and a positive bone marrow result (Fig 4.8). Furthermore, PSA levels at time of biopsy were analysed to identify if there was any correlation with a positive bone marrow. The mean PSA for patients with a positive bone marrow was 66 ng/mL (26 – 87 ng/mL) and slightly lower in negative bone marrows at 42 ng/mL (5 – 261 ng/mL), however this was also not significant (Fig 4.9).

4.1.8 Lymph node, liver and bone biopsies

In total, 2 patients underwent CT guided biopsies of a lymph node, which confirmed the presence of adenocarcinoma consistent with metastatic PCa (Fig 4.10A and B). In total, 4 patients recruited to iPROSPECT developed liver metastases, of which 3 underwent a targeted CT guided biopsy of a liver lesion. Two patient biopsies had confirmed adenocarcinoma (Fig 4.11A and B). PSA expression was positive using IHC, in both adenocarcinoma samples with negative neuroendocrine profiling consistent with metastatic PCa. The third patient had developed neuroendocrine differentiation.

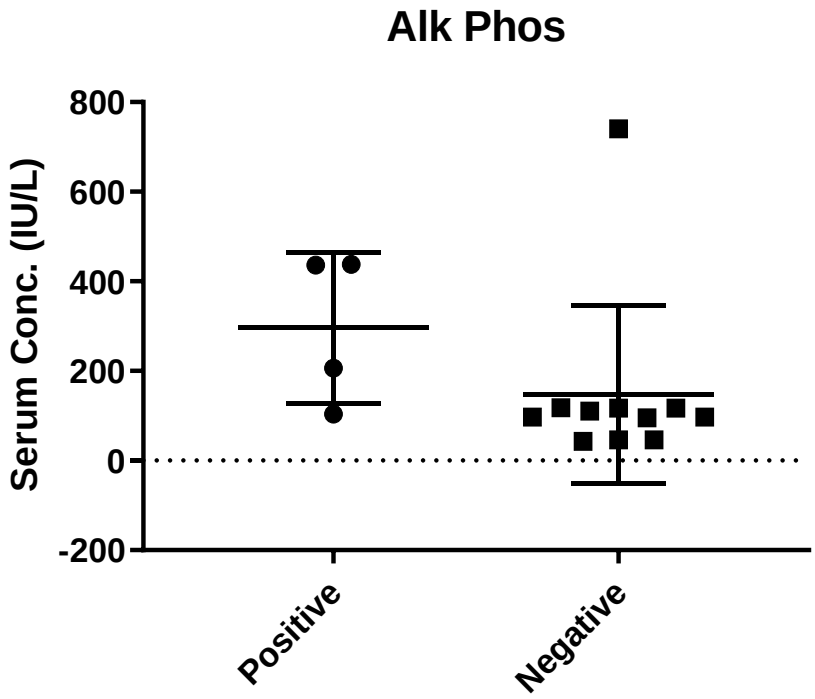

Figure 4.8. Alkaline phosphatase value comparisons of positive and negative bone marrow biopsies. There was no significant difference in values. Data Graphed as mean ± SEM. Unpaired Student t test (P=0.3430)

(Alkaline phosphatase = Alk Phos)

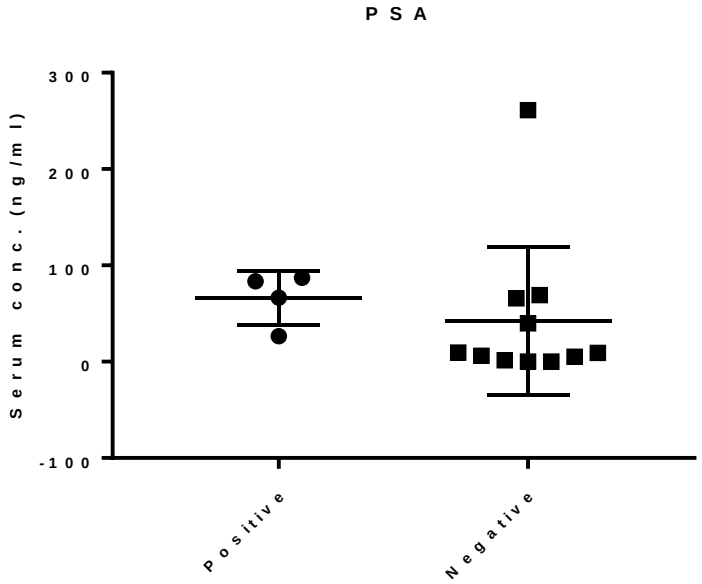

Figure 4.9. PSA value comparisons of positive and negative bone marrow biopsies. There was no significant difference in values. Data Graphed as mean ± SEM. Unpaired Student t test (P=0.08).

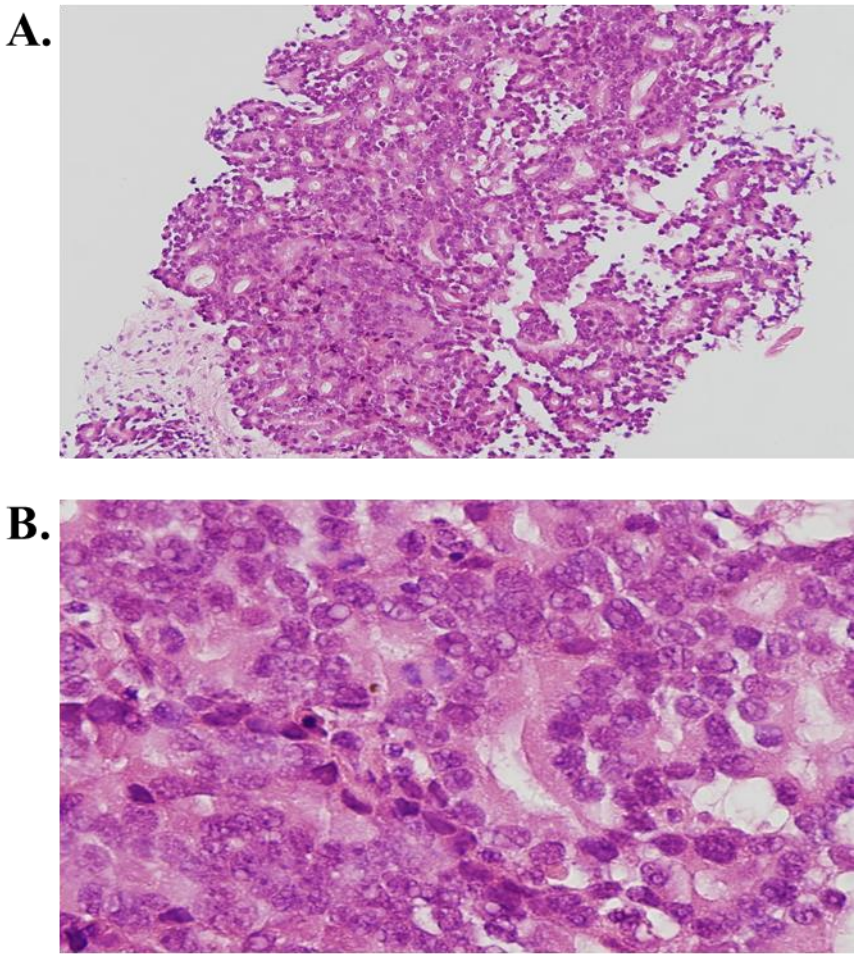

Figure 4.10. Lymph node biopsy showing metastatic adenocarcinoma. Images at (A) 10X and (B) 40X.

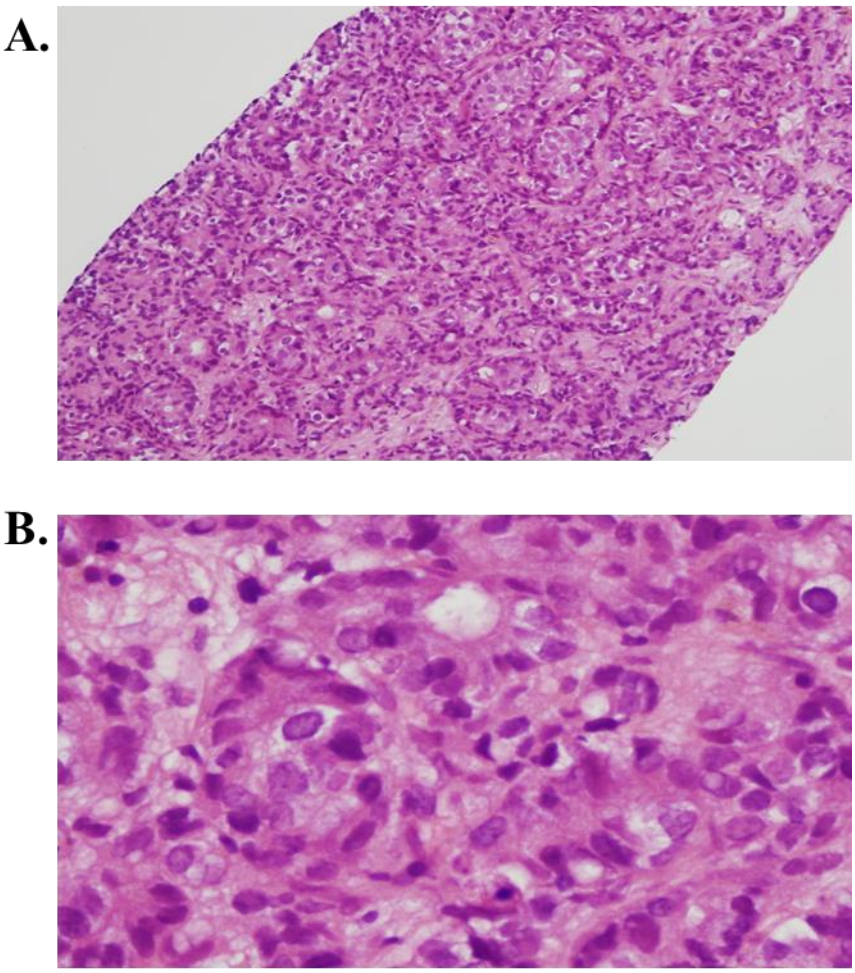

Figure 4.11. Liver biopsy showing metastatic adenocarcinoma.

Images at (A) 10X and (B) 40X.

4.1.9 Neuroendocrine differentiation in PCa

Clinical specimens obtained from metastatic lesions were analysed for evidence of neuroendocrine differentiation. In total, 11 metastatic samples underwent a second review by a pathologist, for evidence of neuroendocrine differentiation. Out of 11 biopsies, a single biopsy showed the presence of neuroendocrine disease. Histopathological review of this biopsy confirmed cores of liver tissue infiltrated by a small cell carcinoma (Fig 4.12A and B). The tumour was positive for neuroendocrine markers pan-cytokeratin (AE1/3), CD56, chromogranin, synaptophysin and thyroid transcription factor 1 (TTF-1). The tumour was negative for PSA, proPSA (PPSA) and prostatic specific acid phosphatase (PSAP). The original diagnostic biopsy had previously shown invasive prostatic adenocarcinoma, which was Gleason Score 3+4=7.

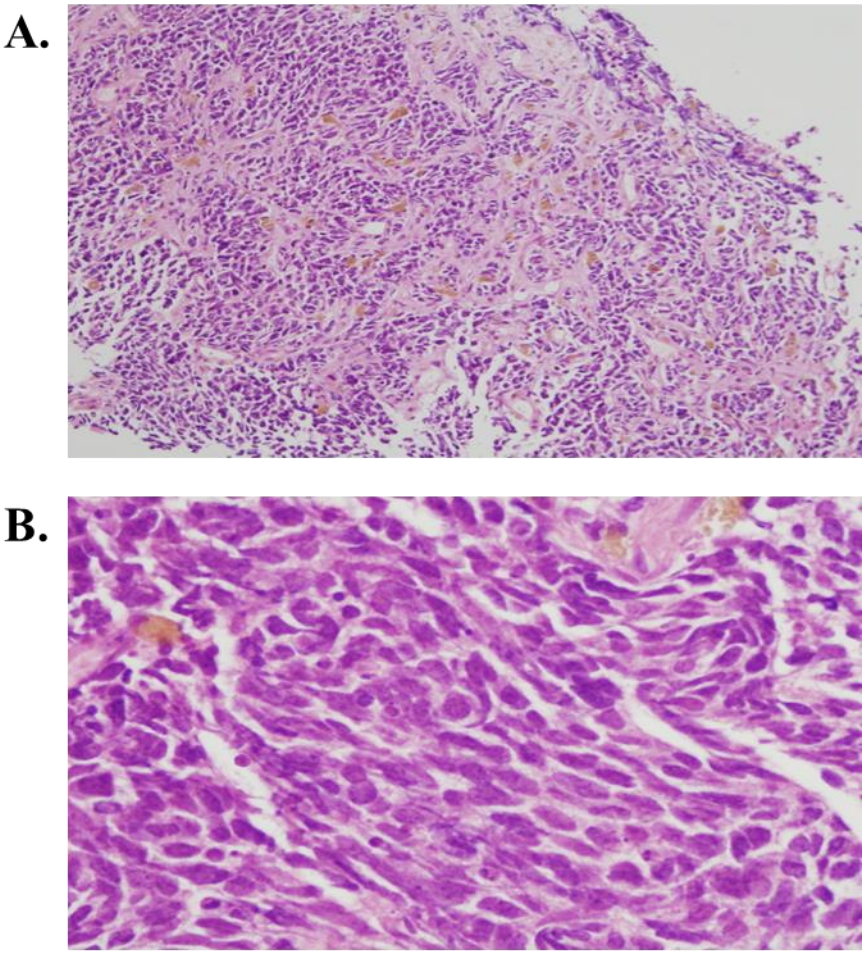

Figure 4.12. H&E of liver biopsy from iPROSPECT sample. Sample infiltrated with small cell carcinoma shown here at (A) 10X and (B) 40X.

4.1.10 Next Generation Sequencing of matched primary and metastatic samples

The matched primary prostate biopsies were obtained for patients, when available, who had their metastatic biopsy sequenced. Four paired primary biopsies had sufficient material available for sequencing (Table 4.3). All biopsies had confirmed adenocarcinoma. Two (50%) out of the 4 biopsies had detectable alterations after sequencing. Both of these biopsies contained a *TMPRSS2-ERG* mutation. One biopsy obtained contained an *ERBB3* mutation.

Ten metastatic biopsies were reviewed by a pathologist to assess suitability for NGS. Metastatic samples were required to have more than 50% cellularity to be suitable for sequencing. In total, 6 biopsies were suitable and selected for sequencing using the Oncomine™ Targeted NGS Assay (Fig 4.13). The Oncomine™ Targeted NGS Assay was selected as it contains fusions, insertion/deletions (indels), single nucleotide variants, and copy number variations from 52 genes detectable in DNA and RNA. Some of these are strongly associated with PCa such as the AR gene and *TMPRSS2-ERG* fusion. It has been shown to have high sensitivity, specificity, and reproducibility (119).The 6 suitable biopsy samples underwent NGS (Table 4.3). Five samples (83%) had confirmed adenocarcinoma and 1 sample (17%) confirmed small cell carcinoma. Five (83.3%) out of the 6 metastatic samples that were sequenced, had detectable mutations or amplifications. *AR* gene amplification was identified in 3 patients (50%) (Table 4.3). One sample (17%) had a *TMPRSS2-ERG* gene fusion. One sample contained a *FGFR3* and

ERBB2 mutation (17%) and one sample (small cell carcinoma) was negative for any mutation.

Table 4.2. NGS Biopsy Results.

BIOPSY	HISTOLOGY	CELLULARITY*	NGS (PRIMARY BIOPSY)	NGS (METASTATIC)	TIME TO DEATH (months)
LIVER	ADENOCARCINOMA	80%	NO FUSIONS/MUTATIONS	AR AMPLIFICATION DETECTED	4
LIVER	SMALL CELL	70%	NO FUSIONS/MUTATIONS	NO MUTATIONS DETECTED	9
LYMPH NODE	ADENOCARCINOMA	70%	TMPRSS2-ERG FUSION, ERBB3 V104M DETECTED	TMPRSS2-ERG FUSION DETECTED	ALIVE
LYMPH NODE	ADENOCARCINOMA	80%	NO PRIMARY AVAILABLE	AR AMPLIFICATION DETECTED	9
BONE	ADENOCARCINOMA	50%	NO PRIMARY AVAILABLE	FGFR3, ERBB2 DETECTED	8
BONE	ADENOCARCINOMA	60%	TMPRSS2-ERG FUSION DETECTED	AR AMPLIFICATION DETECTED	6

*Biopsies selected for NGS based on having >50% cellularity.

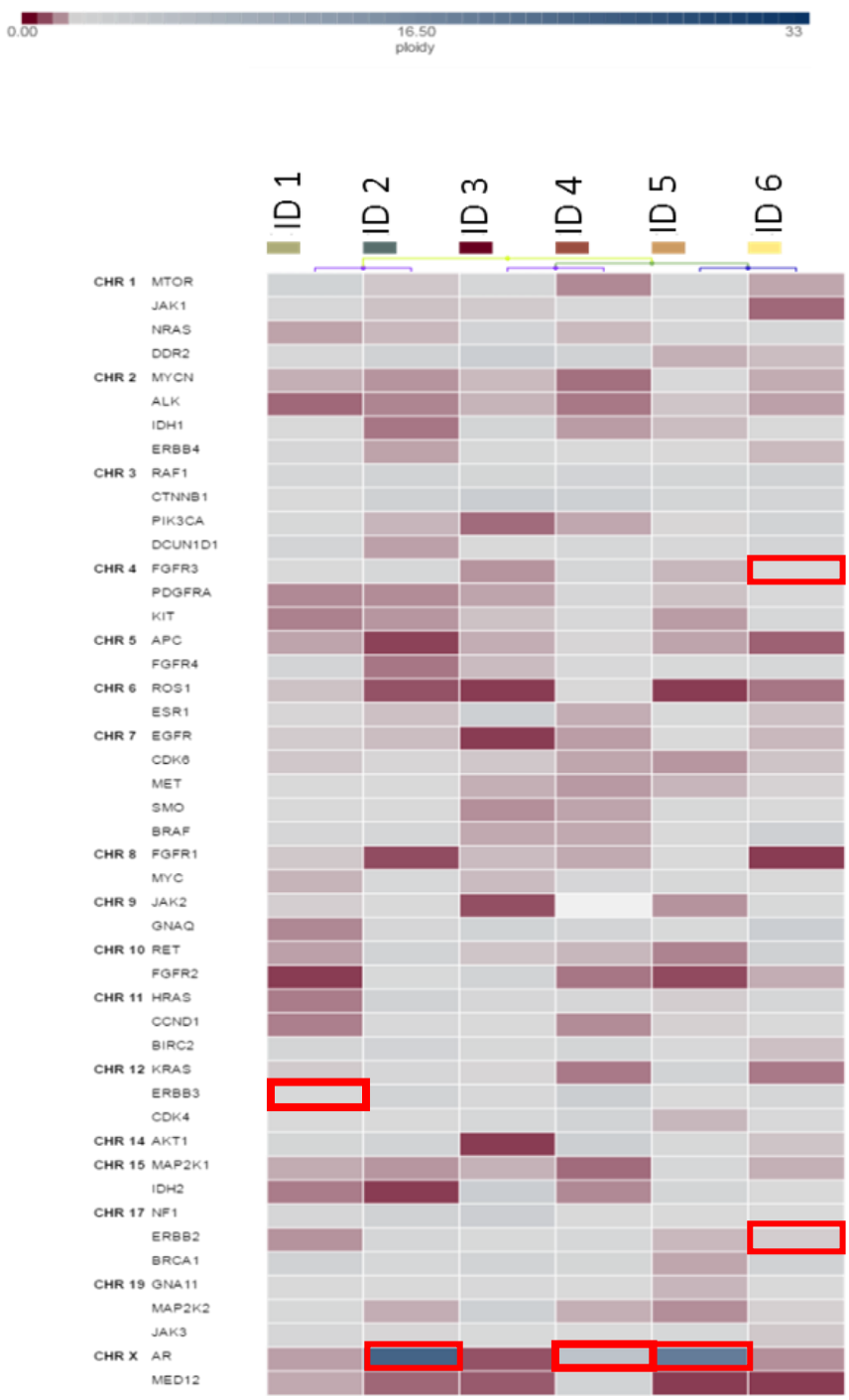

Figure 4.13. Heatmap showing alterations in metastatic biopsy samples using the Oncomine™ panel. Darker blue reflects higher copy number gain. Red boxes indicate alterations identified in genes.

4.1.11 CTCs and metastatic biopsies

Patients undergoing optional biopsies also had CTC levels measured. CTC levels were analysed in samples that were positive for carcinoma (n=3) and in patients who had a normal biopsy with no evidence of carcinoma. In those patients positive for carcinoma CTCs were 16.3/6 mL (SEM ± 4) and those which were negative had a mean CTC count of 12.43/6 mL (SEM ± 3.4). However, due to the small number of carcinoma samples available, it was not possible to perform statistical analysis between the two groups (Fig. 4.14).

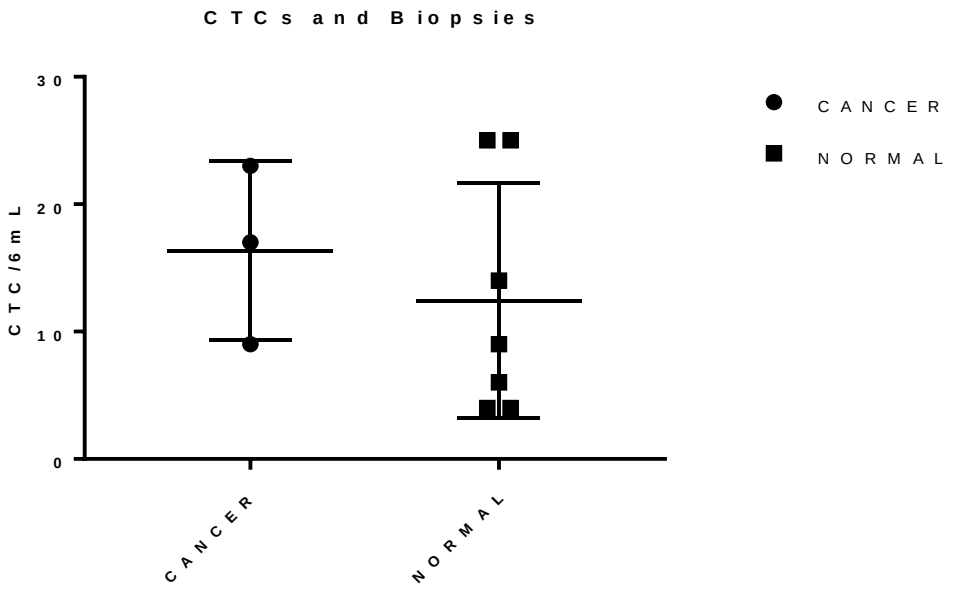

Figure 4.14. CTC counts measured at time of biopsy according to the presence or absence of carcinoma.

(Cancer n=3, normal n=7; Data graphed as raw values)

6.24 Discussion

It is now well established that the nature of PCa changes over many years, from the original diagnosis of localised prostate adenocarcinoma to the development of metastatic castration-resistant disease (120). However, it can be difficult to obtain biopsy samples in patients with metastatic disease due to the long natural history of the disease, and due to the questionable benefit of performing repeat biopsies many years later. Therefore, this study aimed to collect samples from patients with metastatic disease and to use those samples to gather more information that may be used to tailor treatment for patients with metastatic PCa. iPROSPECT was designed to have two cohorts of patients reflecting the varied nature of PCa. The first cohort recruited patients with hormone-sensitive disease; that is patients with metastatic PCa who were responding to ADT. The second cohort recruited patients with castration-resistant disease; that is patients with progressive disease despite receiving ADT. In total, 15 patients were recruited to cohort 1 and 41 patients were recruited to cohort 2.

The mean age of patients recruited to cohort 1 was 67 years of age and the mean age of cohort 2 was 69 years of age. This age profile is similar to other studies recruiting to metastatic PCa trials and reflects the older age profile of men who are diagnosed with PCa (121). The average Gleason Score for both groups was 8 at screening. A Gleason score of 8 is now newly classified as a grade group 4 cancer (122). This new grading system consists of five different prognostic groups which have been validated in large patient cohort studies. The five-year biochemical risk-free survival for the five grade groups were 96%, 88%, 63%, 48% and 26%, respectively (122). Based on this,

the two cohorts in iPROSPECT who both had a Gleason score of 8 would be expected to have a five-year biochemical risk-free survival of 48%. The baseline screening PSA for eligibility for both cohorts in iPROSPECT had to be greater than 2.0 ng/mL. For cohort 1, the baseline PSA was 31 ng/mL and for cohort 2, it was 173 ng/mL. The higher value for cohort 2 reflects the progressive and more aggressive nature of CRPC and the fact that this subtype no longer responds to ADT. Higher levels of LDH and alkaline phosphatase are associated with poorer prognosis in PCa and were measured at baseline and throughout this study. The baseline LDH at recruitment in cohort 1 was 263 IU/L and 378 IU/L in cohort 2. The higher value of LDH in cohort 2 again reflects the more aggressive nature of CRPC in comparison to cohort 1 patients.

Bone metastases are the most common site for PCa metastases. Patients recruited to iPROSPECT had to have confirmed metastatic disease. All patients in both cohorts in this study had confirmed bone metastases. Alkaline phosphatase is elevated in men with metastatic PCa when the bone marrow is infiltrated with carcinoma (123). In cohort 1, the screening value was 298 IU/L *vs*. 173 IU/L in cohort 2. This higher values for patients in cohort 1 with hormone sensitive disease may reflect the fact that these patients have newly diagnosed bone metastases that have never been treated. In comparison, patients in cohort 2 would have had prior treatment to their bone metastases reflecting the lower value for the alkaline phosphatase (124). PCa next commonly spreads to the lymph nodes followed less commonly by visceral involvement. In cohort 1, only 2 patients had lymph node involvement and no

patients had visceral involvement, reflecting the earlier more responsive nature of hormone-sensitive PCa. This contrasts with cohort 2, where 42% of patients had lymph node involvement and 27% of patients had visceral involvement, again reflecting the more aggressive nature of CRPC, which is in line with previously published data (125). All patients recruited to iPROSPECT had CTC counts measured at baseline and every 4 months (± 1 month) during treatment. A decrease in CTC count was noted in both cohorts at their second follow up visit possibly in line with a response to treatment. CTC counts therefore may have a potential role as a marker of response, however longer follow up is required.

The management of PCa can present a challenge in the era of targeted therapy due to the lack of tissue samples available. PCa is heterogeneous in genotype as well as phenotype, even between different metastatic sites within the same patient. With this in mind, all patients who would be eligible for a biopsy were given the option of consenting for a metastatic biopsy sub-study. Two different methods of biopsy were analysed, a bone marrow biopsy traditionally performed at the bedside with minimal preparation, and a targeted biopsy sub-study performed with radiological guidance, which normally requires admission to the hospital as a day case. Fifteen bone marrows were performed compared to only 6 radiologically guided biopsies, perhaps reflecting the easier access to bone marrow procedures. However, when the methods were compared, CT guided biopsies were more accurate at obtaining metastatic tissue compared to bone marrows (100 *vs*. 24%). A previous study by Kantoff *et al.* had similar findings, albeit with a larger cohort (116). One

reason for this discrepancy may be that although the marrow is diffusely involved, there will be sites of normal bone tissue between sites of metastatic disease, and therefore metastatic deposits may be missed. This may be overcome by taking multiple samples of bone, however this could be associated with increased morbidity for the patient. Radiological guidance overcomes this problem by using real-time imaging to guide the biopsy needle to the identified metastatic deposit (118). This has been previously confirmed in other studies showing CT guided biopsies to be superior to bone marrow biopsies for tissue acquisition (126). Previous studies have shown an elevated alkaline phosphatase to be associated with a higher burden of metastatic bone disease, and therefore a higher yield of positive bone marrow results, however, this was not confirmed in this study, perhaps due to the low numbers involved (118).

One of the important findings noted from recent studies examining metastatic samples in PCa is the transformation to neuroendocrine disease such as small cell carcinoma (127). It is not clear if this is a treatment-emergent variant, or if it is the same disease entity as de novo small cell PCa. However, there is an increasing body of evidence to support the development of a high grade neuroendocrine subtype due to therapeutic resistance to AR-targeting therapy (103, 128). Rates of transformation vary in different studies, however a repeat metastatic biopsy to confirm neuroendocrine disease should be considered in any patient with rapidly progressing disease radiologically with minimal PSA change, as neuroendocrine disease rarely secretes PSA. Treatment options change significantly once neuroendocrine disease is

diagnosed as this subtype type of disease more commonly responds to traditional chemotherapy agents such as platinum based agents (129), thus having a significant impact on the clinical management of the patient. Understanding the pathogenesis of transformed neuroendocrine PCa and why some patients with CRPC progress to neuroendocrine disease is an area of active research. One patient who underwent a repeat liver biopsy from iPROSPECT had confirmed neuroendocrine disease after developing multiple liver metastases with only a small increase in PSA levels. This would be consistent with transformed metastatic PCa as there was no evidence of a lung primary on CT imaging. It is possible that this tumour had transformed into a high-grade neuroendocrine phenotype under AR selective pressure, different from the original primary. The patient was subsequently treated with platinum chemotherapy based on this biopsy result. Though the reported frequency of neuroendocrine differentiation varies in the literature, a rate of 10%, similar to this study has been commonly reported (130).

Understanding the genomic landscape of PCa and identifying alterations acquired with disease progression can help in the design of new, effective therapies that specifically target altered biologic pathways. Recent advances in sequencing technologies allow for simultaneous identification of base substitutions, copy number alterations, and mutations at much greater sensitivity then traditional Sanger sequencing (131). In total, 10 samples underwent NGS using the Oncomine™ sequencing panel (119). Six metastatic samples were selected from this study and a further 4 matched primary biopsy samples for these patients underwent sequencing. One of the reasons for the

small volume of biopsies that were sequenced was due to the larger number of bone marrow samples that were obtained. In these samples, there was small volume of tissue available, and decalcification during tissue processing further degraded the tissue quality, an issue that has been highlighted in other sequencing studies (132). Interestingly, there was a higher rate of alterations detected in metastatic biopsies (83%) compared to the primary biopsies sequenced (50%), reflecting the more complex genomic makeup of advanced metastatic disease. There is a paucity of data in this setting due to the lack of metastatic biopsies available, however these results are similar to previous published data and contribute to the understanding of the complex genomic landscape of metastatic PCa (131). Of the metastatic samples sequenced, 3 biopsy samples (50%) had AR copy number gain. AR copy number gain has been shown to be associated with castration resistance in the metastatic setting (133). AR copy number gain has been shown by Attard *et al.* (111) to be associated with a worse prognosis and to be associated with resistance to therapies such as enzalutamide and abiraterone. Two of the patients had been treated with abiraterone and one patient had received enzalutamide. The *TMPRSS2-ERG* gene fusion which has been detected in up to 50% of PCa (134) was similarly detected in 1 metastatic patient sample and in 2 primary biopsy samples. The low level of detection may have been due to the small number of samples sequenced. A second sample had a mutation for the fibroblast growth factor receptor 3 (*FGFR3*) gene, which belongs to the family of tyrosine kinase receptors (135). FGF signalling has been shown to induce differentiation and/or cell proliferation inhibition and/or cell death (136). Deregulation of FGF signalling in carcinogenesis has been widely explored and

it is now well-established that FGFs and FGFRs play oncogenic roles through different intracellular molecular targets leading to increased cell proliferation, cell survival, angiogenesis and promotion of cell migration and invasion (137). Previous studies have reported prevalence rates as high as 20% for radical prostatectomy samples, however data is unknown for metastatic samples (138). Similarly, in the same sample, *ERBB2* was detected, which is a well is known oncogene. It has been previously shown to collaborate with androgen signalling to promote PCa metastases (139). The rate of *ERRB2* in radical prostatectomy samples has been reported as low as 1.5%, however no data is available in metastatic PCa (140). The involvement of FGF pathways in prostate tumorigenesis provides a rationale for the therapeutic blockade of this pathway, and two small-molecule tyrosine kinase inhibitors, dovitinib and nintedanib, are currently in phase 2 clinical development for advanced PCa (141). Preliminary results from these trials suggest that FGF pathway inhibition represents a promising new strategy to treat castrate-resistant disease. ERBB2 signalling is elevated in a subset of patients with CRPC and stabilises the AR protein (142). Combination therapy with ERBB2 antagonists has been analysed in preclinical models and may be effective for treating the subset of CRPC with elevated ERBB2 activity (142). Interestingly, no mutations or copy number gains were detected in the sample with neuroendocrine transformation. Previous studies have confirmed low expression of known androgen-regulated genes in this subtype of cancer (128). This highlights that neuroendocrine transformation is a distinct subtype of PCa with its own unique molecular signature which requires optimisation of targeted treatments.

PCa has a long natural history over many years from the first diagnosis to the development of metastatic disease. Most patients currently do not undergo a repeat biopsy; however, this study shows the feasibility of performing biopsies and the clinical importance of doing so, in this patient cohort. Biopsies performed using real time imaging are superior to biopsies performed without any guidance such as bone marrow biopsies. Furthermore, lymph node or visceral biopsies appear to be superior compared with bone biopsies in yielding adequate tissue for analysis. Neuroendocrine differentiation is an important finding in repeat biopsies, which may dictate a change in treatment if detected. Advances in sequencing continue to detect genomic changes in PCa, which may guide future therapies tailored for patients, and may act as both predictive and prognostic biomarkers, highlighting the importance of serial biopsies in patients.

Chapter 5: Assessment of Methods and Sample types for identifying AR-FL & AR-V7 in Prostate Cancer

6.25 Introduction

AR signalling plays a pivotal role in the progression of PCa. Significant evidence exists demonstrating up-regulation of the AR by a variety of mechanisms in advanced stages of hormone-sensitive PCa (31). Furthermore, research has shown that AR signalling continues to play a critical role in CRPC (143). The majority of CRPC patients respond to androgen signalling inhibitors (ASI) such as enzalutamide or abiraterone; however, there is a subset of patients (20-40%) who never respond, as determined by a lack of response using levels of PSA, and radiological or clinical disease progression (33). The molecular mechanisms driving this resistance, however, are currently unclear, and a deeper understanding is critical for the rational development of alternate therapeutics, and the identification of markers to stratify patients for therapy. Genetic aberrations of the AR caused by mutations, rearrangements, and polymorphisms result in a mutant receptor that has varied functions compared to the wild type AR (37). A recent study by Korpal *et al.* demonstrated that a mutation in the AR LBD, F876L, emerges in enzalutamide resistant clones of LNCaP cell lines, which strongly supports the hypothesis that the emergence of AR mutants may represent a mechanism of resistance to enzalutamide (35).

AR-V7 is a splice variant of the AR, which lacks the LBD in the C-terminus, leading to constitutive ligand independent activation of the receptor (36). Detection of baseline AR-V7, using CTCs, has been shown to predict patients' response to ASIs such enzalutamide or abiraterone therapies (33). It is therefore conceivable that an assay developed to detect AR-V7 could be used to predict response to ASIs, and to AR-V7 targeted therapies that are currently under development (40). Even though a number of assays exist, such as IHC

and qPCR, the detection of AR-V7 in clinical samples remains difficult. As of yet, no assay has transferred readily into clinical use. Furthermore, it is uncertain if there is an association with AR-V7 and F876L, both of which are believed to play a role in the development of resistance to enzalutamide.

The aims of this study were to (i) examine AR-FL and AR-V7 transcript expression in a panel of PCa cell lines (benign and malignant), (ii) determine the expression levels of AR-V7 in an isogenic cell line model of enzalutamide resistance with confirmed expression of F876L, and (iii) determine the expression of AR-FL and AR-V7 in cell lines and tissues, using a novel RISH assay.

6.26 Results

5.1.1 AR-FL expression in a panel of PCa cell lines

Expression of AR-FL was determined in both AR dependent cell lines (22Rv1, LNCaP, VCaP) and independent cell lines (DU 145, PC-3). This was performed using a standard curve method (Fig 5.1). Serial dilutions of a known copy number of the AR gene were used in order to determine gene copy number within samples. It was confirmed by qPCR that AR-FL was present in all known AR dependent cell lines (Fig 5.2). VCaP cell lines had the highest RNA copy number of AR-FL (copy number = 5.75 ± 0.03) compared to LNCaP (copy number = 5.04 ± 0.19) ($p \leq 0.05$), and 22Rv1 (copy number = 4.55 ± 0.19) ($p \leq 0.01$). AR-FL was not detected in known AR independent lines, DU 145 and PC-3, or in any of the normal or BPH-1 cell lines. (Data given as mean ± SEM).

5.1.2 AR-V7 expression in a panel of PCa cell lines

AR-V7 was also examined in the cell line panel. This was performed using a standard curve method using a transcript for AR-V7 as per AR-FL (Fig 5.3). AR-V7 transcript RNA copy number was highest in 22Rv1 (copy number = 3.51 ± 0.05) compared to LNCaP (copy number = 1.73 ± 0.02) ($p \leq 0.0001$) and VCaP (copy number = 3.04 ± 0.18) ($p \leq 0.05$) (Fig 5.4). AR-V7 transcript copy number was significantly higher in VCaP cell lines compared to LNCaP ($p \leq 0.001$). AR-V7 was not detected in known AR independent lines, DU 145 and PC-3, or in any of the normal or BPH-1 cell lines. (Data given as mean ± SEM).

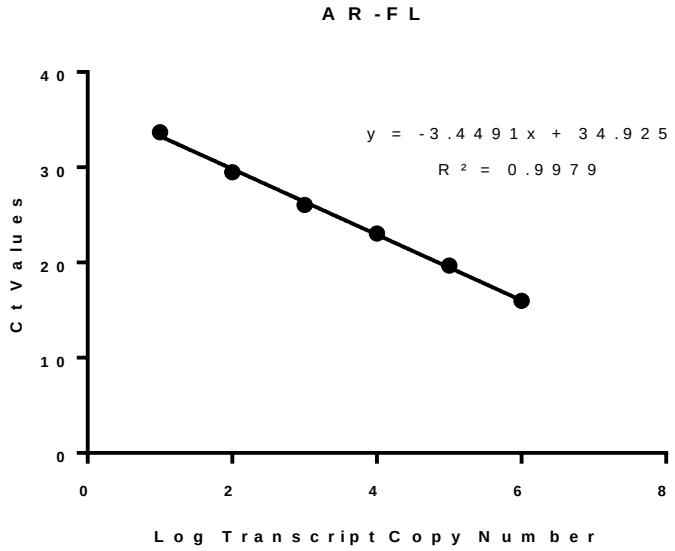

Figure 5.1. Standard curve method for AR-FL. Standard dilution curve for AR-FL is shown. Threshold cycle numbers (Y axis) in qPCR reactions were determined for cDNA specific to the AR-FL gene at 6 dilutions containing the indicated number of copies of each transcript (X axis). Formula as shown was derived to quantify the absolute copy numbers on the basis of Ct values.

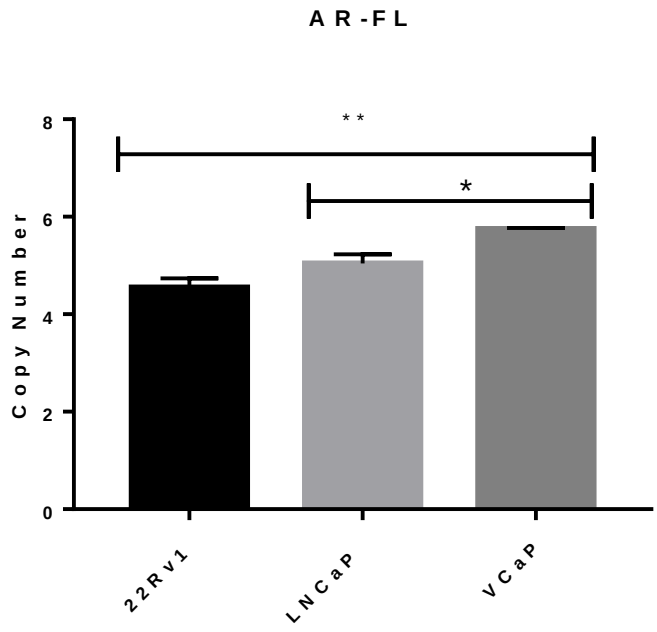

Figure 5.2. AR-FL copy number expression. AR-FL was expressed in all 3 cell lines. Data graphed as mean ± SEM (n=3). Statistical analysis performed using ordinary one-way ANOVA (* $p \leq 0.05$, ** $p \leq 0.01$).

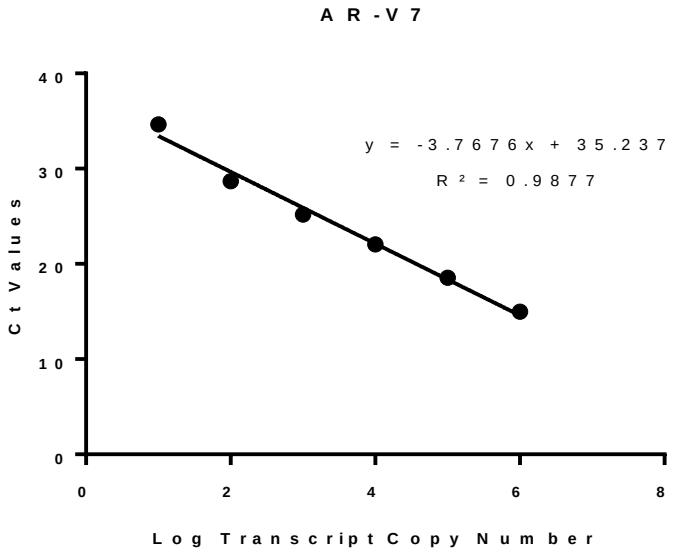

Figure 5.3. AR-V7 standard curve. Standard dilution curve for AR-V7 are shown. Threshold cycle numbers (Y axis) in quantitative PCR reactions were determined for cDNA specific to the AR-V7 gene at 6 dilutions containing the indicated number of copies of each transcript (X axis). Formula as shown was derived to quantify the absolute copy numbers on the basis of Ct values.

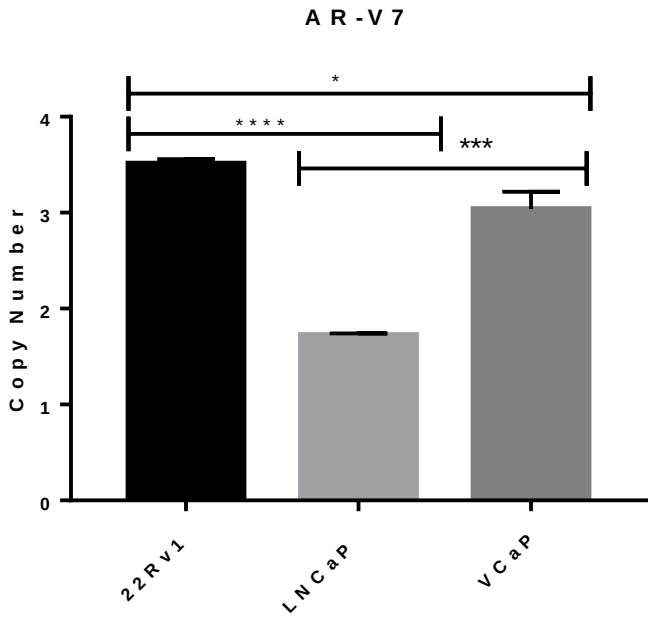

Figure 5.4. RNA copy number expression of AR-V7. AR-V7 was expressed in all 3 lines. Data graphed as mean ± SEM (n=3). Statistical analysis performed using ordinary one-way ANOVA (* $p \leq 0.05$, *** $p \leq 0.001$, **** $p \leq 0.0001$).

5.1.3 AR-FL and AR-V7 expression in an isogenic model of enzalutamide resistance

An isogenic cell line model of enzalutamide resistance was used to determine the levels of AR-FL and AR-V7 associated with drug resistance (35). The model consisted of an age matched control cell line (enzalutamide sensitive) and two sub-lines; clone 1 (strongly resistance to enzalutamide) and clone 9 (moderately resistance to enzalutamide). An experiment was performed to confirm expression of AR-FL in these lines as previously described. As expected, all three lines showed similar transcript expression levels of AR-FL with no significant difference in expression between cell lines (Fig 5.5). AR-V7 expression was also assessed in the isogenic panel as previously described. AR-V7 RNA copy number was highest in LNCaP clone 1 (copy number = 4.11 ± 0.17) compared to LNCaP control (copy number = 2.04 ± 0.11) ($p \leq 0.001$) and LNCaP clone 9 (copy number = 2.10 ± 0.17) ($p \leq 0.001$) (Fig 5.6). (Data given as mean ± SEM).

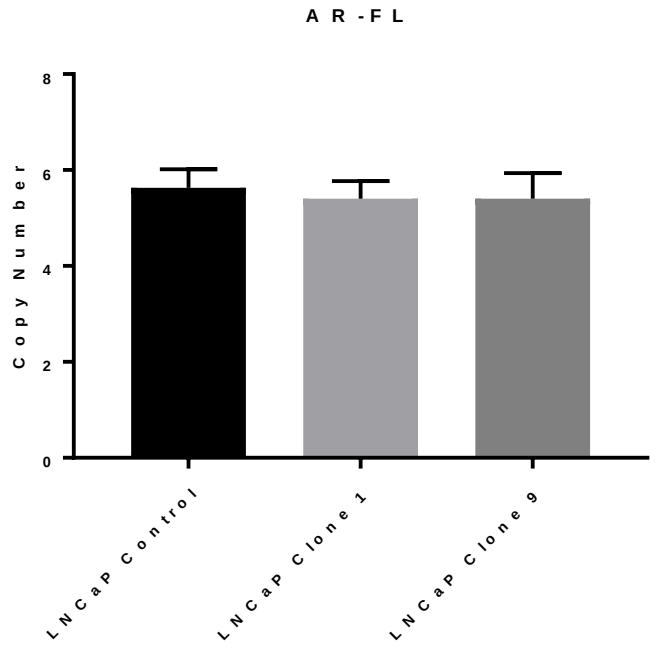

Figure 5.5. AR-FL expression in a cell line model of enzalutamide resistance.

AR-FL was expressed in all 3 lines. Data graphed as mean ± SEM (n=3).

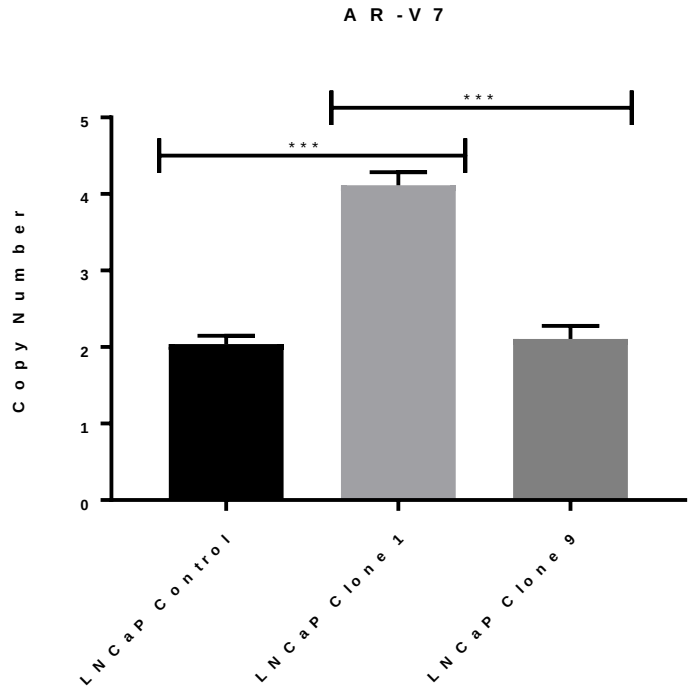

Figure 5.6. AR-V7 expression in a cell line model of enzalutamide resistance. Data graphed as mean ± SEM (n=3). Statistical analysis performed using ordinary one-way ANOVA performed (*** $p \leq 0.001$).

5.1.4 AR-V7 expression using IHC

Experiments using IHC to detect AR-V7 were performed. This was performed using a rabbit recombinant monoclonal AR-V7 specific antibody (ab198394). The target of the antibody was a splice variant of the AR (UniProt P10275) that lacks the C-terminal androgen-binding site. The androgen independent cell line DU 145 showed no expression of AR-V7 and served as a cell line negative control (Fig 5.7A). Testing was performed in 22Rv1, which showed weak positivity with AR-V7 (Fig 5.7B). Testing was similarly performed in normal LNCaP cell lines, which showed no expression of AR-V7 (Fig 5.7C). Omission of the primary antibody with PBS served as an IHC negative control.

5.1.5 Comparison of RISH methods to detect AR-FL and AR-V7

An alternative method to detect AR-V7 was examined. Two novel RISH assays were used, RNAscope® and BaseScope™, which can detect target RNA within intact cells. The sensitivity and specificity of these different RISH methods using novel custom designed probes for AR-FL and AR-V7, were assessed.

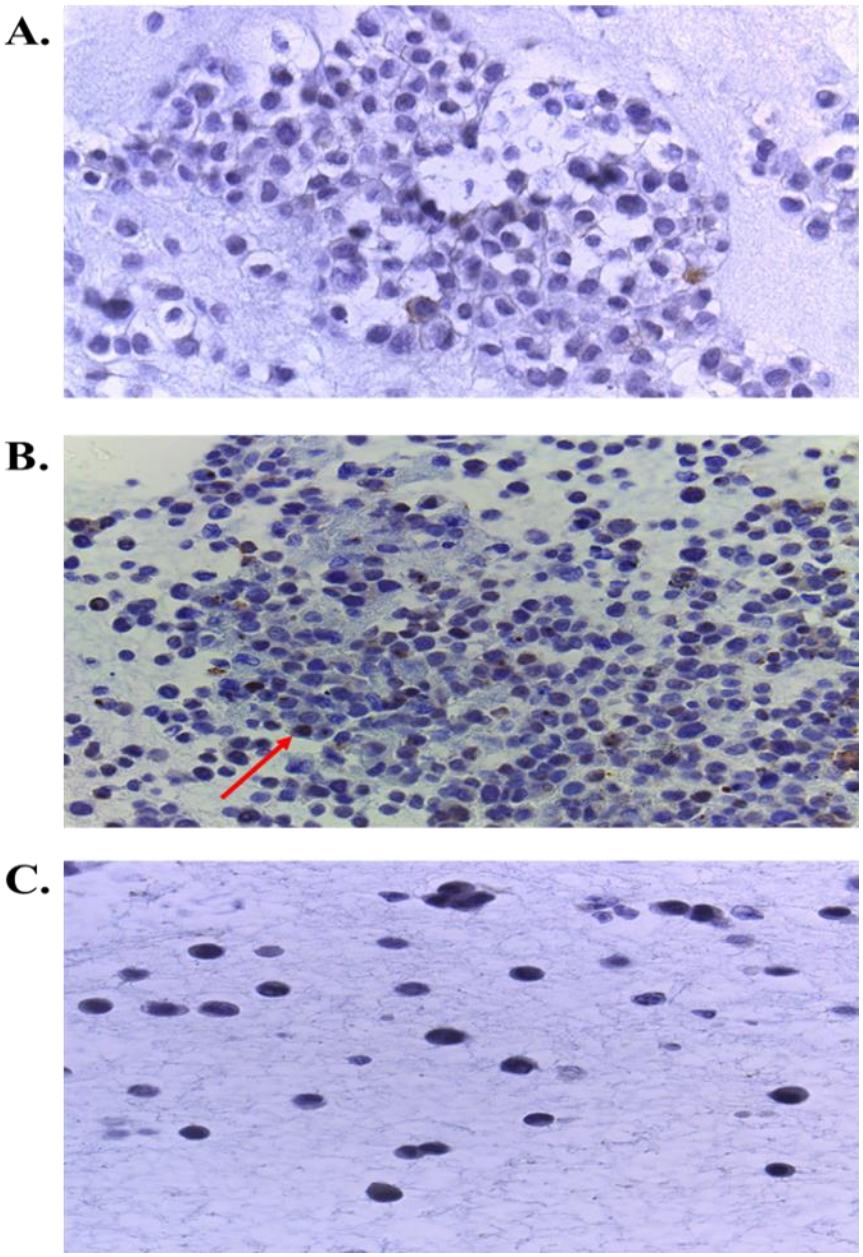

Figure 5.7. IHC for AR-V7. (A) DU 145 showed no nuclear staining, (B) 22Rv1 had weak expression (red arrow), and (C) LNCaP showed no expression (All images at 40X).

5.1.6 Assessment of RISH techniques

BaseScope™ and RNAscope® workflows were tested and compared using HeLa FFPE sections. For BaseScope™, the bacterial gene dapB was used as a negative control, which allowed for the assessment of cell integrity (Fig 5.8A). The peptidyl-prolyl cis-trans isomerase B (PPIB) gene was used as a positive control to assess the workflow. BaseScope™ positive staining was visible as red punctate staining (Fig 5.8C). For RNAscope®, dapB was used as a negative control for the assessment of cell integrity (Fig 5.8B). The PPIB gene was used as a positive control to assess the workflow. RNAscope® positive staining was visible as brown punctate staining within the cytoplasm (Fig 5.8D).

A.

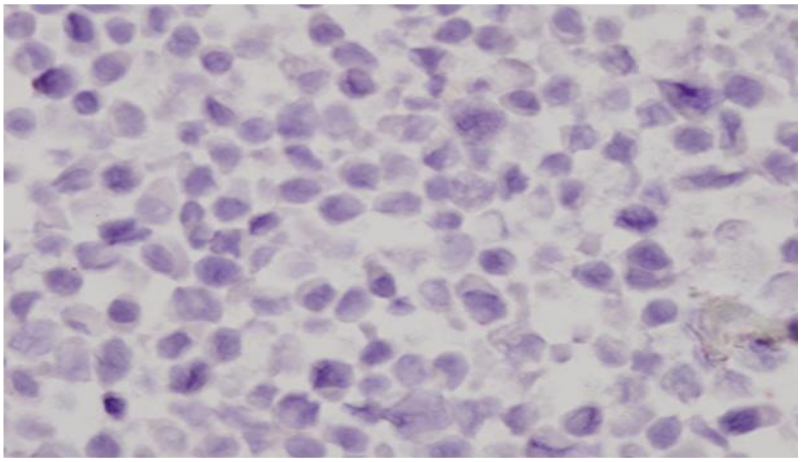

B.

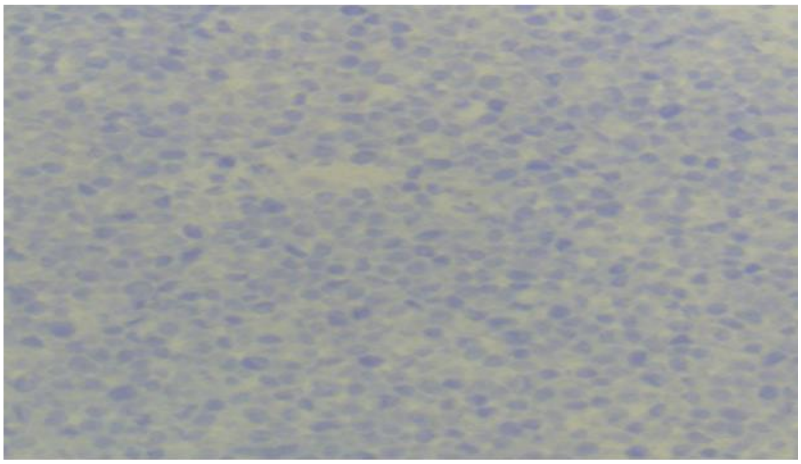

C.

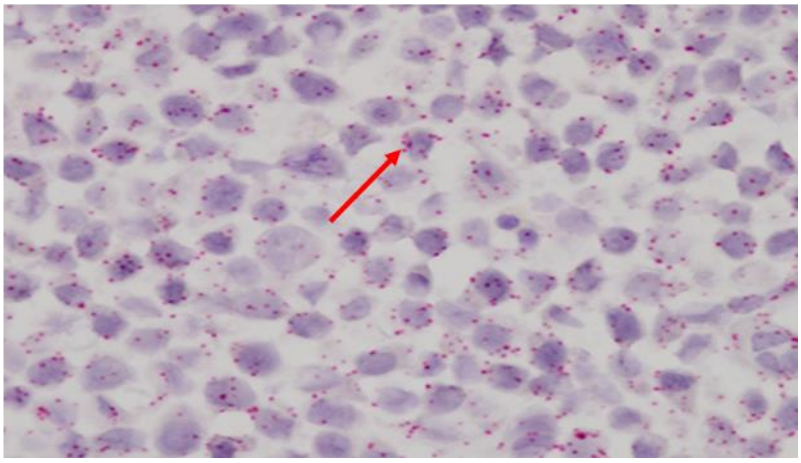

D.

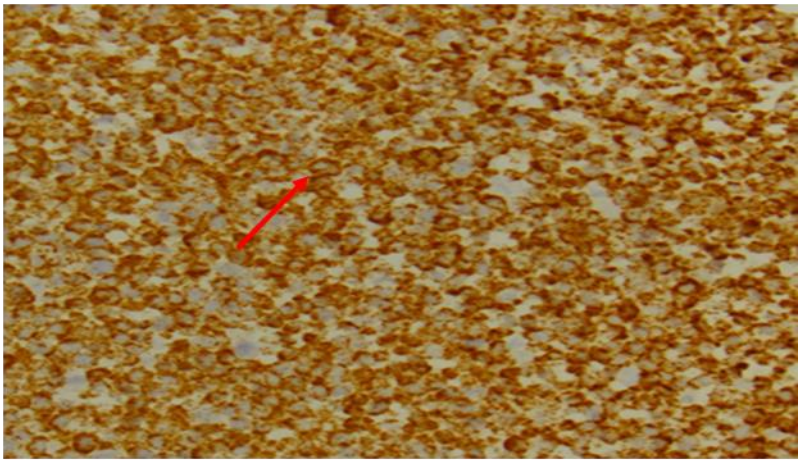

Figure 5.8. RNAscope® and BaseScope™ positive and negative controls using HeLa cells. (A) BaseScope™ dapB negative control probe at 20X, (B) RNAscope® dapB negative control at 40X, (C) BaseScope™ PPIB positive control probe displaying red punctate staining (red arrow) at 20X and (D) RNAscope® PPIB positive control demonstrating brown staining (red arrow) at 40X.

5.1.7 AR-FL and AR-V7 expression using RISH

Having confirmed the RNAscope® and BaseScope™ workflow in HeLa Cells, the RNAscope® assay was used initially to test AR-FL and AR-V7 expression in the 22Rv1, VCaP and PC-3 cell lines. 22Rv1 and VCaP cell lines showed robust expression of AR-FL and AR-V7 by qPCR. PC-3 is a known androgen independent cell line that does not express AR-FL or AR-V7. 22Rv1, VCaP and PC-3 cells were cultured directly on Nunc™ Lab-Tek™ II Chamber Slides and RISH was performed using RNAscope® directly on the slides. Negative control staining with dapB (Fig 5.9A) and positive control staining with PPIB (Fig 5.9B) genes were used to confirm the workflow and to assess cell morphology, which were well preserved. AR-FL expression was confirmed in 22Rv1 (Fig 5.9C). Similarly, AR-V7 was expressed in this cell line (Fig 5.9D).

In VCaP cell lines, positive (Fig 5.10A) and negative (Fig 5.10B) control staining confirmed the assay workflow. In VCaP cells, both AR-FL (Fig 5.10C) and AR-V7 (Fig 5.10D) were highly expressed, similar to the expression levels previously confirmed by qPCR. PC-3 was used as a negative cell line control as it did not express any AR-FL or AR-V7 (Fig 5.11).

A.

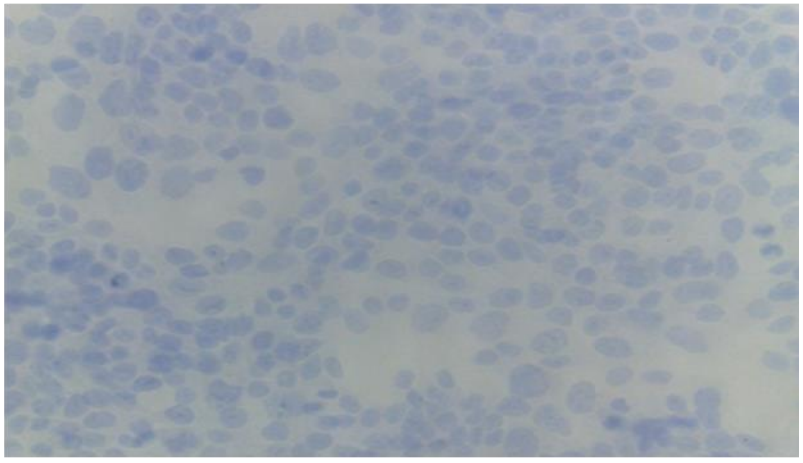

B.

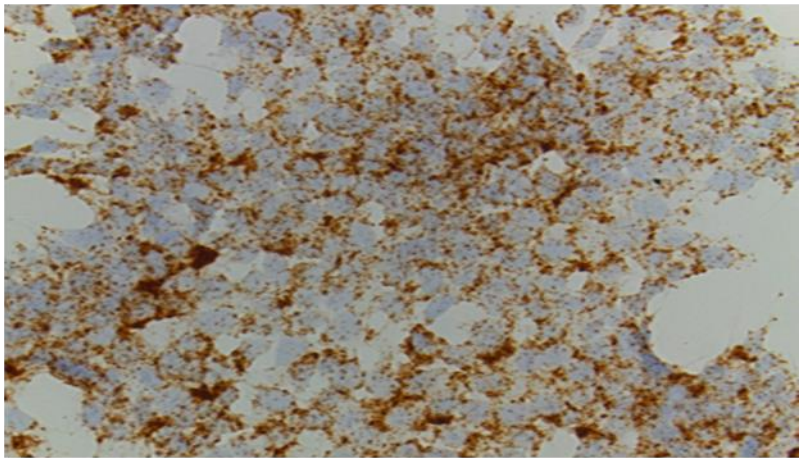

C.

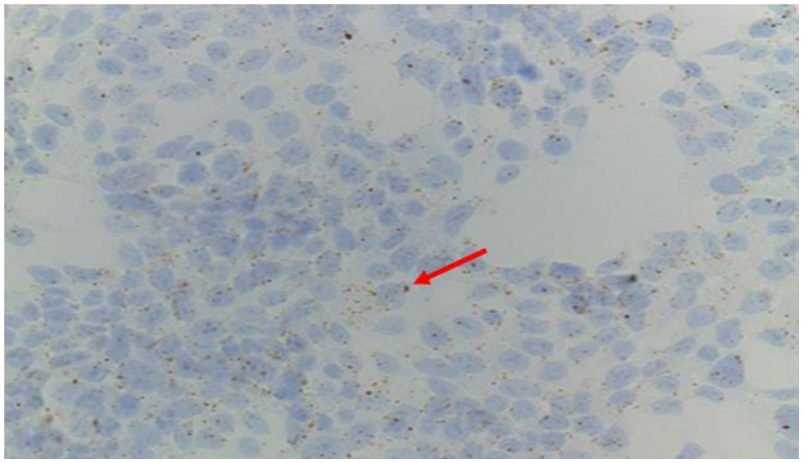

D.

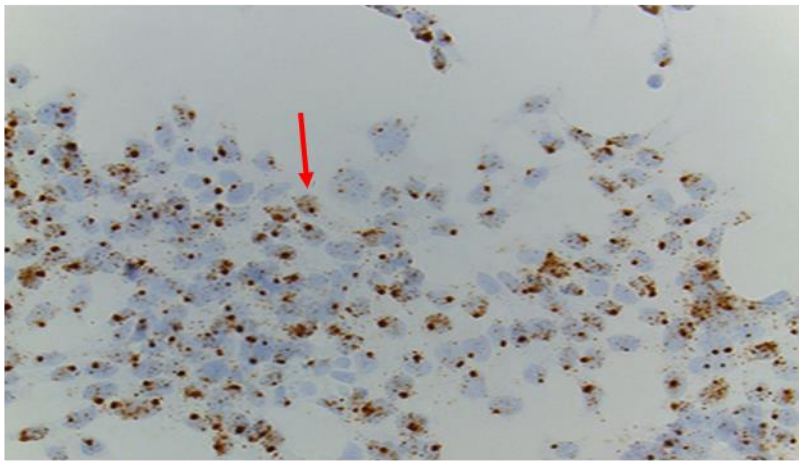

Figure 5.9. AR-FL and AR-V7 expression in 22Rv1 cell lines using RNAscope®. (A) Negative control with dapB transcript at 40X, (B) Positive control showing positive brown staining with PPIB gene at 40X, (C) AR-FL probe showing positive (score 2+) brown punctate staining (red arrow) at 40X, and (D) AR-V7 probe showing positive (score 2+) brown punctate staining (red arrow) at 40X.

A.

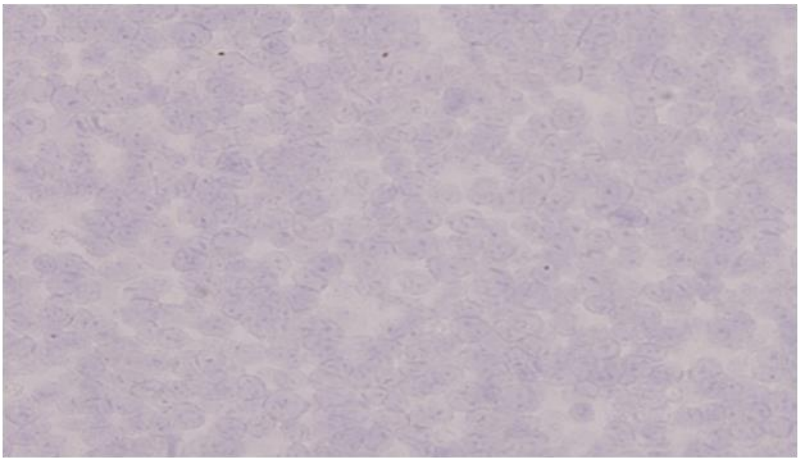

B.

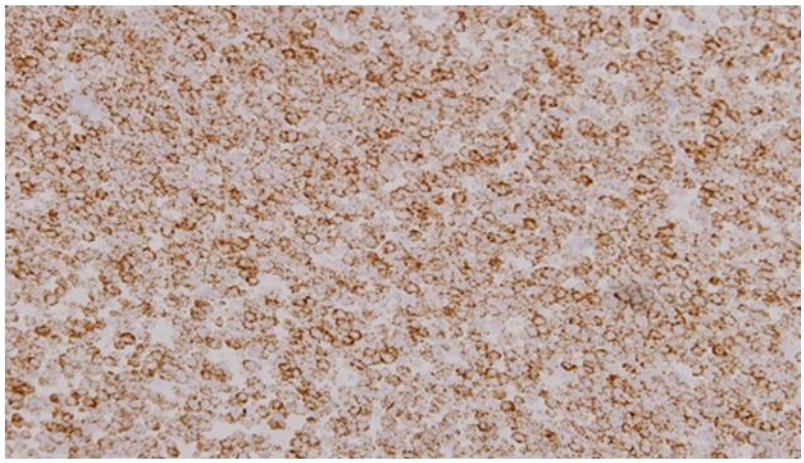

C.

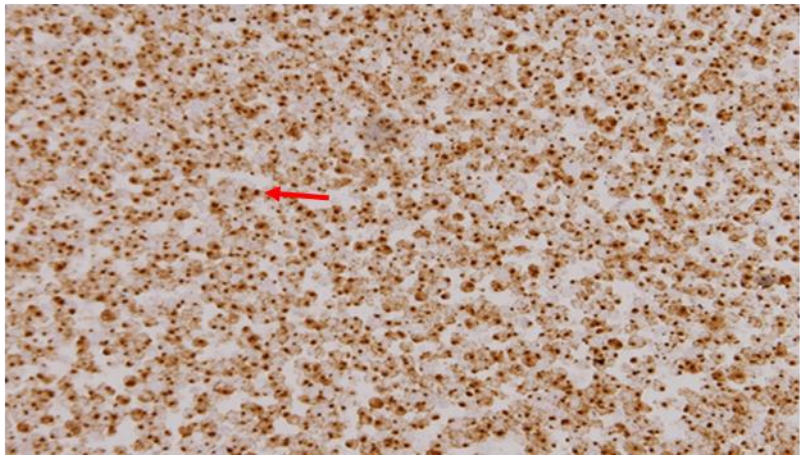

D.

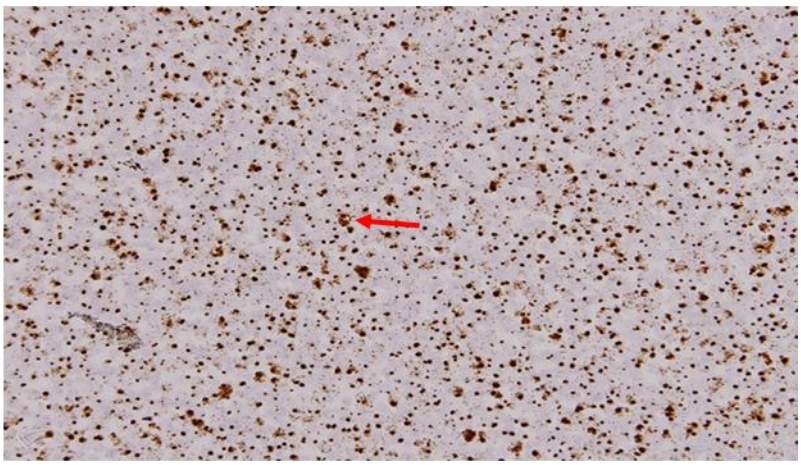

Figure 5.10. AR-FL and AR-V7 expression in VCaP cell lines using RNAscope®. (A) Negative control with dapB gene at 40X, (B) Positive control showing brown staining with PPIB gene at 40X, (C) AR-FL probe showing positive (score 3+) brown punctate staining (red arrow) at 40X, and (D) AR-V7 probe showing positive (score 2+) brown punctate staining (red arrow) at 40X.

A.

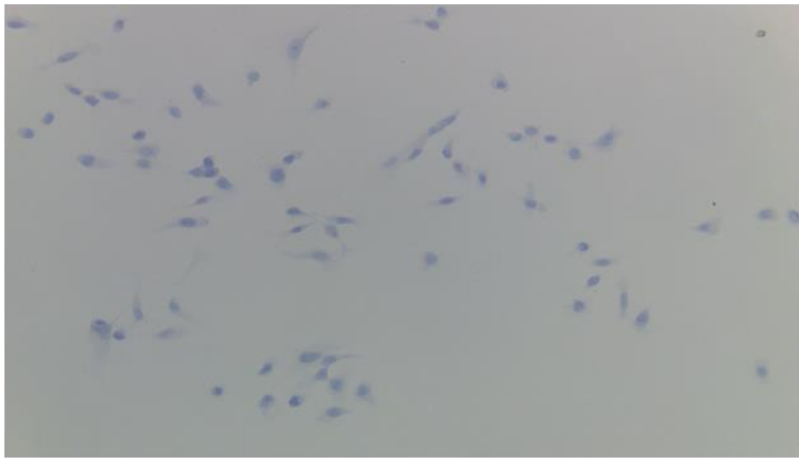

B.

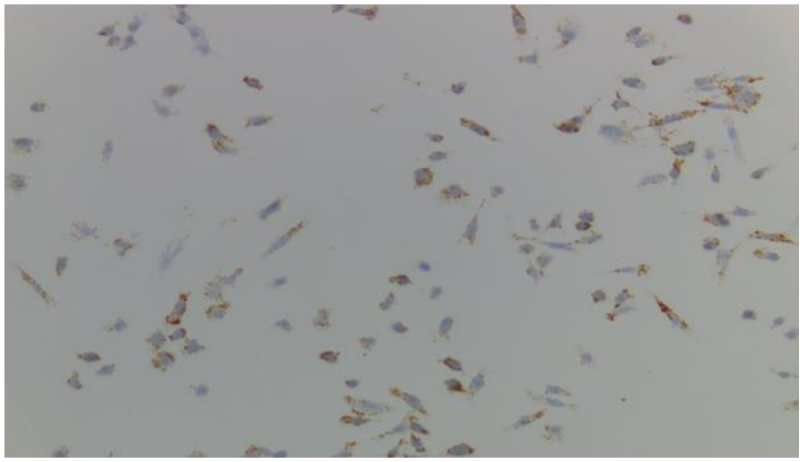

C.

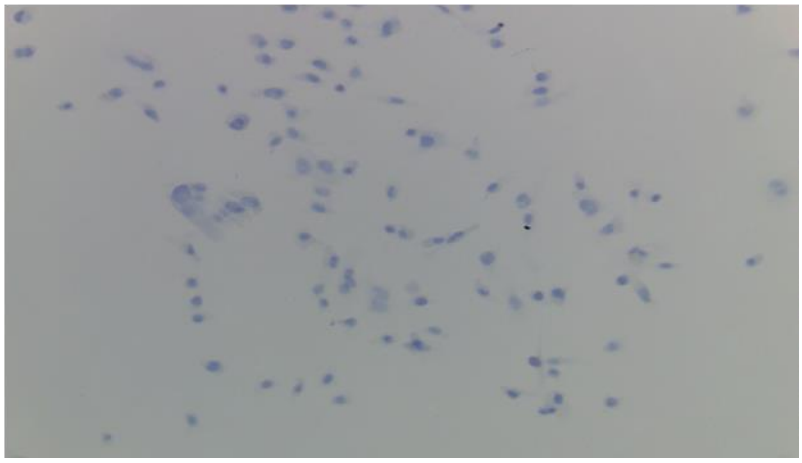

D.

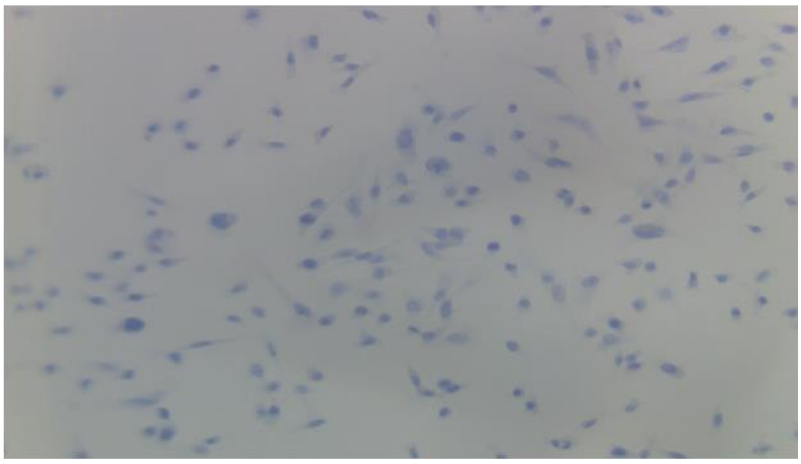

Figure 5.11. AR-FL and AR-V7 expression in PC3 cell lines using RNAscope®. (A) Negative control with dapB gene at 20X, (B) Positive control showing brown staining with PPIB gene at 20X, (C) AR-FL probe showing no staining at 20X, and (D) AR-V7 probe showing no staining at 20X.

5.1.8 RISH using BaseScope™

BaseScope™ is RISH based technology that enables the specific detection of mutations, exon junctions, short target sequences and highly homologous sequences, with single molecule detection sensitivity in a broad range of tissues, samples and species (Fig 5.12). Custom designed probes for both AR-FL and AR-V7 and a probe that detects combined AR-FL and AR-V7 expression were used (Table 5.1).

Figure 5.12. Custom designed BaseScope™ probes for AR-FL and AR-V7. Representation of AR-FL and AR-V7 showing their exons and targets for BaseScope™ probes.

Image taken from ACD Bio website (144).

Table 5.1. Custom designed BaseScope™ probes for AR-FL and AR-V7.

Probe	Target
BA-Hs-AR-V7-E3CE3	E3-Ec3 junction, detects AR-V7
BA-Hs-AR-E3E4	E3-E4 junction, detects AR-FL
BA-Hs-AR-E2E3	E3-E4 junction, detects both AR-V7 and AR-FL

The BaseScope™ assay was optimised using VCaP cell lines. Cell morphology was well preserved. Red punctuate staining within the cell cytoplasm was consistent with AR-FL and AR-V7 staining (Fig 5.13). VCaP cell lines were chosen as they strongly expressed AR-V7. Following optimisation with the VCaP cell lines, sections from FFPE blocks of LNCaP control, LNCaP clone 1 and LNCaP clone 9, were examined for AR-FL and AR-V7 expression. LNCaP control line showed expression of AR-FL, however there was an absence of staining for AR-V7 (Fig 5.14). LNCaP clone 1 (most resistant) showed strong staining for AR-FL and AR-V7 (Fig 5.15). LNCaP clone 9 (less resistant) showed staining for AR-FL and AR-V7 (Fig 5.16). Interestingly, qualitatively, AR-V7 expression was higher in the most enzalutamide resistant clone 1 compared to the less resistant clone 9. Androgen independent PC-3 cell lines were used as a negative control and showed no staining for AR-FL or AR-V7 (Fig 5.17).

A.

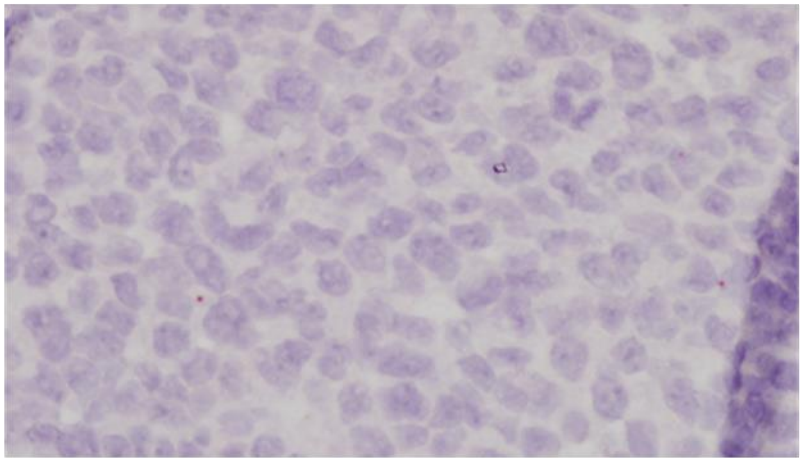

B.

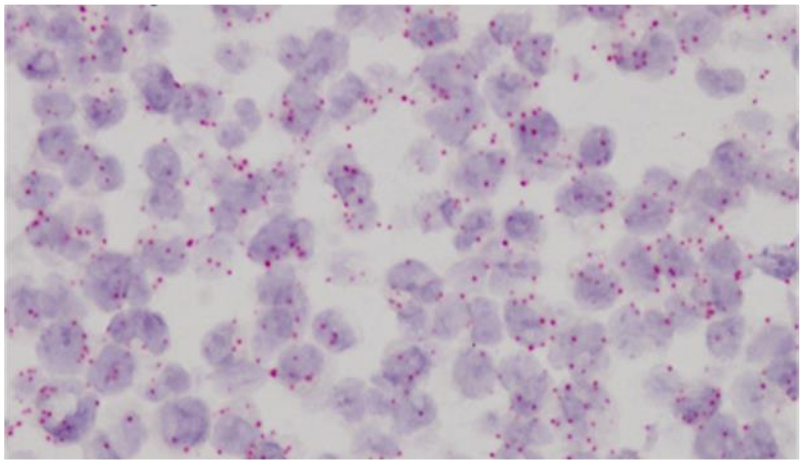

C.

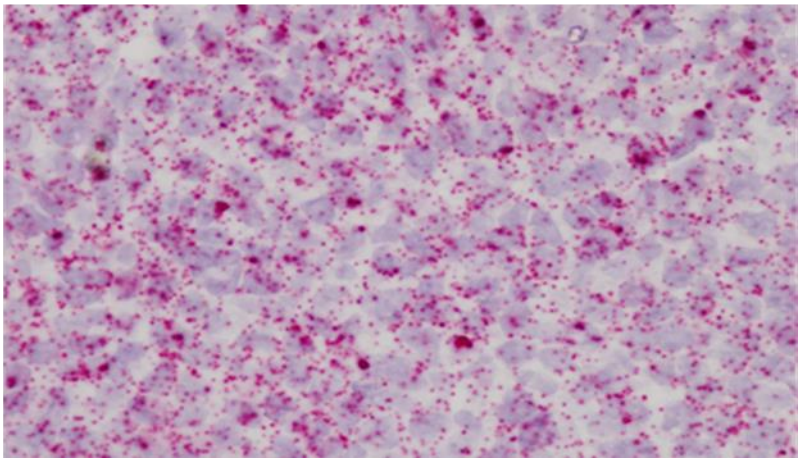

D.

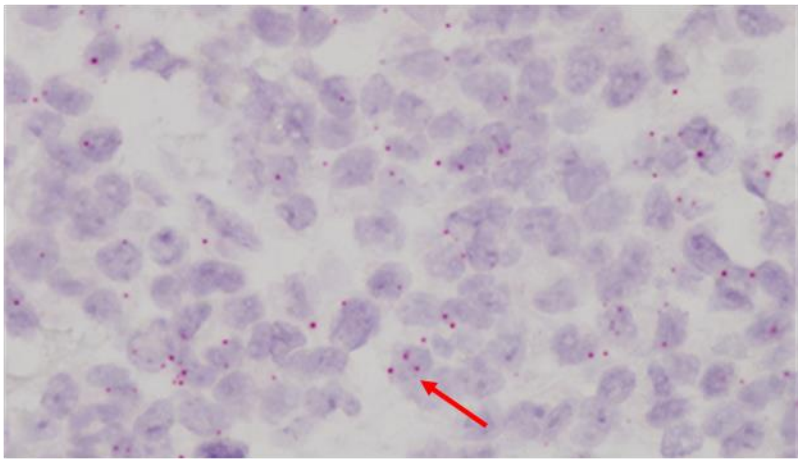

Figure 5.13. AR-FL and AR-V7 expression in VCaP using BaseScope™. (A) Negative control, (B) Positive control, (C) AR-FL probe showing positive (score 3+) red punctate staining, and (D) AR-V7 probe showing positive (score 1+) red punctate staining (red arrow). All images taken at 40X magnification.

A.

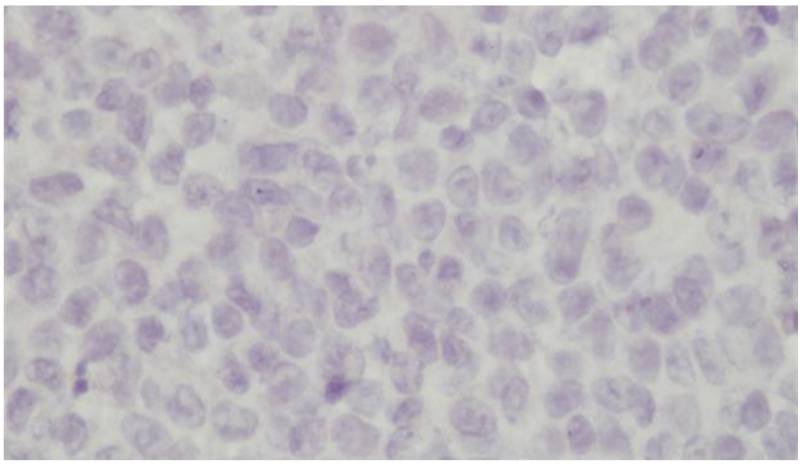

B.

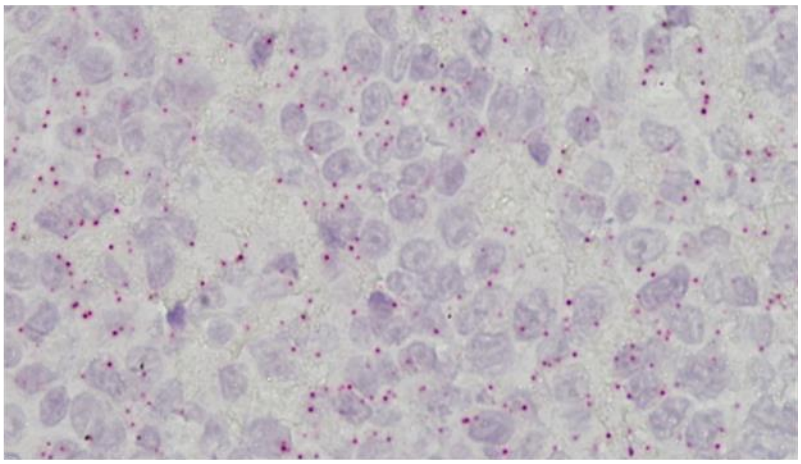

C.

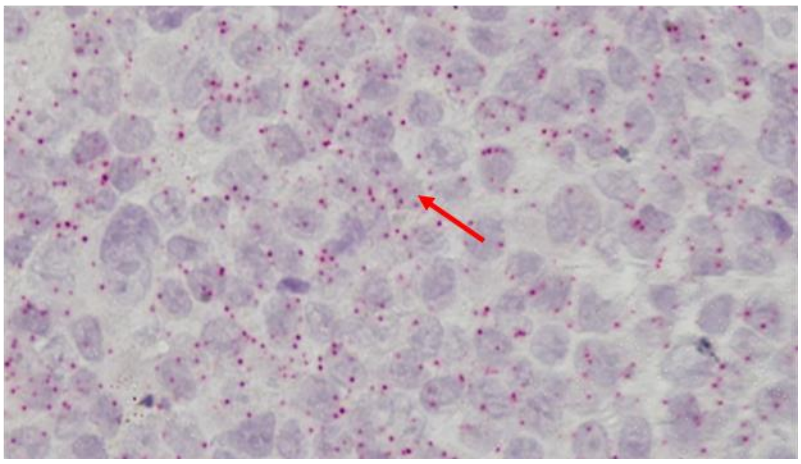

D.

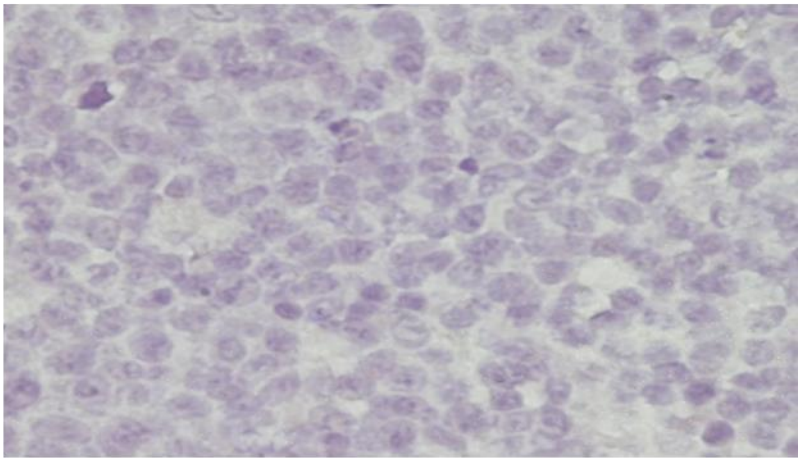

Figure 5.14. LNCaP Control cell line stained using BaseScope™. (A) Negative control (40X), (B) Positive control (40X), (C) AR-FL staining (score 2+) (red arrow) (40X), and (D) AR-V7 staining (40X).

A.

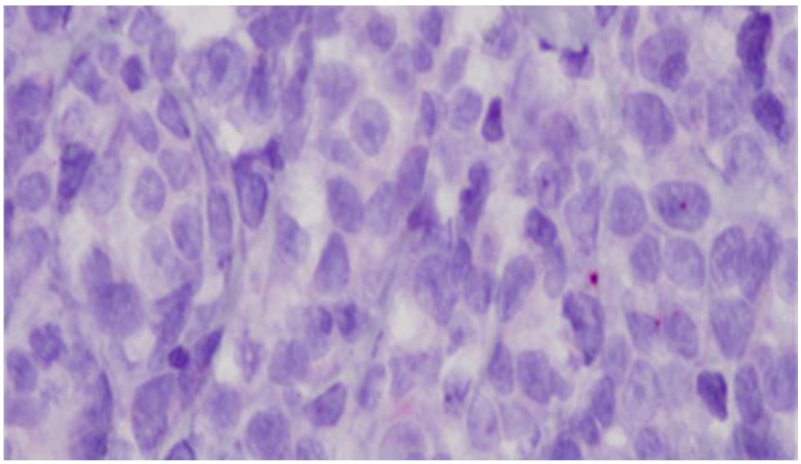

B.

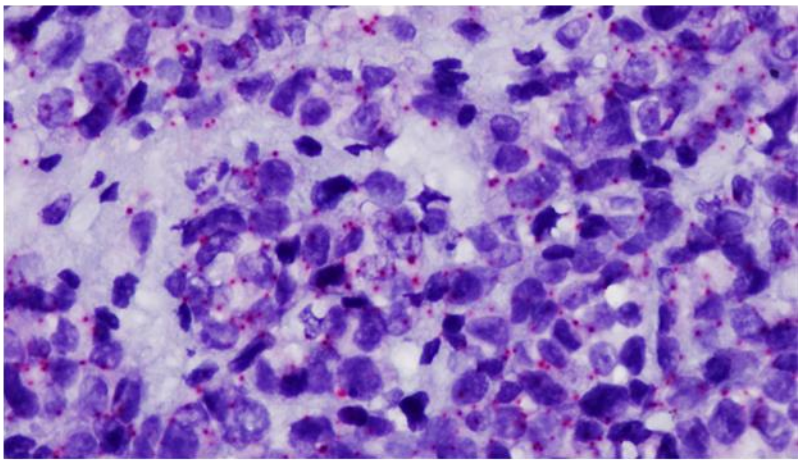

C.

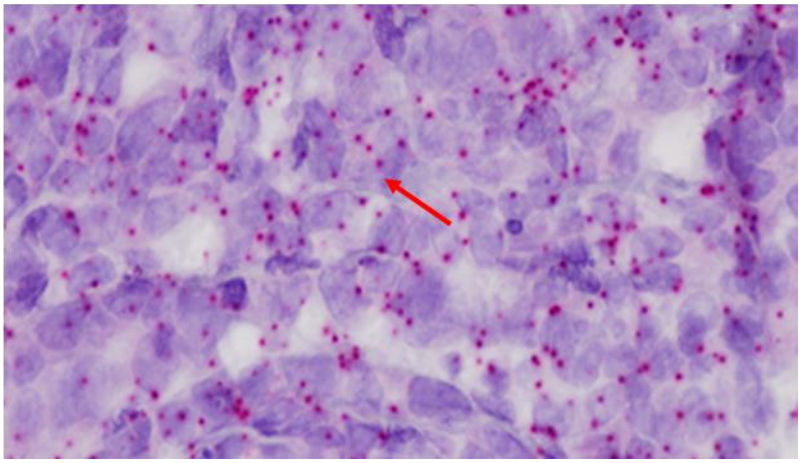

D.

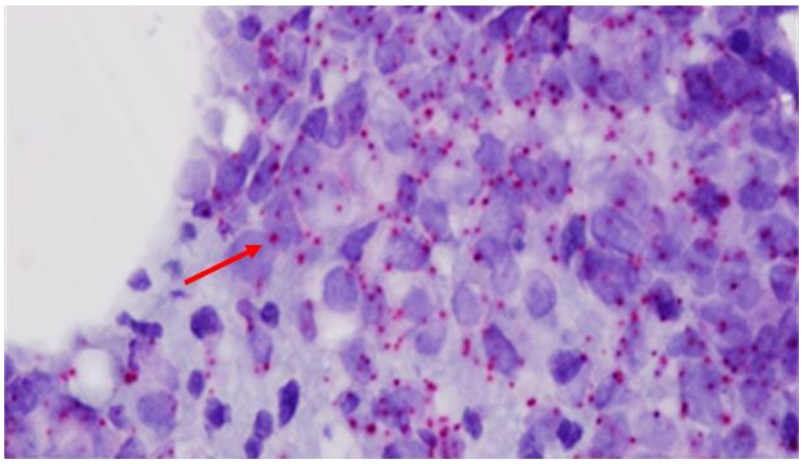

Figure 5.15. LNCaP clone 1 cell line stained using BaseScope™. (A) Negative control (40X), (B) Positive control (40X), (C) AR-FL staining (red arrow, score 2+) (40X), and (D) AR-V7 staining (red arrow, score 2+) (40X).

A.

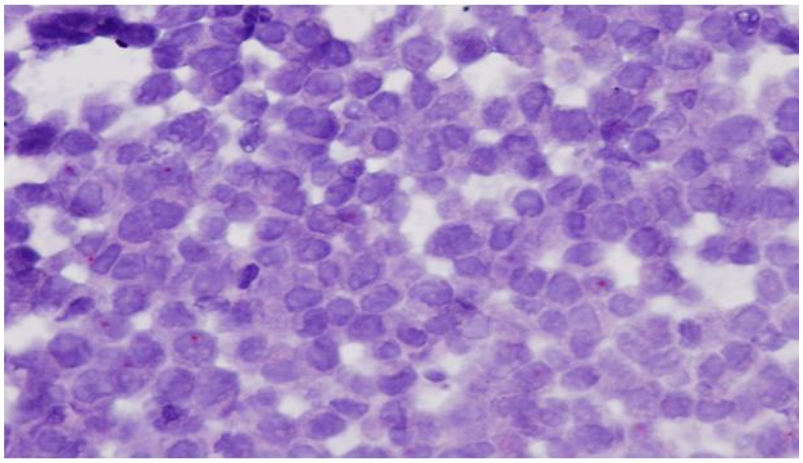

B.

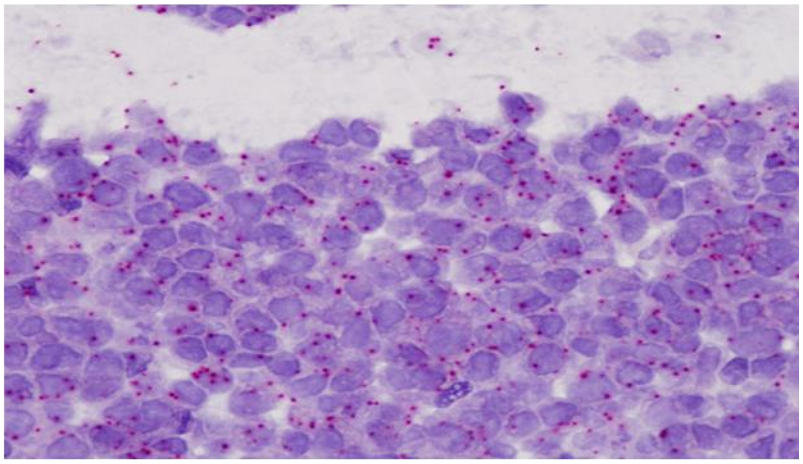

C.

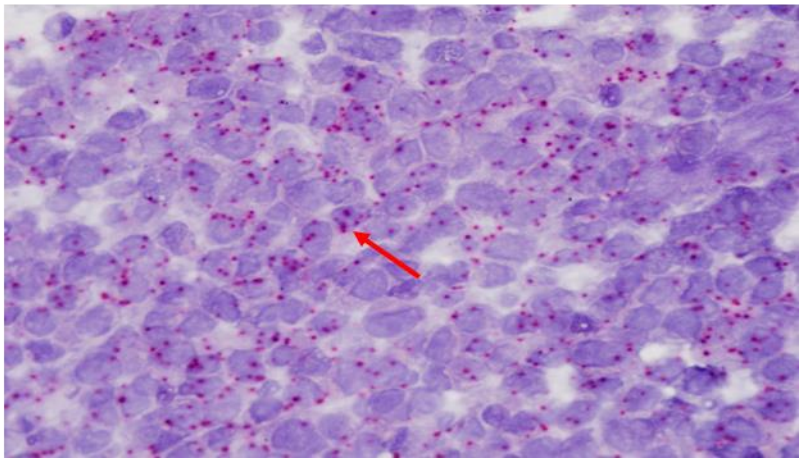

D.

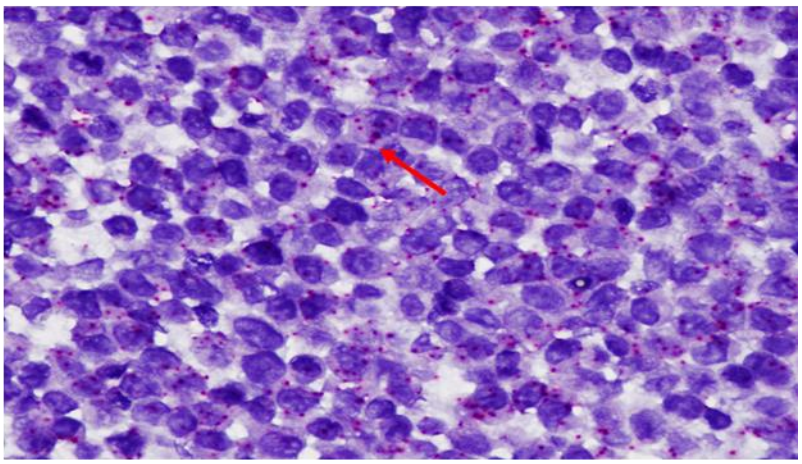

Figure 5.16. LNCaP clone 9 stained using BaseScope™. (A) Negative control (40X), (B) Positive control (40X), (C) AR-FL staining (red arrow, score 2+) (40X) and (D) AR-V7 staining (red arrow, score 1+) (40X).

A.

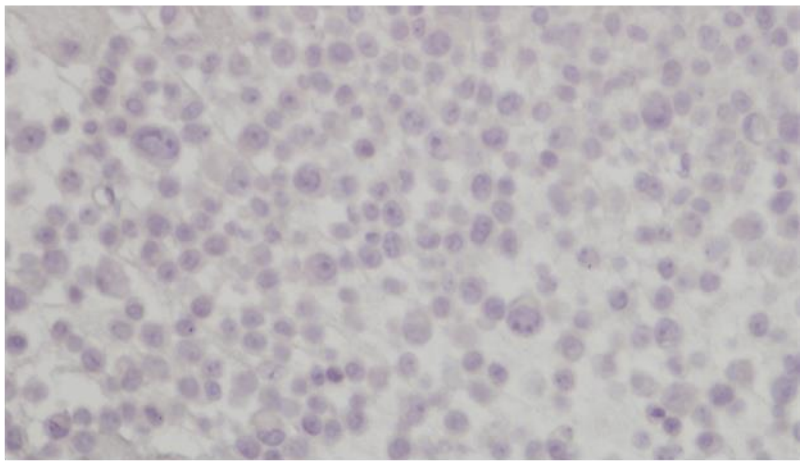

B.

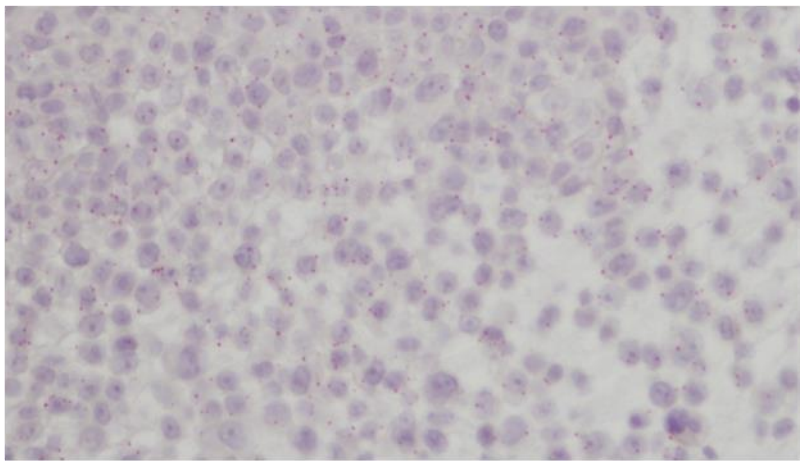

C.

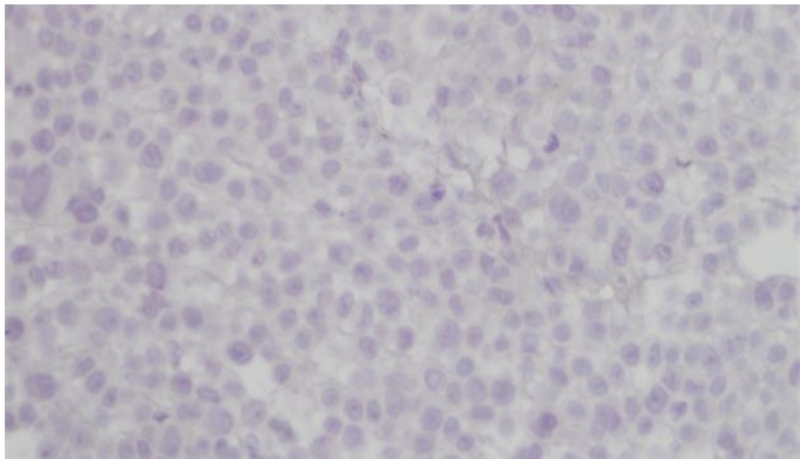

D.

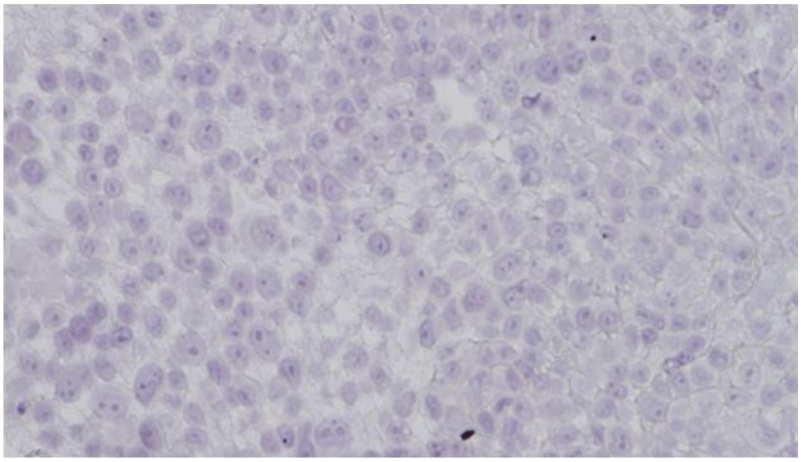

Figure 5.17. Androgen independent PC-3 using BaseScope™ showing no expression of AR expression. (A) Negative control (40X), (B) Positive control (40X), (C) AR-FL (40X), and (D) AR-V7 (40X).

5.1.9 Assessment of RISH on patient tissue samples

RNAScope® was performed initially on radical prostatectomy specimens (n=4). Prior to testing, a pathologist reviewed the clinical specimens, and the presence of invasive carcinoma was confirmed. Staining with negative and positive controls were used to confirm the workflow. In 2 samples, there was no staining with the positive control, indicating that the workflow was not compatible with these specimens. These were radical prostatectomy specimens. In the third sample (a radical prostatectomy specimen), expression was observed for the positive control confirming the workflow, however, there was no staining present with either AR-FL or AR-V7 (Fig 5.18). In the fourth sample (a radical prostatectomy specimen), there was sub-optimal positive control staining, and there was no signal observed for either AR-FL or AR-V7.

A.

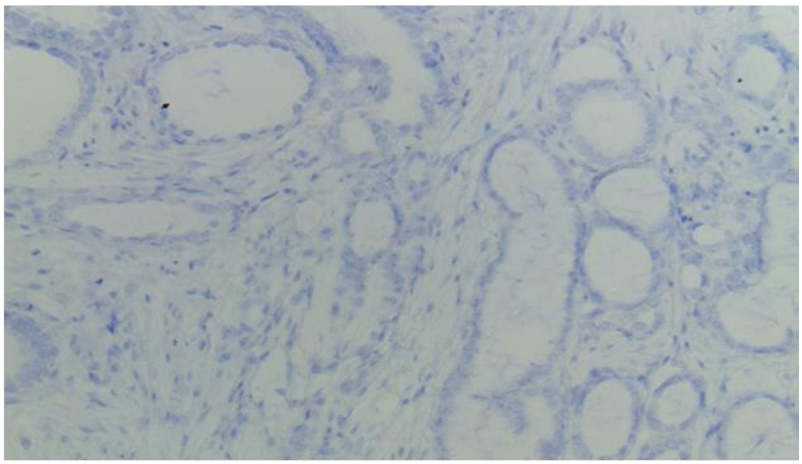

B.

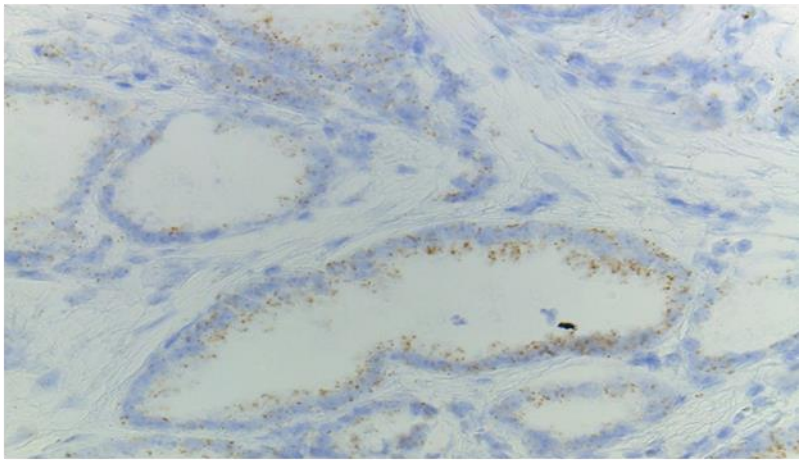

C.

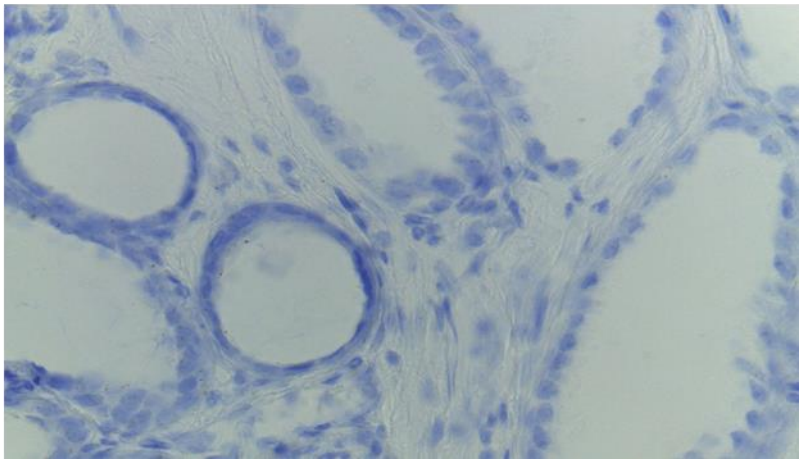

D.

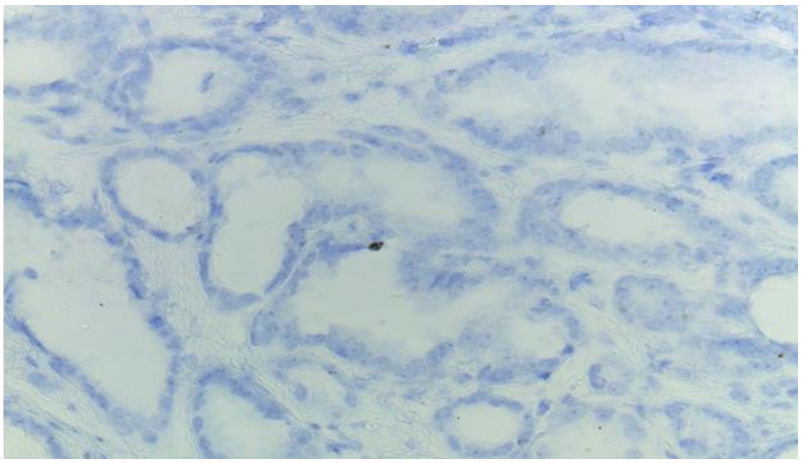

Figure 5.18. Images obtained from RNAscope® staining on radical prostatectomy sample specimen. This specimen was a pT2c prostate adenocarcinoma with a Gleason score of 3+4=7. FFPE sections showing (A) negative control, and (B) positive control with brown staining. Background is clear, positive control was present and cell morphology was preserved. The probes AR-FL (C) and AR-V7 (D) were not detectable in this sample. All images taken at 40X magnification.

5.1.10 AR-FL and AR-V7 using BaseScope™ RISH

BaseScope™ was next used to assess AR-FL and AR-V7 expression on patient tissues. Metastatic biopsies obtained from the iPROSPECT study were used to test the assay after optimisation in cell lines. A sample was selected from a patient with mCRPC who had undergone a CT guided biopsy of a metastatic lymph node. Histology confirmed poorly differentiated carcinoma with positive staining for PPSA and PSA, which was consistent with metastatic prostatic adenocarcinoma. To assess the BaseScope™ workflow prior to testing, positive (PPIB) and negative (dapB) controls genes were tested first. Cell morphology was well preserved throughout the workflow (Fig 5.19A) and the workflow was confirmed (Fig 5.19B). Both AR-FL (Fig 5190C) and AR-V7 (Fig 5.19D) was detected in the metastatic biopsy sample.

5.1.11 Assessing the sensitivity of BaseScope™ in other PCa subtypes

To assess if BaseScope™ was suitable on other types of tissue, RISH was performed using bone and liver biopsy samples (n = 2). In the liver biopsy sample, there was no expression of either AR-FL or AR-V7. IHC was performed on this sample and it showed neuroendocrine differentiation. Similarly, RISH using BaseScope™ was performed on a bone sample obtained from a patient enrolled on iPROSPECT. Histopathological review of the slides showed a significant reduction in the quality of the cells due to decalcification, which explains the lack of positive staining for AR-FL or AR-V7. Further testing was not performed due to the lack of available tissue samples in metastatic patients.

A.

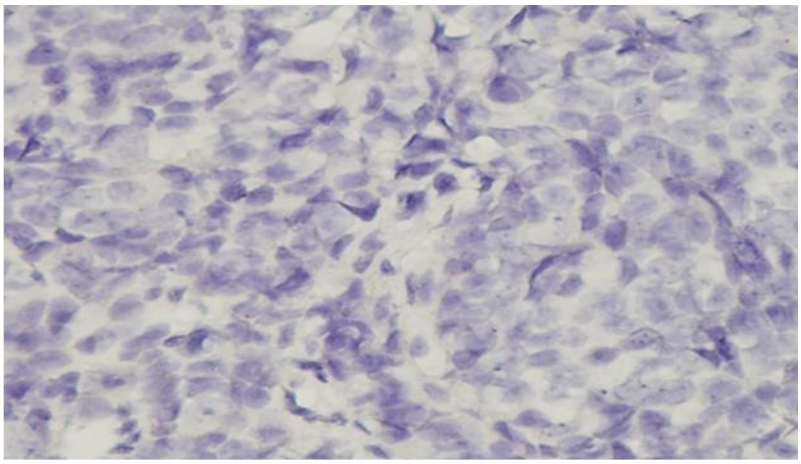

B.

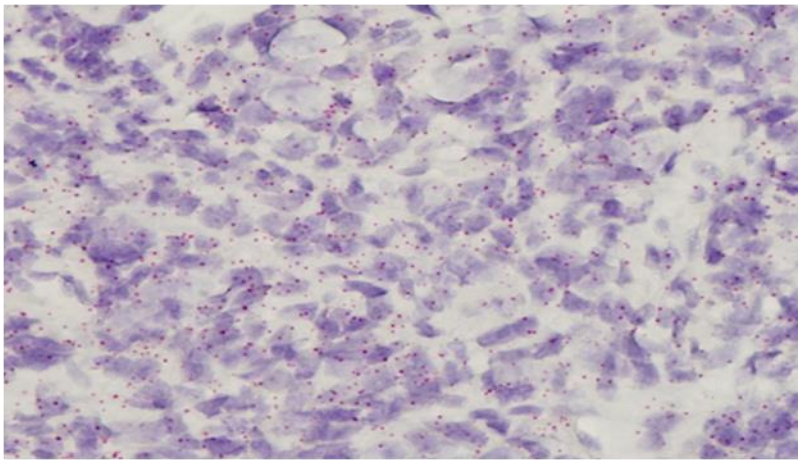

C.

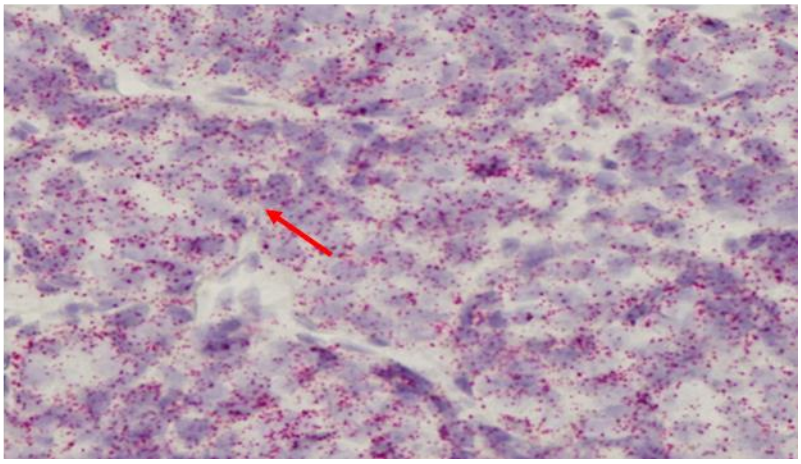

D.

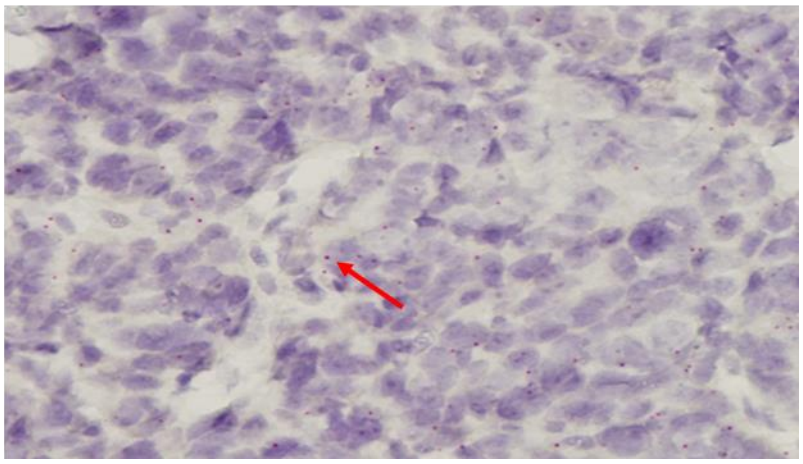

Figure 5.19. AR-FL and AR-V7 expression in a patient sample using BaseScope™. (A) Negative control with dapB gene (40X), (B) Positive control showing red punctate staining with PPIB gene (40X), (C) AR-FL probe showing red positive punctate staining (score 3+) (red arrow) (40X), and (D) AR-V7 probe showing red positive punctate staining (score 1+) (red arrow) (40X).

5.1.12 CTC filters and RISH

ScreenCell® devices are designed to capture CTCs directly on a filter. This allows for downstream procedures such as IHC to be performed directly on to the filters. RNAscope® had not been previously been tested on these types of filters. Healthy donor blood spiked with 22Rv1 cells was used to test the suitability of the use of RNAscope® with ScreenCell® filters. 22Rv1 cells were successfully captured on the CTC filter and stained with MGG (Fig 5.20). Staining with positive control PPIB and negative control dapB was used, however there was no staining visible after completion of the workflow. Thus, indicating that RNAscope® is currently not compatible with ScreenCell® filters.

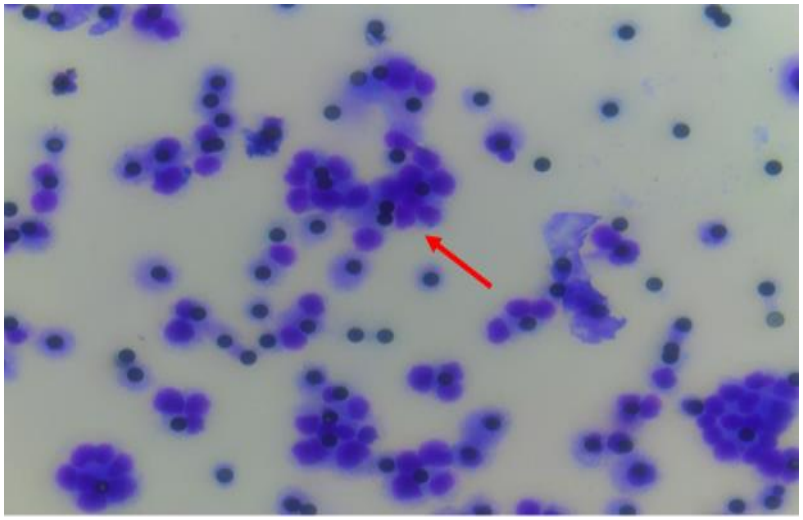

Figure 5.20. Compatibility of RNAscope® with ScreenCell® filters. Blood spiked with 22Rv1 cells was filtered using ScreenCell®. Clustering of 22Rv1 cells is shown after staining with MGG (red arrow) (40X).

6.27 Discussion

The aim of this chapter was to analyse the expression of AR-FL and AR-V7 *in vitro* and *in vivo*. This study also explored the association of AR-V7 and the F876L mutation. Androgens and the AR play essential roles in the initiation and progression of PCa (31). AR gene amplification emerges during ADT and facilitates tumour growth in low androgen concentrations (145). Furthermore, the presence of the splice variant, AR-V7, has been established to be associated with resistance to ASIs, such as enzalutamide, which functions by impairing AR signalling (17). However, a robust clinical assay to detect AR-V7 has not yet been fully established, many years after its initial discovery. Several hypotheses for treatment failure have been suggested such as hypersensitivity to non-testicular antiandrogens, increased androgen biosynthesis from adrenal precursor steroids or mutations in the androgen receptor gene (145).

For *in vitro* experiments in this study, a panel of malignant, androgen dependent and independent cell lines were used. Both AR-FL and AR-V7 were confirmed in AR-dependent cell lines. Interestingly AR-V7 expression was highest in 22Rv1, a cell line previously known to be resistant to enzalutamide (146). To further assess the association of enzalutamide resistance and AR-V7 expression, a panel of cell lines with varying resistance to enzalutamide was utilised. The resistant cell lines (Clone 1/9) possessed the F876L mutation in the AR that potently drives genetic/phenotypic resistance to enzalutamide (35). The mutation alters the AR allowing it to use enzalutamide as an agonist and has been demonstrated to promote an addictive phenotype *in vivo* (35). The AR-V7 transcript copy number was highest in LNCaP clone 1, a cell line displaying strong resistance to enzalutamide and this is most likely due to the

presence of the AR-F876L mutation (35). This demonstrated for the first time the levels of AR-V7 in this cell line model.

In order to further develop applicable clinical AR-V7 assays, different histopathological methods were analysed. Detection of clinically significant AR-V7 expression has been achieved by IHC using antibodies raised against the AR-V7–specific peptide, however, detection of nonspecific, unidentified protein targets in AR/AR-V7 negative cells has been reported (144). In this study, previous testing with IHC for AR-V7 had proven suboptimal. Earlier reports have observed discrepancies in IHC data, possibly reflecting some nonspecific binding by the antibody or differences in protein levels (147). As IHC methods could not be optimised successfully, a more sensitive RISH assay was explored. RISH detection techniques have been available for some time, but have been previously shown to lack robustness and sensitivity to reliably detect the expression of most human genes (148). This may be because DNA and protein surrogates do not always correlate with RNA expression patterns due to pre- and post-translational modifications. Novel assays such as RNAscope® and BaseScope™ represent an advance in RISH approaches with their proprietary probe design. The advantages of both the RNAscope® and BaseScope™ include improved sensitivity of the detection of each single RNA molecule (148). The technology utilizes ‘Z’ probes, each of which contains an 18- to 25-base region complementary to the RNA sequence of interest, followed by a spacer sequence, then a short “tail” sequence that is recognized by the signal amplification system. The key concept in this technology is that signal amplification requires two ‘Z’ probes binding adjacent to each other in

order for a signal-generating “tree” to form at the target site (149). Single probes binding to nonspecific sites should not produce a full binding site for the pre-amplifier, thus preventing amplification of non-specific signals and enhancing specificity, which can then be visualised under a standard microscope. Optimisation was initially performed with the RNAscope® assay, which confirmed positivity in cells lines but could not be optimised in clinical specimens. The results for RNAscope® in radical prostatectomy tissue samples were suboptimal with strong nuclear background visible after treatment in 2 patient samples, and no positive control signal visible in 2 other samples. The RNAscope® probes for AR-FL and AR-V7, generated nuclear staining which may have been due to the detection of pre-mRNA within the nucleus (148). It is possible the intra-nuclear RISH signals may represent nuclear retention of unspliced RNA species at the transcription site, a phenomenon that has been reported in other transcripts that are inefficiently processed (148).

The BaseScope™ assay was tested and optimised in cell lines followed by clinical samples. Compared to RNAscope®, BaseScope™ incorporates an additional signal amplification step to further boost detection sensitivity without increasing background noise. As a result, BaseScope™ requires only a single ZZ pair instead of the standard 20 ZZ pairs used in RNAscope®, allowing detection of short RNA sequences and the discrimination between single nucleotide alterations (149). AR-FL and AR-V7 expression were confirmed in cell lines, including a panel of enzalutamide resistant cell lines, which showed higher AR-V7 expression in the more resistant clones. The BaseScope™ assay detected mature mRNA exclusively in the cytoplasm of

cell lines with both cytoplasmic and intra-nuclear signals detected. In a patient with advanced CRPC, BaseScope™ demonstrated positive AR-FL and AR-V7 staining in a sample obtained from a lymph node infiltrated with prostate adenocarcinoma. However, it was not possible to detect AR-V7 expression in a metastatic bone sample or liver metastatic sample. Decalcification is required to process metastatic bone samples which can lead to a significant reduction in the quality of the specimen. The reason for the lack of expression of AR-V7 in the bone biopsy could be due to the well-described degradation of tissue integrity and RNA quality that occurs in bone biopsy samples after the decalcification process (150). The liver biopsy analysed in this study did not express AR-FL or AR-V7. It did show evidence of neuroendocrine differentiation, which may be the reason for the lack of expression of AR, as this phenotype rarely expresses AR (151).

This data suggests that BaseScope™ provides superior sensitivity to RNAscope® for the detection of AR-FL and AR-V7 at the RNA level. However, BaseScope™ may only be suitable for soft tissue biopsies rather than bone marrow biopsies or image guided bone biopsies, as standard laboratory processing of samples affects the robustness of the BaseScope™ assay. Nevertheless, BaseScope™ may provide a clinically useful assay for the determination of AR status in soft tissue biopsies with confirmed adenocarcinoma.

In the era of ‘liquid biopsies’, developing an AR-V7 assay that could be used directly on CTCs is of interest, as this would allow serial monitoring of AR-V7 status throughout treatment without the need for repeat invasive

biopsies (52). Initial testing of RISH on CTC filters was negative in this study. However, further optimisation of RISH with other CTC isolation methods, may provide the means to develop this into a potentially clinically useful assay.

In conclusion, multiple techniques to detect AR-FL and AR-V7 were compared including IHC, qPCR and RISH. RISH using BaseScope™ was identified as the most sensitive assay for identifying AR-FL and AR-V7 gene expression in clinical FFPE samples. Ongoing work to validate this assay in larger cohorts of tissue samples is needed. If validated, this assay could be used routinely in the clinical setting to identify patients who may not respond to ASIs and could allow for improved tailored treatment plans for patients.

Chapter 6: Circular RNA expression in Prostate Cancer

6.28 Introduction

ncRNA is made up of several different classes including miRNAs and lncRNAs, both of which are areas of active investigation in PCa (13). Another recently discovered type of ncRNA, called circRNA, exists and appears to have an important role in cancer initiation, development, and progression (14, 15). circRNAs are RNA molecules with covalently joined 3′- and 5′-ends formed by back-splice events, thus presenting as closed continuous loops, which makes them highly stable (16, 17). They typically comprise of one to several coding exons of otherwise linear mRNAs and range between a few hundreds and thousands of nucleotides in length (18). They can be identified and predicted from back-splice junctions, if the alignments of the two terminal parts can be extended to obtain the original read sequence (60). They can be validated using qPCR, normally after enriching with RNase R, a magnesium-dependent 3′→5′ exoribonuclease that digests essentially all linear RNAs but does not digest lariat or circRNA structures (73). Their high abundance, stability and evolutionary conservation between species suggests that they may have an important biological regulatory role. Interestingly, circRNAs have been identified in a number of cancers including PCa suggesting a potential role as a biomarker or target for therapeutics in cancer (90). One such method is by regulating the function of miRNAs. miRNAs have been previously shown to have a wide array of biological processes and have an important role in regulating gene expression in cancer, where they act through the repression of downstream tumour-suppressive mRNAs (20). It has been proposed that circRNAs can act as a miRNA ‘sponge’ thereby modifying miRNA activity through sequestration, thus modifying mRNA target gene expression (34).

Currently, PSA is the only marker used to screen men for the presence of PCa, however it is sub-optimal given issues with specificity and sensitivity. Therefore, there is a need to identify new diagnostic markers for use in the clinical setting. circRNAs could potentially become one such marker.

The aims of this chapter were to (i) investigate the pattern of circRNA expression in a panel of benign and PCa cell lines, (ii) determine the circRNA signature in AR independent *vs*. AR dependent cell lines and (iii) identify the circRNA-miRNA pathways linked to PCa.

6.29 Results

6.29.1 circRNA profiling of Prostate Cancer cell lines

A circRNA microarray (Arraystar) was performed across a panel of eight cell lines in triplicate (Table 6.1). The human circular RNA microarray version 2.0 covers 13,617 previously discovered human circRNAs. circRNAs were enriched by treatment with Ribonuclease R (RNase R), which degrades all linear RNAs, but not circRNAs. Quantile normalization of raw data and subsequent data processing were performed using the R software package (108). After normalization of the raw data (Fig 6.1), low intensity filtering was performed, and the circRNAs that were flagged as "present" or "marginal" ("all targets value") were retained for further analyses. In total 9,757 circRNAs were classified as present across the panel of cell lines. Hierarchical clustering was performed based on all target value circRNAs across 8 samples performed in triplicate.

Table 6.1. Human Prostate Cancer Cell Lines.

Groups	**Cell Lines**	**Source**
AR dependent	22Rv1	
	VCaP	Androgen-dependent xenograftVertebral bone metastasis
	LNCaP	Lymph node metastasis
AR independent	PC-3	Bone metastasis
	DU 145	Brain metastasis
Benign	BPH-1	Human prostate tissue
	PWR-1E	Prostatic epithelial cells
	RWPE-1	Human prostate tissue

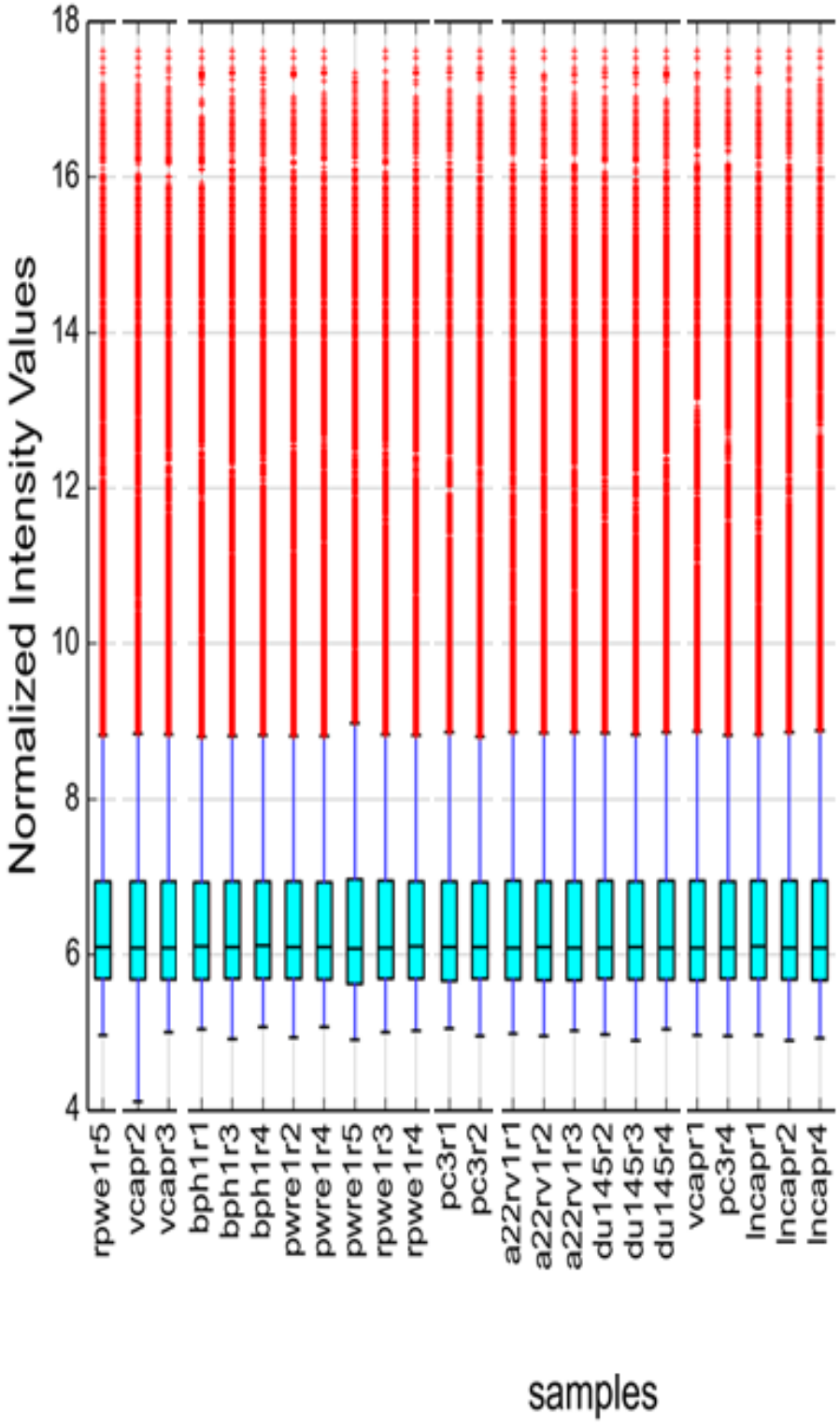

Figure 6.1. Boxplot distributions of circRNA expression. Values for the samples after normalization. CircRNAs were differentially expressed across all cell lines.

6.29.2 Differentially expressed circRNAs

circRNA expression levels between the different cell lines based on malignancy and androgen dependency were investigated. Cell lines were examined using biological replicates performed in triplicate. Differentially expressed circRNAs were examined by computing the fold change (FC) (i.e. the ratio of the group averages) for each circRNA between malignant *vs.* benign cell lines and androgen dependent *vs.* independent cell lines. A student's paired *t* test was then used to identify significantly altered circRNAs. The false discovery rate (FDR) was applied to determine the threshold of p value. An FDR of < 0.05 was used. circRNAs with a FC ≥ 1.5 and $p < 0.05$ were considered to be significantly differentially expressed between malignant *vs.* benign cell lines and androgen dependent *vs.* independent cell lines. Grouped analysis of detected circRNAs between the different cell line groups according to FC is shown using a principle component analysis (PCA) (Fig 6.2). This allows the direct visualisation of the different levels of circRNA expression between the different defined groups of cell lines. Unsupervised clustering (euclidean distance measure and the 'average' agglomeration method) was used for analysis (n=3).

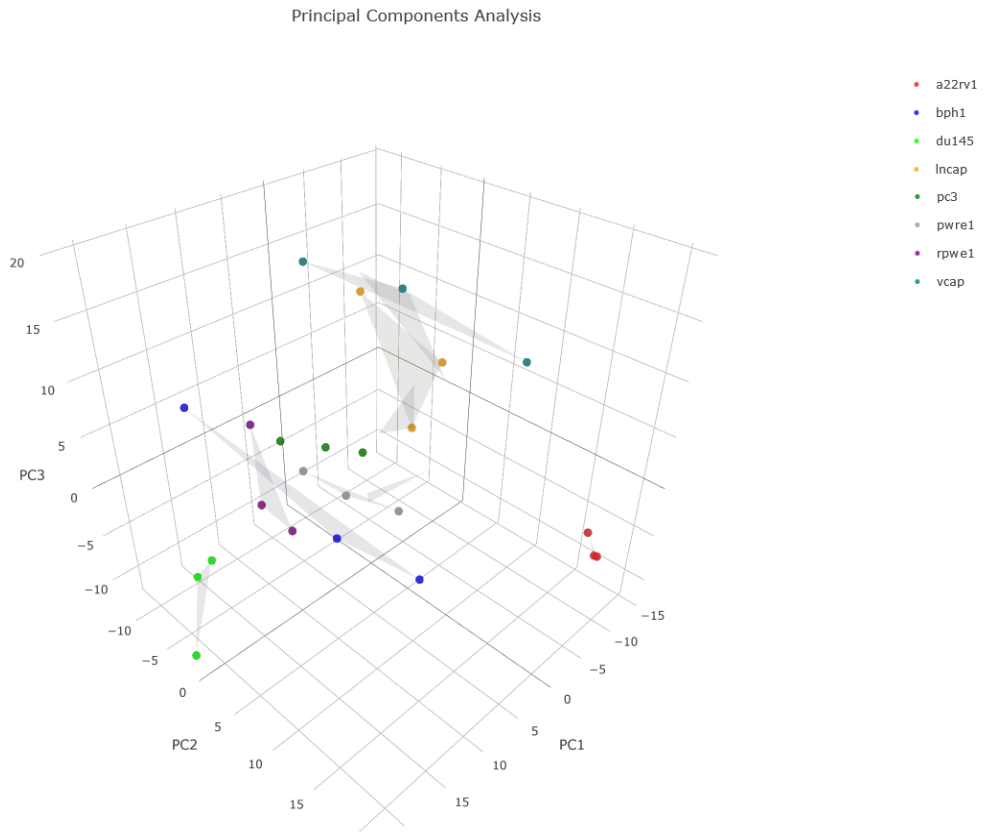

Figure 6.2. Principle Component Analysis plot. Analysis showing circRNA expression levels for the 8 cell lines. Unsupervised clustering (euclidean distance measure and the ‘average’ agglomeration method) was used for analysis (n=3).

6.29.3 Proof of concept to determine the utility of qPCR to detect circRNAs

A previously discovered intronic circRNA termed circBICC1, associated with the gene, *BICC1*, is composed of four separated fragments in the human genome (152) and was used as a proof of concept to determine the utility of qPCR to detect circRNAs. Outward facing primers for circBICC1 were designed using the sequence published by Gao *et al.* (152) and qPCR was performed on HeLa cell lines. Expression of BICC1 circRNA was confirmed using standard qPCR after enrichment with RNase R, which confirmed the feasibility of analysing cell lines for circRNAs using a qPCR-based method (Fig 6.3).

6.29.4 RNAse R

RNAse R was used to degrade linear RNAs and therefore enrich for circRNAs. A number of experiments were performed to optimise RNase R treatment in order to enrich for circRNAs. RNase R was used initially as a proof of concept to confirm circBICC1 expression and in the initial microarray study. As an example, RNase R was used to enrich hsa_circ_0090923 (Fig 6.4), however there was no significant change in expression levels after treatment. Further additional experiments examining RNAse R are listed in Table 6.2.

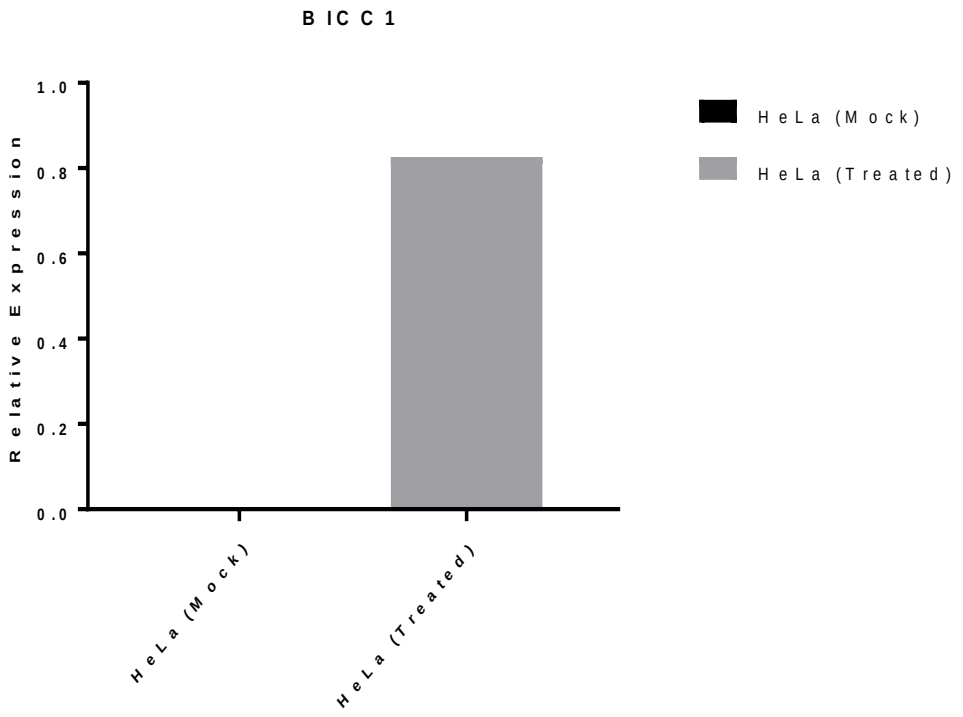

Figure 6.3. circBICC1 expression in HeLa Cells. HeLa cells with no RNase R treatment (Mock) compared to Hela Cells treated with RNase R (Treated). (n=1)

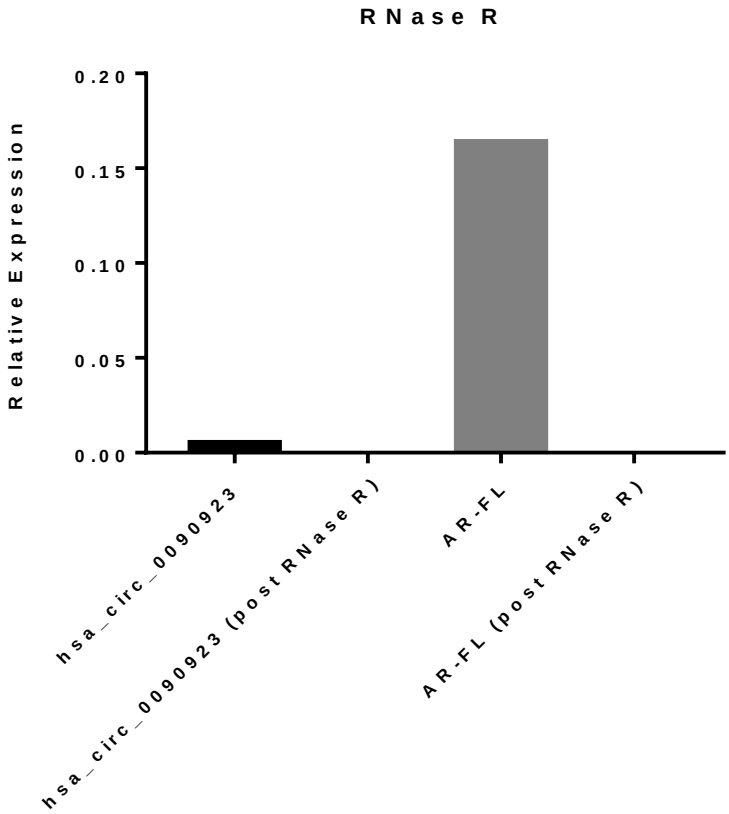

Figure 6.4. Expression of hsa_circ_0090923 and AR-FL with and without RNase R. (n = 1).

Table 6.2. Different methods attempted to optimise RNase R.

Method
1. Increasing RNA concentration
2. Increasing RNase R concentration
3. Increasing qPCR cycle length >55
4. Performing RNA clean-up
5. Designing TaqMan probe for circRNAs
6. Using RNase R from a different manufacturer
7. Performing RNase R without DNase

6.29.5 circRNAs and their miRNA binding sites

circRNAs for validation were selected based on the detected MREs. MREs are miRNA binding sites that were predicted using TargetScan (110) and miRanda (109) bioinformatic platforms based on the circRNA-miRNA-mRNA network. For each identified circRNA, the top 5 most likely miRNA binding sites were predicted. Twenty-one miRNAs associated with PCa were used to rank the top circRNAs. CircRNAs that matched these miRNAs are listed in Table 6.3. These circRNAs were then selected for validation.

6.29.6 circRNAs and their associated miRNAs identified from microarray

circRNAs were filtered based on their association with known miRNAs that are associated with PCa. Five upregulated and 5 downregulated circRNAs based on miRNA filtering were selected to perform validation testing, in a panel of PCa cell lines (Table 6.4).

Outward facing primers for the 10 circRNAs were designed. Seven out of the 10 cirRNAs had Ct values beyond 30, which were not tested further (Table 6.5). Further testing identified 3/10 circRNAs with acceptable Ct values. The expression of 2/3 circRNAs (hsa_circ_0083092, hsa_circ_0004870) was consistent with the microarray data and were further validated in cell lines.

Table 6.3. List of miRNAs and their predicted circRNAs.

miRNA	**Function**	**Predicted circRNA**
mir-141	miR-141 obstructs tumour growth and metastasis(153)	hsa_circ_0063526 hsa_circ_0083694
mir-145	downregulated in CRPC (154)	hsa_circ_0004870 hsa_circ_0063577 hsa_circ_0004622 hsa_circ_0007351
mir-205	downregulated in PCa and acts as a tumour suppressor (155)	hsa_circ_0083756
mir-21	inhibits tumour suppressor gene PTEN to promote PCa cell proliferation and invasion (156)	hsa_circ_0065760
mir-106b	promotes proliferation and metastasis of PCa (157)	hsa_circ_0013204
mir-449b	high expression associated with biochemical recurrence after radical prostatectomy (158)	hsa_circ_0003249 hsa_circ_0040994 hsa_circ_0058988 hsa_circ_0049657
mir-25	downregulated in PCa (159)	hsa_circ_0000673
mir-124	inhibits invasion and proliferation of PCa cells (160)	hsa_circ_0022383 hsa_circ_0003505 hsa_circ_0088059
mir-221	downregulated in CRPC (161)	hsa_circ_0001721
mir-125b	tumour suppressor (162)	hsa_circ_0083092

Table 6.4. List of circRNAs selected for validation. circRNAs are given with their corresponding gene, MREs and miRNA function.

Alias	**Expression**	**Parental Gene**	**MRE**	**miRNA role in PCa**
hsa_circ_0004870	Down	*RBM39*	miR-145	Cancer cell migration and invasion (163)
hsa_circ_0002807	Down	*TMCO3*	miR-141	Suppresses stem cells (153)
hsa_circ_0022383	Down	*FADS2*	miR-124	Inhibits invasion and proliferation (164)
hsa_circ_0003505	Down	*USP22*	miR-124	as per miR-124
hsa_circ_0088059	Down	*SUSD1*	miR-124	as per miR-124
hsa_circ_0000673	Up	*RSL1D1*	miR-25	Modulates invasiveness and dissemination (159)
hsa_circ_0002754	Up	*KAT6A*	miR-145	Cancer cell migration and invasion (159, 165, 166)
hsa_circ_0001278	Up	*STT3B*	miR-205	ERG target gene (155)
hsa_circ_0001721	Up	*CDK14*	miR-221	Promotes cell proliferation and represses apoptosis (161)
hsa_circ_0083092	Up	*RBM33*	miR-125b	Tumour suppressor (162)

Table 6.5. List of circRNAs qPCR values beyond 30 cycles that were not further tested.

CircRNA	**Ct Value**
hsa_circ_0000673	31
hsa_circ_0002754	33
hsa_circ_0002807	32
hsa_circ_0088059	30
hsa_circ_0001278	30
hsa_circ_0022383	35
hsa_circ_0003505	34

6.29.7 circRNAs are differentially expressed in Prostate Cancer

An overall group analysis based on malignancy was performed between malignant and benign groups. circRNA expression levels between malignant cell lines (22Rv1, LNCaP, PC-3 and VCaP) were compared to benign cell lines (BPH-1, PWR-1E, RWPE-1). circRNAs were significantly differentially expressed between these groups according to FC and P value (Fig 6.5).

The list of the top ten upregulated circRNAs in malignant PCa cell lines compared to benign cell lines are listed in Table 6.6. The top two expressed circRNAs in PCa cell lines were hsa_circ_0082672 and hsa_circ_0082680, both located on chromosome 7 and associated with the Homeodomain-interacting protein kinase 2 (*HIPK2)* gene. Depletion of HIPK2 in PCa cells is associated with decreased AR target gene expression (167).

The top 10 downregulated circRNAs according to FC are listed in Table 6.7. hsa_circ_0001016, and two others downregulated circRNAs (hsa_circ_0001017 and hsa_circ_0054882) are associated with the *XP01* gene. XPO1 has been shown to force the retention and activation of tumour suppressor proteins resulting in tumour cell death in preclinical models (168).

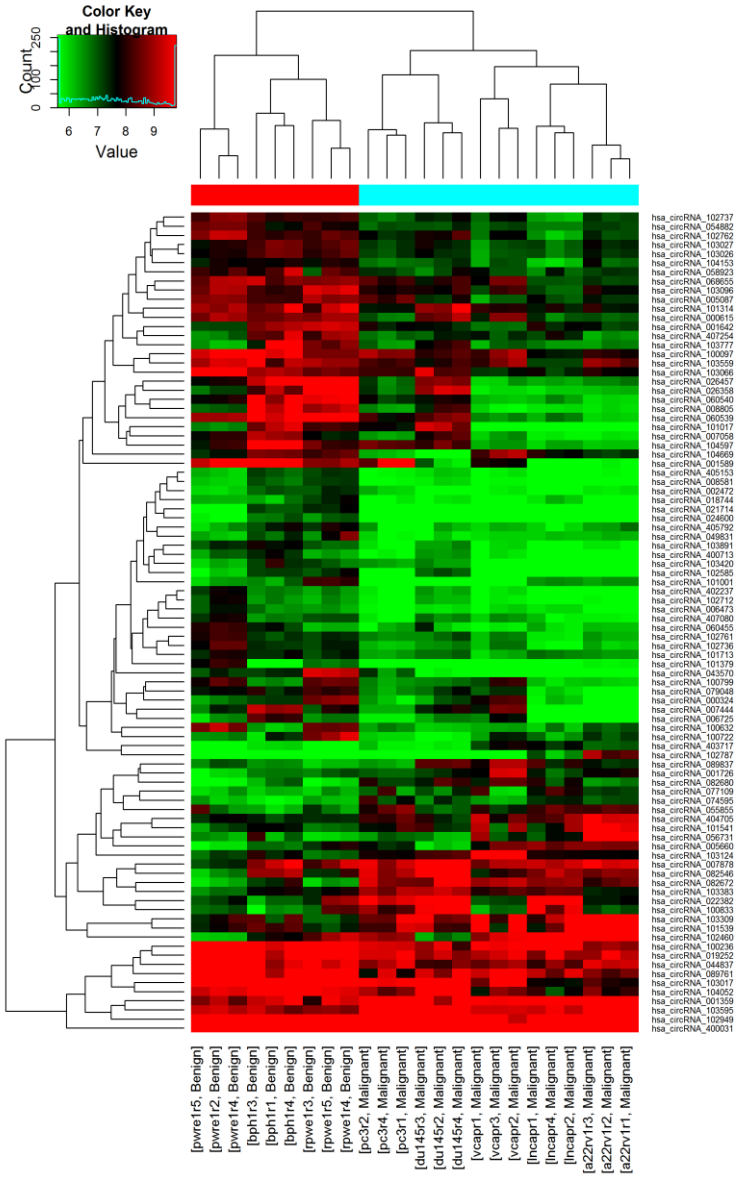

Figure 6.5. Clustering heat map of microarray data showing differential expression of circRNAs between malignant and benign cell lines. Unsupervised clustering (euclidean distance measure and the 'average' agglomeration method) was used for analysis (n=3).

Table 6.6. Top ten upregulated circRNAs in PCa (malignant *vs.* benign cell lines).

CircRNA	Chromosome	Gene
hsa_circ_0082672	chr7	*HIPK2*
hsa_circ_0082680	chr7	*HIPK2*
hsa_circ_0074595	chr5	*ANXA6*
hsa_circ_0089837	chrX	*AK000470*
hsa_circ_0065871	chr3	*MAPKAPK3*
hsa_circ_403717	chr6	*ARFGEF3*
hsa_circ_0001187	chr21	*DOPEY2*
hsa_circ_0014022	chr1	*TARS2*
hsa_circ_0069086	chr4	*MAN2B2*
hsa_circ_0049657	chr19	*NFIX*

Table 6.7. Top ten downregulated circRNA in PCa (malignant *vs.* benign cell lines).

CircRNA	Chromosome	Gene
hsa_circ_0001016	chr2	*XPO1*
hsa_circ_0003394	chr2	*PGAP1*
hsa_circ_0004942	chr15	*RMDN3*
hsa_circ_0004405	chr5	*FAM169A*
hsa_circ_0037972	chr16	*PARN*
hsa_circ_0026457	chr12	*KRT5*
hsa_circ_0060539	chr20	*SDC4*
hsa_circ_0001017	chr2	*XPO1*
hsa_circ_0054882	chr2	*XPO1*
hsa_circ_0008805	chr17	*ARHGAP23*

hsa_circ_0004870

Two representative malignant cell lines (22Rv1 and LNCaP) and 1 representative benign line (BPH-1) were used to assess expression of hsa_circ_0004870 according to malignancy status. hsa_circ_0004870 was significantly downregulated in the malignant lines 22Rv1 ($p \leq 0.01$) and LNCaP ($p \leq 0.01$) compared to the benign line BPH-1 (Fig. 6.6). This corresponds to the array data, which showed this circRNA significantly downregulated in these cell lines.

hsa_circ_0083092

hsa_circ_0083092 is an exonic circRNA that has been shown to be associated with miR-125b expression and appears to be an early event in tumourigenesis in PCa (169). Expression of hsa_circ_0083092 was examined in malignant cell lines (22Rv1 and LNCaP) *vs.* benign cell line (BPH-1). There was no significant difference in expression of hsa_circ_0083092 between these cell lines (Fig. 6.7). This was consistent with the microarray data.

6.29.8 circRNAs are differentially expressed according to AR status

circRNA expression levels between androgen dependent and independent cell line were examined. Androgen dependency was confirmed by analysing AR-FL expression in this cell line panel as previously described in chapter 5. circRNAs were differentially expressed between androgen dependent (2125 circRNAs) *vs*. independent cell lines (2235 circRNAs) (Fig 6.8).

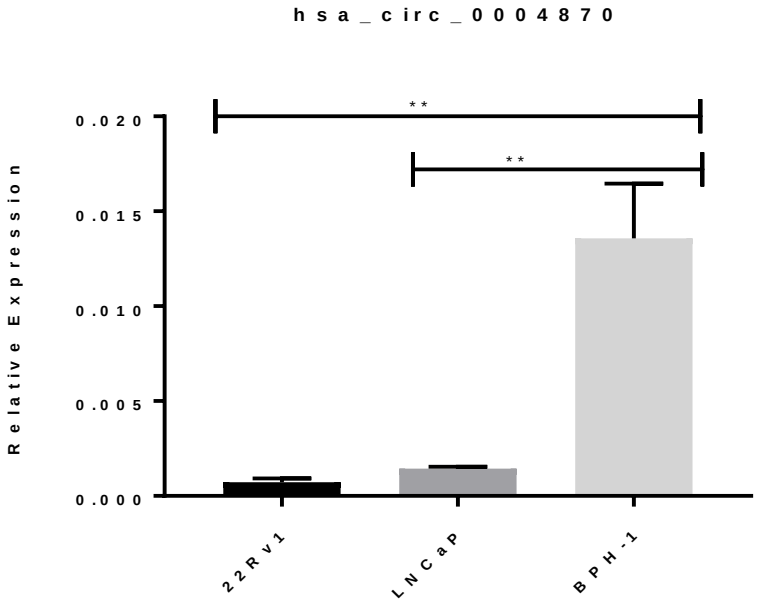

Figure 6.6. hsa_circ_0004870 expression according to malignancy status. Two malignant cell lines (22Rv1 and LNCaP) were compared to the benign line BPH1. Data graphed as mean ± SEM (n=3). Ordinary one-way ANOVA. ** p≤ 0.01.

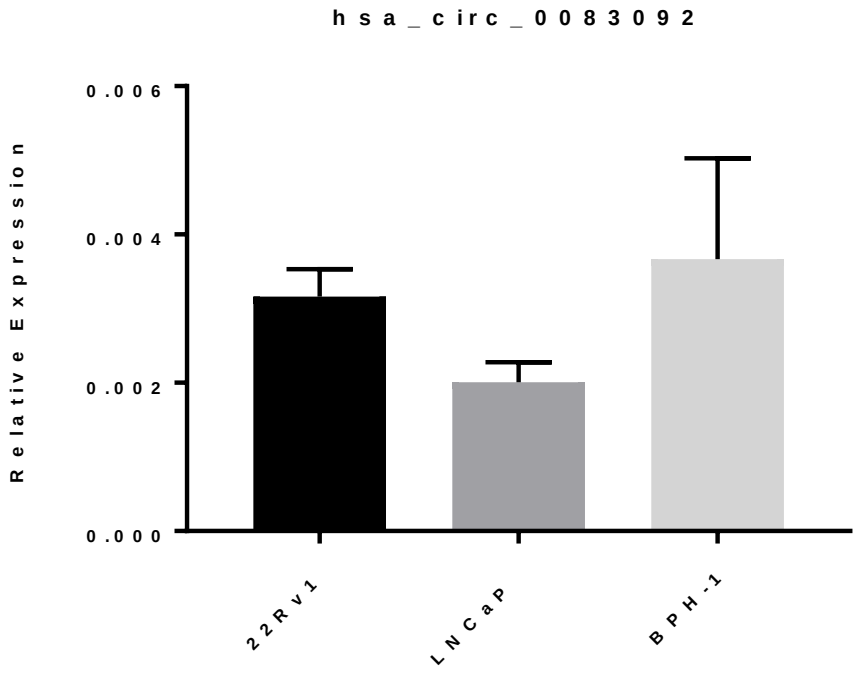

Figure 6.7. hsa_circ_0083092 expression in PCa. Two malignant cell lines (22Rv1 and LNCaP) were compared to the benign line BPH-1. Data graphed as mean ± SEM (n=3).

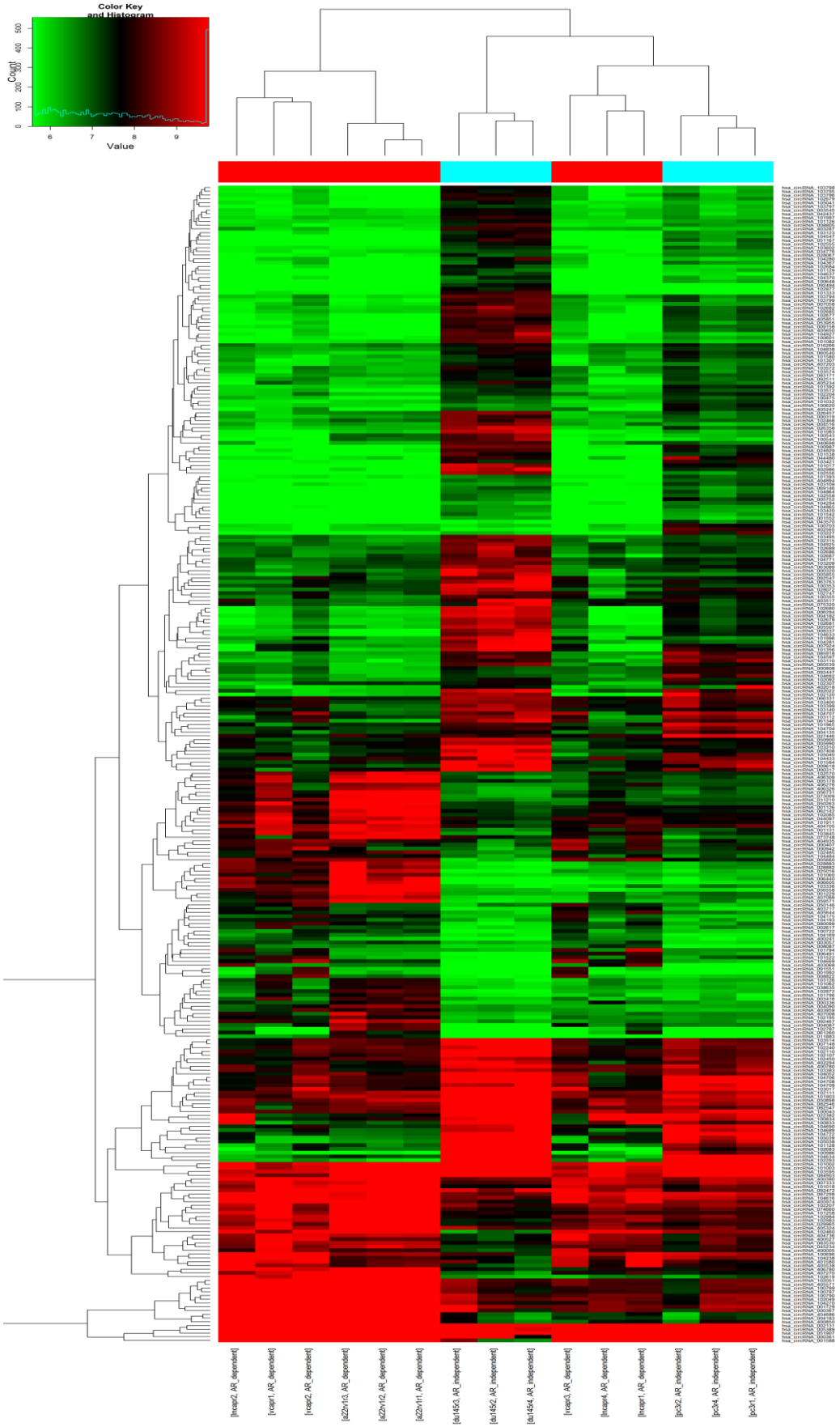
Color Key and Histogram
Count
Value
[lncap2, AR_dependent]
[vcap1, AR_dependent]
[vcap2, AR_dependent]
[ar2v1r3, AR_dependent]
[ar2v1r2, AR_dependent]
[ar2v1r1, AR_dependent]
[dr145-3, AR_independent]
[dr145-2, AR_independent]
[dr145-4, AR_independent]
[vcap3, AR_dependent]
[lncap4, AR_dependent]
[lncap1, AR_dependent]
[pc3-2, AR_independent]
[pc3-4, AR_independent]
[pc3-1, AR_independent]

Figure 6.8. Clustering heat map of microarray data. Heatmap showing differential expression of circRNAs between androgen dependent LNCaP, 22rv1 and VCaP (hormone sensitive) and independent cell lines DU145 and PC3 (castration resistant). Unsupervised clustering (euclidean distance measure and the 'average' agglomeration method) was used for analysis (n=3).

Grouped analysis was performed of differentially expressed circRNAs between androgen dependent and independent cell line groups. The grouped analysis listed the highest upregulated circRNAs in AR dependent PCa (Table 6.8). The upregulated hsa_circ_0083171 is an exonic circRNA located on chromosome 7 and associated with the gene *DNAJB6*. DNAJB6 is a known tumour suppressor (170).

Table 6.8. Top ten upregulated circRNAs in androgen independent cell lines.

circRNA	**FC**	**Chromosome**	**Gene**
hsa_circ_0083171	2.2	chr7	*DNAJB6*
hsa_circ_0092022	10.5	ChrX	*FLNA*
hsa_circ_0006646	3.2	chr8	*PTK2*
hsa_circ_0018086	2.0	chr10	*ZEB1*
hsa_circ_0084615	14.2	chr8	*ASPH*
hsa_circRNA_402986	4.4	chr3	*PLOD2*
hsa_circ_0008337	2.9	chr8	*ASPH*
hsa_circ_0085918	4.1	chr8	*PLEC*
hsa_circ_0003578	2.3	chr2	*CRIM1*
hsa_circ_0005442	2.5	chr2	*CRIM1*

The grouped analysis listed downregulated circRNAs in AR independent PCa (Table 6.9). The downregulated hsa_circ_0005954 is an exonic circRNA located on chromosome 6 and associated with the gene *AMD1*. AMD1 is upregulated in PCa (171).

Table 6.9. Top ten upregulated circRNAs in androgen dependent cell lines.

circRNA	**FC**	**Chromosome**	**Gene**
hsa_circ_0005954	3.0	chr6	*AMD1*
hsa_circRNA_403068	2.5	chr4	*ZNF732*
hsa_circ_0085173	4.0	chr8	*GRHL2*
hsa_circ_0002822	1.9	chr2	*KANSL1L*
hsa_circ_0001633	2.0	chr6	*SOBP*
hsa_circ_0072492	1.8	chr5	*PPAP2A*
hsa_circRNA_403717	3.4	chr6	*ARFGEF3*
hsa_circ_0003057	1.6	chr5	*ANKH*
hsa_circ_0083530	2.9	chr8	*XPO7*
hsa_circ_0023255	1.7	chr11	*CPT1A*

hsa_circ_0004870

hsa_circ_0004870 is an exonic circRNA that is associated with miR-145 expression, a known tumour suppressor (166). Testing was performed with qPCR using RNA (n=3) from androgen dependent cell lines (22Rv1, LNCaP) and androgen independent cell lines (DU 145). hsa_circ_0004870 was significantly downregulated in the AR dependent line 22Rv1 ($p \leq 0.01$) compared to the AR independent line DU 145 (Fig 6.9). There was no significant difference between 22Rv1 and LNCaP or DU 145.

hsa_circ_0083092

The expression of hsa_circ_0083092 in known androgen dependent lines (22Rv1 and LNCaP) and AR independent lines (DU 145) was examined. hsa_circ_0083092 was expressed in all lines with no significant difference between the AR dependent or independent lines (P value for 22Rv1 compared to DU 145 was 0.0855) (Fig. 6.10).

CircBase (http://www.circbase.org/) is an online database, where merged and unified data sets of circRNAs and the evidence supporting their expression can be accessed, downloaded and browsed within the genomic context (77). CircBase also provides scripts to identify known and novel circRNAs in sequencing data. The FASTA sequence for both the *AR* gene and AR-V7 transcript were submitted to circBase. Data from circBase identified four circRNAs (hsa_circ_0090923, hsa_circ_0090922, hsa_circ_0090924, hsa_circ_0090925) associated with the AR, shown in Figure 6.11.

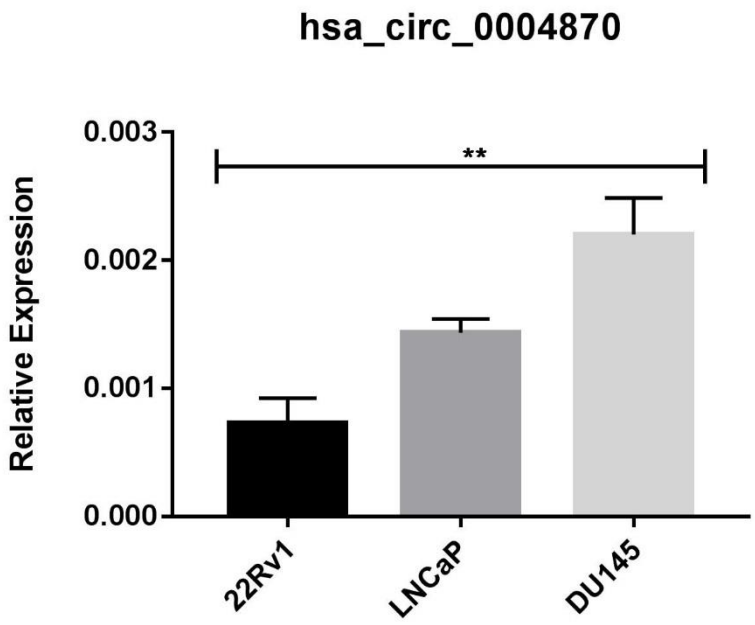

Figure 6.9. hsa_circ_0004870 expression according to androgen dependency. Two androgen dependent lines (22Rv1 and LNCaP) were compared to the androgen independent line DU 145. Data graphed as mean ± SEM (n=3). Ordinary one-way ANOVA. ** $p \leq 0.01$.

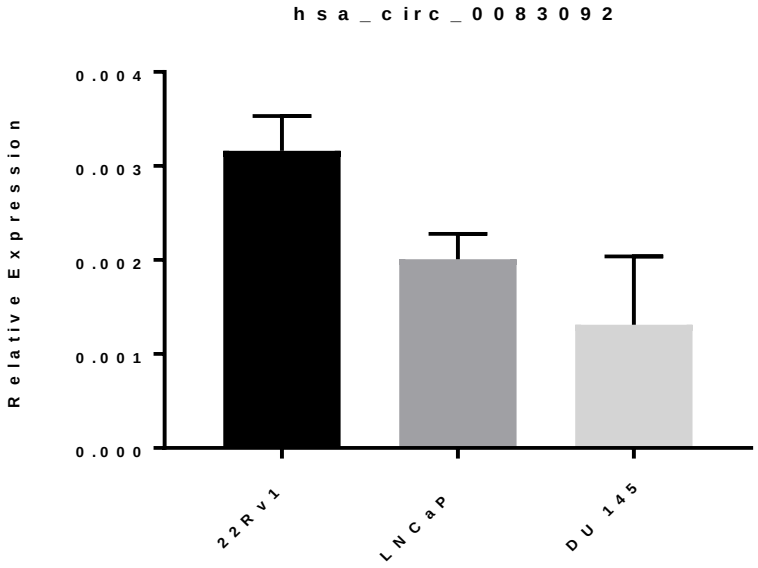

Figure 6.10. hsa_circ_0083092 expression according to androgen dependency. Two androgen dependent cell lines (22Rv1 and LNCaP) were compared to the androgen independent line DU 145. Data graphed as mean ± SEM (n=3).

organism	position (genome browser link)	strand	circRNA ID	genomic length	spliced length	samples	scores	repeats	annotation	best transcript	gene symbol	circRNA study
hsa	chrX:66788682-66950461	+	hsa_circ_0090922	161779	8107	H1hesc	NA	NA	ANNOTATED, CDS, coding, OVCODE, OVERLAPTX, OVEXON, UTR3, UTR5	NM_001011645	AR	Salzman2013
hsa	chrX:66863097-66863249	+	hsa_circ_0090923	152	152	Huvec	1	NA	ANNOTATED, CDS, coding, INTERNAL, OVCODE, OVEXON	NM_000044	AR	Salzman2013
hsa	chrX:66863097-66937464	+	hsa_circ_0090924	74367	702	H1hesc	NA	NA	ANNOTATED, CDS, coding, INTERNAL, OVCODE, OVEXON	NM_000044	AR	Salzman2013
hsa	chrX:66905851-66905968	+	hsa_circ_0090925	117	117	H1hesc	5	NA	ANNOTATED, CDS, coding, INTERNAL, OVCODE, OVEXON	NM_000044	AR	Salzman2013

Figure 6.11. circRNAs identified from circBase using the AR and AR-V7 sequences.

Using the FASTA sequences for all 4 circRNAs, a bioinformatic analyses was performed to assess for any genomic matches to the AR sequence (Fig 6.12). The sequence for the AR gene (NM_000044.3) was obtained from Human Genome Resources (https://www.ncbi.nlm.nih.gov/genome/guide/human/) at the National Centre for Biotechnology Information (NCBI) and the sequence for AR-V7 was obtained from previous published resources (37). AR-V7 has no LBD, explaining the shorter spliced sequence. All 4 circRNAs aligned to both the AR-FL transcript and AR-V7.

Outward facing primers were designed for each identified circRNA (n=4) using the sequence obtained from circBase (Fig 6.13) and qPCR was performed.

hsa_circ_0090922, hsa_circ_0090924, and hsa_circ_0090925 were beyond the level of detection by Ct value. hsa_circ_0090923 was significantly expressed compared to the house keeping gene *GAPDH*. hsa_circ_0090923 is located on the X chromosome and its matching gene transcript is NM_000044, corresponding to the *AR* gene. It has a spliced sequence length of 152 bp. The expression was highest in 22Rv1 cells (Fig 6.14), which are known to express AR-V7, and to be associated with resistance to enzalutamide, however there was no significant difference between cell lines. After qPCR was performed, the PCR product for hsa_circ_0090923 was electrophoresed on a gel (Fig 6.15). The product size was 150 bp, which confirmed the splice transcript. hsa_circ_0090925 was not detected, which was expected given qPCR results.

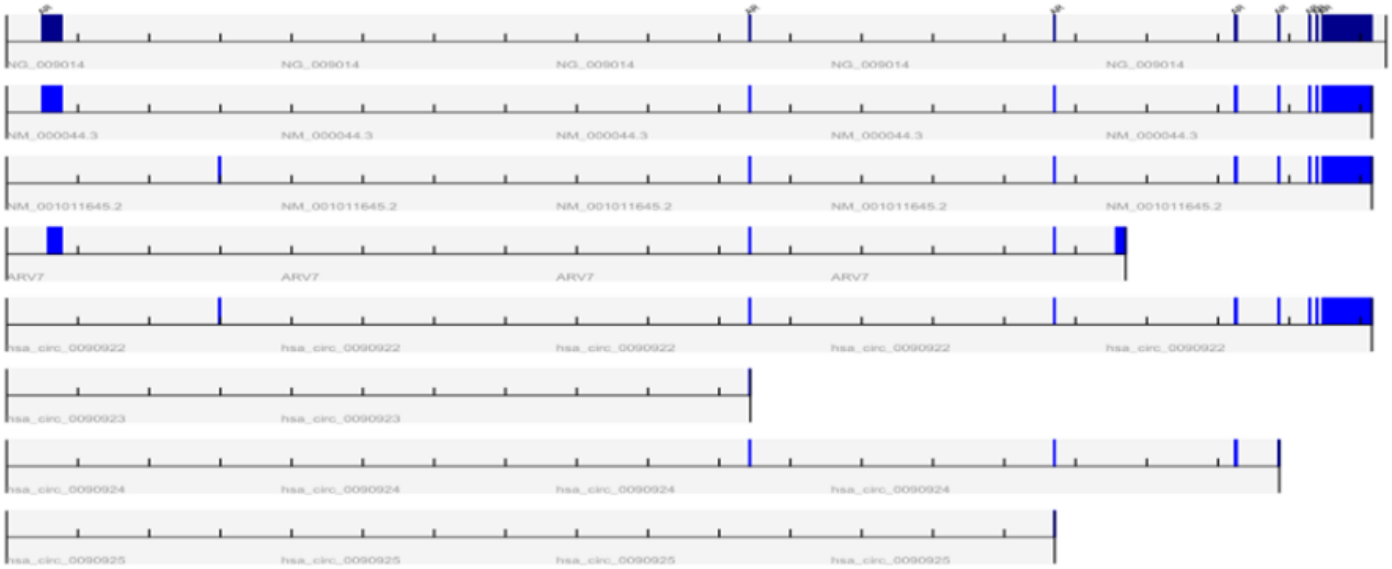

Figure 6.12. Alignment of the four identified circRNAs from circBase to the AR transcript (NM00044.3) and AR-V7. AR-V7 is shown compared to the full-length AR transcript. Exons shown in blue

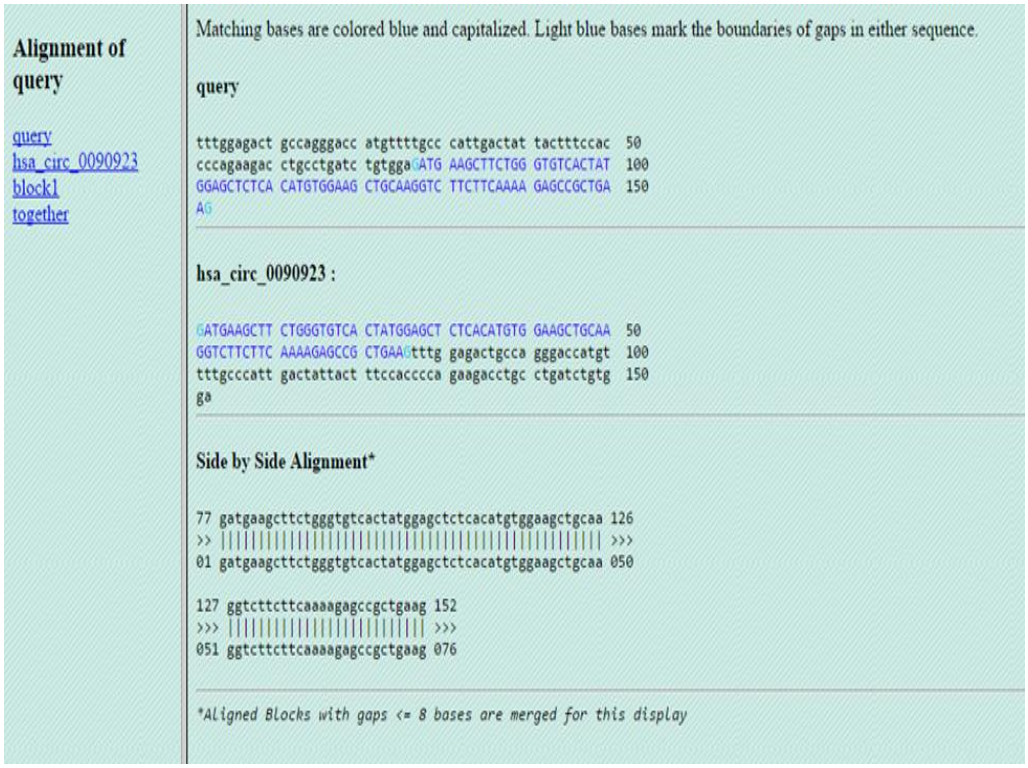

Figure 6.13. hsa_circ_0090923 sequence and alignment to the AR from circBase.

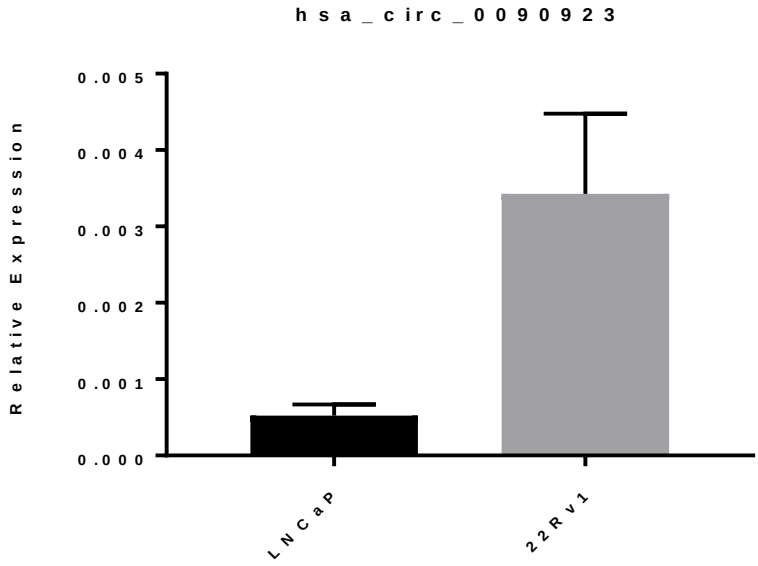

Figure 6.14. Relative expression of hsa_circ_0090923 in known AR dependent cell lines. Data graphed as ± SEM (n=3).

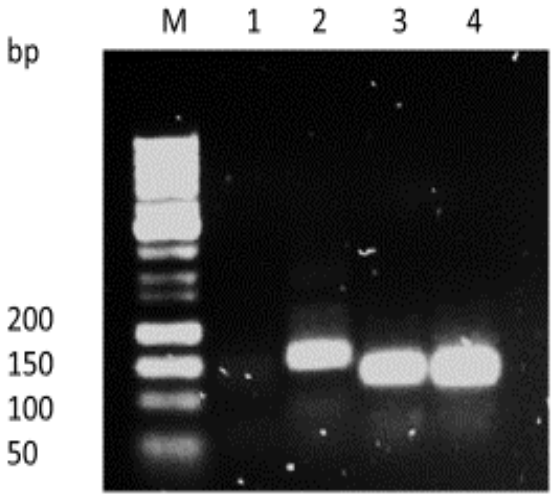

Figure 6.15. circRNA products post qPCR. Lane 1 = hsa_circ_0090925. Lane 2 = hsa_circ_0090923. Lane 3 = AR-FL. Lane 4 = AR-V7.

6.30 Discussion

circRNAs have been shown to be extremely stable and resistant to RNA degradation, and as such they could translate into clinically useful markers, detectable in blood without the need for isolation of CTCs or the need for invasive biopsy procedures. Due to their unique structures, circRNAs can be detected using outward facing primers. The potential impact of circRNAs on human disease has been demonstrated. For example, changes in the level of ciRS-7/CDR1as (a miR-7 circRNA sponge) alters the levels of miR-7 target genes (86). This is relevant as miR-7 has been characterized as having both oncogenic and tumour suppressive properties (172). Further studies have found an association of up and downregulated circRNAs with carcinoma including gastric cancer and colon cancer (91, 92). This study aimed to examine the expression of circRNAs in PCa.

To investigate circRNAs associated with PCa, circRNA profiling was performed on a panel of PCa cell lines using a high throughout microarray assay. Bioinformatic analysis identified a number of differentially expressed circRNAs between different malignant *vs.* benign and androgen dependent *vs.* independent cell lines. A total of 3409 circRNAs were significantly upregulated in malignant cell lines *vs.* benign cell lines. In a grouped analysis of androgen dependent *vs.* independent cell lines, there were 2127 upregulated circRNAs in AR dependent cell lines and 2236 in AR independent cell lines. This suggests that circRNA expression is highly dysregulated in PCa and may identify a clinical signature that could be used to stratify patients. Two of the highly expressed circRNAs (hsa_circ_0082672, hsa_circ_0082680) in PCa,

according to FC, were associated with the *HIPK2* gene. Depletion of HIPK2 in PCa has been shown to be associated with decreased AR target gene expression and, importantly, reduced the proliferation of androgen-dependent and castration-resistant PCa cells (167). Similarly, a number of downregulated circRNAs (hsa_circ_0001016, hsa_circ_0001017**,** and hsa_circ_0054882) were found to be associated with the *XPO1* gene. *XPO1* has been shown to force the retention and activation of tumour suppressor proteins resulting in tumour cell death in preclinical models making this association an interesting finding in this setting (168).

circRNA expression profiles were analysed between androgen dependent and independent cell lines. Profiling detected significant differential expression of circRNAs between these cell lines and identified a potential circRNA signature reflective of androgen dependency. circRNAs can compete for the pool of miRNA binding sites to influence the activities of miRNAs in regulating gene expression (172). Interestingly, most of the miRNAs that have been altered in CRPC are linked to the AR pathway (173). One such miRNA is miR-145, which has been shown to suppress the AR in PCa (166). miRNAs can be regulated by androgens through direct binding to androgen-responsive elements in the promoter. Direct regulation of AR transcripts by miRNAs has also been demonstrated (174). Downregulation of miRNAs in PCa tissue has been commonly reported and could partly explain the increased expression of the AR in CRPC (175). In this study, 5 miRNA binding sites were predicted, using a bioinformatic pipeline, for each detected circRNA. miRNAs were stratified based on previous known associations with PCa (173). circRNA

expression was examined using qPCR. Expression of hsa_circ_0083092 (predicted miRNA: miR-125b) and hsa_circ_0004870 (predicted miRNA: miR-145) was detected in cell lines that highly express both AR and AR-V7.

AR-V7 is associated with resistance to treatment in advanced PCa and is associated with a worse prognosis (33). The online circRNA database, circBase, identified 4 circRNAs associated with AR-V7. Further analysis showed these 4 circRNAs matched the full-length AR genomic sequence. Only one, hsa-circ_0090923, was detected by qPCR in malignant cell lines.

RNase R was used to enrich RNA prior to performing the microarray. It is an enrichment step sometimes used in the validation of circRNAs (66). As a proof of concept, an initial attempt to detect circRNAs after RNase R using qPCR was performed using a previously validated circRNA (circBICC1) in HeLa cells. This demonstrated that this circRNA was detectable in this cell line even after treatment with RNase R. However, an attempt to enrich the 4 identified circRNAs with RNase R treatment did not result in circRNA enrichment. Previous qPCR validation studies have shown that a number of experimentally validated circRNAs are depleted by RNase R (73). Some circRNAs may be prone to nicking during library preparation, allowing them to be degraded by RNase R, although it is unclear whether there are specific features of specific circRNAs that systematically result in RNase R sensitivity (60). In addition, there can be a high variability in results between RNase R-treated replicates, with fewer than 50% of the circRNAs that are resistant in one replicate also resistant in the second replicate prepared by the same laboratory (152). Previous research has shown that very high concentrations of

RNA are required due to the degradation of RNA from the RNase R (176). This may have been a factor in this research, however increasing the concentration of RNA had no effect on the overall yield of circRNA detection. It is also possible that the majority of circRNAs have a single as yet unknown function or act together to serve one unified role, though it has been proposed that some expressed circRNAs may be non-functional and merely 'noisy' by-products of splicing (73).

In conclusion, for the first time, this study profiled the circRNA expression signatures of normal prostate cell lines and advanced PCa cell lines. The circRNA profiles were deregulated between benign and malignant cell lines, which may impact both miRNA and mRNA expression profiles, in addition to influencing the regulation of gene expression. Therefore, specific circRNA expression profiles may be significant in determining not only the disease state but may also be useful as a potential screening marker for PCa.

Chapter 7: Circular RNAs and their association with resistance to enzalutamide

6.31 Introduction

Multiple new treatments that target the AR such as enzalutamide have become available for men with advanced PCa, however, despite these advances, resistance to treatment continues to occur. ADT is the mainstay of treatment (4), with an average initial response of approximately 18 months, however resistance inevitably develops. This results in CRPC, which is currently incurable (9). CRPC continues to rely on androgens via AR signalling (177). Enzalutamide is a targeted AR inhibitor that competitively binds to the LBD of the AR. The drug inhibits AR translocation, recruitment of AR co-factors, and AR binding to DNA (23). While the exact mechanisms for developing enzalutamide resistance are yet to be fully understood, it is known that AR gene amplification emerges during ADT and facilitates tumour growth in low androgen concentrations (31). It has been shown that ncRNAs such as miRNAs play a role in the development of resistance to AR targeted agents in PCa (178). However, it is unknown if circRNAs play a role in the development of resistance or not.

Additionally, AR-V7 is a truncated form of the AR that may play a role in developing resistance, as it lacks the LBD (37) and has been shown to be associated with resistance to enzalutamide (33, 39-41). A model of spontaneous resistance to enzalutamide in LNCaP prostate cancer cells has been developed that contains an F876L mutation in AR that is correlated with a blunted AR response to enzalutamide (35). It is not yet known, if there is an association with the F876L mutation and AR-V7, and an assay to detect AR-V7 has not yet reached the clinic. Deregulation of circRNAs may influence proliferative signalling, EMT, angiogenesis, apoptosis or drug resistance (Fig

7.1) and, in this manner, directly have a role in the development of cancer (179). circRNA expression may also affect the development of enzalutamide resistance through as yet unidentified mechanisms, or through a regulation function influencing the expression of AR and AR-V7.

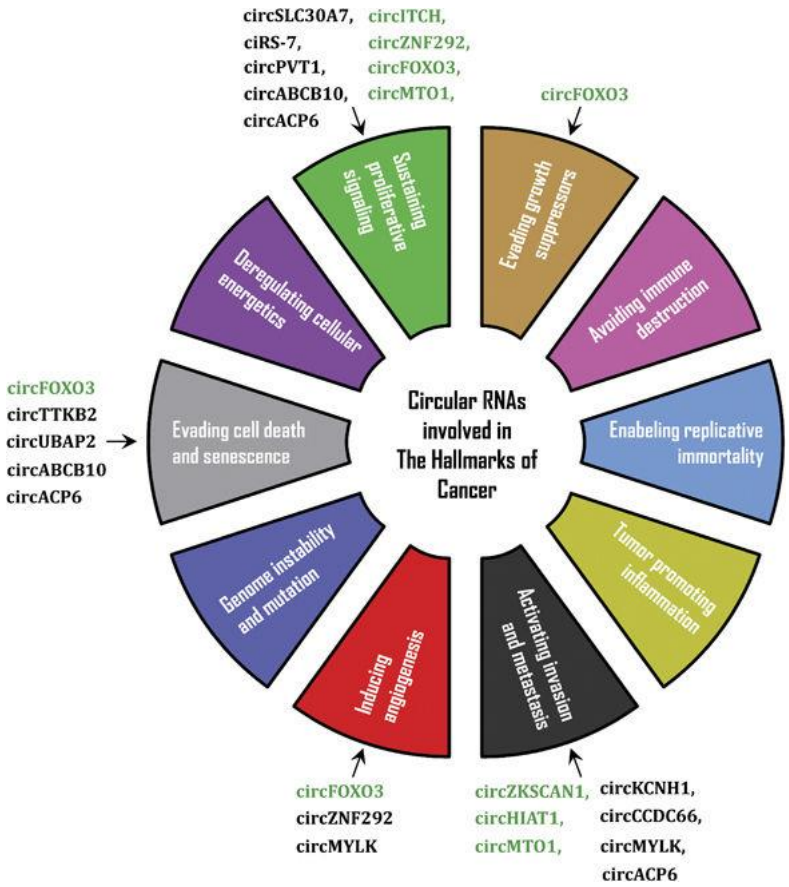

Figure 7.1. circRNAs and cancer development. Tumour-suppressor circRNAs are indicated in green and circRNAs with oncogenic properties are indicated in black.

Image taken from Kirstensen *et al*. (179).

The aim of this chapter was to (i) examine the pattern of circRNA expression in a panel of isogenic enzalutamide resistant cell lines, (ii) identify genes associated with the circRNA-miRNA-mRNA pathway, and (iii) determine the association between circRNA expression and the generation of AR-V7.

6.32 Results

7.1.1 circRNA screening identified differentially expressed profiles within an isogenic enzalutamide resistant cell line model

The panel of isogenic cell lines were screened for circRNA expression using a circRNA microarray as described in the previous chapter. The panel consisted of a control cell line (drug sensitive), clone 1 (strongly drug resistant) and clone 9 (moderately drug resistant) (35). Significantly altered circRNAs were identified as described in Chapter 6. circRNAs with a FC $\geq$ 1.5 and $p < 0.05$ were considered to be significantly differentially expressed. In total, 930 circRNAs were classified as present across the combined panel of isogenic enzalutamide resistant cell lines. These target circRNAs were used for further differential analysis. Grouped analysis (Control *vs.* combined Clone1/9) of detected circRNAs according to FC was performed. Overall, circRNAs were significantly down-regulated in the enzalutamide resistant cell lines compared to the less resistant control (Fig 7.2). There were 278 circRNAs up-regulated ($p<0.05$, Control *vs.* combined Clone1/9) and 588 circRNAs that were down-regulated ($p <0.05$, Control *vs.* combined Clone1/9).

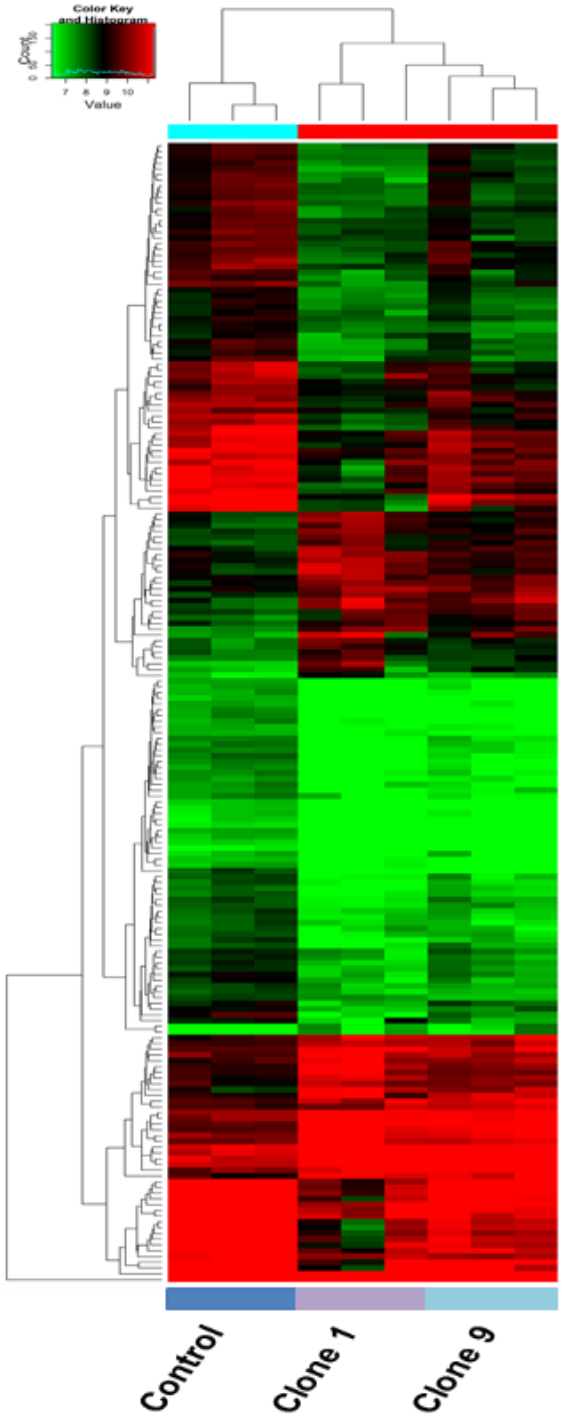

Figure 7.2. Clustered heatmap of enzalutamide resistant clones 1 and 9 vs. less resistant control. Heatmap reflects changes in expression using unsupervised clustering analysis (euclidean distance measure and the 'average' agglomeration method) (n=3).

7.1.2 Associated circRNA parental genes are involved in pro-oncogenic activities and is further altered depending on the extent of enzalutamide resistance.

Control *vs.* clone 1

Overall, circRNAs were significantly down-regulated in the enzalutamide resistant cell lines compared with the control. In control *vs.* clone 1 (most resistant to enzalutamide), 230 up-regulated circRNAs were identified ($p<0.05$, *vs.* control), and 465 that were down-regulated ($p<0.05$, *vs.* control). Data is shown as a scatterplot and associated heatmap in Fig 7.3. The top 5 up-regulated and down-regulated circRNAs in control *vs.* clone 1, ranked by FC, are shown in Table 7.1. hsa_circ_0001275 was up-regulated in control *vs.* clone 1 ($p<0.05$), and it's associated parental gene is *PLCL2*. *PLCL2* (codes for Inactive phospholipase C-like protein 2) was identified as part of a 23-gene signature, which predicted metastatic-lethal PCa outcomes in men diagnosed with clinically localised PCa (180). hsa_circ_0022392 was down-regulated in control *vs.* clone 1 ($p<0.001$) and associates with the gene *FADS2* (codes for Fatty acid desaturase 2), which has been shown to play a role in PCa development (181).

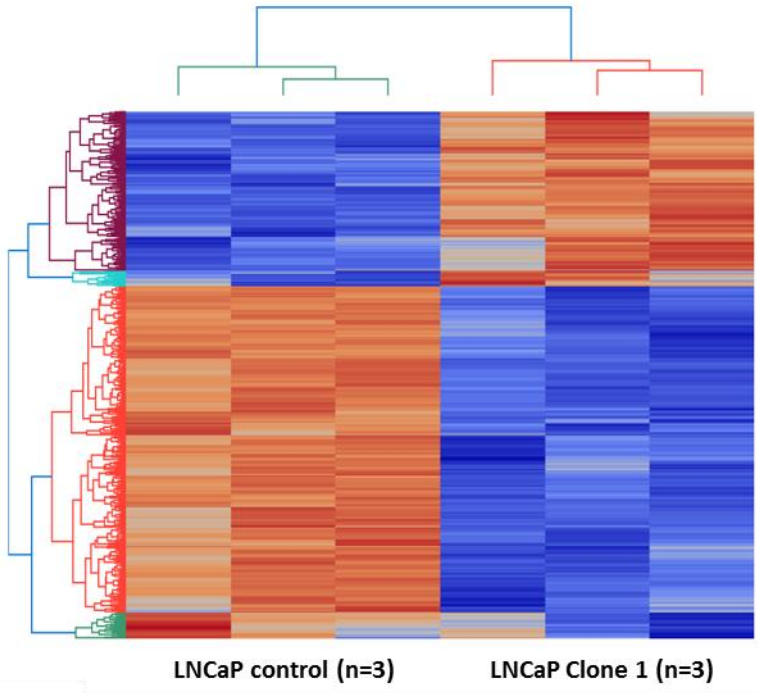

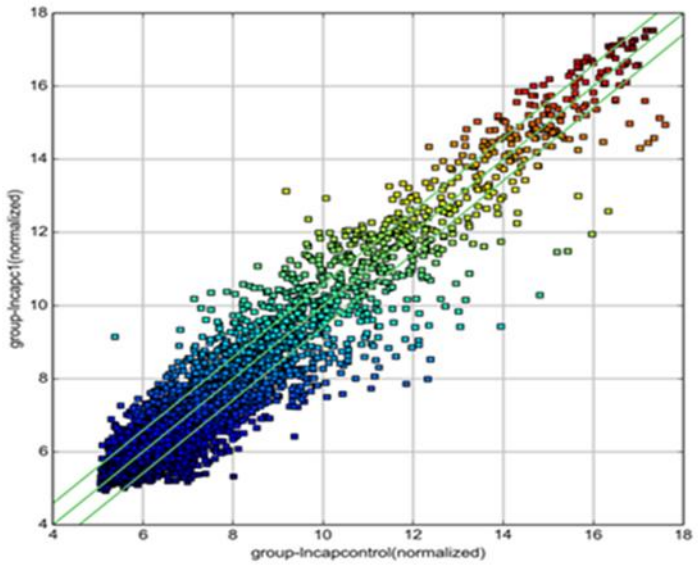

Figure 7.3. Heatmap and corresponding scatterplot showing expression levels for control *vs.* clone 1 cells. The values of X and Y axes in the scatterplot are the normalized signal values of the samples (log2 scaled) or the averaged normalized signal values of groups of samples (log2 scaled). The green lines in the scatterplot are FC lines. (lncapc1= L clone 1, r= replicate). Heatmap reflects changes in expression using unsupervised clustering analysis

(euclidean distance measure and the 'average' agglomeration method) (n=3). Red indicates higher levels of expression, while blue indicates lower levels.

Table 7.1 The top 5 up-regulated and down-regulated circRNAs in control *vs.* clone 1 based on FC.

CircRNA	**Expression**	**Parental Gene**	**Gene Function**
hsa_circ_0001275	Up	*PLCL2*	Complimentary to Gleason score for the prognostic classification of patients with PCa (180)
hsa_circ_0026462	Up	*KRT1*	Target receptor highly expressed on breast cancer cells (182)
hsa_circ_0033144	Up	*BCL11B*	Methylated in PCa (183)
hsa_circ_0000673	Up	*RSL1D1*	Overexpression is associated with an aggressive phenotype and a poor prognosis in patients with PCa (184)
hsa_circ_0000129	Up	*VPS72*	May have a role in regulating long-term hematopoietic stem cell activity (185)
hsa_circ_0022392 hsa_circ_0022383 hsa_circ_0022382	Down	*FADS2*	Polymorphisms in the FADS gene cluster which alters desaturase may have an impact on the effect of ω3 and ω6 PUFA on PCa risk among different populations (186)
hsa_circ_0000518 hsa_circ_0071174	Down	*RPPH1*	NcRNA involved in processing of tRNA precursors by cleaving the trailer sequence from the 5′-end (187)

Control *vs.* clone 9

In control *vs*. clone 9 cells, 60 circRNAs were up-regulated and 175 circRNAs were down-regulated (Fig 7.4). The top 5 up-regulated and down-regulated circRNAs in control *vs*. clone 9, ranked by FC, are shown in Table 7.2. In clone 9, hsa_circ_0045697 is up-regulated ($p < 0.05$, *vs.* control) and is associated with the oncogene *ITGB4* (codes for Integrin Subunit Beta 4). Previous studies have shown that *ITGB4* promotes prostate tumorigenesis (188).

7.1.3 miRNAs associated with circRNAs

MREs are miRNA binding sites that were predicted using TargetScan (189) and miRanda (190) bioinformatic platforms based on the circRNA-miRNA-mRNA network. For each identified circRNA, the top five most likely miRNA binding sites were predicted (Fig. 7.5). The top 5 up-regulated and down-regulated circRNAs were filtered based on their miRNA interaction as per chapter 6 and these were selected for validation studies.

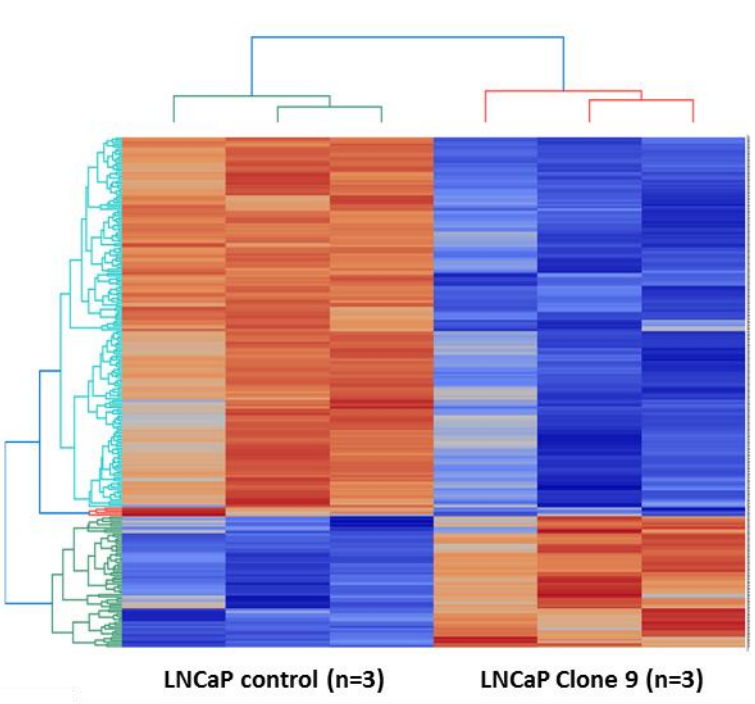

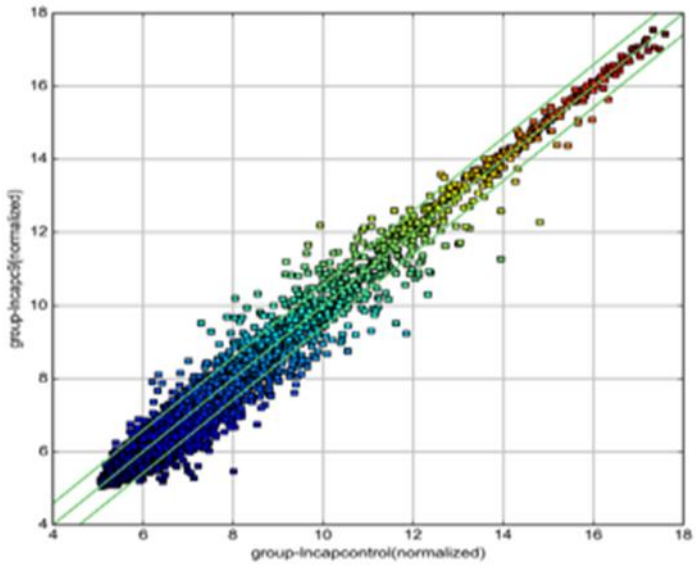

Figure 7.4. Heatmap and corresponding scatterplot showing expression levels for control vs. clone 9 cells. Heatmap reflects changes in expression using unsupervised clustering analysis (euclidean distance measure and the 'average' agglomeration method) (n=3).

Red indicates higher levels of expression, while blue indicates lower levels.

Table 7.2 The top five up-regulated and down-regulated circRNAs in clone 9 *vs.* control based on FC.

CircRNA	**Expression**	**Parental Gene**	**Gene Function**
hsa_circ_0045697	Up	*ITGB4*	Involved in prostate tumorigenesis and cancer invasiveness (188)
hsa_circ_0000463	Up	*EP400NL*	Pseudogene
hsa_circ_0026462	Up	*KRT1*	Target receptor highly expressed on breast cancer cells (182)
hsa_circ_0000673	Up	*RSL1D1*	overexpressed in PCa (184)
hsa_circ_407059	Up	*FGFR1*	Role in prostate tumorigenesis (191)
hsa_circ_0000326	Down	*XLOC_l2_002352*	Undefined
hsa_circ_0022383 hsa_circ_0022392	Down	*FADS2*	As per table 7.1
hsa_circ_0078607	Down	*SLC22A3*	Contributes to PCa pathogenesis (192)
hsa_circ_0002082	Down	*MALAT1*	Plays a role in AR-V7 resistance (193)

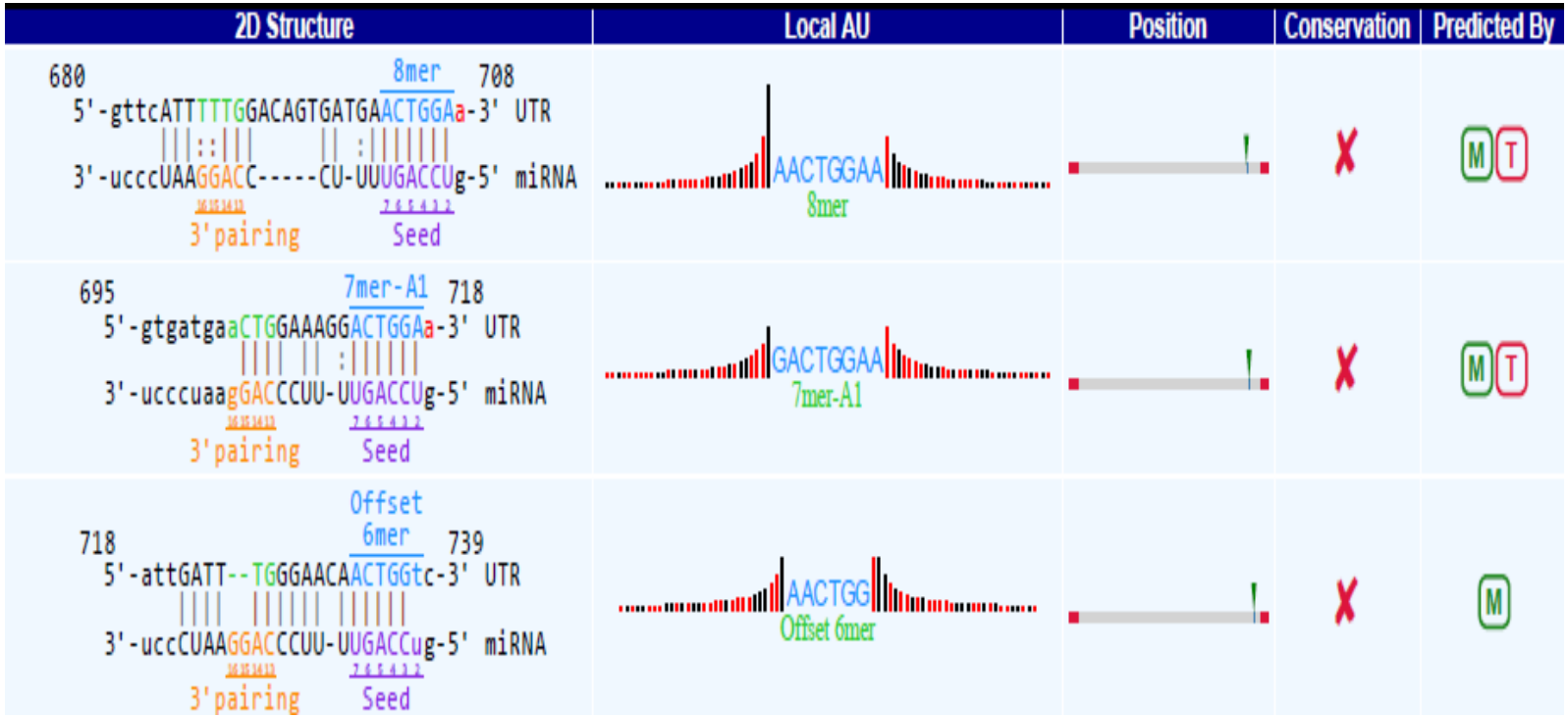

Figure 7.5. Detailed annotation for predicting circRNA/miRNA interaction for miR-145 and hsa_circ_000487.

7.1.4 Validation of circRNAs

Custom designed outward facing primers were used for validation via qPCR for 10 selected upregulated and downregulated circRNAs that have known associations with PCa. Out of the 10 circRNAs, 2 circRNAs were validated. hsa_circ_0001721 was also significantly upregulated in the more resistant cell line clone 1 compared to the less resistant clone 9 (FC 0.7 SEM ± 0.1) ($p \leq 0.05$). This corresponded to the microarray data. hsa_circ_0001721 is an exonic circRNA, located on chromosome 7 and is associated with the gene *CDK14*. hsa_circ_0004870 was significantly down-regulated in clone 1 and clone 9 *vs.* the LNCaP control ($p \leq 0.05$), which corresponded to the array data (Fig. 7.6C). hsa_circ_0004870 is an exonic circRNA located on chromosome 20 and is associated with the gene *RBM39*.

A

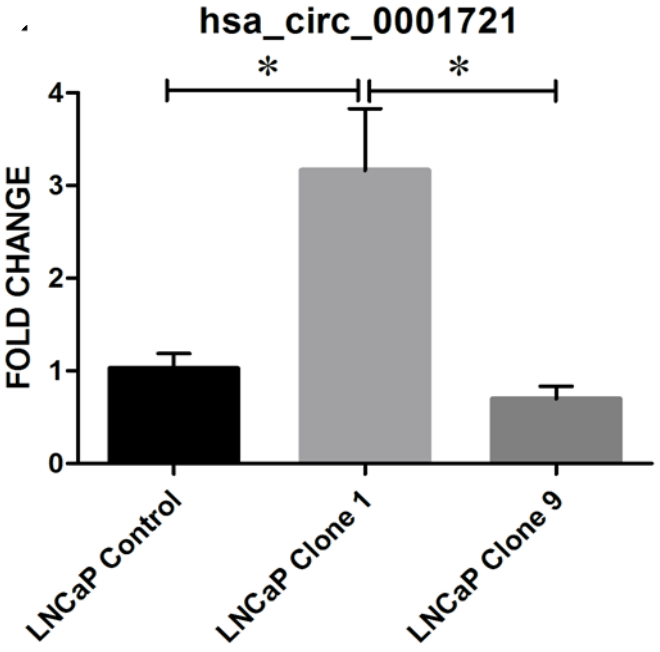
hsa_circ_0001721
*
*
FOLD CHANGE
4
3
2
1
0
LNCaP Control
LNCaP Clone 1
LNCaP Clone 9

B

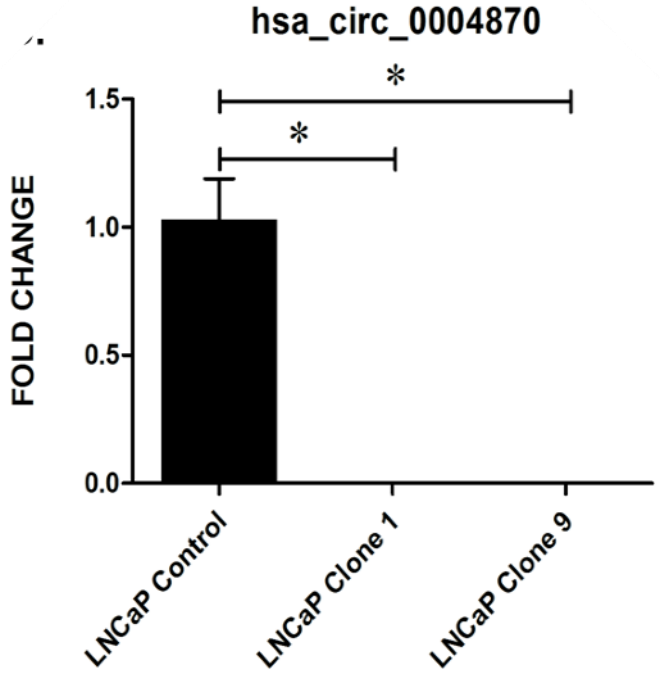
hsa_circ_0004870
*
*
FOLD CHANGE
1.5
1.0
0.5
0.0
LNCaP Control
LNCaP Clone 1
LNCaP Clone 9

Figure 7.6. Validation of circRNAs. (A) Validation of hsa_circ_0001721 in enzalutamide resistant LNCaP cell lines and (B) Validation of hsa_circ_0004870 in enzalutamide resistant LNCaP cell lines. Data graphed as mean ± SEM (n=3). Data analysed using an ordinary one-way ANOVA. (*$p \leq 0.05$).

7.1.5 hsa_circ_0004870 is downregulated in cancer cells and androgen dependent PCa

hsa_circ_0004870 was downregulated in the microarray data group comparisons according to malignancy and AR status. Validation of this circRNA in cell lines was performed. hsa_circ_0004870 was significantly downregulated in the malignant lines 22Rv1 ($p \leq 0.01$) and LNCaP ($p \leq 0.01$) compared to the benign line BPH-1 (Fig 7.7A). Similarly, hsa_circ_0004870 was downregulated in the AR dependent line 22Rv1 ($p \leq 0.01$) compared to the AR independent line DU 145 (Fig 7.7B).

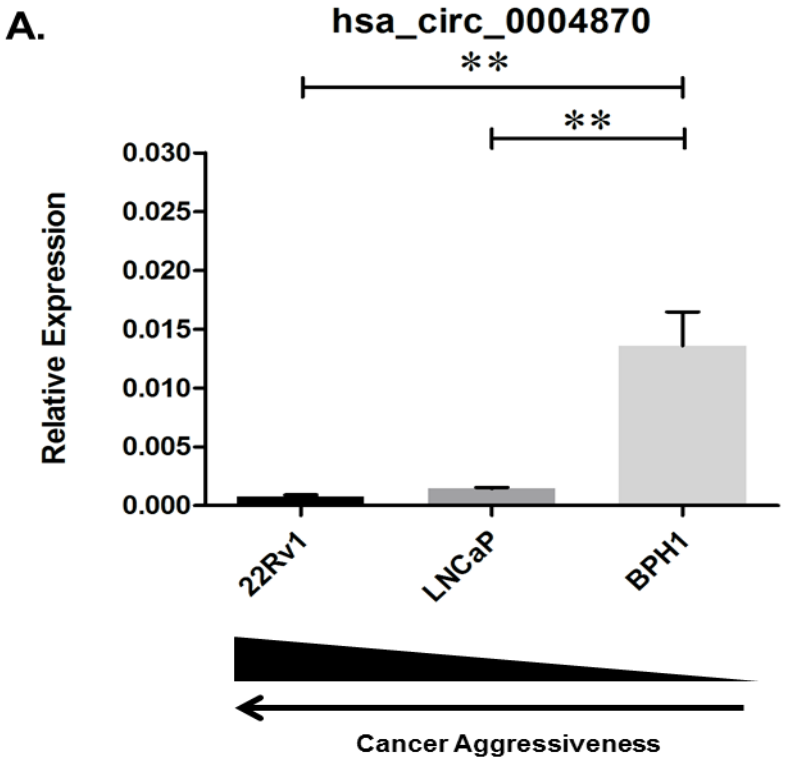
A.
hsa_circ_0004870
**
**
Relative Expression
0.030
0.025
0.020
0.015
0.010
0.005
0.000
22Rv1
LNCaP
BPH1
Cancer Aggressiveness

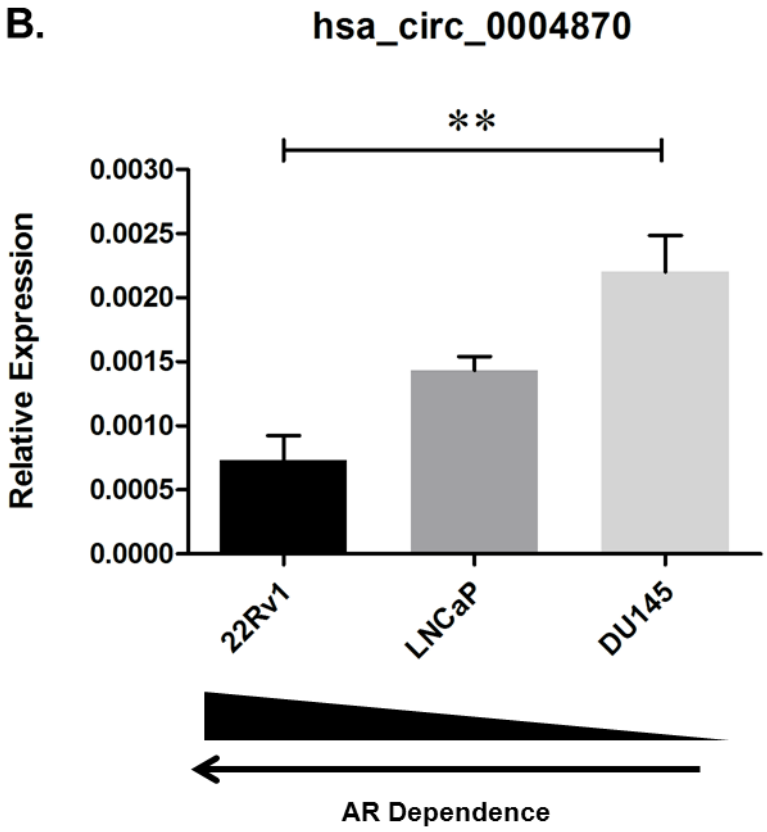
B.
hsa_circ_0004870
**
Relative Expression
0.0030
0.0025
0.0020
0.0015
0.0010
0.0005
0.0000
22Rv1
LNCaP
DU145
AR Dependence

Figure 7.7. hsa_circ_0004870. (A) hsa_circ_0004870 expression according to malignancy status and (B) hsa_circ_0004870 expression according to androgen dependency. Data graphed as mean ± SEM (n=3). Data analysed using an ordinary one-way ANOVA. (**p≤ 0.01) .

7.1.6 RBM39 and U2AF65 are down-regulated in enzalutamide resistant PCa

As hsa_circ_0004870 was significantly down-regulated in the enzalutamide resistant clones 1 and 9 compared to control, this circRNA was selected for further study. The coordinates (chr20:34,302,106-34,313,077) for hsa_circ_0004870 correspond to the gene *RBM39* on the UCSC Genome Browser. Expression of RBM39 was confirmed in the cell line panel with RBM39 significantly down-regulated in the resistant clones 1 ($p \leq 0.0001$) and clone 9 ($p \leq 0.0001$) compared with control (Fig 7.8). *RBM39* encodes a member of the U2AF65 family of proteins and it has previously been shown that, U2AF65 leads to expression of AR-V7 via the lncRNA PCGEM1, binding to AR pre-mRNA. Expression of U2AF65 was confirmed in the cell line panel, which was significantly down-regulated in the most resistant clone 1 ($p \leq 0.05$) (Fig 7.9).

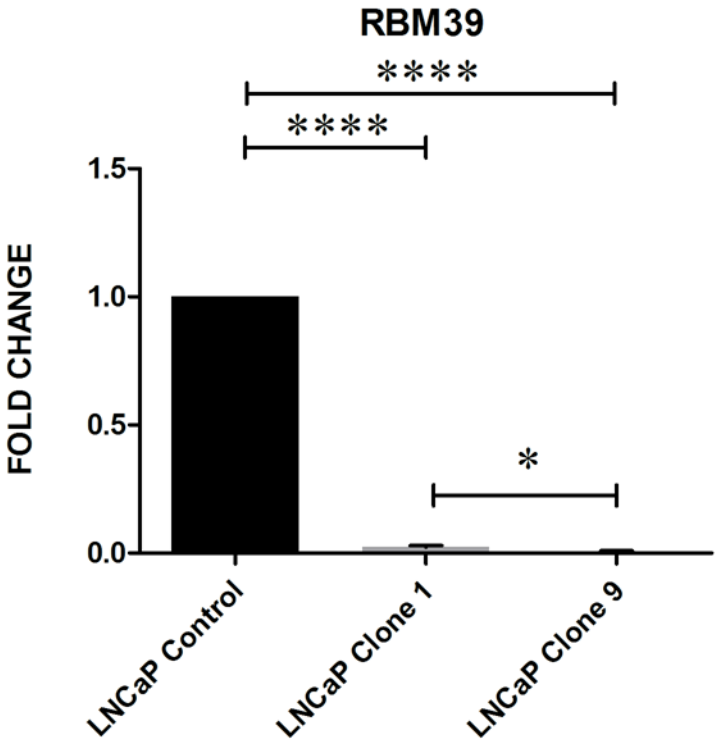

Figure 7.8. RBM39 expression. Data graphed as mean ± SEM (n=3). Data analysed using an ordinary one-way ANOVA. (*p ≤ 0.05, **** p≤ 0.0001)

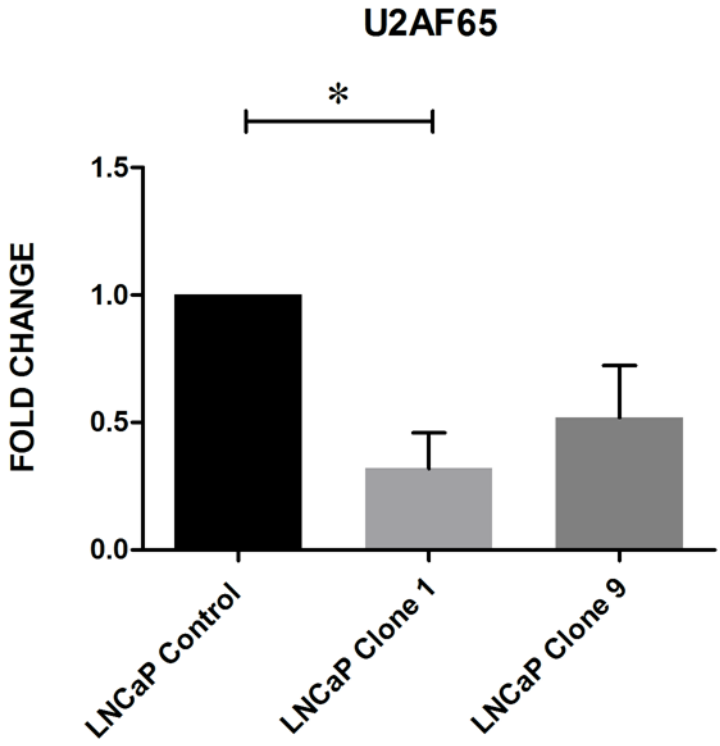

Figure 7.9. U2AF65 expression. Data graphed as mean ± SEM (n=3). Data analysed using an ordinary one-way ANOVA. (*p≤ 0.05)

7.1.7 miRNAs

Due to the association of circRNAs with miRNAs, cell lines were analysed for expression of their predicted miRNA. The predicted miRNA for

hsa_circ_0083092 is miR-125b, a known tumour suppressor gene (169). Using qPCR, miR-125b was significantly downregulated in clones 1 ($p \leq 0.01$) and clone 9 ($p \leq 0.05$) compared to control (Fig 7.10). miR-145 was the predicted miRNA for hsa_circ_0004870 and it was found not to be expressed in control, clone 1 or clone 9, suggesting this miRNA expression may be lost in these cancer cell lines.

7.1.8 circRNA expression in media

To test for extracellular expression of circRNAs as proof of principle, the culture media of control, clone 1 and clone 9 were analysed for circRNA expression. Primers for hsa_circ_0083092 were used in order to detect expression by qPCR. hsa_circ_0083092 was expressed in all three lines, with the highest expression in clone 1 (Fig 7.11).

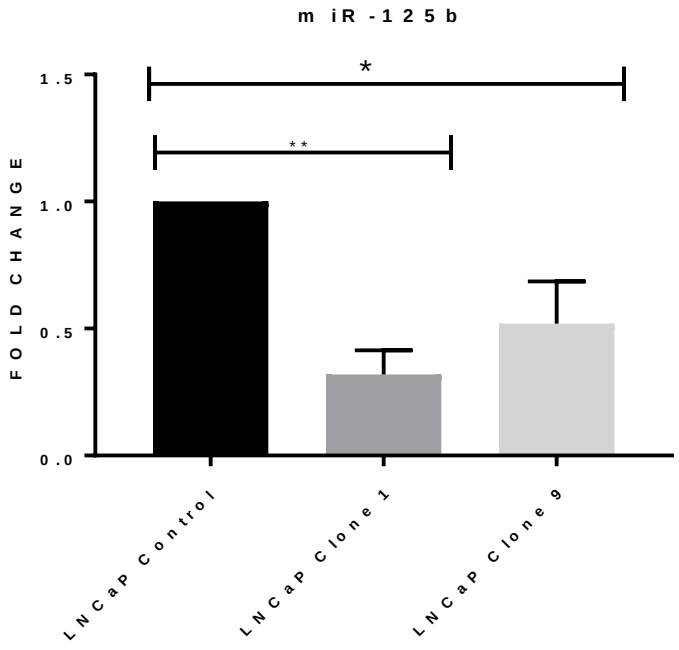

Figure 7.10. miR-125b expression. Data graphed as mean ± SEM (n=3). Data analysed using an ordinary one-way ANOVA. (*$p \leq 0.05$, ** $p \leq 0.01$)

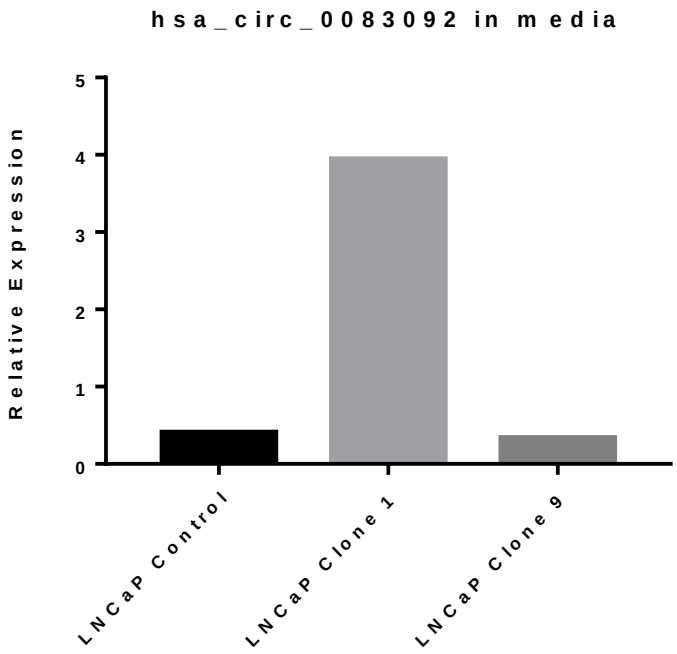

Figure 7.11. Relative expression of hsa_circ_0083092 in cell culture media. (n=1)

7.1.9 RISH for circRNA detection

In order to assess if hsa_circ_0083092 was expressed in tissue, BaseScope® technology was used. The probes were designated: BA-Hs-RBM33circRNA-E5E4, 1zz targets NM_053043.2, 899-552 and BA-Hs-STT3BcircRNA-E3E2, 1zz targets NM_178862.2, 1170-828 (Fig. 7.12). These probes specifically targeted the exon junction identified for hsa_circ_0083092.

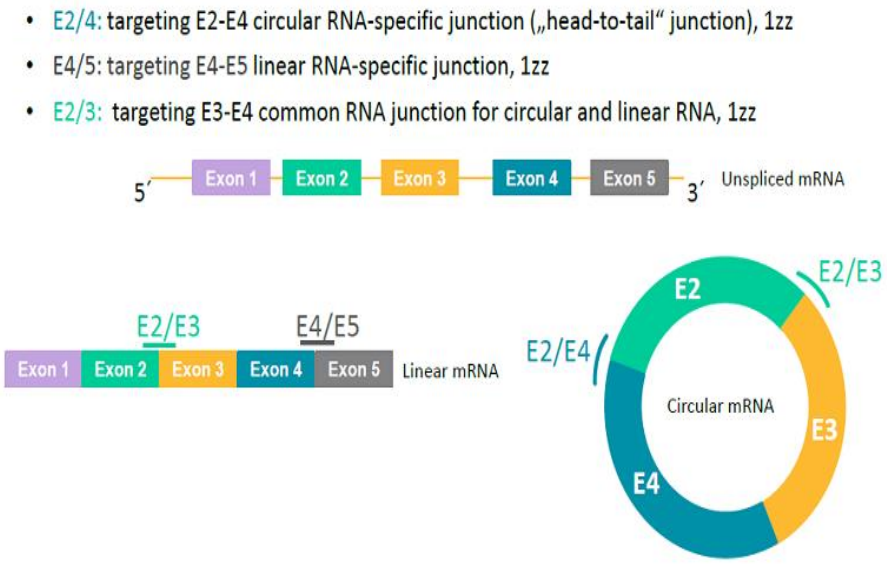

Figure 7.12. Using BaseScope® technology to design circRNAs probes. (Image taken from BaseScope® protocol insert.)

hsa_circ_0083092 was chosen for RISH testing as it was significantly upregulated in clone 1 compared to control. hsa_circ_0083092 was not expressed in tissue from cell lines (Fig 7.13) or patient samples (Fig 7.14).

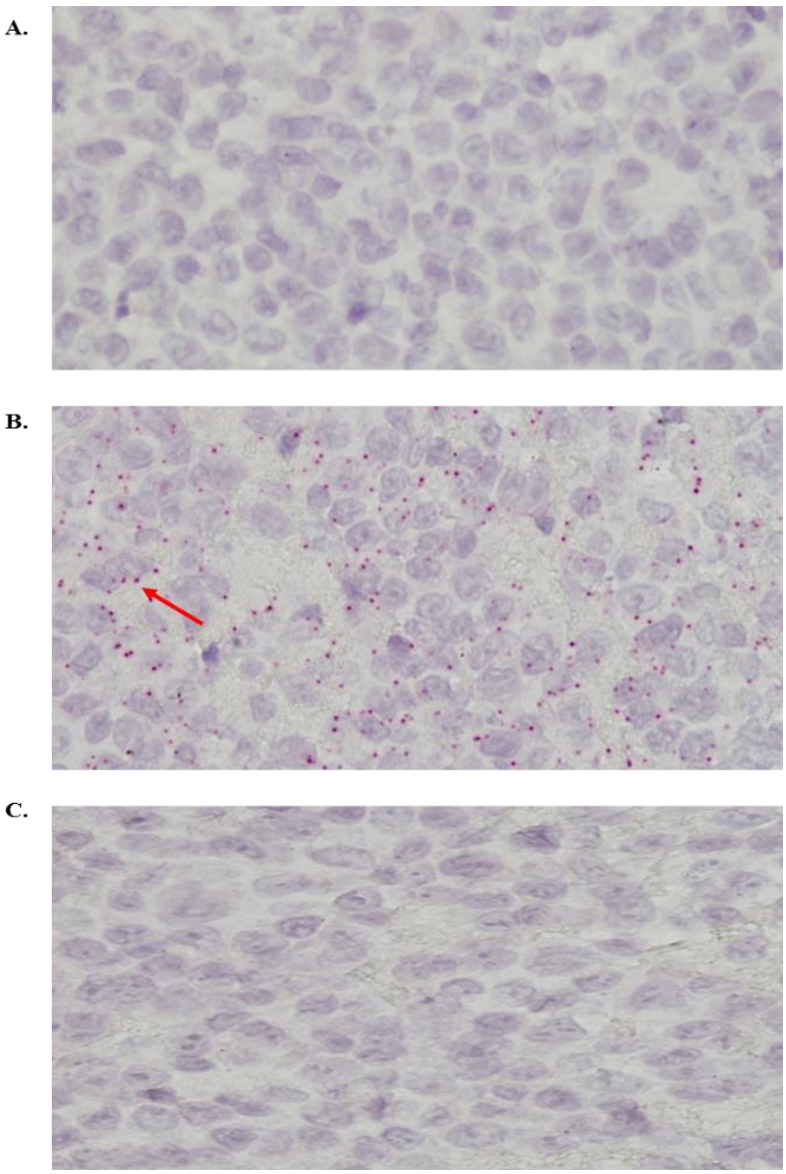

Figure 7.13. RISH in cell lines for hsa_circ_0083092 using BaseScope®. (A) LNCaP negative control cell line (40X), (B) LNCaP positive control cell line (red arrow) (40X) and (C) LNCaP cell line showing no expression of hsa_circ_0083092 (40X).

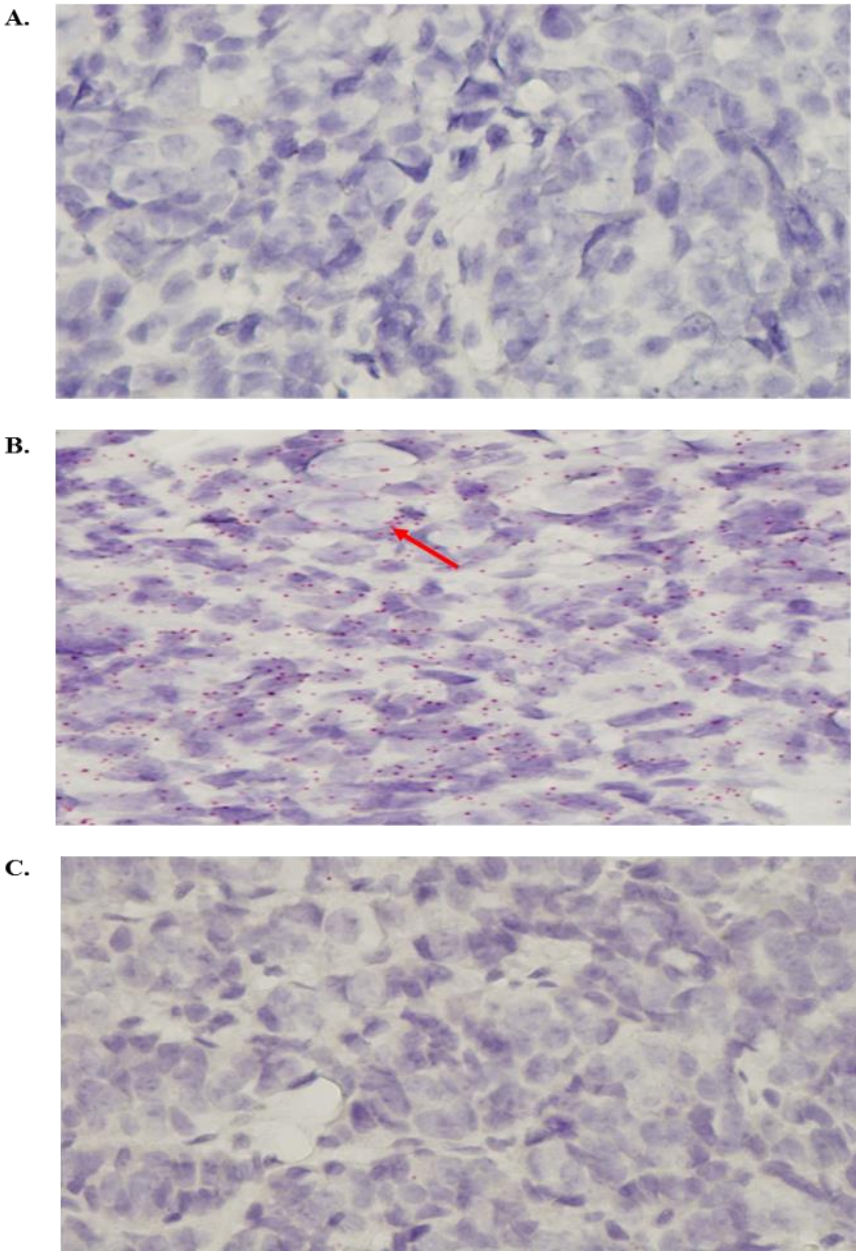

Figure 7.14. RISH in metastatic lymph node biopsy sample for hsa_circ_0083092 using BaseScope®. (A) Negative control (40X), (B) Positive control (red arrow) (40X) and (C) Biopsy showing no expression of hsa_circ_0083092 (40X).

6.33 Discussion

circRNAs have been identified in a number of different cancers (90), suggesting a potential role as a biomarker or therapeutic target. Although, their role in cancer has yet to be fully elucidated, recent research suggests they can act as miRNA sponges (172), bind RNA-binding proteins (RBPs), translate peptides (83) and may confer resistance to therapy (194). In the present study, the expression of circRNA profiles in PCa cell lines that are resistant to enzalutamide are reported. This analysis revealed 278 circRNAs that were aberrantly up-regulated and 588 circRNAs that were down-regulated in enzalutamide resistant PCa (clone 1 and clone 9 combined) compared to the less resistant control. circRNAs were significantly more down-regulated in cell lines which displayed enhanced resistance to enzalutamide (465 circRNAs were down-regulated in clone 1, compared to 175 circRNAs in clone 9). circRNAs were filtered according to their predicted miRNAs that were strongly associated with PCa in the literature, thus producing a list of relevant circRNAs (173). Using qPCR, hsa_circ_0001721 (predicted miRNA: hsa-miR-221) were validated, confirming that they were both significantly upregulated in the more resistant clone 1 *vs.* control. hsa_circ_0004870 (predicted miRNA: miR-145), was significantly downregulated in enzalutamide resistant clone 1 and clone 9 cell lines *vs.* control. miR-125b, a known tumour suppressor was shown to be decreased in the enzalutamide resistant clones. Previously, alterations in miR-125b expression have also been shown to be an early event in prostate tumorigenesis (162). Similarly, miR-145, a known tumour suppressor was not expressed in the enzalutamide resistant clones. Loss of miR-145 has been shown to have significant effects in PCa by suppressing the AR, and this appears to correlate with a worse overall prognosis

(166). Therefore, loss of miR-145 may be a factor in driving resistance to enzalutamide.

hsa_circ_0004870 was selected for further investigation, as it was consistently downregulated in the microarray data and was associated with miR-145. In this study, it was significantly downregulated in malignant cell lines and AR dependent cell lines. hsa_circ_0004870's parental gene is *RBM39,* a serine/arginine-rich RNA-binding protein thought to activate or inhibit the alternative splicing of specific mRNA by interacting with the spliceosomal components within splice sites (195). Furthermore, RBM39 is a U2AF65-related protein, with U2AF65 appearing to be a critical regulator involved with the generation of AR-V7 (196). AR-V7 is associated with intrinsic and acquired resistance to enzalutamide, however the exact mechanism is unknown (33). One proposed mechanism is that U2AF65 may play a role in generating resistance by regulating AR-V7 via the lncRNA, PCGEM1, through binding to AR pre-mRNA (196). It has been shown here, that both RBM39 and U2AF65 are downregulated in the enzalutamide resistant cell lines. Furthermore, it has been shown that AR-V7 is significantly higher expressed in enzalutamide resistant cells compared with control. It is therefore proposed that expression of AR-V7 may be further regulated by U2AF65 via the circRNA, hsa_circ_0004870.

A novel RISH technology was tested to assess if circRNAs could be directly visualised in FFPE tissue samples. Custom probes were designed that span the exon junction of the circRNA splice ends. hsa_circ_0083092 was chosen to validate this technology in both cell lines and metastatic biopsy samples as it had been shown as significantly upregulated by qPCR. Expression of

hsa_circ_0083092 was not confirmed by RISH in both cell lines and in tissue samples. As circRNAs are more commonly downregulated in cancer, it may be useful to assess loss of circRNA expression in future experiments. This technology needs further testing and validation to assess suitability for further analysis in terms of circRNAs.

In conclusion, this study characterised circRNAs profiles in enzalutamide resistant PCa for the first time and showed that they are differentially expressed depending upon drug sensitivity. Thousands of circRNAs have been identified, however, it is not clear whether all circRNAs function as miRNA sponges, as has been previously proposed (172). A number of miRNAs associated with PCa were identified that have been proposed to regulate these circRNAs, however further validation and mechanistic studies are required. Similar studies have shown circRNAs to be abundant, highly stable and to be detectable in human saliva, tissue and blood samples (197, 198). These findings indicate that circRNAs, may represent potentially valuable diagnostic biomarkers in PCa. Moving forward, additional work is warranted to validate circRNAs in patient samples in order to develop a potential circRNA signature that could be useful in the clinical setting.

Chapter 8: Discussion and future directions

6.34 Overall discussion

There is a need to discover biomarkers that could allow clinicians to provide improved personalised treatment to their patients. PSA has been used for many years to guide treatment decisions, however, PSA doesn't always accurately detect recurrent disease or disease that is refractory to current treatment modalities (199). Currently, a large body of evidence supports the ability of multiple biomolecular markers to predict patient outcome, however none of these are being used to guide clinical decision-making (200). More recently, splice variants of the AR, including AR-V7 have been discovered which have been shown, in small studies, to be associated with resistance to certain treatments in PCa (33). Ongoing research has documented the use of translational approaches to profile the spectrum of molecular anomalies associated with PCa progression (201).

In chapter 3, the combination of the radioisotope, radium-223 and an ASI, enzalutamide, in progressive mCRPC was investigated. This combination was of interest due to differing modes of action and non-overlapping toxicity profiles, leading to the potential for synergy. The safety and efficacy of this combination has not previously been reported in the literature. The implementation of this study, including the collection of the biospecimens (e.g. CTCs), patient characteristics and the safety data for the first six months of the study were analysed. Patients received 6 cycles of radium-223 (50 kBq/kg IV Q4W) in combination with enzalutamide (160 mg/day), followed by enzalutamide alone until disease progression, unacceptable toxicity or consent withdrawal. The primary endpoint was safety for the 6 months of combination therapy. From July 2015 to July 2017, 45 patients were accrued. A total of 13 patients (28.9 %) had

grade 3/4 adverse events. The most frequent grade 3/4 adverse events were neutropenia (6.6%) and fatigue (6.6%). There were no therapy-related deaths. The combination treatment was well tolerated with acceptable early safety and toxicity profiles consistent with those seen when they are used as single agents, therefore allowing for concomitant administration.

CTCs are an increasingly important biomarker in all cancers (45). CTCs can provide further knowledge relating to tumour burden in these patients, while additionally allowing clinicians to determine response to treatments and therefore act as a potential surrogate endpoint in PCa treatment (50). A translational study examining the effect of the combination of drugs on CTC numbers was performed as part of CTRIAL 13-21. All enrolled patients in ICORG 13-21 had blood drawn at baseline for CTC analysis and throughout therapy. The technology used allows for direct visualisation of CTCs by a trained histopathologist. After treatment with radium-223 and enzalutamide combination therapy, there was a noticeable reduction in CTC numbers in both groups, however this was not statistically significant. Longer follow up is required to fully assess variations in CTC numbers over time. The European Organisation for Research and Treatment of Cancer (EORTC) is now recruiting patients to the PEACE III trial (ClinicalTrials.gov Identifier: NCT02194842), a randomized phase III open label trial assessing if upfront combination of enzalutamide and radium-223 improves outcomes compared to enzalutamide single agent in patients with asymptomatic or mildly symptomatic CRPC with bone metastases. The recent ERA 223 trial reported on outcomes on patients who had metastatic CRPC and were treated with a combination of radium-223 and abiraterone (202). The addition of radium-223

to abiraterone acetate did not improve survival in patients with CRPC and bone metastases, and was associated with an increased frequency of bone fractures compared with placebo. This finding was not confirmed in our study, however ongoing analysis is being performed on SREs in this study and the ongoing phase II study should help to clarify if it is safe to combine radium-223 and enzalutamide.

Chapter 4 described results from iPROSPECT, a translational study that collected biospecimens from men with hormone-sensitive PCa and men with CRPC. iPROSPECT was developed to address the need to further molecularly characterise PCa. In some patients, there can be a period of many years between the original diagnostic prostate biopsy and the development of metastatic disease (201). It is now known that over this period, PCa can undergo many changes including neuroendocrine differentiation (127). However, it has not been routine to repeat a biopsy in patients with metastatic disease. This is in part due to the difficulty and morbidity associated with repeat biopsies in PCa. With the development of sequencing technologies that identify potential drug targets, and the development of novel therapeutics, iPROSPECT focused on collecting metastatic biopsy samples that could be analysed for potential actionable mutations, further IHC testing and molecular profiling. Two biopsy methods were analysed; a non-targeted bone marrow biopsy traditionally performed at the bedside, and a targeted biopsy performed with radiological guidance, which normally requires admission to the hospital as a day case. When the methods were compared, CT guided biopsies were more accurate at obtaining metastatic tissue compared to bone marrow biopsies. An important finding of iPROSPECT was the

identification of transformation of PCa to neuroendocrine disease or small cell carcinoma on biopsy. Neuroendocrine PCa is a lethal disease subset with median overall survival of less than 1 year from time of detection (127). Patients presenting with *de novo* small cell carcinoma arising from the prostate is a rare entity observed in approximately 1% of all PCa cases, and is normally treated with a platinum agent plus etoposide, similar to the treatment for small cell lung cancer (129). Rates of this occurring vary in different studies; in this study one patient had neuroendocrine differentiation highlighting the importance of a repeat metastatic biopsy in any patient with rapidly progressing disease. Treatment options vary significantly once neuroendocrine disease is diagnosed as the subtype type of disease more commonly responds to traditional platinum based chemotherapy (129), therefore changing a patient's course of treatment. Detecting neuroendocrine disease significantly alters the management of these patients, as they require treatment with platinum based chemotherapy (130).

Recent advances in sequencing technologies allow for simultaneous identification of base substitutions, copy number alterations, and mutations at much greater sensitivity then traditional Sanger sequencing (131). Six metastatic samples and four matched primary samples were sequenced using the Oncomine™ Comprehensive Assay. In this study a higher number of mutations and alterations were detected in metastatic biopsies compared to primary biopsy samples. This chapter highlights the importance of performing repeat biopsies in patients with progressive metastatic PCa. NGS of these samples has confirmed numerous mutations and alterations that could be potential drug targets in the

future. A number of potential targets were detected including FGFR3 and amplification of the AR.

In chapter 5, the development of resistance to enzalutamide is discussed. The aim of this part of the study was to analyse the expression of AR-FL and AR-V7 *in vitro* and *in vivo*. Androgens and the AR play essential roles in the initiation and progression of PCa (31). AR gene amplification emerges during ADT and facilitates tumour growth in low androgen concentrations (35). Furthermore, the presence of the splice variant, AR-V7, has been established to be associated with resistance to anti-androgen treatment, such as enzalutamide, that functons by impairing AR signalling (26). Several hypotheses for treatment failure have been suggested such as hypersensitivity to non-testicular anti-androgens, increased androgen biosynthesis from adrenal precursor steroids or mutations in the AR gene (20). The best mechanism to detect AR-V7 has not been fully established. In this chapter, AR-V7 expression was examined in a panel of enzalutamide resistant cell lines and then analysed using two RISH methods to assess AR-FL and AR-V7 expression. Novel assays such as RNAscope® and BaseScope® represent a change in RISH approaches with their proprietary probe design that simultaneously amplify target-specific signals and suppress background noise from non-specific hybridisation (44). The BaseScope® assay was more sensitive in determining AR-V7 expression in cell lines and tissue samples compared to RNAscope®. This is in keeping with previously published data for AR-V7 using RISH (148), however, this was the first time both assays were compared to each other.

In chapter 6, a recently discovered novel class of ncRNAs called circRNAs are discussed. This was the first time circRNAs had been extensively researched in PCa. To investigate circRNAs associated with PCa, circRNA profiling was performed on a panel of PCa cell lines using a high throughout microarray assay. Bioinformatic analysis identified a number of differentially expressed circRNAs between different malignant *vs.* benign, and androgen dependent *vs.* independent cell lines. This suggests for the first time that circRNA expression is highly dysregulated in PCa and may identify a clinical signature that could be used to stratify patients for treatment or have use as diagnostic biomarkers.

In chapter 7, the expression of circRNA profiles in enzalutamide resistant PCa cell lines are reported. circRNAs were consistently found to be significantly more down-regulated in cell lines, which displayed enhanced resistance to enzalutamide. As circRNAs were predicted to bind miRNAs, miRNAs previously published in the literature were used that were strongly associated with PCa to select circRNAs for validation (173). Using qPCR, both hsa_circ_0083092 (predicted miRNA: miR-125b), hsa_circ_0001721 (predicted miRNA: hsa-miR-221) and hsa_circ_0004870 (predicted miRNA: miR-145), were validated, across the panel of cell lines. hsa_circ_0004870 was significantly down-regulated in enzalutamide resistant cell lines. hsa_circ_0004870's parental gene is *RBM39*, a serine/arginine-rich RNA-binding protein thought to activate or inhibit the alternative splicing of specific mRNA by interacting with the spliceosomal components within splice sites (195). Furthermore, *RBM39* is an U2AF65-related protein, with U2AF65 appearing to be a critical regulator involved with the

generation of AR-V7 (196). It is therefore possible that hsa_circ_0004870 may have an indirect role in regulating RBM39 expression, which has been previously shown to have a role in regulating AR-V7.

Biomarkers have an important role in monitoring a patient's disease and response to treatment in an efficient and effective manner. For a biomarker to be effective, there must be the ability to have access to repeat samples and to identify biomarkers from those samples that are reproducible in real time in the clinical setting. Biomarkers such as CTCs, must have sufficiently high sensitivity and specificity to be used in patients. When a biomarker has been clinically validated, it must also prove that it has clinical utility by improving outcomes in patients, therefore highlighting the importance of translational trials running parallel with clinical trials (203).

6.35 Future work

iPROSPECT collected a bank of biospecimens from men with metastatic PCa. This biobank includes CTCs, serum/plasma and metastatic biopsy samples. These valuable specimens will allow researchers to continue to monitor disease responses to treatment and to investigate methods of resistance. Future work includes analysis of CTC counts, which will allow researchers to follow CTC counts during treatment and see if these correlate with disease progression in the hormone sensitive setting. Further work could include IHC, RISH, and NGS (from the DNA collected from the CTCs), additionally characterising the complex molecular makeup of metastatic PCa.

Radium-223 combined with enzalutamide (30) was safe and well tolerated and may become a standard of care treatment for men with mCRPC. Evaluation of secondary endpoints including skeletal related events, PFS, OS and QoL data with longer follow up is on-going and outside the scope of this thesis.

In this study, an AR-V7 assay using RISH was validated using metastatic biopsy samples from iPROSPECT. Future work will validate these techniques in larger cohorts. The presence of AR-V7 will be correlated with the clinical data collected from patients in iPROSPECT. If validated, further testing for AR-V7 could be performed on the CTC filters collected from patients, which could then be used to diagnose patients without the need for biopsy. Ultimately building on this research, these assays may provide more robust yet feasible methods to acquire translational data to answer fundamental questions about ARV-7 biology, such as the role of other variants of the AR, and the significance of AR-V7 as a driver mutation (204). The RISH technology could be applied to detect other mutations in PCa. One such mutation could be PTEN, which has been shown to be associated with a poor prognosis in patients with metastatic CRPC. In a trial examining combined blockade with abiraterone and the AKT inhibitor, ipatasertib, there was superior anti-tumour activity in patients with PTEN-loss tumours, suggesting this as a marker that could be in future detected by RISH, allowing for tailored treatments for patients (205).

This study revealed for the first time the circRNA expression signatures of advanced PCa. It established a novel approach for comprehensively screening circRNAs that could be involved in cancer-related pathways. Furthermore, the regulatory role of the circRNA/miRNA/mRNA pathway (such as

hsa_circ_0004870/miR-145/RBM39) was preliminarily established in PCa. Further experimentation is required to further delineate the association with resistance to enzalutamide. The biological functions and mechanisms underlying hsa_circ_0004870 need to further established. This may lay the foundation for further diagnostic, therapeutic and functional research of circRNAs in PCa. Furthermore, the deregulation of miRNAs in disease conditions could be harnessed by either miRNA replacement therapy using miRNA mimics or inhibition of miRNA function by antimiRs (85). Based on these findings in miRNA research, the possibility of the validated circRNAs in this project having similar functions and uses in PCa is possible, but yet to be fully explored.

In summary, this body of work lays the foundations to identify potential biomarkers that could be used to identify patients who have more aggressive and treatment resistant disease. One such biomarker are circRNAs which may be associated with resistance to AR targeted therapies. Future work will involve validation studies of candidate circRNAs in clinical specimens.

6.36 Overall conclusions

In this thesis, novel treatment methods were explored for mCRPC as were methods of detecting response to these treatments by analysing CTC numbers. The feasibility of performing biopsies in patients with PCa has also been demonstrated. Biopsies performed using real time imaging are superior to biopsies performed without any guidance such as bone marrow biopsies. Neuroendocrine differentiation is an important finding in repeat biopsies, which may dictate a change in treatment if detected. This study explored a number of methods to analyse AR-V7 and confirmed the known association with resistance to

enzalutamide. This study characterised circRNAs profiles in PCa for the first time and demonstrated that they are differentially expressed in enzalutamide resistant cell lines with confirmed AR-V7 expression. These findings indicate that circRNAs may represent potentially valuable diagnostic biomarkers for detecting resistance in men receiving treatment for PCa.

The development of novel treatment combinations was safe and should be further explored. However, identifying patients who will respond to these treatments is a key goal in ongoing research. This study has identified a number of novel molecular targets that could be developed into clinically useful assays that may guide future treatment decisions and improve outcomes for patients.

References

1. PA H. Cancers of the male reproductive organs. In: World Cancer Report, Stewart BW, Wild CP (Eds), World Health Organization, Lyon 2014.

2. Ireland NCR. www.ncri.ie. 2015.

3. Department of Health. Diagnosis, staging and treatment of patients with prostate cancer. National Clinical Guideline No8. 2015.

4. Nelson WG, De Marzo AM, Isaacs WB. Prostate Cancer. New England Journal of Medicine. 2003;349(4):366-81.

5. de Moor JS, Mariotto AB, Parry C, Alfano CM, Padgett L, Kent EE, et al. Cancer survivors in the United States: prevalence across the survivorship trajectory and implications for care. Cancer epidemiology, biomarkers & prevention : a publication of the American Association for Cancer Research, cosponsored by the American Society of Preventive Oncology. 2013;22(4):561-70.

6. James ND, Spears MR, Clarke NW, Dearnaley DP, De Bono JS, Gale J, et al. Survival with Newly Diagnosed Metastatic Prostate Cancer in the "Docetaxel Era": Data from 917 Patients in the Control Arm of the STAMPEDE Trial (MRC PR08, CRUK/06/019). Eur Urol. 2015;67(6):1028-38.

7. Karantanos T, Corn PG, Thompson TC. Prostate cancer progression after androgen deprivation therapy: mechanisms of castrate resistance and novel therapeutic approaches. Oncogene. 2013;32:5501.

8. Cicek MS, Conti DV, Curran A, Neville PJ, Paris PL, Casey G, et al. Association of prostate cancer risk and aggressiveness to androgen pathway genes: SRD5A2, CYP17, and the AR. The Prostate. 2004;59(1):69-76.

9. Heidenreich A, Bastian PJ, Bellmunt J, Bolla M, Joniau S, van der Kwast T, et al. EAU guidelines on prostate cancer. Part II: Treatment of advanced, relapsing, and castration-resistant prostate cancer. Eur Urol. 2014;65(2):467-79.

10. Loblaw DA, Virgo KS, Nam R, Somerfield MR, Ben-Josef E, Mendelson DS, et al. Initial hormonal management of androgen-sensitive metastatic, recurrent, or progressive prostate cancer: 2006 update of an American Society of Clinical Oncology practice guideline. Journal of clinical oncology : official journal of the American Society of Clinical Oncology. 2007;25(12):1596-605.

11. Basch E, Loblaw DA, Oliver TK, Carducci M, Chen RC, Frame JN, et al. Systemic therapy in men with metastatic castration-resistant prostate cancer:American Society of Clinical Oncology and Cancer Care Ontario clinical practice guideline. Journal of clinical oncology : official journal of the American Society of Clinical Oncology. 2014;32(30):3436-48.

12. Mostaghel EA, Plymate SR, Montgomery B. Molecular pathways: targeting resistance in the androgen receptor for therapeutic benefit. Clin Cancer Res. 2014;20(4):791-8.

13. Sweeney CJ, Chen Y-H, Carducci M, Liu G, Jarrard DF, Eisenberger M, et al. Chemohormonal Therapy in Metastatic Hormone-Sensitive Prostate Cancer. New England Journal of Medicine. 2015;373(8):737-46.

14. James ND, Sydes MR, Clarke NW, Mason MD, Dearnaley DP, Spears MR, et al. Addition of docetaxel, zoledronic acid, or both to first-line long-term hormone therapy in prostate cancer (STAMPEDE): survival results from an adaptive, multiarm, multistage, platform randomised controlled trial. Lancet. 2016;387(10024):1163-77.

15. Fizazi K, Tran N, Fein L, Matsubara N, Rodriguez-Antolin A, Alekseev BY, et al. Abiraterone plus Prednisone in Metastatic, Castration-Sensitive Prostate Cancer. New England Journal of Medicine. 2017;377(4):352-60.

16. James ND, de Bono JS, Spears MR, Clarke NW, Mason MD, Dearnaley DP, et al. Abiraterone for Prostate Cancer Not Previously Treated with Hormone Therapy. New England Journal of Medicine. 2017;377(4):338-51.

17. Beer TM, Armstrong AJ, Rathkopf DE, Loriot Y, Sternberg CN, Higano CS, et al. Enzalutamide in metastatic prostate cancer before chemotherapy. The New England journal of medicine. 2014;371(5):424-33.

18. de Bono JS, Logothetis CJ, Molina A, Fizazi K, North S, Chu L, et al. Abiraterone and increased survival in metastatic prostate cancer. The New England journal of medicine. 2011;364(21):1995-2005.

19. de Bono JS, Oudard S, Ozguroglu M, Hansen S, Machiels J-P, Kocak I, et al. Prednisone plus cabazitaxel or mitoxantrone for metastatic castration-resistant prostate cancer progressing after docetaxel treatment: a randomised open-label trial. The Lancet.376(9747):1147-54.

20. Balbas MD, Evans MJ, Hosfield DJ, Wongvipat J, Arora VK, Watson PA, et al. Overcoming mutation-based resistance to antiandrogens with rational drug design. Elife. 2013;2:e00499.

21. Ryan CJ, Smith MR, Fizazi K, Saad F, Mulders PF, Sternberg CN, et al. Abiraterone acetate plus prednisone versus placebo plus prednisone in chemotherapy-naive men with metastatic castration-resistant prostate cancer (COU-AA-302): final overall survival analysis of a randomised, double-blind, placebo-controlled phase 3 study. The Lancet Oncology. 2015;16(2):152-60.

22. Scher HI, Fizazi K, Saad F, Taplin M-E, Sternberg CN, Miller K, et al. Increased Survival with Enzalutamide in Prostate Cancer after Chemotherapy. New England Journal of Medicine. 2012;367(13):1187-97.

23. Scher HI, Fizazi K, Saad F, Taplin ME, Sternberg CN, Miller K, et al. Increased survival with enzalutamide in prostate cancer after chemotherapy. The New England journal of medicine. 2012;367(13):1187-97.

24. Beer TM, Armstrong AJ, Rathkopf DE, Loriot Y, Sternberg CN, Higano CS, et al. Enzalutamide in Metastatic Prostate Cancer before Chemotherapy. New England Journal of Medicine. 2014;371(5):424-33.

25. Loriot Y, Bianchini D, Ileana E, Sandhu S, Patrikidou A, Pezaro C, et al. Antitumour activity of abiraterone acetate against metastatic castration-resistant prostate cancer progressing after docetaxel and enzalutamide (MDV3100). Ann Oncol. 2013;24(7):1807-12.

26. Schrader AJ, Boegemann M, Ohlmann CH, Schnoeller TJ, Krabbe LM, Hajili T, et al. Enzalutamide in castration-resistant prostate cancer patients progressing after docetaxel and abiraterone. Eur Urol. 2014;65(1):30-6.

27. Berthold DR, Pond GR, Soban F, de Wit R, Eisenberger M, Tannock IF. Docetaxel plus prednisone or mitoxantrone plus prednisone for advanced prostate cancer: updated survival in the TAX 327 study. Journal of clinical oncology : official journal of the American Society of Clinical Oncology. 2008;26(2):242-5.

28. Gandaglia G, Karakiewicz PI, Briganti A, Passoni NM, Schiffmann J, Trudeau V, et al. Impact of the Site of Metastases on Survival in Patients with Metastatic Prostate Cancer. Eur Urol. 2015;68(2):325-34.

29. Fizazi K, Carducci M, Smith M, Damiao R, Brown J, Karsh L, et al. Denosumab versus zoledronic acid for treatment of bone metastases in men with castration-resistant prostate cancer: a randomised, double-blind study. Lancet. 2011;377(9768):813-22.

30. Parker C, Nilsson S, Heinrich D, Helle SI, O'Sullivan JM, Fossa SD, et al. Alpha emitter radium-223 and survival in metastatic prostate cancer. The New England journal of medicine. 2013;369(3):213-23.

31. Visakorpi T, Hyytinen E, Koivisto P, Tanner M, Keinanen R, Palmberg C, et al. In vivo amplification of the androgen receptor gene and progression of human prostate cancer. Nature genetics. 1995;9(4):401-6.

32. Lorente D, Mateo J, Zafeiriou Z, Smith AD, Sandhu S, Ferraldeschi R, et al. Switching and withdrawing hormonal agents for castration-resistant prostate cancer. Nat Rev Urol. 2015;12(1):37-47.

33. Antonarakis ES, Lu C, Wang H, Luber B, Nakazawa M, Roeser JC, et al. AR-V7 and resistance to enzalutamide and abiraterone in prostate cancer. The New England journal of medicine. 2014;371(11):1028-38.

34. Eisermann K, Wang D, Jing Y, Pascal LE, Wang Z. Androgen receptor gene mutation, rearrangement, polymorphism. Translational Andrology and Urology. 2013;2(3):137-47.

35. Korpal M, Korn JM, Gao X, Rakiec DP, Ruddy DA, Doshi S, et al. An F876L mutation in androgen receptor confers genetic and phenotypic resistance to MDV3100 (enzalutamide). Cancer Discov. 2013;3(9):1030-43.

36. Hu R, Dunn TA, Wei S, Isharwal S, Veltri RW, Humphreys E, et al. Ligand-independent androgen receptor variants derived from splicing of cryptic exons signify hormone-refractory prostate cancer. Cancer research. 2009;69(1):16-22.

37. Liu LL, Xie N, Sun S, Plymate S, Mostaghel E, Dong X. Mechanisms of the androgen receptor splicing in prostate cancer cells. Oncogene. 2014;33(24):3140-50.

38. Yu Z, Chen S, Sowalsky AG, Voznesensky OS, Mostaghel EA, Nelson PS, et al. Rapid induction of androgen receptor splice variants by androgen deprivation in prostate cancer. Clin Cancer Res. 2014;20(6):1590-600.

39. Onstenk W, Sieuwerts AM, Kraan J, Van M, Nieuweboer AJ, Mathijssen RH, et al. Efficacy of Cabazitaxel in Castration-resistant Prostate Cancer Is Independent of the Presence of AR-V7 in Circulating Tumor Cells. Eur Urol. 2015;15(15):00611-9.

40. Antonarakis ES, Lu C, Luber B, Wang H, Chen Y, Nakazawa M, et al. Androgen Receptor Splice Variant 7 and Efficacy of Taxane Chemotherapy in Patients With Metastatic Castration-Resistant Prostate Cancer. JAMA Oncol. 2015;4(10).

41. Nakazawa M, Lu C, Chen Y, Paller CJ, Carducci MA, Eisenberger MA, et al. Serial Blood-Based Analysis of AR-V7 in Men with Advanced Prostate Cancer. Ann Oncol. 2015;27.

42. Qu Y, Dai B, Ye D, Kong Y, Chang K, Jia Z, et al. Constitutively active AR-V7 plays an essential role in the development and progression of castration-resistant prostate cancer. Scientific reports. 2015;5:7654.

43. Watson PA, Arora VK, Sawyers CL. Emerging mechanisms of resistance to androgen receptor inhibitors in prostate cancer. Nat Rev Cancer. 2015;15(12):701-11.

44. Wang F, Flanagan J, Su N, Wang LC, Bui S, Nielson A, et al. RNAscope: a novel in situ RNA analysis platform for formalin-fixed, paraffin-embedded tissues. The Journal of molecular diagnostics : JMD. 2012;14(1):22-9.

45. Danila DC, Fleisher M, Scher HI. Circulating tumor cells as biomarkers in prostate cancer. Clin Cancer Res. 2011;17(12):3903-12.

46. Lianidou ES, Strati A, Markou A. Circulating tumor cells as promising novel biomarkers in solid cancers. Crit Rev Clin Lab Sci. 2014;51(3):160-71.

47. Scher HI, Jia X, de Bono JS, Fleisher M, Pienta KJ, Raghavan D, et al. Circulating tumour cells as prognostic markers in progressive, castration-resistant prostate cancer: a reanalysis of IMMC38 trial data. The lancet oncology. 2009;10(3):233-9.

48. Thalgott M, Rack B, Maurer T, Souvatzoglou M, Eiber M, Kress V, et al. Detection of circulating tumor cells in different stages of prostate cancer. Journal of cancer research and clinical oncology. 2013;139(5):755-63.

49. Abrahamsson PA. Neuroendocrine differentiation in prostatic carcinoma. The Prostate. 1999;39(2):135-48.

50. de Bono JS, Scher HI, Montgomery RB, Parker C, Miller MC, Tissing H, et al. Circulating tumor cells predict survival benefit from treatment in metastatic castration-resistant prostate cancer. Clin Cancer Res. 2008;14(19):6302-9.

51. Danila DC, Anand A, Schultz N, Heller G, Wan M, Sung CC, et al. Analytic and clinical validation of a prostate cancer-enhanced messenger RNA detection assay in whole blood as a prognostic biomarker for survival. Eur Urol. 2014;65(6):1191-7.

52. Flores LM, Kindelberger DW, Ligon AH, Capelletti M, Fiorentino M, Loda M, et al. Improving the yield of circulating tumour cells facilitates molecular characterisation and recognition of discordant HER2 amplification in breast cancer. British Journal of Cancer. 2010;102(10):1495-502.

53. Awe JA, Saranchuk J, Drachenberg D, Mai S. Filtration-based enrichment of circulating tumor cells from all prostate cancer risk groups. Urologic Oncology: Seminars and Original Investigations. 2017;35(5):300-9.

54. Desitter I, Guerrouahen BS, Benali-Furet N, Wechsler J, Janne PA, Kuang Y, et al. A new device for rapid isolation by size and characterization of rare circulating tumor cells. Anticancer Res. 2011;31(2):427-41.

55. Scher HI, Beer TM, Higano CS, Anand A, Taplin M-E, Efstathiou E, et al. Antitumour activity of MDV3100 in castration-resistant prostate cancer: a phase 1-2 study. Lancet. 2010;375(9724):1437-46.

56. Shih JW, Wang LY, Hung CL, Kung HJ, Hsieh CL. Non-Coding RNAs in Castration-Resistant Prostate Cancer: Regulation of Androgen Receptor Signaling and Cancer Metabolism. International journal of molecular sciences. 2015;16(12):28943-78.

57. Misawa A, Takayama KI, Inoue S. Long non-coding RNAs and prostate cancer. Cancer science. 2017;108(11):2107-14.

58. Lin H-M, Mahon KL, Spielman C, Gurney H, Mallesara G, Stockler MR, et al. Phase 2 study of circulating microRNA biomarkers in castration-resistant prostate cancer. British Journal Of Cancer. 2017;116:1002.

59. Esteller M. Non-coding RNAs in human disease. Nat Rev Genet. 2011;12(12):861-74.

60. Jeck WR, Sorrentino JA, Wang K, Slevin MK, Burd CE, Liu J, et al. Circular RNAs are abundant, conserved, and associated with ALU repeats. Rna. 2013;19(2):141-57.

61. Warner JR. The economics of ribosome biosynthesis in yeast. Trends in biochemical sciences. 1999;24(11):437-40.

62. Cocquerelle C, Mascrez B, Hetuin D, Bailleul B. Mis-splicing yields circular RNA molecules. FASEB journal : official publication of the Federation of American Societies for Experimental Biology. 1993;7(1):155-60.

63. Nigro JM, Cho KR, Fearon ER, Kern SE, Ruppert JM, Oliner JD, et al. Scrambled exons. Cell. 1991;64(3):607-13.

64. Kos A, Dijkema R, Arnberg AC, van der Meide PH, Schellekens H. The hepatitis delta (delta) virus possesses a circular RNA. Nature. 1986;323(6088):558-60.

65. Salzman J, Gawad C, Wang PL, Lacayo N, Brown PO. Circular RNAs are the predominant transcript isoform from hundreds of human genes in diverse cell types. PLoS One. 2012;7(2):1.

66. Jeck WR, Sharpless NE. Detecting and characterizing circular RNAs. Nat Biotechnol. 2014;32(5):453-61.

67. Li Z, Huang C, Bao C, Chen L, Lin M, Wang X, et al. Exon-intron circular RNAs regulate transcription in the nucleus. Nat Struct Mol Biol. 2015;22(3):256-64.

68. Zhang Y, Zhang X-O, Chen T, Xiang J-F, Yin Q-F, Xing Y-H, et al. Circular Intronic Long Noncoding RNAs. Molecular Cell.51(6):792-806.

69. Greene J, Baird AM, Brady L, Lim M, Gray SG, McDermott R, et al. Circular RNAs: Biogenesis, Function and Role in Human Diseases. Frontiers in molecular biosciences. 2017;4:38.

70. Memczak S, Jens M, Elefsinioti A, Torti F, Krueger J, Rybak A, et al. Circular RNAs are a large class of animal RNAs with regulatory potency. Nature. 2013;495(7441):333-8.

71. Suzuki H, Zuo Y, Wang J, Zhang MQ, Malhotra A, Mayeda A. Characterization of RNase R-digested cellular RNA source that consists of lariat and circular RNAs from pre-mRNA splicing. Nucleic Acids Res. 2006;34(8):e63.

72. Guo JU, Agarwal V, Guo H, Bartel DP. Expanded identification and characterization of mammalian circular RNAs. Genome Biol. 2014;15(7):409.

73. Szabo L, Salzman J. Detecting circular RNAs: bioinformatic and experimental challenges. Nat Rev Genet. 2016;17(11):679-92.

74. Wang Y-h, Yu X-h, Luo S-s, Han H. Comprehensive circular RNA profiling reveals that circular RNA100783 is involved in chronic CD28-associated CD8(+)T cell ageing. Immunity & Ageing : I & A. 2015;12:17.

75. Zhong Z, Lv M, Chen J. Screening differential circular RNA expression profiles reveals the regulatory role of circTCF25-miR-103a-3p/miR-107-CDK6 pathway in bladder carcinoma. Scientific reports. 2016;6:30919.

76. Danan M, Schwartz S, Edelheit S, Sorek R. Transcriptome-wide discovery of circular RNAs in Archaea. Nucleic Acids Res. 2012;40(7):3131-42.

77. Glazar P, Papavasileiou P, Rajewsky N. circBase: a database for circular RNAs. Rna. 2014;20(11):1666-70.

78. Thomson DW, Dinger ME. Endogenous microRNA sponges: evidence and controversy. Nat Rev Genet. 2016;17(5):272-83.

79. Salzman J. Circular RNA Expression: Its Potential Regulation and Function. Trends in genetics : TIG. 2016;32(5):309-16.

80. Felekkis K, Touvana E, Stefanou C, Deltas C. microRNAs: a newly described class of encoded molecules that play a role in health and disease. Hippokratia. 2010;14(4):236-40.

81. Burd CE, Jeck WR, Liu Y, Sanoff HK, Wang Z, Sharpless NE. Expression of linear and novel circular forms of an INK4/ARF-associated non-coding RNA correlates with atherosclerosis risk. PLoS Genet. 2010;6(12):e1001233.

82. Wang F, Nazarali AJ, Ji S. Circular RNAs as potential biomarkers for cancer diagnosis and therapy. American journal of cancer research. 2016;6(6):1167-76.

83. He J, Xie Q, Xu H, Li J, Li Y. Circular RNAs and cancer. Cancer Letters. 2017;396:138-44.

84. Kent OA, Mendell JT. A small piece in the cancer puzzle: microRNAs as tumor suppressors and oncogenes. Oncogene. 2006;25(46):6188-96.

85. Peng Y, Croce CM. The role of MicroRNAs in human cancer. Signal Transduction And Targeted Therapy. 2016;1:15004.

86. Hansen TB, Jensen TI, Clausen BH, Bramsen JB, Finsen B, Damgaard CK, et al. Natural RNA circles function as efficient microRNA sponges. Nature. 2013;495(7441):384-8.

87. Wang F, Nazarali AJ, Ji S. Circular RNAs as potential biomarkers for cancer diagnosis and therapy. American Journal of Cancer Research. 2016;6(6):1167-76.

88. Zheng Q, Bao C, Guo W, Li S, Chen J, Chen B, et al. Circular RNA profiling reveals an abundant circHIPK3 that regulates cell growth by sponging multiple miRNAs. Nature Communications. 2016;7:11215.

89. Scotti MM, Swanson MS. RNA mis-splicing in disease. Nat Rev Genet. 2016;17(1):19-32.

90. Kong Z, Wan X, Zhang Y, Zhang P, Zhang Y, Zhang X, et al. Androgen-responsive circular RNA circSMARCA5 is up-regulated and promotes cell proliferation in prostate cancer. Biochem Biophys Res Commun. 2017;493(3):1217-23.

91. Li P, Chen S, Chen H, Mo X, Li T, Shao Y, et al. Using circular RNA as a novel type of biomarker in the screening of gastric cancer. Clin Chim Acta. 2015;444:132-6.

92. Bachmayr-Heyda A, Reiner AT, Auer K, Sukhbaatar N, Aust S, Bachleitner-Hofmann T, et al. Correlation of circular RNA abundance with proliferation - exemplified with colorectal and ovarian cancer, idiopathic lung fibrosis, and normal human tissues. Scientific reports. 2015;5:8057.

93. Dou Y, Cha DJ, Franklin JL, Higginbotham JN, Jeppesen DK, Weaver AM, et al. Circular RNAs are down-regulated in KRAS mutant colon cancer cells and can be transferred to exosomes. Scientific reports. 2016;6:37982.

94. Huang G, Zhu H, Shi Y, Wu W, Cai H, Chen X. cir-ITCH plays an inhibitory role in colorectal cancer by regulating the Wnt/beta-catenin pathway. PLoS One. 2015;10(6):e0131225.

95. Qin M, Liu G, Huo X, Tao X, Sun X, Ge Z, et al. Hsa_circ_0001649: A circular RNA and potential novel biomarker for hepatocellular carcinoma. Cancer Biomark. 2016;16(1):161-9.

96. Shang X, Li G, Liu H, Li T, Liu J, Zhao Q, et al. Comprehensive Circular RNA Profiling Reveals That hsa_circ_0005075, a New Circular RNA Biomarker, Is Involved in Hepatocellular Crcinoma Development. Medicine. 2016;95(22):e3811.

97. Yu L, Gong X, Sun L, Zhou Q, Lu B, Zhu L. The Circular RNA Cdr1as Act as an Oncogene in Hepatocellular Carcinoma through Targeting miR-7 Expression. PLoS One. 2016;11(7):e0158347.

98. Li F, Zhang L, Li W, Deng J, Zheng J, An M, et al. Circular RNA ITCH has inhibitory effect on ESCC by suppressing the Wnt/beta-catenin pathway. Oncotarget. 2015;6(8):6001-13.

99. Wan L, Zhang L, Fan K, Cheng ZX, Sun QC, Wang JJ. Circular RNA-ITCH Suppresses Lung Cancer Proliferation via Inhibiting the Wnt/beta-Catenin Pathway. Biomed Res Int. 2016;2016:1579490.

100. Clegg N, Ferguson C, True LD, Arnold H, Moorman A, Quinn JE, et al. Molecular characterization of prostatic small-cell neuroendocrine carcinoma. The Prostate. 2003;55(1):55-64.

101. Tetu B, Ro JY, Ayala AG, Johnson DE, Logothetis CJ, Ordonez NG. Small cell carcinoma of the prostate. Part I. A clinicopathologic study of 20 cases. Cancer. 1987;59(10):1803-9.

102. Humphrey PA. Histological variants of prostatic carcinoma and their significance. Histopathology. 2012;60(1):59-74.

103. Aggarwal R, Huang J, Alumkal JJ, Zhang L, Feng FY, Thomas GV, et al. Clinical and Genomic Characterization of Treatment-Emergent Small-Cell Neuroendocrine Prostate Cancer: A Multi-institutional Prospective Study. Journal of Clinical Oncology. 2018;36(24):2492-503.

104. Horoszewicz JS, Leong SS, Kawinski E, Karr JP, Rosenthal H, Chu TM, et al. LNCaP model of human prostatic carcinoma. Cancer research. 1983;43(4):1809-18.

105. Webber MM, Bello D, Kleinman HK, Wartinger DD, Williams DE, Rhim JS. Prostate specific antigen and androgen receptor induction and characterization of an immortalized adult human prostatic epithelial cell line. Carcinogenesis. 1996;17(8):1641-6.

106. Bello D, Webber MM, Kleinman HK, Wartinger DD, Rhim JS. Androgen responsive adult human prostatic epithelial cell lines immortalized by human papillomavirus 18. Carcinogenesis. 1997;18(6):1215-23.

107. Young L, Sung J, Stacey G, Masters JR. Detection of Mycoplasma in cell cultures. Nature protocols. 2010;5(5):929-34.

108. R RCTRAlaefsc, Foundation for Statistical Computing V, Austria. ISBN 3-900051-07-0, URL, http://www.R-project.org/.

109. John B, Enright AJ, Aravin A, Tuschl T, Sander C, Marks DS. Human MicroRNA Targets. PLOS Biology. 2004;2(11):e363.

110. Agarwal V, Bell GW, Nam J-W, Bartel DP. Predicting effective microRNA target sites in mammalian mRNAs. eLife. 2015;4:e05005.

111. Conteduca V, Wetterskog D, Sharabiani MTA, Grande E, Fernandez-Perez MP, Jayaram A, et al. Androgen receptor gene status in plasma DNA associates with worse outcome on enzalutamide or abiraterone for castration-resistant prostate cancer: a multi-institution correlative biomarker study. Ann Oncol. 2017.

112. Scher HI, Halabi S, Tannock I, Morris M, Sternberg CN, Carducci MA, et al. Design and end points of clinical trials for patients with progressive prostate cancer and castrate levels of testosterone: recommendations of the Prostate Cancer Clinical Trials Working Group. Journal of clinical oncology : official journal of the American Society of Clinical Oncology. 2008;26(7):1148-59.

113. Bitting RL, Boominathan R, Rao C, Kemeny G, Foulk B, Garcia-Blanco MA, et al. Development of a method to isolate circulating tumor cells using mesenchymal-based capture. Methods (San Diego, Calif). 2013;64(2):10.1016/j.ymeth.2013.06.034.

114. Bitting RL, Schaeffer D, Somarelli JA, Garcia-Blanco MA, Armstrong AJ. The role of epithelial plasticity in prostate cancer dissemination and treatment resistance. Cancer metastasis reviews. 2014;33(0):441-68.

115. Meyerson M, Gabriel S, Getz G. Advances in understanding cancer genomes through second-generation sequencing. Nat Rev Genet. 2010;11(10):685-96.

116. Ross RW, Halabi S, Ou SS, Rajeshkumar BR, Woda BA, Vogelzang NJ, et al. Predictors of prostate cancer tissue acquisition by an undirected core bone marrow biopsy in metastatic castration-resistant prostate cancer--a Cancer and Leukemia Group B study. Clin Cancer Res. 2005;11(22):8109-13.

117. Rubinstein MA, Smelin A. Superiority of iliac over sternal marrow aspiration in recovery of neoplastic cells. AMA Archives of Internal Medicine. 1952;89(6):909-13.

118. Holmes MG, Foss E, Joseph G, Foye A, Beckett B, Motamedi D, et al. CT-Guided Bone Biopsies in Metastatic Castration-Resistant Prostate Cancer: Factors Predictive of Maximum Tumor Yield. Journal of vascular and interventional radiology : JVIR. 2017;28(8):1073-81.e1.

119. Hovelson DH, McDaniel AS, Cani AK, Johnson B, Rhodes K, Williams PD, et al. Development and Validation of a Scalable Next-Generation Sequencing System for Assessing Relevant Somatic Variants in Solid Tumors()(). Neoplasia (New York, NY). 2015;17(4):385-99.

120. Boyd LK, Mao X, Lu Y-J. The complexity of prostate cancer: genomic alterations and heterogeneity. Nat Rev Urol. 2012;9(11):652-64.

121. Stangelberger A, Waldert M, Djavan B. Prostate Cancer in Elderly Men. Reviews in Urology. 2008;10(2):111-9.

122. Pierorazio PM, Walsh PC, Partin AW, Epstein JI. Prognostic Gleason grade grouping: data based on the modified Gleason scoring sys- tem. BJU Int. 2013;111.

123. Metwalli AR, Rosner IL, Cullen J, Chen Y, Brand T, Brassell SA, et al. Elevated Alkaline Phosphatase Velocity Strongly Predicts Overall Survival and the Risk of Bone Metastases in Castrate Resistant Prostate Cancer. Urologic oncology. 2014;32(6):761-8.

124. Mikah P, Krabbe L-M, Eminaga O, Herrmann E, Papavassilis P, Hinkelammert R, et al. Dynamic changes of alkaline phosphatase are strongly associated with PSA-decline and predict best clinical benefit earlier than PSA-

changes under therapy with abiraterone acetate in bone metastatic castration resistant prostate cancer. BMC Cancer. 2016;16:214.

125. Gandaglia G, Abdollah F, Schiffmann J, Trudeau V, Shariat SF, Kim SP, et al. Distribution of metastatic sites in patients with prostate cancer: A population-based analysis. The Prostate. 2014;74(2):210-6.

126. Hilton JF, Amir E, Hopkins S, Nabavi M, DiPrimio G, Sheikh A, et al. Acquisition of metastatic tissue from patients with bone metastases from breast cancer. Breast cancer research and treatment. 2011;129(3):761-5.

127. Parimi V, Goyal R, Poropatich K, Yang XJ. Neuroendocrine differentiation of prostate cancer: a review. American Journal of Clinical and Experimental Urology. 2014;2(4):273-85.

128. Beltran H, Rickman DS, Park K, Chae SS, Sboner A, MacDonald TY, et al. Molecular Characterization of Neuroendocrine Prostate Cancer and Identification of New Drug Targets. Cancer discovery. 2011;1(6):487-95.

129. Vlachostergios PJ, Papandreou CN. Targeting Neuroendocrine Prostate Cancer: Molecular and Clinical Perspectives. Frontiers in Oncology. 2015;5:6.

130. Epstein JI, Amin MB, Beltran H, Lotan TL, Mosquera J-M, Reuter VE, et al. Proposed Morphologic Classification of Prostate Cancer With Neuroendocrine Differentiation. The American journal of surgical pathology. 2014;38(6):756-67.

131. Robinson D, Van Allen Eliezer M, Wu Y-M, Schultz N, Lonigro Robert J, Mosquera J-M, et al. Integrative Clinical Genomics of Advanced Prostate Cancer. Cell.161(5):1215-28.

132. Schrijver WAME, van der Groep P, Hoefnagel LDC, ter Hoeve ND, Peeters T, Moelans CB, et al. Influence of decalcification procedures on immunohistochemistry and molecular pathology in breast cancer. Mod Pathol. 2016;29(12):1460-70.

133. Salvi S, Casadio V, Conteduca V, Lolli C, Gurioli G, Martignano F, et al. Circulating AR copy number and outcome to enzalutamide in docetaxel-treated metastatic castration-resistant prostate cancer. Oncotarget. 2016;7(25):37839-45.

134. Tomlins SA, Laxman B, Varambally S, Cao X, Yu J, Helgeson BE, et al. Role of the TMPRSS2-ERG Gene Fusion in Prostate Cancer. Neoplasia (New York, NY). 2008;10(2):177-88.

135. Williams SV, Hurst CD, Knowles MA. Oncogenic FGFR3 gene fusions in bladder cancer. Human Molecular Genetics. 2013;22(4):795-803.

136. Ornitz DM, Itoh N. The Fibroblast Growth Factor signaling pathway. Wiley Interdisciplinary Reviews Developmental Biology. 2015;4(3):215-66.

137. Babina IS, Turner NC. Advances and challenges in targeting FGFR signalling in cancer. Nature Reviews Cancer. 2017;17:318.

138. Hernandez S, de Muga S, Agell L, Juanpere N, Esgueva R, Lorente JA, et al. FGFR3 mutations in prostate cancer: association with low-grade tumors. Mod Pathol. 2009;22(6):848-56.

139. Tome-Garcia J, Li D, Ghazaryan S, Shu L, Wu L. ERBB2 Increases Metastatic Potentials Specifically in Androgen-Insensitive Prostate Cancer Cells. PLOS ONE. 2014;9(6):e99525.

140. Baek KH, Hong ME, Jung YY, Lee CH, Lee TJ, Park ES, et al. Correlation of AR, EGFR, and HER2 Expression Levels in Prostate Cancer: Immunohistochemical Analysis and Chromogenic In Situ Hybridization. Cancer Research and Treatment : Official Journal of Korean Cancer Association. 2012;44(1):50-6.

141. Corn P, Wang F, McKeehan WL, Navone N. Targeting Fibroblast Growth Factor Pathways in Prostate Cancer. Clinical cancer research : an official journal of the American Association for Cancer Research. 2013;19(21):5856-66.

142. Gao S, Ye H, Gerrin S, Wang H, Sharma A, Chen S, et al. ErbB2 Signaling Increases Androgen Receptor Expression in Abiraterone-Resistant Prostate Cancer. Clin Cancer Res. 2016;22(14):3672-82.

143. Li R, Wheeler T, Dai H, Frolov A, Thompson T, Ayala G. High level of androgen receptor is associated with aggressive clinicopathologic features and decreased biochemical recurrence-free survival in prostate: cancer patients treated with radical prostatectomy. The American journal of surgical pathology. 2004;28(7):928-34.

144. Zhu Y, Sharp A, Anderson CM, Silberstein JL, Taylor M, Lu C, et al. Novel Junction-specific and Quantifiable In Situ Detection of AR-V7 and its Clinical Correlates in Metastatic Castration-resistant Prostate Cancer. European Urology.

145. Koivisto P, Kononen J, Palmberg C, Tammela T, Hyytinen E, Isola J, et al. Androgen receptor gene amplification: a possible molecular mechanism for androgen deprivation therapy failure in prostate cancer. Cancer research. 1997;57(2):314-9.

146. Li Y, Chan SC, Brand LJ, Hwang TH, Silverstein KAT, Dehm SM. Androgen receptor splice variants mediate enzalutamide resistance in castration-resistant prostate cancer cell lines. Cancer research. 2013;73(2):483-9.

147. Crumbaker M, Savdie R, Joshua AM. Refining the Assessment and Implications of AR-V7 in Castrate-resistant Prostate Cancer. European Urology.

148. Guedes LB, Morais CL, Almutairi F, Haffner MC, Zheng Q, Isaacs JT, et al. Analytic Validation of RNA In Situ Hybridization (RISH) for AR and AR-V7 Expression in Human Prostate Cancer. Clin Cancer Res. 2016;22(18):4651-63.

149. Baker A-M, Huang W, Wang X-MM, Jansen M, Ma X-J, Kim J, et al. Robust RNA-based in situ mutation detection delineates colorectal cancer subclonal evolution. Nature Communications. 2017;8(1):1998.

150. Alers JC, Krijtenburg PJ, Vissers KJ, van Dekken H. Effect of bone decalcification procedures on DNA in situ hybridization and comparative genomic hybridization. EDTA is highly preferable to a routinely used acid

decalcifier. The journal of histochemistry and cytochemistry : official journal of the Histochemistry Society. 1999;47(5):703-10.

151. Kleb B, Estecio MR, Zhang J, Tzelepi V, Chung W, Jelinek J, et al. Differentially methylated genes and androgen receptor re-expression in small cell prostate carcinomas. Epigenetics. 2016;11(3):184-93.

152. Gao Y, Wang J, Zhao F. CIRI: an efficient and unbiased algorithm for de novo circular RNA identification. Genome Biol. 2015;16(4):014-0571.

153. Liu C, Liu R, Zhang D, Deng Q, Liu B, Chao HP, et al. MicroRNA-141 suppresses prostate cancer stem cells and metastasis by targeting a cohort of pro-metastasis genes. Nat Commun. 2017;8:14270.

154. Goto Y, Kurozumi A, Arai T, Nohata N, Kojima S, Okato A, et al. Impact of novel miR-145-3p regulatory networks on survival in patients with castration-resistant prostate cancer. British journal of cancer. 2017;117(3):409-20.

155. Wang N, Li Q, Feng N-H, Cheng G, Guan Z-L, Wang Y, et al. miR-205 is frequently downregulated in prostate cancer and acts as a tumor suppressor by inhibiting tumor growth. Asian Journal of Andrology. 2013;15(6):735-41.

156. Yang Y, Guo J-X, Shao Z-Q. miR-21 targets and inhibits tumor suppressor gene PTEN to promote prostate cancer cell proliferation and invasion: An experimental study. Asian Pacific Journal of Tropical Medicine. 2017;10(1):87-91.

157. Luo B, Kang N, Chen Y, Liu L, Zhang Y. Oncogene miR-106a promotes proliferation and metastasis of prostate cancer cells by directly targeting PTEN in vivo and in vitro. Minerva medica. 2018;109(1):24-30.

158. Kumar P, Sharad S, Petrovics G, Mohamed A, Dobi A, Sreenath TL, et al. Loss of miR-449a in ERG-associated prostate cancer promotes the invasive phenotype by inducing SIRT1. Oncotarget. 2016;7(16):22791-806.

159. Zoni E, van der Horst G, van de Merbel AF, Chen L, Rane JK, Pelger RC, et al. miR-25 Modulates Invasiveness and Dissemination of Human Prostate Cancer Cells via Regulation of alphav- and alpha6-Integrin Expression. Cancer research. 2015;75(11):2326-36.

160. Shi X-B, Ma A-H, Xue L, Li M, Nguyen HG, Yang JC, et al. miR-124 and androgen receptor signaling inhibitors repress prostate cancer growth by downregulating androgen receptor splice variants, EZH2 and Src. Cancer research. 2015;75(24):5309-17.

161. Wang L, Liu C, Li C, Xue J, Zhao S, Zhan P, et al. Effects of microRNA-221/222 on cell proliferation and apoptosis in prostate cancer cells. Gene. 2015;572(2):252-8.

162. Budd WT, Seashols-Williams SJ, Clark GC, Weaver D, Calvert V, Petricoin E, et al. Dual Action of miR-125b As a Tumor Suppressor and OncomiR-22 Promotes Prostate Cancer Tumorigenesis. PLoS One. 2015;10(11):e0142373.

163. Chen J, Li Y, Zheng Q, Bao C, He J, Chen B, et al. Circular RNA profile identifies circPVT1 as a proliferative factor and prognostic marker in gastric cancer. Cancer Letters. 2017;388:208-19.

164. Shi XB, Xue L, Ma AH, Tepper CG, Gandour-Edwards R, Kung HJ, et al. Tumor suppressive miR-124 targets androgen receptor and inhibits proliferation of prostate cancer cells. Oncogene. 2013;32(35):4130-8.

165. Chen Y, Sun Y, Rao Q, Xu H, Li L, Chang C. Androgen receptor (AR) suppresses miRNA-145 to promote renal cell carcinoma (RCC) progression independent of VHL status. Oncotarget. 2015;6(31):31203-15.

166. Larne O, Hagman Z, Lilja H, Bjartell A, Edsjo A, Ceder Y. miR-145 suppress the androgen receptor in prostate cancer cells and correlates to prostate cancer prognosis. Carcinogenesis. 2015;36(8):858-66.

167. Imberg-Kazdan K, Ha S, Greenfield A, Poultney CS, Bonneau R, Logan SK, et al. A genome-wide RNA interference screen identifies new regulators of androgen receptor function in prostate cancer cells. Genome research. 2013;23(4):581-91.

168. Yoo S, Choi SY, You D, Kim C-S. New drugs in prostate cancer. Prostate International. 2016;4(2):37-42.

169. Budd WT, Seashols-Williams SJ, Clark GC, Weaver D, Calvert V, Petricoin E, et al. Dual Action of miR-125b As a Tumor Suppressor and OncomiR-22 Promotes Prostate Cancer Tumorigenesis. PLOS ONE. 2015;10(11):e0142373.

170. Mitra A, Fillmore RA, Metge BJ, Rajesh M, Xi Y, King J, et al. Large isoform of MRJ (DNAJB6) reduces malignant activity of breast cancer. Breast Cancer Research. 2008;10(2):R22.

171. Zabala-Letona A, Arruabarrena-Aristorena A, Martin-Martin N, Fernandez-Ruiz S, Sutherland JD, Clasquin M, et al. mTORC1-dependent AMD1 regulation sustains polyamine metabolism in prostate cancer. Nature. 2017;547(7661):109-13.

172. Hansen TB, Kjems J, Damgaard CK. Circular RNA and miR-7 in cancer. Cancer research. 2013;73(18):5609-12.

173. Fabris L, Ceder Y, Chinnaiyan AM, Jenster GW, Sorensen KD, Tomlins S, et al. The Potential of MicroRNAs as Prostate Cancer Biomarkers. European Urology. 2016;70(2):312-22.

174. Ostling P, Leivonen SK, Aakula A, Kohonen P, Makela R, Hagman Z, et al. Systematic analysis of microRNAs targeting the androgen receptor in prostate cancer cells. Cancer research. 2011;71(5):1956-67.

175. ChunJiao S, Huan C, ChaoYang X, GuoMei R. Uncovering the roles of miRNAs and their relationship with androgen receptor in prostate cancer. IUBMB life. 2014;66(6):379-86.

176. Meng X, Li X, Zhang P, Wang J, Zhou Y, Chen M. Circular RNA: an emerging key player in RNA world. Briefings in bioinformatics. 2016.

177. Mellado B, Codony J, Ribal MJ, Visa L, Gascon P. Molecular biology of androgen-independent prostate cancer: the role of the androgen receptor pathway. Clinical & translational oncology : official publication of the Federation of Spanish Oncology Societies and of the National Cancer Institute of Mexico. 2009;11(1):5-10.

178. Lin H-M, Nikolic I, Yang J, Castillo L, Deng N, Chan C-L, et al. MicroRNAs as potential therapeutics to enhance chemosensitivity in advanced prostate cancer. Scientific reports. 2018;8(1):7820.

179. Kristensen LS, Hansen TB, Venø MT, Kjems J. Circular RNAs in cancer: opportunities and challenges in the field. Oncogene. 2017;37:555.

180. Rubicz R, Zhao S, Wright JL, Coleman I, Grasso C, Geybels MS, et al. Gene expression panel predicts metastatic-lethal prostate cancer outcomes in men diagnosed with clinically localized prostate cancer. Molecular oncology. 2017;11(2):140-50.

181. Park WJ, Kothapalli KSD, Lawrence P, Brenna JT. FADS2 Function Loss at the Cancer Hotspot 11q13 Locus Diverts Lipid Signaling Precursor Synthesis to Unusual Eicosanoid Fatty Acids. PLOS ONE. 2011;6(11):e28186.

182. Soudy R, Etayash H, Bahadorani K, Lavasanifar A, Kaur K. Breast Cancer Targeting Peptide Binds Keratin 1: A New Molecular Marker for Targeted Drug Delivery to Breast Cancer. Molecular pharmaceutics. 2017;14(3):593-604.

183. Mahapatra S, Klee EW, Young CY, Sun Z, Jimenez RE, Klee GG, et al. Global methylation profiling for risk prediction of prostate cancer. Clin Cancer Res. 2012;18(10):2882-95.

184. Li X-P, Jiao JU, Lu LI, Zou Q, Zhu SHU, Zhang Y. Overexpression of ribosomal L1 domain containing 1 is associated with an aggressive phenotype and a poor prognosis in patients with prostate cancer. Oncology Letters. 2016;11(4):2839-44.

185. Horikawa I, Tanaka H, Yuasa Y, Suzuki M, Shimizu M, Oshimura M. Forced expression of YL-1 protein suppresses the anchorage-independent growth of Kirsten sarcoma virus-transformed NIH3T3 cells. Experimental cell research. 1995;220(1):11-7.

186. Berquin IM, Edwards IJ, Kridel SJ, Chen YQ. Polyunsaturated fatty acid metabolism in prostate cancer. Cancer metastasis reviews. 2011;30(0):10.1007/s10555-011-9299-7.

187. Martens-Uzunova ES, Olvedy M, Jenster G. Beyond microRNA – Novel RNAs derived from small non-coding RNA and their implication in cancer. Cancer Letters. 2013;340(2):201-11.

188. Yoshioka T, Otero J, Chen Y, Kim Y-M, Koutcher JA, Satagopan J, et al. β4 Integrin signaling induces expansion of prostate tumor progenitors. The Journal of Clinical Investigation. 2013;123(2):682-99.

189. Lewis BP, Burge CB, Bartel DP. Conserved seed pairing, often flanked by adenosines, indicates that thousands of human genes are microRNA targets. Cell. 2005;120(1):15-20.

190. Betel D, Wilson M, Gabow A, Marks DS, Sander C. The microRNA.org resource: targets and expression. Nucleic Acids Res. 2008;36(Database issue):D149-53.

191. Yang F, Zhang Y, Ressler SJ, Ittmann MM, Ayala GE, Dang TD, et al. FGFR1 is essential for prostate cancer progression and metastasis. Cancer research. 2013;73(12):3716-24.

192. Grisanzio C, Werner L, Takeda D, Awoyemi BC, Pomerantz MM, Yamada H, et al. Genetic and functional analyses implicate the NUDT11, HNF1B, and SLC22A3 genes in prostate cancer pathogenesis. Proceedings of the National Academy of Sciences of the United States of America. 2012;109(28):11252-7.

193. Wang R, Sun Y, Li L, Niu Y, Lin W, Lin C, et al. Preclinical Study using Small Interfering RNA or Androgen Receptor Splicing Variant 7 Degradation Enhancer ASC-J9to Suppress Enzalutamide-resistant Prostate Cancer Progression. European Urology.72(5):835-44.

194. Guarnerio J, Bezzi M, Jeong JC, Paffenholz SV, Berry K, Naldini MM, et al. Oncogenic Role of Fusion-circRNAs Derived from Cancer-Associated Chromosomal Translocations. Cell. 2016;165(2):289-302.

195. Mai S, Qu X, Li P, Ma Q, Cao C, Liu X. Global regulation of alternative RNA splicing by the SR-rich protein RBM39. Biochimica et biophysica acta. 2016;1859(8):1014-24.

196. Zhang Z, Zhou N, Huang J, Ho TT, Zhu Z, Qiu Z, et al. Regulation of androgen receptor splice variant AR3 by PCGEM1. Oncotarget. 2016;7(13):15481-91.

197. Salzman J, Chen RE, Olsen MN, Wang PL, Brown PO. Cell-type specific features of circular RNA expression. PLoS Genet. 2013;9(9):5.

198. Bahn JH, Zhang Q, Li F, Chan TM, Lin X, Kim Y, et al. The landscape of microRNA, Piwi-interacting RNA, and circular RNA in human saliva. Clin Chem. 2015;61(1):221-30.

199. Gaudreau P-O, Stagg J, Soulières D, Saad F. The Present and Future of Biomarkers in Prostate Cancer: Proteomics, Genomics, and Immunology Advancements. Biomarkers in Cancer. 2016;8(Suppl 2):15-33.

200. Makarov DV, Humphreys EB, Mangold LA, Carducci MA, Partin AW, Eisenberger MA, et al. The natural history of men treated with deferred androgen deprivation therapy in whom metastatic prostate cancer developed following radical prostatectomy. The Journal of urology. 2008;179(1):156-61; discussion 61-2.

201. Haffner MC, Mosbruger T, Esopi DM, Fedor H, Heaphy CM, Walker DA, et al. Tracking the clonal origin of lethal prostate cancer. The Journal of clinical investigation. 2013;123(11):4918-22.

202. Smith M, Parker C, Saad F, Miller K, Tombal B, Ng QS, et al. Addition of radium-223 to abiraterone acetate and prednisone or prednisolone in patients with castration-resistant prostate cancer and bone metastases (ERA 223): a randomised, double-blind, placebo-controlled, phase 3 trial. The Lancet Oncology. 2019;20(3):408-19.

203. Teutsch SM, Bradley LA, Palomaki GE, Haddow JE, Piper M, Calonge N, et al. The Evaluation of Genomic Applications in Practice and Prevention (EGAPP) Initiative: methods of the EGAPP Working Group. Genet Med. 2009;11(1):3-14.

204. Xu D, Zhan Y, Qi Y, Cao B, Bai S, Xu W, et al. Androgen Receptor Splice Variants Dimerize to Transactivate Target Genes. Cancer research. 2015;75(17):3663-71.

205. de Bono JS, De Giorgi U, Nava Rodrigues D, Massard C, Bracarda S, Font A, et al. Randomized Phase II Study of Akt Blockade With or Without Ipatasertib in Abiraterone-Treated Patients With Metastatic Prostate Cancer With and Without PTEN Loss. Clinical Cancer Research. 2018:clincanres.0981.2018.